MULTISTAGE ALTERATION OF THE EXTRUSIVE SEQUENCE,

TROODOS OPHIOLITE, CYPRUS

by

KATHRYN M. GILLIS

Submitted in partial fulfillment of the requirements

for the degree of Doctorate of Philosophy

at

Dalhousie University

Halifax, Nova Scotia

November, 1986

i

DALHOUSIE UNIVERSITY

FACULTY OF GRADUATE STUDIES

The undersigned hereby certify that they have read and
recommend to the Faculty of Graduate Studies for acceptance
a thesis entitled " Multi-stage Alteration of the Extrusive
Sequence Troodos Ophiolite, Cyprus "

by   Kathryn Mary Gillis

in partial fulfillment of the requirements for the degree of
Doctor of Philosophy.

$$\textcircled{C}$$

Dated   November 4, 1986

External Examiner

Research Supervisor

Examining Committee

ii

DALHOUSIE UNIVERSITY

Date Nov. 17, 1986.

Author   Kathryn M. Gillis

Title   Multistage Alteration of the Extrusive Sequence, Troodos Ophiolite,

Cyprus

Department or School   Geology

Degree   Ph.D.   Convocation   Spring   Year   1987

iii

TABLE OF CONTENTS

iv

DALHOUSIE UNIVERSITY

Date ___Nov. 17, 1986.___

Author ___Kathryn M. Gillis___

Title ___Multistage Alteration of the Extrusive Sequence, Troodos Ophiolite,___

___Cyprus___

___

Department or School ___Geology___

Degree ___Ph.D.___ Convocation ___Spring___ Year ___1987___

Permission is herewith granted to Dalhousie University to
circulate and to have copied for non-commercial purposes, at its
discretion, the above title upon the request of individuals or
institutions.

███████████████

Signature of Author

iii

ABSTRACT

Several stages of alteration documented in the upper 1 - 2 km of
the Troodos ophiolite have been related to the evolution of hydrothermal
systems, crustal aging, and the subsequent uplift and emplacement of the
ophiolite. Six alteration zones, defined by their mineralogical
signatures, have been mapped along the northern flank of the ophiolite
and outlined in the ICRDG drillcores, CY-1 and CY-1a. The depositional
sequence of the groundmass-replacing and void-filling secondary minerals
in each of these zones reflects localized change in physical and
chemical conditions through time.

The rocks in the upper tens of metres of the extrusive sequence
are pervasively altered, oxidized, enriched in K_2O, CO_2, H_2O, Rb, and
Ba, and depleted in SiO_2 and Sr. Where synvolcanic umbers overlie the
volcanic pile, the rocks are not oxidized and fresh glassy rinds are
commonly preserved, indicating that the rocks were sealed from
penetrating seawater. Below these zones, the rocks are variably altered
to assemblages of smectite, celadonite, zeolites, and carbonate and
locally enriched in alkalis and MgO and depleted in SiO_2, CaO, and Sr.
The low temperature minerals are replaced at the base of this zone by
laumontite, mixtures of smectite/chlorite, and quartz. Over a 100- to
150-m-thick interval, the rocks become progressively more recrystallized
and assemblages of chlorite + quartz + albite + pyrite $\pm$ epidote
dominate. Rock-dominated conditions resulted in the enrichment of Na_2O
and depletion of CaO, K_2O, Rb, and Sr. Local enrichment of MnO, Cu, and
Zn are attributed to localized zones of discharge.

Outside the localized zones of hydrothermal discharge, the rocks

have not been pervasively metamorphosed. The intensity of alteration is not directly related to depth but rather depends on permeability, temperature, and the rate of sedimentation. A sharp transition occurs between the low temperature zones and the higher temperature zones with greenschist facies mineral assemblages at different levels within the extrusive sequence and sheeted dyke complex. This indicates that the geothermal gradient was stepped and responded to localized conditions, such as changes in permeability that restricted the penetration of unreacted, cold seawater into the lower zone.

LIST OF FIGURES

x

LIST OF TABLES

xiii

LIST OF PLATES

ACKNOWLEDGEMENTS

CHAPTER I

INTRODUCTION

1.1 GENERAL STATEMENT

The discovery of hydrothermal vents at both fast (e.g. $21^{\circ}N$, EPR, Edmond et al. 1979) and slow (e.g. 23° N, MAR, Leg 106 Scientific Party, in press) spreading centres and the regular flucutation of heat flow measurements away from mid-ocean ridges (Green et al. 1981; Williams et al. 1974) confirm that hydrothermal circulation is an important process in the modern oceanic crust. In fact, the presence of polymetallic sulfide deposits in oceanic crust of all ages indicates that hydrothermal circulation of seawater has been an important process throughout geologic time (Franklin et al. 1981). Estimates for the duration of this circulation from heat flow measurements range from 5-6 Ma (Galapagos) to 60-70 Ma (Atlantic) (Anderson & Skilbeck 1981), depending upon the rates of spreading and sedimentation (Anderson et al. 1977; Anderson & Hobart 1976). Chemical and isotopic studies of drilled and dredged rocks of various ages from different geologic settings show that the oceanic crust has reacted with circulating seawater (Honnorez 1981). These observations have led some investigators to speculate that the oceanic crust is an important sink and source for chemical exchanges that control the composition of seawater (Thompson 1983; Edmond et al. 1979; Humphris & Thompson 1978; Wolery & Sleep 1976) and that the recycling of this chemically modified oceanic crust at destructive plate margins may influence arc magmatism and the composition of the mantle (Spooner 1980). Before models for geochemical mass-balancing may be properly constrained, however, a much better understanding of how the

1

composition and structure of the oceanic crust evolves is required.

The drillcores recovered by the Deep Sea Drilling Project (DSDP) and Ocean Drilling Project (ODP) have provided valuable information about the upper 1000 m of the oceanic crust. The diversity of the recovered core, however, has shown that the rocks have undergone several progressive and commonly overlapping stages of alteration, generally at low temperatures (Honnorez 1981). Three holes drilled in Cretaceous crust during DSDP legs 51-53, Holes 417A, 417D, and 418A, indicate that the lateral and vertical variation in the pervasiveness of alteration in the uppermost crust is significant and that below this zone of intense alteration the rocks are variably altered with fresh glass being locally preserved (Shipboard Scientific Crew, Legs 51, 51, & 53, 1979 a&b). The rocks recovered at Hole 504B, the only deep basement hole, showed the same zonation in alteration, with the upper pillows being more intensely altered than the underlying pillows (Honnorez et al. 1983). The lithologic transition zone from the extrusive sequence into the sheeted dyke complex, where alteration conditions change from low to high temperature, was also sampled at this site (Alt et al. 1985). Measurments of "in situ" permeability (Anderson et al. 1985) and bulk porosity (Becker 1985) indicate that permeability decreases almost exponentially with depth whereas the temperature gradient during the earliest stages of alteration was stepped, with nearly isothermal conditions in the permeable extrusive sequence, a sharp increase across the lithologic transition zone, and near normal gradient in the sheeted dyke complex (Alt et al. 1986). These observations provide new boundary conditions for mathematical models of hydrothermal circulation and new constraints for models of crustal aging. How representative these

conditions are of normal crust, however, is not known. The only other recovered "in situ" oceanic rocks altered at higher temperatures were dredged from fault scarps and are therefore not necessarily representative of alteration deep in the crust.

Many early models for the structure and evolution of oceanic crust came from studies of ophiolites (e.g. Gass 1980; Coleman 1977). Geophysical studies showed that the gross structure of "in situ" crust is analogous to ophiolites (e.g. Salisbury & Christensen 1978), even though most ophiolites are now believed to have formed at spreading axes in marginal basins (e.g. Sarmentio, Stern & Elthon 1979) or subduction-related environments (e.g. Troodos, Robinson et al. 1983) rather than at typical mid-ocean ridges. The presence of exhalative sulfide deposits in many ophiolites (e.g. Troodos, Semail, Bett's Cove) and the alteration of the exposed rocks led to the prediction that deep hydrothermal circulation was associated with magmatism close to ridge axes and the development of regional metamorphic zones whose grade and intensity of alteration increase with increasing depth (McCulloch et al. 1980; Stern & Elthon 1979; Liou & Ernst 1979; Spooner et al. 1977 a&b; Constantinou & Govett 1973; Gass & Spooner 1973; Spooner & Fyfe 1973).

The Troodos ophiolite is probably the most studied ophiolite in the world and hence has influenced the formulation of models for crustal accretion and hydrothermal circulation (e.g. Gass 1980; Spooner 1977; Spooner et al. 1977b; Gass & Smewing 1973; Moores & Vine 1971). In 1982, a major re-investigation of the Troodos ophiolite, including extensive field mapping and deep drilling, was undertaken by the International Crustal Research Drilling Group (ICRDG). During the early stages of the project, field investigations showed that fresh glass was

preserved throughout the extrusive sequence indicating that the rocks were not pervasively metamorphosed (Robinson et al. 1983; Robinson, pers. comm., 1982) as had previously been proposed (Gass & Smewing 1973). These observations suggested that the pattern of alteration in the extrusive sequence is analogous to "in situ" oceanic crust sampled by DSDP.

This thesis was undertaken to test this hypothesis and to re-evaluate the models for alteration and hydrothermal circulation in the Troodos ophiolite, concentrating on the broad zones of downwelling. The combination of field outcrops with ICRDG drillcore provided a unique opportunity to study the three-dimensional relationships among hydrothermal circulation, ore deposition, and crustal aging. The stratigraphic and petrologic framework developed for the extrusive sequence (Mehegan & Robinson 1985; Bailey 1984; Robinson et al. 1983; Schmincke et al. 1983) and investigations of the ore deposits (e.g. ICRDG 1984; Adamides 1984; Lydon 1984; Constantinou 1980) greatly enhanced this study.

The objective of this thesis was to develop a spatial and temporal model for the alteration of the extrusive sequence along the northern flank of the Troodos ophiolite which distinguishes the effects of hydrothermal circulation, crustal aging, and the uplift and subsequent emplacement of the ophiolite. Detailed field studies combined with mineralogic and chemical investigations provided a framework for the delineation of progressive stages of alteration with constant physical and chemical conditions. Comparison of the observed alteration pattern in Troodos with alteration studies of "in situ" oceanic crust is important to evaluate the "representativeness" of

Troodos of more normal oceanic crust.

1.2 PREVIOUS STUDIES

Alteration studies of the Troodos ophiolite date back to ancient times when the Phoenicians and Romans used gossans as an exploration tool in the search for sulfide deposits. Focus since that time has remained upon the ore deposits because, until recently, their exploitation served as an important base of the Cypriot economy.

The spatial distribution of characteristic secondary minerals, combined with stratigraphic and primary mineralogic criteria, was used to divide the extrusive sequence into the Upper Pillow Lavas (UPL) and Lower Pillow Lavas (LPL) (Bear 1960; Carr & Bear 1960; Gass 1960). Gass & Smewing (1973) proposed that the UPL/LPL subdivision corresponded to a metamorphic discontinuity. They suggested that the LPL and sheeted dyke complex formed at a constructive plate margin and were pervasively metamorphosed within 100 km of the spreading centre. The metamorphic grade of this "axis" sequence increased gradually with increasing depth, from zeolite to greenschist facies, and was not correlated with a change in the intrusive/extrusive ratio. The overlying, "off-axis" sequence (UPL) formed after this metamorphism, away from the spreading centre. It was also metamorphosed to the zeolite facies but with different characteristic minerals than those of the "axis" sequence (LPL) (Smewing 1975).

Stable isotopic studies of altered rocks (Spooner et al. 1977b; Chapman & Spooner 1977; Heaton & Shepperd 1977) and fluid inclusion studies (Spooner & Bray 1977) have shown that the altering fluid was seawater. Oxidation (Spooner et al. 1977b) and $d^{18}O$ (Heaton & Shepperd

1977) depth profiles have shown that away from the sulfide deposits, the direction of seawater flow was dominantly downward. These observations led to the prediction that hydrothermal circulation of seawater through the upper 3-5 km of the ophiolite resulted in the formation of the massive sulphide deposits (Parmientier & Spooner 1978; Spooner 1977; Heaton & Shepperd 1977; Spooner & Bray 1977; Chapman & Spooner 1977; Spooner et al. 1977b). It was envisaged that seawater penetrated the crust in broad zones of downwelling, was heated at depth, and returned to the surface in focussed conduits (Parmentier & Spooner 1978). The recharge zones are characterised by the regional metamorphism described by Gass & Smewing (1973) and the discharge zones are marked by the sulfide deposits. Spooner et al. (1977b) estimated water/rock ratios for this alteration ranging from 15:1 (Sr isotopes) to 3×10^3:1 (oxidation). In contrast, Heaton & Shepperd (1977) suggested on the basis of O isotopes that the water/rock ratios decrease from >1 in the zeolite facies pillow lavas to 0.1 in the greenschist facies rocks.

Until recently, investigators generally agreed with the model for increasing metamorphic grade with depth developed by Gass & Smewing (1973) (Gass 1980; Constantinou 1980; Kay & Senechal 1976; Adamides 1975; Pearce & Cann 1973; Constantinou & Govett 1972). The recognition of fresh glass throughout the extrusive sequence (Robinson et al. 1983), however, indicated that the rocks were not pervasively metamorphosed and that alteration facies were not stratigraphically controlled. Clearly, further investigations were in order to understand the nature of alteration of the Troodos ophiolite.

CHAPTER II

GEOLOGY OF CYPRUS

2.1 INTRODUCTION

The Troodos ophiolite is located on the island of Cyprus in the
eastern Mediterranean Sea (Figure II-1). It is the north-western
end-member of a belt of Cretaceous ophiolites which are discontinuously
exposed along the margin of the Arabian plate (Moores et al. 1984).
Although it is generally accepted that the complex formed at a spreading
axis (Schmincke et al. 1983; McCulloch & Cameron 1983; Robertson &
Woodcock 1980; Pearce 1975; Moores & Vine 1971), controversy still
exists as to its specific tectonic environment. A mature island arc
(Miyashiro 1973), an immature arc (Rautenschlein et al. 1985; Thy et al.
1985; Moores et al. 1984; Robinson et al. 1983) and a marginal basin
(Smewing et al. 1975; Pearce & Cann 1973) have all been suggested.

In the following chapter, the geology of Cyprus is briefly
reviewed, the field area is defined, and the igneous stratigraphy of
specific localities within the field area is summarized. Typical
lithologic features of the extrusive sequence are also described.

2.2 GEOLOGY OF CYPRUS

The Troodos ophiolite forms an elongate WNW-trending domal
structure in central Cyprus which occupies approximately one-third of
the island's 9520 km^2. Three tectonic zones comprise the remaining
areas of the island: the Mamonia Complex, the Kyrenia Range, and a
sedimentary succession (Figure II-2).

7

Figure II-1. Map of the eastern Mediterranean showing the location of
the Troodos ophiolite and other Cretaceous ophiolites in the region
(modified after Robertson & Woodcock 1980).
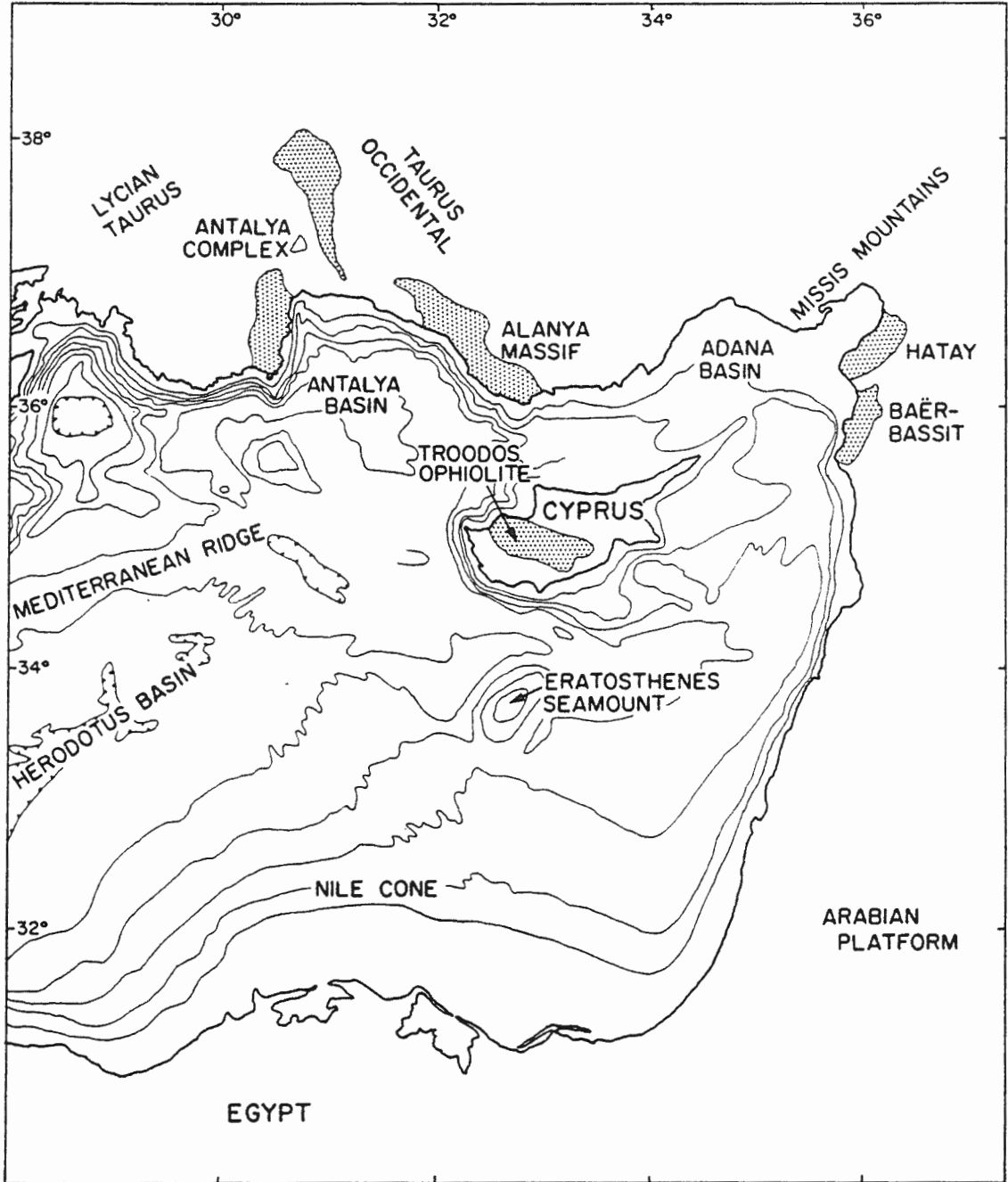
Figure II-2. Geologic map of Cyprus.

CYPRUS

Kyrenia

Nicosia

Famagusta

Larnaca

Paphos

Limasol

0 5 10 15 20 25 kilometers

35°
30'

35°
00'

32° 30'

33° 30'

35°
30'

35°
00'

32° 30'

33° 30'

LEGEND

Sedimentary Rocks

+ + Mamonia Complex

Kyrenia Range

Troodos Ophiolite

Extrusive Complex

Sheeted Dyke Complex

Plutonic Complex

11
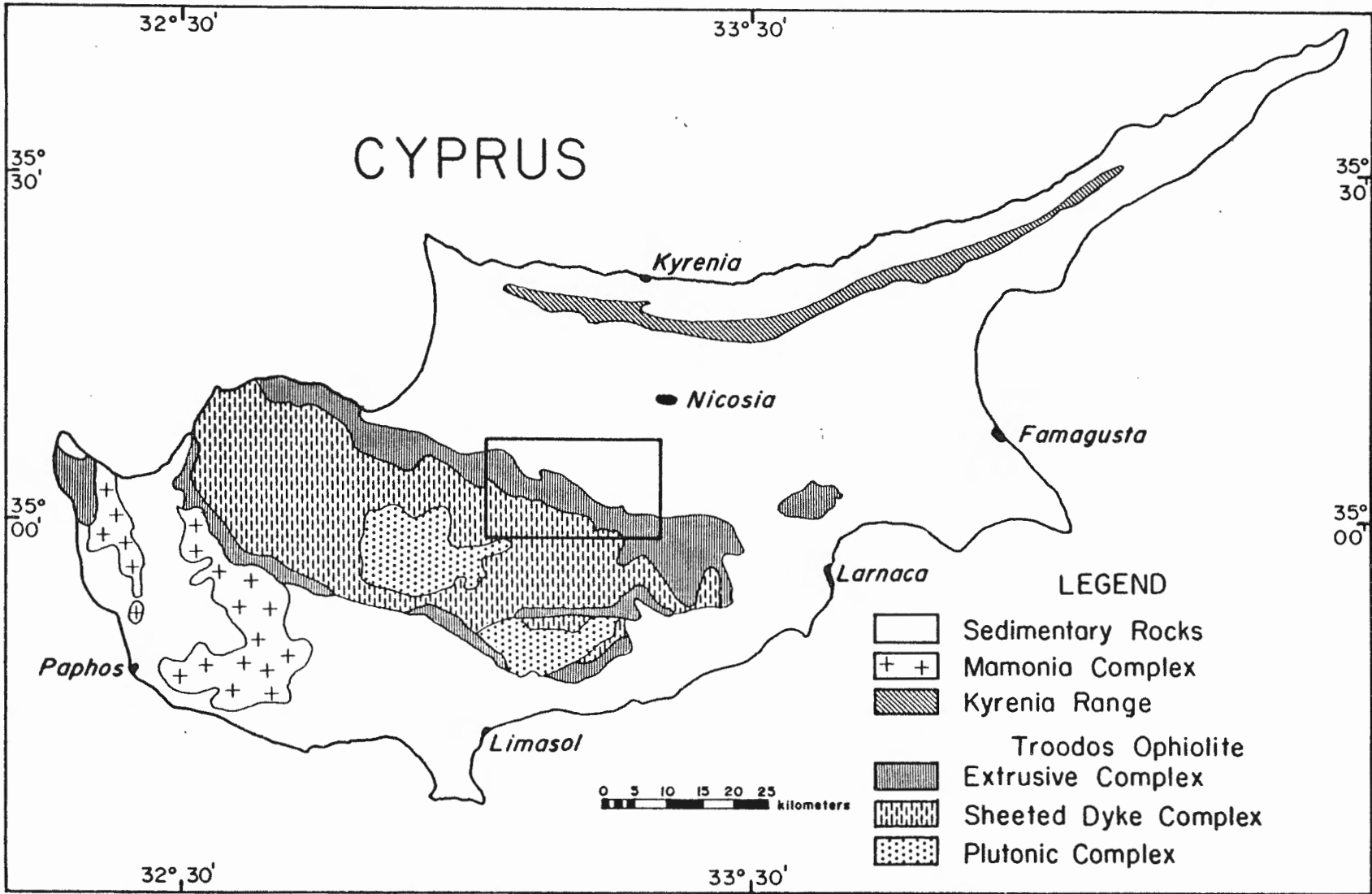
2.2.1 Kyrenia Range

The Kyrenia Range forms an arcuate, east-west trending belt of autochthonous and allochthonous rocks along the northern coast of Cyprus. The allochthonous rocks include a sequence of Permian to Miocene limestones, pelagic chalks, radiolarites, and volcanic rocks which are locally intermixed with undated serpentinites and metamorphic rocks. The volcanic rocks include a Maastrichtian alkaline (Pearce 1975) to calc-alkaline (Baroz et al. 1975) suite and a Paleocene shoshonitic suite (Baroz 1980). These rocks are stacked in four north- to northeast-dipping thrust slices that have been internally folded (Baroz et al. 1976; Biju-Duval et al. 1976) and are flanked both to the north and south by terrigenous flysch deposits (Baroz 1977). The allochthonous rock sequences, which include remnants of a volcanic arc, were emplaced during the late Oligocene to early Miocene (Robertson & Woodcock 1980; Baroz et al. 1975). The mountain range is bounded to the south by a strike-slip fault and is not underlain by mafic or ultramafic rocks at shallow depths (Aubert & Baroz 1974).

2.2.2 Mamonia Complex

The Mamonia Complex is exposed south and southwest of the Troodos ophiolite. Two rock assemblages dominate the complex: 1) the Late Triassic Dhiarizos Group which contains mafic volcanic rocks, reef limestones, and hemipelagic sedimentary rocks and 2) the Late Triassic to Middle Cretaceous Ayios Photios Group which contains quartzose sandstone, platform and hemipelagic limestone, and pelagic siliceous sedimentary rocks (Swarbrick 1980). These rocks are stacked in sub-horizontal thrust sheets. A major east-west trending arcuate belt

of serpentinite and associated igneous and metamorphic rocks cuts across the complex (Robertson & Woodcock 1980). Emplacement from the northeast, either as thrust sheets over an autochthonous Troodos Massif or entrained beneath, and emplaced with, an allochthonous Troodos Massif has been suggested (Baroz et al. 1976; Biju-Duval et al. 1976; Lapierre 1975; Turner 1973). Alternatively, Swarbrick (1980) has proposed that the allochthonous rocks of the Mamonia Complex were emplaced from the southwest and are separated from the ophiolite by a transcurrent fault.

2.2.3 Sedimentary Rocks

The sedimentary sequences that overlie the Troodos ophiolite and the Mamonia Complex record a complex history of episodic uplift, subsidence, erosion, and peneplanation (Robertson 1977). Metalliferous sediments of the basal Perapedhi Formation were deposited during the waning stages of volcanism in small hollows and fault-bounded depressions along the top of the lava sequence (Robertson & Boyle 1983). Umbers, radiolarites, and bentonitic claystones form beds which are generally < 4 m thick but may be up to 35 m thick. These Turonian sediments (Blome & Irwin 1985) are commonly underlain by altered and fragmented, pale grey pillows with fresh glassy margins.

Maastrichtian volcanogenic and bentonitic clays of the Kannaviou Formation comformably overlie the Perapedhi Formation or unconformably overlie the Troodos lavas and the Mamonia Complex. South and west of the ophiolite, sequences are up to 600 m thick whereas scattered beds < 10 m thick are present on the north and east.

Pelagic calcareous sediments of the Lefkara Formation were deposited during the next major period of sedimentation (Pantazis 1967).

Thick sequences of fine-grained, finely laminated chalks were deposited during the late Maastrichtian in the south whereas to the north, beds < 25 m thick accumulated in broad hollows. Deposition of massive to weakly bedded chalks and intercalated cherts in sequences up to 300 m thick followed during the Paleocene and Lower Eocene. The overlying sequence of chert-free chalks, marls, reef limestones, and calcarenites, deposited during the Upper Eocene and Lower Miocene, records a gradual regression and the cessation of Lefkara sedimentation (Robertson & Woodcock 1980).

During the Middle Miocene, reef limestones, chalks, marls, calcarenites, conglomerates, and evaporites of the Pahkna and Koronia Formations record several periods of transgression and regression triggered by uplift in the Limassol Forest area.

The final emplacement of the Kyrenia Range from the north and major faulting in the Troodos volcanic basement during the Late Miocene and Pliocene influenced the next episode of sedimentation. Thick sequences of the Nicosia, Myrthou Marl, and Athalassa Formations were transgressively deposited over the older formations and locally over the volcanic rocks.

Uplift during the Pleistocene led to deposition of the Fanglomerate Series. Uplift has continued since the Quaternary, resulting in minor erosion of the Fanglomerates and incision of most streams.

2.2.4 Troodos Ophiolite

The Troodos ophiolite is a pseudostratified igneous succession composed of three main rock units: a plutonic complex, a sheeted dyke

complex, and an extrusive sequence. Uplift of approximately 2000 m during the Tertiary and subsequent erosion have exposed all stratigraphic levels of the massif with the lowermost plutonic complex being exposed in the core of the Troodos mountains and the extrusive sequence along its periphery.

The plutonic complex consists of tectonized harzburgite, dunite, olivine pyroxenite, isotropic olivine gabbro, and plagiogranite (Moores & Vine 1971). Two suites have been recognised within the complex on the basis of intrusive contacts and deformation styles: an early suite of tectonized harzburgite, dunite with chromite, and layered olivine pyroxenite which has undergone high-temperature deformation, and a later suite of poikilitic plagioclase peridotite, pyroxenite, and pyroxene-hornblende gabbro which is weakly and inhomogeneously deformed (Dunsworth & Calon 1984).

The boundary between the plutonic complex and the overlying sheeted dyke complex is variable. Dykes intruding gabbros, gabbros intruding dykes, and dykes in fault contact with gabbros have all been documented in the field (Malpas, pers. comm., 1984).

Dyke swarms within the sheeted complex have variable orientation and individual dykes range in thickness from a few centimetres to a few metres (Baragar et al. 1984). Most dykes are aphyric but some contain sparse phenocrysts of clinopyroxene and olivine. The dykes are typically fine to medium grained, greyish-green, and variably altered to greenschist or amphibolite mineral assemblages. The Basal Group, with screens of pillows between the dykes, comprises the upper portion of the sheeted dyke complex (Bear 1960; Wilson 1959; Gass 1960). These pillow screens vary from thin bands of highly altered material to homogeneous

zones up to 15 m wide in which the original pillow morphology is preserved. The Basal Group grades upward into the extrusive sequence over a 100 to 150 m interval where the dyke density decreases from >90% to <50%.

The extrusive sequence is composed of pillows, massive and sheet flows, volcanic breccias, and hyaloclastites. It was divided by early workers into the Upper Pillow Lavas (UPL) and the Lower Pillow Lavas (LPL) on the basis of color, abundance of olivine, assemblages of secondary minerals, and the location of massive sulfide orebodies (Bear 1960; Gass 1960). Gass & Smewing (1973) divided the sequence into an axis sequence, consisting of the Lower Pillow Lavas and the sheeted dykes, and a younger, off-axis sequence, represented by the Upper Pillow Lavas, based upon a supposed metamorphic boundary within the complex.

Two distinct geochemical suites have been outlined for the lavas from the northern flank of the ophiolite based on glass and whole rock compositions: 1) a lower andesite - dacite - rhyodacite assemblage of arc tholeiite affinity and 2) an upper picritic basalt - andesitic basalt assemblage with a depleted arc tholeiite affinity (Mehegan & Robinson 1985; Thy et al. 1985; Robinson et al. 1983). These suites are hereafter referred to as the arc tholeiite suite and the high MgO - high SiO_2 suite, respectively (Robinson et al. 1983). The stratigraphic level of this geochemical boundary is variable within the extrusive sequence in relation to the former UPL/LPL boundary (Figure II-3). A third suite of highly depleted basalts with "boninitic" affinities has been recognised on the southern flank of Troodos (Mehegan & Robinson 1985).

Radiolarian fauna in the umbers interbedded with and overlying

Figure II-3. Schematic stratigraphic column which illustrates the
historical development of the divisions in the extrusive sequence
and Basal Group. 1 Bear (1960), Gass (1960), and others, 2 Gass &
Smewing (1973), 3 Robinson et al. 1983, 4 lithostratigraphic
sequences used in this study.

1	2	3	4
UPL	OFF-AXIS SEQUENCE	HIGH MgO HIGH SiO$_2$ SUITE	III
LPL	AXIS SEQUENCE	ARC THOLEIITE SUITE	II
			I
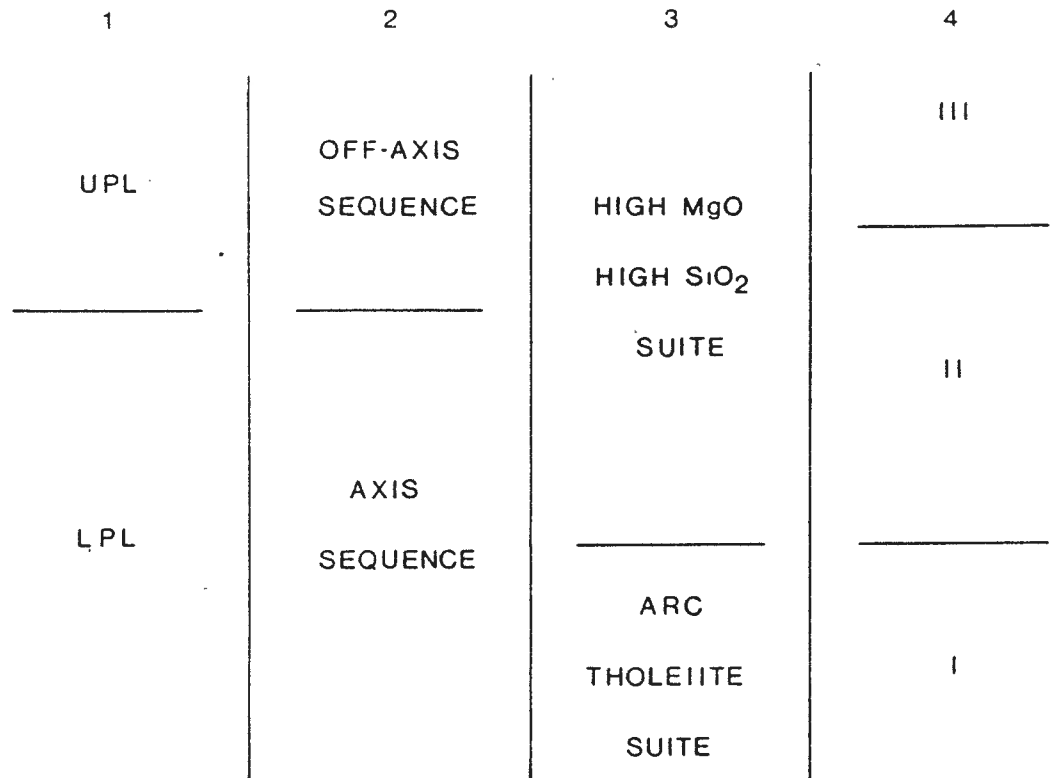
the extrusive sequence (Blome & Irwin 1985) and U-Pb zircon ages from the plagiogranites (Mukasa & Ludden 1986) indicate that the ophiolite formed during or prior to the Turonian (88.5 - 91.5 Ma, Hartland et al. 1982). K/Ar ages from whole rock samples are generally lower and were probably re-set after igneous emplacement (Staudigel et al. 1986; Delaloye et al. 1980).

2.3 FIELD AREAS

The study area includes the region between the villages of Peristerona and Margi along the northern flank of the ophiolite, extending from the top of the lavas to the Basal Group (Figure II-4). Within this area, several locations were studied in considerable detail. The volcanic stratigraphy and structure of each of these localities, presented in the following section, are based upon the field mapping of J. Mehegan, D. Bailey, P. Robinson, M. Rautenschlein, and H.-U. Schmincke during the 1981-1982 field seasons.

The extrusive sequence in each of these areas was subdivided into several lithologic units based upon mineralogy, cooling-unit type, and color. These units cannot be correlated on a regional scale because they are laterally discontinuous and because of poor exposures between river sections. For simplicity, these lithologic units have been grouped into three major lithostratigraphic sequences which are mappable on a regional scale (Mehegan, unpublished data, 1985; Robinson et al. 1983). They are, from oldest to youngest:

Sequence I: aphyric to sparsely plagioclase- and clinopyroxene-phyric lavas

Sequence II: aphyric to sparsely olivine-clinopyroxene-phyric lavas

Figure II-4. Geologic map of the study area. The areas studied in
detail are outlined (modified after Bear 1960 and Gass 1960).

Sedimentary Formations

Fanglomerate Series

Mesaoria Group

Dhali Group

Letkara Formation

Perapedhi Formation

Igneous Rocks

Extrusive Sequence

Basal Group & Sheeted Dyke Complex

Gabbros

★ massive sulfide mine

0   1   2 km
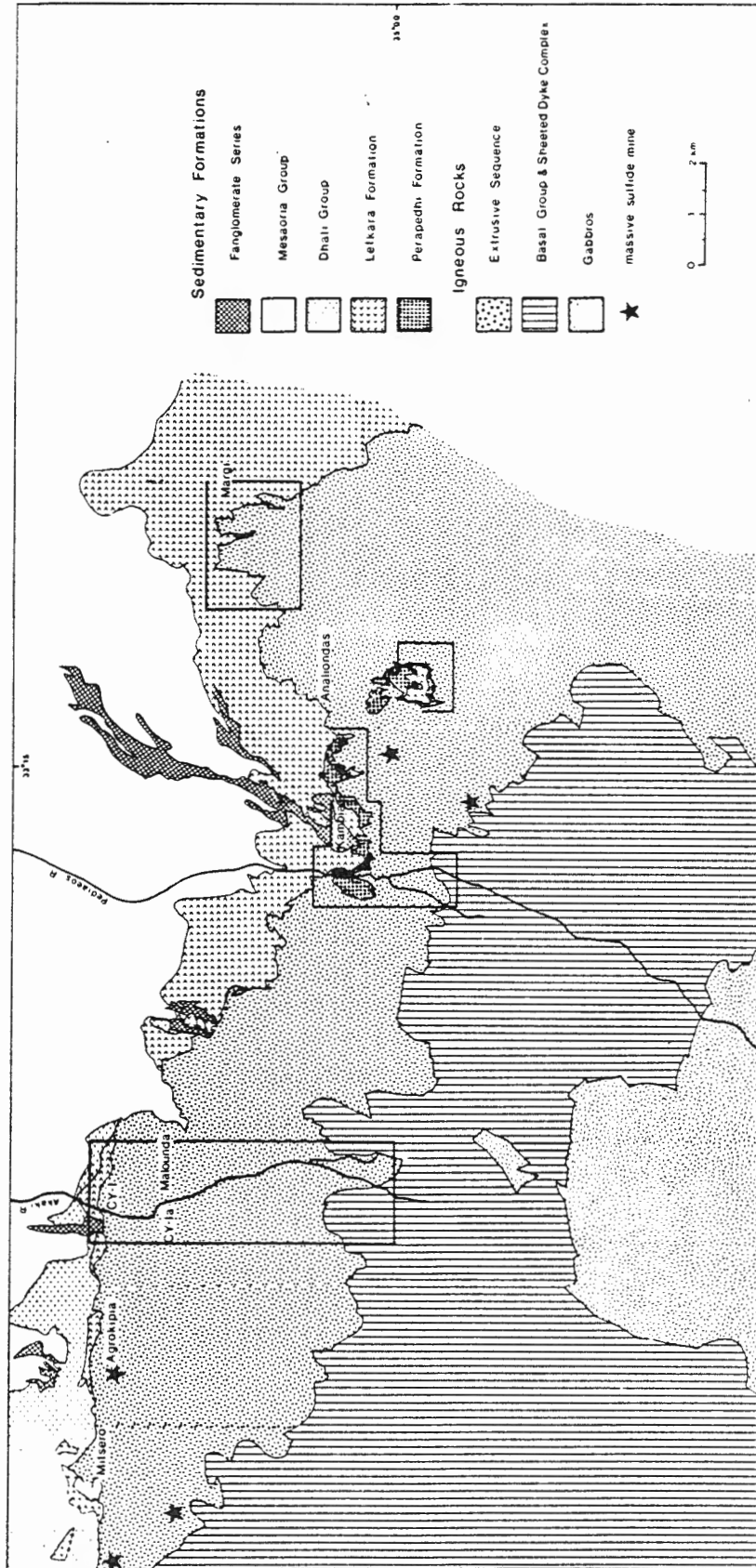
<u>Sequence III</u>: aphyric, olivine-clinopyroxene-phyric, and picritic lavas

In the study area, Sequences I and III are ubiquitous whereas locally Sequence II may be absent. In the Kambia - Mathiati area, Sequence III is separated from Sequence I by a <1-10 m thick horizon of umbers and very fine-grained massive to finely laminated mudstones. Elsewhere, Sequence I is directly overlain by Sequence II or III.

The basal Sequence I, dominated by massive and sheet flows with lesser pillows, breccias, and hyaloclastites, is andesitic - dacitic - rhyolitic in composition and corresponds to the arc tholeiite suite of Robinson <u>et al.</u> (1983) (Figure II-3). Its thickness, difficult to estimate due to dyke intrusion at its base, is 300 - 500 m. Flows and pillows are locally separated by thin (<1 m) layers of hyaloclastite.

The overlying Sequence II lavas, basalt to basaltic andesite in composition, belong to the high MgO-high SiO_2 geochemical suite. This sequence may be up to 600 m thick and is composed of alternating sequences of pillows and flows. Subvertical dykes and sills are less abundant than in the lower sequence. Coarse-grained, doleritic intrusive bodies, several tens of metres in width, often have a layered appearance although they have no discernable grain size or mineralogical variation. They have been interpreted as the synvolcanic feeders for the pillowed units (M. Rautenschlein, pers. comm., 1985).

Sequence III lavas, also part of the high MgO-high SiO_2 suite, are dominated by olivine-phyric and picritic pillows with lesser amounts of massive and sheet flows, pillow fragment breccias, and hyaloclastites. The stratigraphic distribution of the aphyric to olivine- and clinopyroxene-phyric units and picrites is variable (Bailey 1984; Boyle & Robertson 1984; Malpas & Langdon 1984). Lenticular pillow

fragments in a clay-carbonate matrix overlie heavily veined and
fractured pillows near the top of the lava pile. Yellowish-brown,
ferrunginous interpillow sediment is locally abundant at the top of the
lava pile but decreases rapidly with depth. Intrusive bodies are rare
or absent at this stratigraphic level.

2.3.1 Peristerona

The extrusive sequence exposed along the Peristerona River, 5 km
south of the village of Orounda, is overlain by Recent alluvium and
fanglomerates. West of the river section, small patchily distributed
deposits of umber are overlain by the Myrotou Marl or Pahkna Formations
(Carr & Bear 1960).

Alteration studies in this area were confined to the upper
aphyric to olivine-clinopyroxene phyric pillows, breccias, and thin
flows of Sequence III.

2.3.2 Malounda

One of the thickest sections of the Troodos extrusive sequence is
exposed along the Akaki River, west of the villages of Malounda and
Klirou (Figure II-4). The lavas in this area are overlain by chalks of
the upper Lefkara Formation (Figure II-5). The 1500-m-thick section has
been subdivided into 11 lithologic units dominated by either pillowed
lavas or massive and sheet flows (Schmincke et al. 1983), (Figure II-6).
Some parts of the section may be structurally repeated, reducing the
true thickness to 1250 m (Mehegan, unpublished data, 1986). The
regional dip is 20-30° to the northwest and the dykes trend north to
northwest. When the lavas are rotated to a horizontal position, the

Figure II-5. Comparative sections illustrating the variable thicknesses
of the sedimentary formations in the study area (modified after
Bear 1960).

Mitsero   Agrokipia   Akaki   Aradiou   Politiko   Pediaeos   Margi

W   E

2 km ── 1 5 km ── 1 km ── 3 km ── 3 km ── 3 km

Koronia Limestone
Pakhna Chalks & Marls
Upper Lefkara Chalks
Middle Lefkara Marls & Chalks
Perapedhi Shales
Extrusive Sequence

Vertical scale

0   30 m
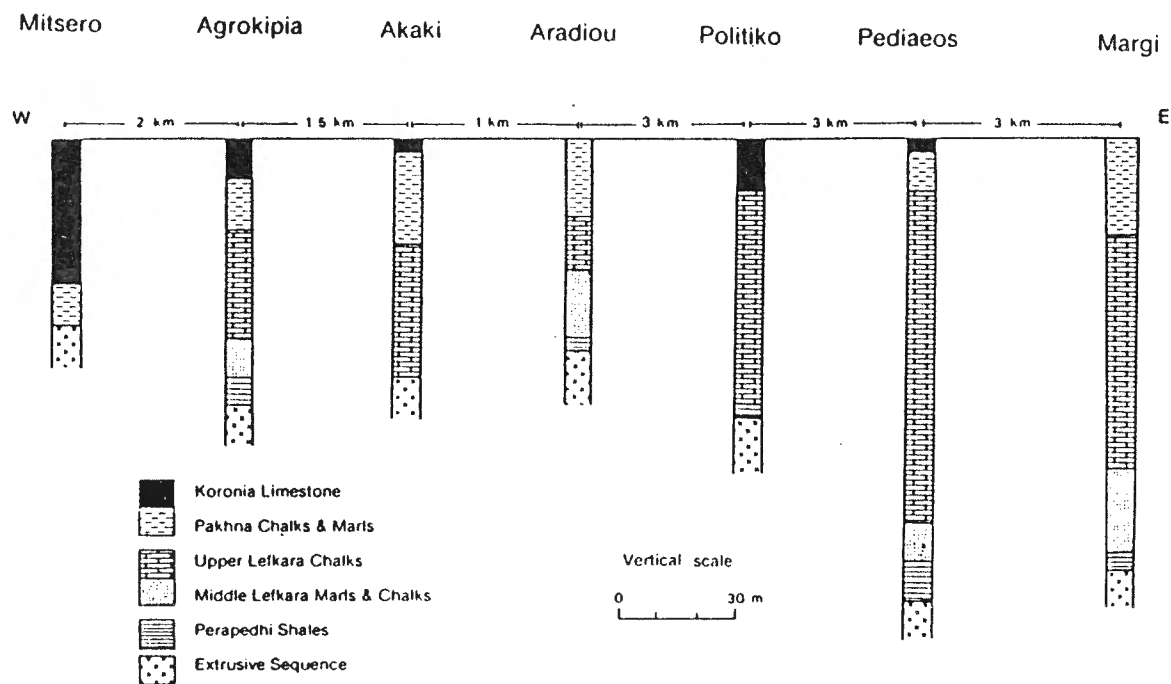
Figure II-5. Comparative sections illustrating the variable thicknesses

of the sedimentary formations in the study area (modified after

Bear 1960). Datum is the base of the Pliocene marls.

Figure II-6. Lithology of the extrusive sequence along the Akaki River
and the locations of the CY-1 and CY-1a drillsites. Inset is a
schematic stratigraphic section which shows the lithologic units of
Schmincke et al. (1983) and the lithostratigraphic units of this
study (modified after Mehegan, unpublished data, 1986 and Schmincke
et al. 1983).
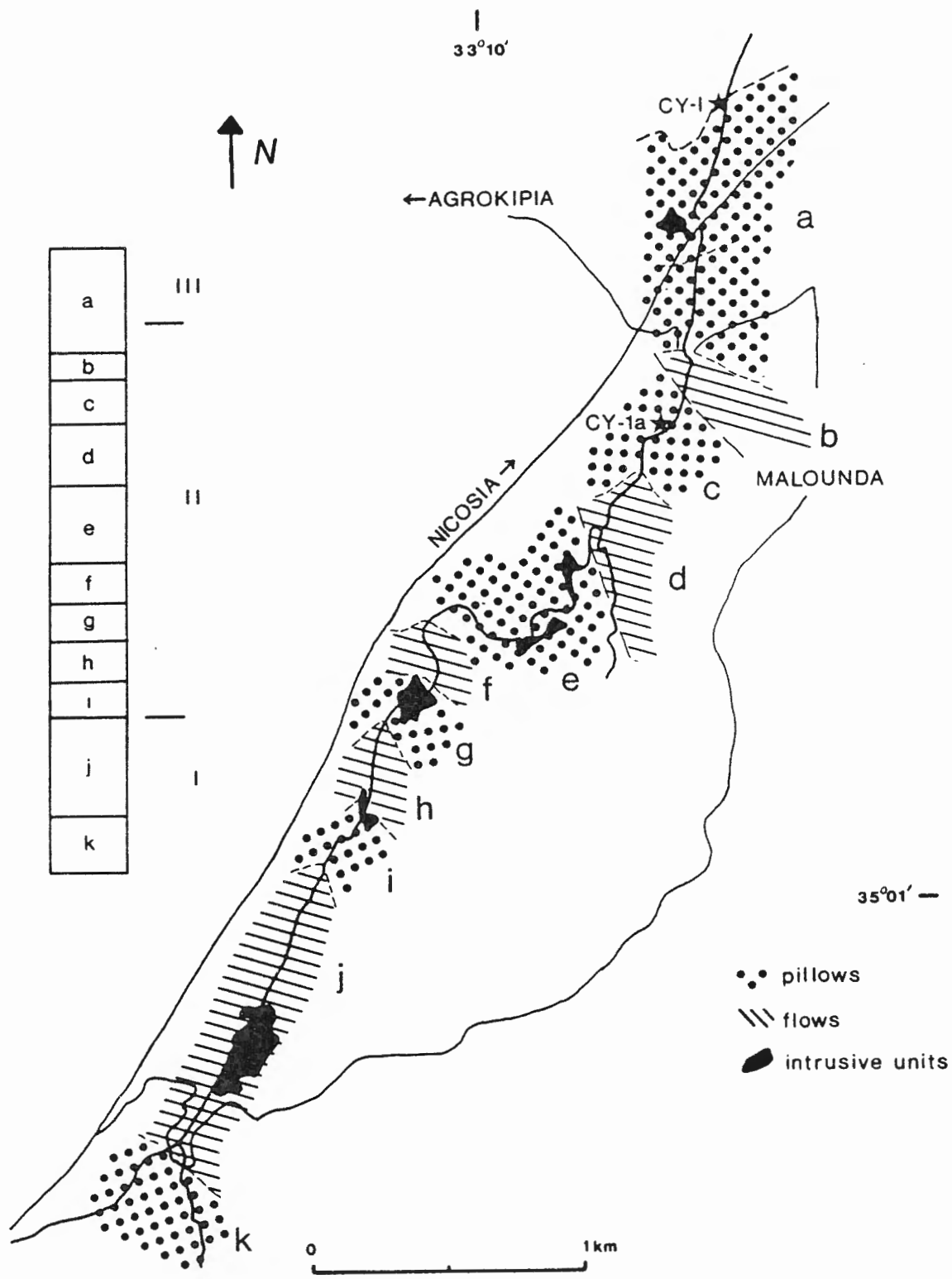
dykes are vertical to near vertical.

The lower 300 m consists of aphyric to sparsely clinopyroxene- and plagioclase-microphyric pillows, flows, and hyaloclastites which belong to Sequence I. Most rocks are grey to greyish-green, alteration is erratic, and fresh glass is commonly preserved.

Sequence II in this area consists of 700-1000 m of dominantly pillows and massive or sheet flows. Towards the base of this section, the abundance of flows and hyaloclastites increases. Overlying the Sequence II rocks are reddish- to yellowish-brown, aphyric to olivine-phyric and picritic pillows and pillow breccias up to 250 m thick which are assigned to Sequence III. The pillow margins in Sequence III are totally altered and interpillow voids are filled with carbonate and clay.

Resistant vertical zones, composed of reddish-grey basalt fragments in a sparry calcite matrix occur throughout Sequences I and II. These zones are 1 - 2 m wide and often have an oxidation halo which extends several meters into the surrounding rock. Schmincke et al. (1983) suggested that they represent syn- to post-volcanic fault zones.

Two holes were drilled in the extrusive sequence in the Akaki River canyon by the ICRDG during the summers of 1982 and 1984. CY-1, spudded in at the lava-sediment interface 1.5 km northwest of Malounda, penetrated the upper 475 m of the sequence (Figure II-6). Thirty lithologic units, which vary in thickness from 5 - 50 m, have been defined (Robinson & Gibson 1983). Pillowed lavas comprise 42%, massive and thin flows 32%, pillow fragment breccias 12%, and intrusions 2% of the recovered core. A few dykes, 5 - 20 cm wide, intrude the section below 350 m and a 1.4-m-wide fault cuts the section at 438.0 m.

The lithologies of CY-1 are similar to the upper 500 m of the Akaki River section (Figure II-7). Reddish-green, olivine- to sparsely olivine-phyric and picritic pillows and breccias comprise the upper 250 m of the section. These Sequence III rocks grade into greenish-grey to grey, aphyric to sparsely olivine-phyric pillows and flows. The boundary between Sequences II and III occurs at 250 m depth.

CY-1a, drilled due west of Malounda to allow for 50-75 m of stratigraphic overlap with the drilled core of CY-1, penetrated 702 m. Thirty lithologic units have been defined that are dominated either by pillows, glassy and crystalline flows, massive flows, or dykes (Figure II-8). Pillows comprise 7.2%, massive and sheet flows 45.5%, undifferentiated flows and dykes 6.6%, dykes 34.2%, and hyaloclastites 5.0% of the recovered core.

The lithologies of CY-1a are similar to those of the lower half of the Akaki River section. Dykes increase in abundance, however, at a shallower depth than in the exposed section. Greyish-green, aphyric to sparsely olivine- and clinopyroxene-phyric pillows and flows comprise the upper 200 m of CY-1a. Aphyric dykes increase in abundance below this depth and interfinger with aphyric to sparsely plagioclase- and clinopyroxene-phyric flows and glassy breccias. The lavas in the upper 350 - 400 m and the dykes throughout the drillcore belong to the high MgO - high SiO_2 suite (Sequence II). Below this depth, the lavas belong to the arc tholeiite suite (Sequence I).

2.3.3 Kambia

A 600-m-thick volcanic sequence is exposed along the Pediaeous River in the Kambia area (Figure II-4). The sequence has been divided

CY-1

depth (m)

f.g. aphyric to oliv-cpx phyric pillows; minor picritic pillows, volcanic breccia, & sediment (Units 1-4)

f.-m.g., massive flows, aphyric to oliv-cpx phyric tops with picritic bases (Unit 5)

f.g. aphyric to oliv-cpx phyric pillows; minor breccia; few dykes (Units 6-8)

f.-m.g. aphyric massive flows (Unit 9)

oliv phyric in upper 10 m; aphyric to sparsely phyric pillows; minor pillow lobe breccia & hyaloclastite (Units 10-12)

f.-m.g. aphyric massive flows; minor interbedded f.g. aphyric pillows; several dykes (Units 13-15)

f.-m.g. aphyric pillows; 2 aphyric dykes (Unit 16)

aphyric massive flows; cut by an oliv phyric and aphyric dyke; minor hyaloclastite (Unit 17-18)

f.g. aphyric pillows; oliv phyric dyke; minor interpillow sediment & breccia (Unit 19)

f.-m.g. aphyric massive and sheet flows; minor aphyric pillows; few aphyric dykes (Units 20-22)

aphyric to sparsely oliv-cpx phyric pillows; minor breccia & hyaloclastite (Units 23-26)

aphyric massive flows & aphyric to sparsely cpx phyric pillows; minor hyaloclastite (Units 27-30)

III

II

Figure II-7. Schematic lithologic column of the CY-1 drillcore. The lithostratigraphic units of this study are marked to the right of the lithologic descriptions (modified after Douma & Robinson 1984).
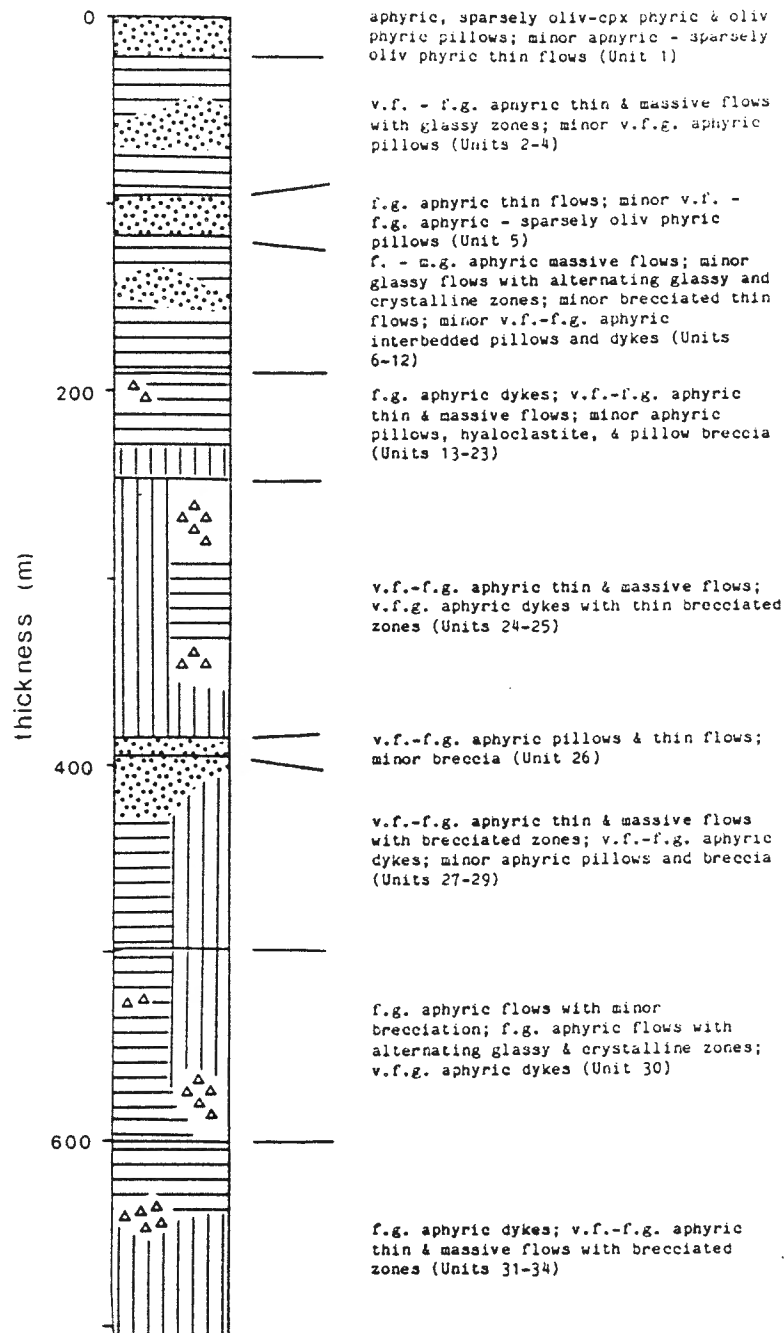
Figure II-8. Schematic lithologic column of the CY-1a drillcore. The lithostratigraphic units of this study are shown to the right of the lithologic descriptions (modified after Horne & Robinson 1986).

into seven major lithologic units, each 20 - 200 m thick (Mehegan, unpublished data, 1986). The lowermost units A-E correspond to Sequence I whereas the overlying units E-G correspond to Sequence III (Figure II-9). Sequence II is absent in this section and the boundary between Sequnces I and III represents the UPL/LPL boundary in the area.

Aphyric to sparsely clinopyroxene- and plagioclase-phyric flows and pillows with minor hyaloclastite comprise Sequence I. Toward the base of this 500-m-thick sequence, dykes become markedly more abundant, increasing from 20% to >90%.

The lavas in Sequence III are overlain locally by umbers of the Perapedhi Formation (Figure II-4) and are not pervasively oxidized. Pillows in the uppermost 2-5 m have grey, crumbly interiors and commonly have well preserved glassy margins. Below this zone, pillows are grey to greyish-green with patchily distributed zones of oxidation. Interpillow umberiferous, yellowish-brown sediment is most abundant towards the lava/sediment boundary.

2.3.4 Kataliondas

South of the village of Analiondas, an isolated block of the Perapedhi Formation overlies lavas which were mapped previously as LPL (Figure II-4). Recent investigation has indicated that these rocks belong to the high MgO - high SiO_2 suite (Mehegan, unpublished data, 1984) and the lack of olivine suggests that they belong to Sequence II.

Immediately below the umbers there is a 5-m-thick unit of grey to greyish-green, aphyric pillows. A thin breccia zone, containing basalt fragments in a hematite-smectite matrix, is interbedded between the pillowed unit and underlying green to brown massive and thin flows.
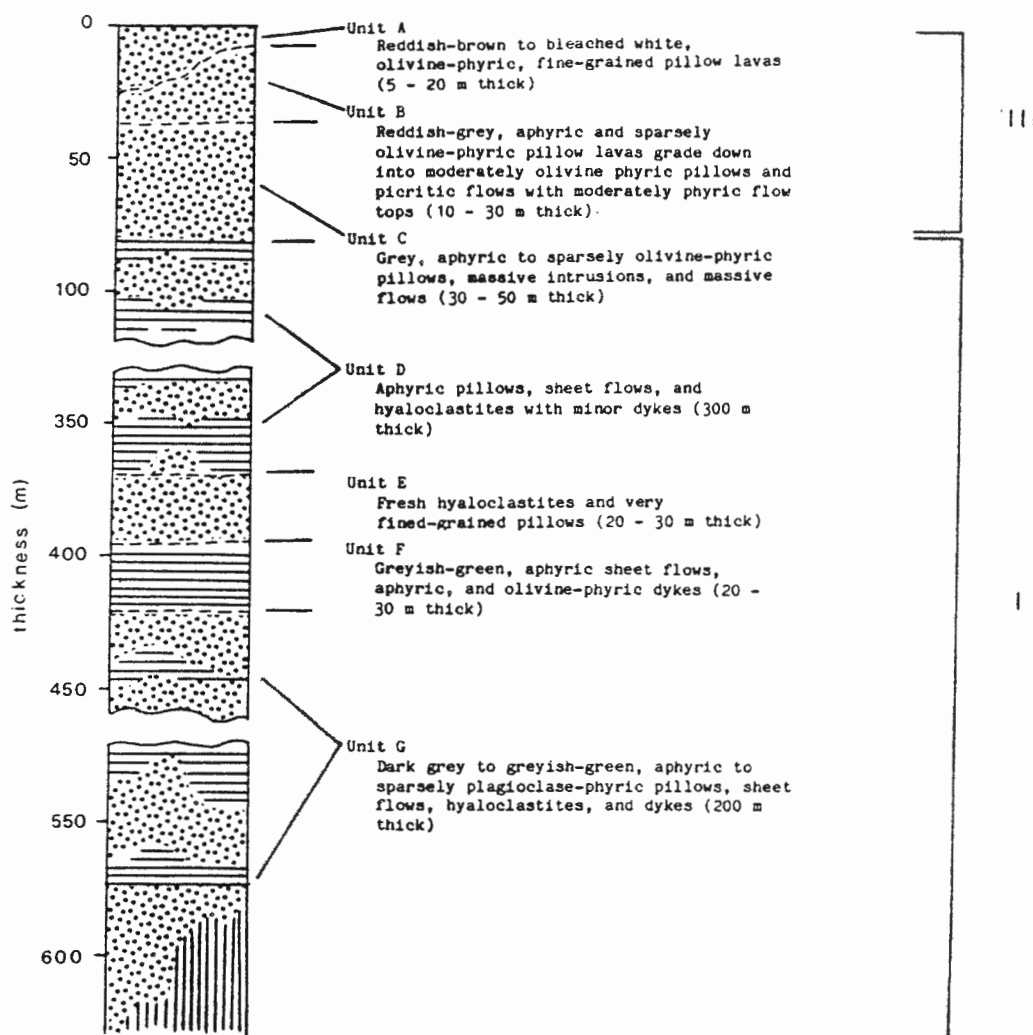
Figure II-9. Schematic lithologic column of the extrusive sequence along the easternmost tributary of the Pediaeos River. The regional lithostratigraphic sequences of this study are outlined to the right of the lithologic descriptions (after Mehegan, unpublished data, 1985).

Fresh glass occurs along flow margins in the lower flow unit but none was observed within the pillow unit. Yellowish-brown, umberiferous sediment locally fills interpillow voids towards the top of the section.

A few vuggy zones, with basalt fragments in a sparry calcite matrix, cross-cut the lavas.

2.3.5 Margi

South and west of the village of Margi there are excellent exposures of the extrusive sequence in fault contact with the overlying Perapedhi and Lefkara Formations (Figure II-5). An area of 4 km^2 containing a 350-m-thick stratigraphic sequence (Bailey 1984) was studied in detail and reconnaissance mapping was carried out in the neighbouring areas.

The volcanic sequence has been subdivided into 3 lithostratigraphic units by Bailey (1984) of which the two upper units belong to Sequence III (Figure II-10). The lower unit corresponds to Sequence I and is separated from the overlying units by a 10-30-cm-thick horizon of umberiferous sediment. This horizon is present throughout the eastern portion of the study area (Boyle & Robertson 1983; L. Lewczuk, pers. comm., 1985).

The Sequence I lavas are chiefly dark brown to grey aphyric to sparsely clinopyroxene- and plagioclase-phyric pillows and massive and sheet flows which are locally separated by <1-m-thick, discontinuous hyaloclastite layers.

Aphyric and olivine-phyric pillows and thin flows comprise the overlying units which belong to Sequence III. Fresh glassy margins are locally preserved where the lavas are directly overlain by the umbers

Chalks

Umbers/Cherts

Unit III
  A. Aphyric pillows and thin flows
  B. sparsely olivine phyric pillows
     and flows

Unit II
  A. Crystalline olivine phyric pillows
     and thin flows
  B. Glassy olivine phyric pillows
  C. Picritic pillows
  D. Picritic-based flows
  E. Aphyric massive flows
  F. Olivine microphyric flows
  G. Clinopyroxene microphyric flows

Unit I
  Aphyric and
  plagioclase-clinopyroxene-phyric pillows
  and flows

Figure II-10. Schematic lithologic column of the Margi area. The regional lithostratigraphic sequences of this study are outlined to the right of the lithologic descriptions (modified after Bailey 1984).

of the Perapedhi Formation. The underlying 175-m-thick sequence is dominated by olivine-phyric pillows and thin flows which vary in form and modal mineralogy. Other minor lithologies are: olivine-phyric pillows, picritic pillows, thick flows with picritic bases, aphyric massive flows, clinopyroxene-phyric flows, and <1-m-thick hyaloclastite layers (Bailey 1984). Sequence III in the Margi area is unusual in its high abundance of fresh picritic pillows and flows.

2.4 LITHOLOGIC FEATURES

The extrusive sequence of the Troodos ophiolite consists largely of pillowed lavas, sheet, thin and massive flows with lesser amounts of breccias and hyaloclastites. These rocks are cut by dykes, sills, and irregular intrusions.

Round to ellipsoid pillows, 0.3-1.0 m in diameter, comprise the bulk of the extrusive sequence. Most pillows have subradial cooling fractures and spherical vesicles, which occupy 1-5% by volume and are generally concentrated in the pillow tops. Variably altered glassy rinds, 1-5 cm thick, commonly are present. Large irregular to rounded pillows up to 3 m in diameter usually have well developed radial columnar jointing. These "megapillows" often interfinger with or form at the base of more typical pillow piles and may be feeder tubes (Rautenschlein, unpublished report, 1983).

Massive flows, generally 2-5 m thick but up to 15 m thick, vary laterally in thickness and may be traced up to 200 m along strike. Flow tops are marked by brecciated, glassy zones, 2 to 20 cm thick, which often contain elongate vugs 1-10 cm in diameter. Most basal contacts display narrow chilled margins which grade upward into a zone with

spherical and/or pipe vesicles (Schmincke et al. 1983). In the Margi area, flows up to 30 m thick are common in Sequence III. These flows commonly have picritic bases which grade upward into aphyric flow interiors and olivine-phyric flow tops (Bailey 1984). Thin flows, less than 2 m thick, are interbedded with pillows and massive flows. Columnar joints grade upward into finer-grained rubbly zones which in turn grade into a narrow chilled margins that are commonly brecciated. This rubbly zone is often poorly developed. Sheet flows, less than 0.5 m thick, are also common.

Breccias are common throughout the entire volcanic pile. In Sequence I, pillow breccias with spherical minipillows and angular, chilled fragments set in a lapilli size glassy matrix are often interbedded with sheet flows and pillowed units (Schmincke et al. 1983). In the overlying sequences, pillow fragment breccias which contain lenticular fragments with a few chilled margins in a clay-carbonate or umberiferous matrix, overlie heavily veined and fractured pillows.

Layers of hyaloclastite which are generally <1 m but up to 5 m thick form discontinuous layers between sheet flows. Most hyaloclastites are fresh with glass spalls embedded in a matrix of altered glass and basalt fragments.

Medium- to coarse-grained sills are generally parallel to the regional dip and have well developed columnar joints. These 1- to 5-m-thick intrusive units are most abundant in Sequences I and II. Dykes generally range from 0.1 to 2 m in width and are vertical to subvertical with a sinuous strike. They are massive, although some display columnar jointing. Where present, vesicles and vugs are elongate parallel to the margins.

CHAPTER III

DEFINITION AND DISTRIBUTION OF ALTERATION ZONES

3.1   INTRODUCTION

Rocks of the extrusive sequence and the upper portion of the sheeted dyke complex have a complex alteration history. Lateral and vertical variation in both the intensity and style of alteration on the scale of metres to hundreds of metres makes the task of concise description difficult. For simplicity, six alteration zones have been defined and mapped. No genetic interpretation is implied by these zones. Each zone is merely a mappable unit which has a uniform field appearance and consistent secondary mineral assemblages.

In the following sections, each alteration zone is defined and its distribution in the study area is described. The zones are then compared to alteration and metamorphic zones which have been outlined for "in situ" oceanic crust and other ophiolites.

3.2   DEFINITION OF ALTERATION ZONES

The distribution of secondary minerals in the study area was mapped and representative samples of these phases, carefully collected with respect to their stratigraphic position, were identified using petrographic and x-ray diffraction techniques (Appendices I & II). Alteration zones were then defined on the basis of field appearance and consistent assemblages of secondary minerals (Figures III-1 to III-4). Each zone, listed below, was named for its typical secondary mineral assemblage.

38

Figure III-1. Distribution of secondary minerals in the Akaki River

section. The small dots represent units dominated by pillows,

horizontal lines represent units dominated by massive and thin

flows. Vertical solid lines indicate that the secondary phase is

found throughout the unit and dashed lines indicate that it is

locally present.
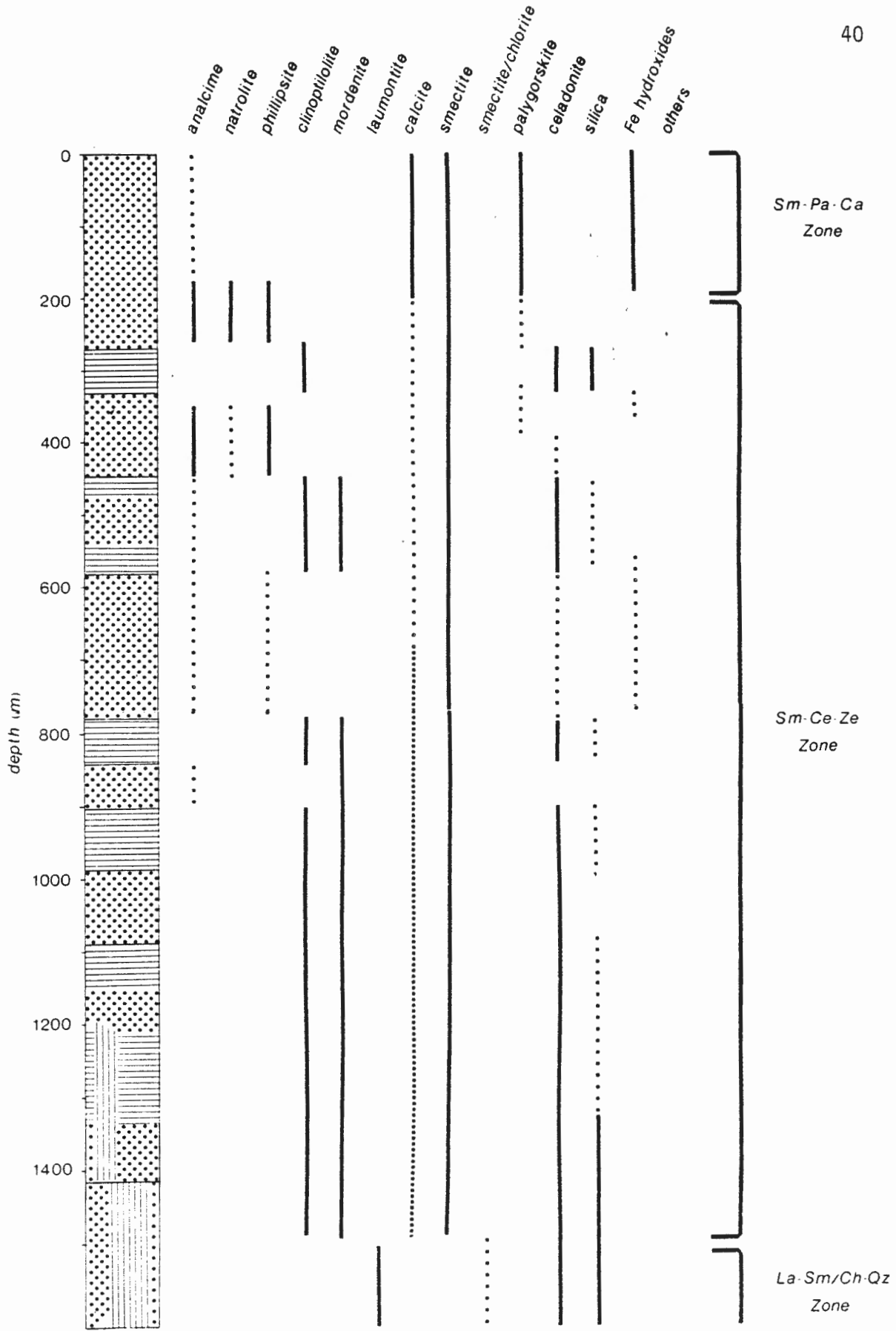
Figure III-2. Distribution of secondary minerals in the CY-1 and CY-1a

drillcores. Symbols as in Figure III-1. Vertical lines represent

units dominated by dykes, triangles represent units dominanted by

breccias or hyaloclastites.

42
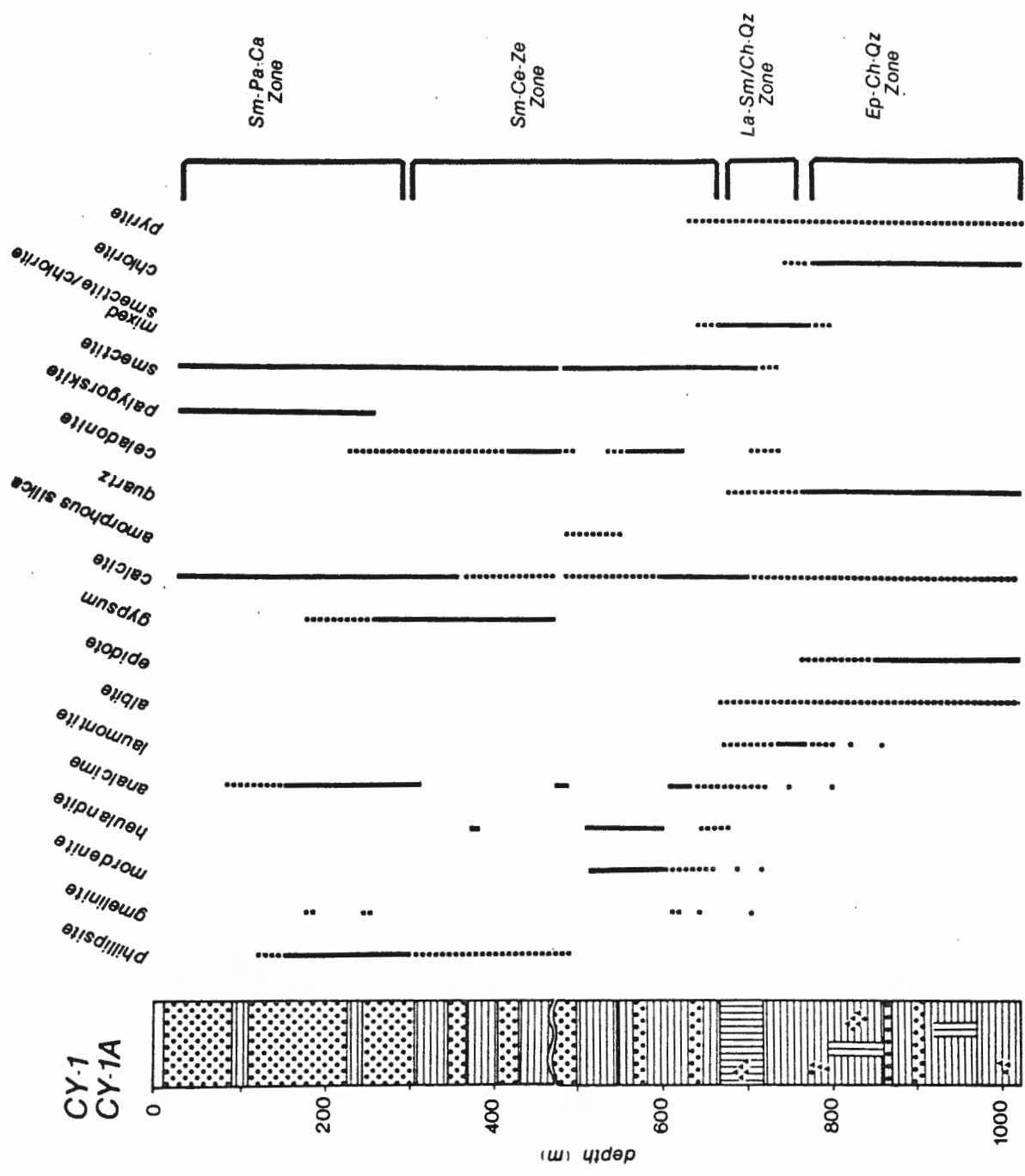
Figure III-3. Distribution of secondary minerals in the Pediaeos River

section. Symbols as in Figure III-1. Others: ch=chabazite,

na=natrolite; go=gossan
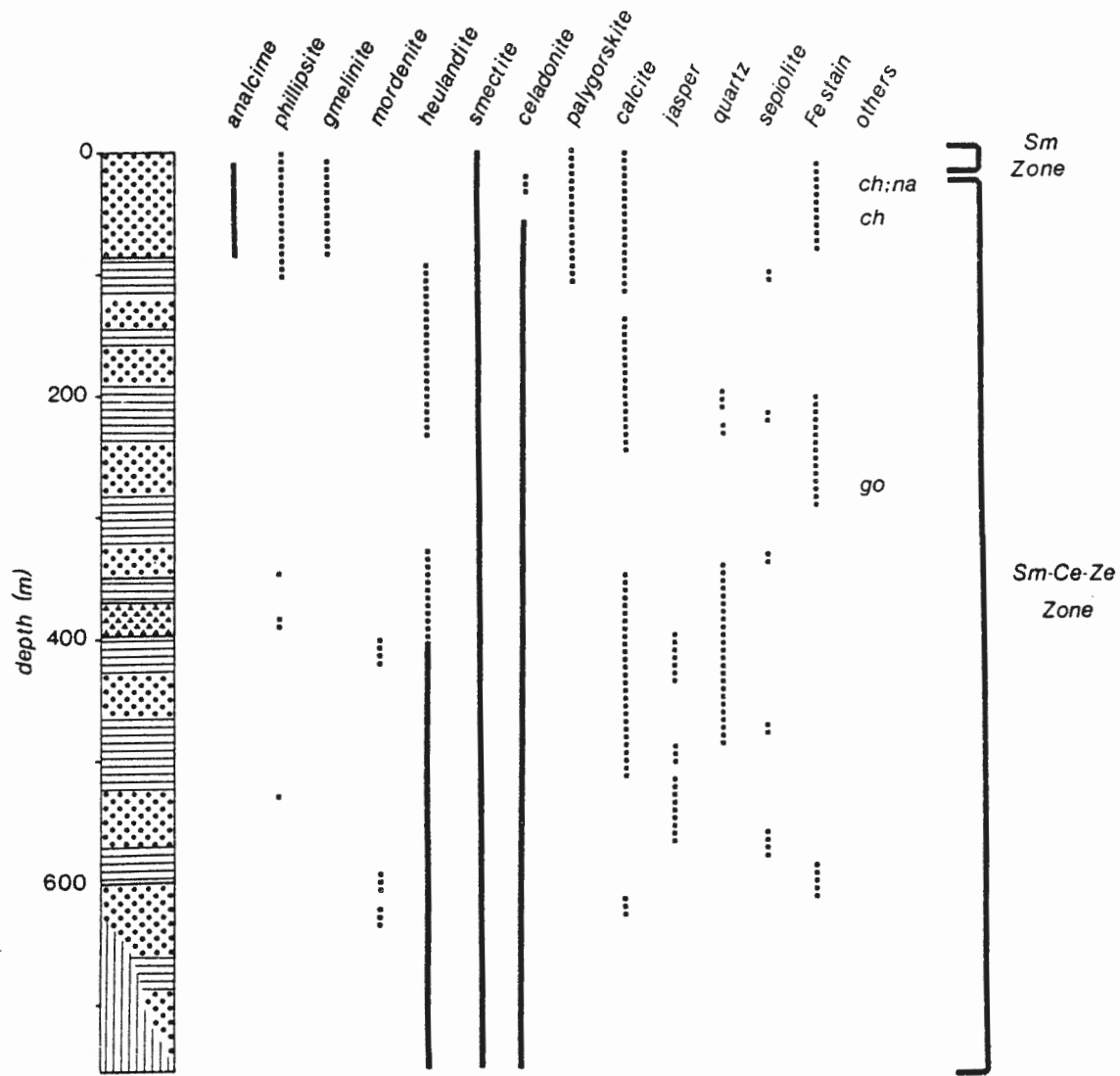
Figure III-4. Distribution of secondary minerals in the Margi area. Symbols as in Figure III-1. V represents units dominated by picritic pillows and flows. Others: ph=phillipsite, py=pyrolusite (present study, Bailey 1984).
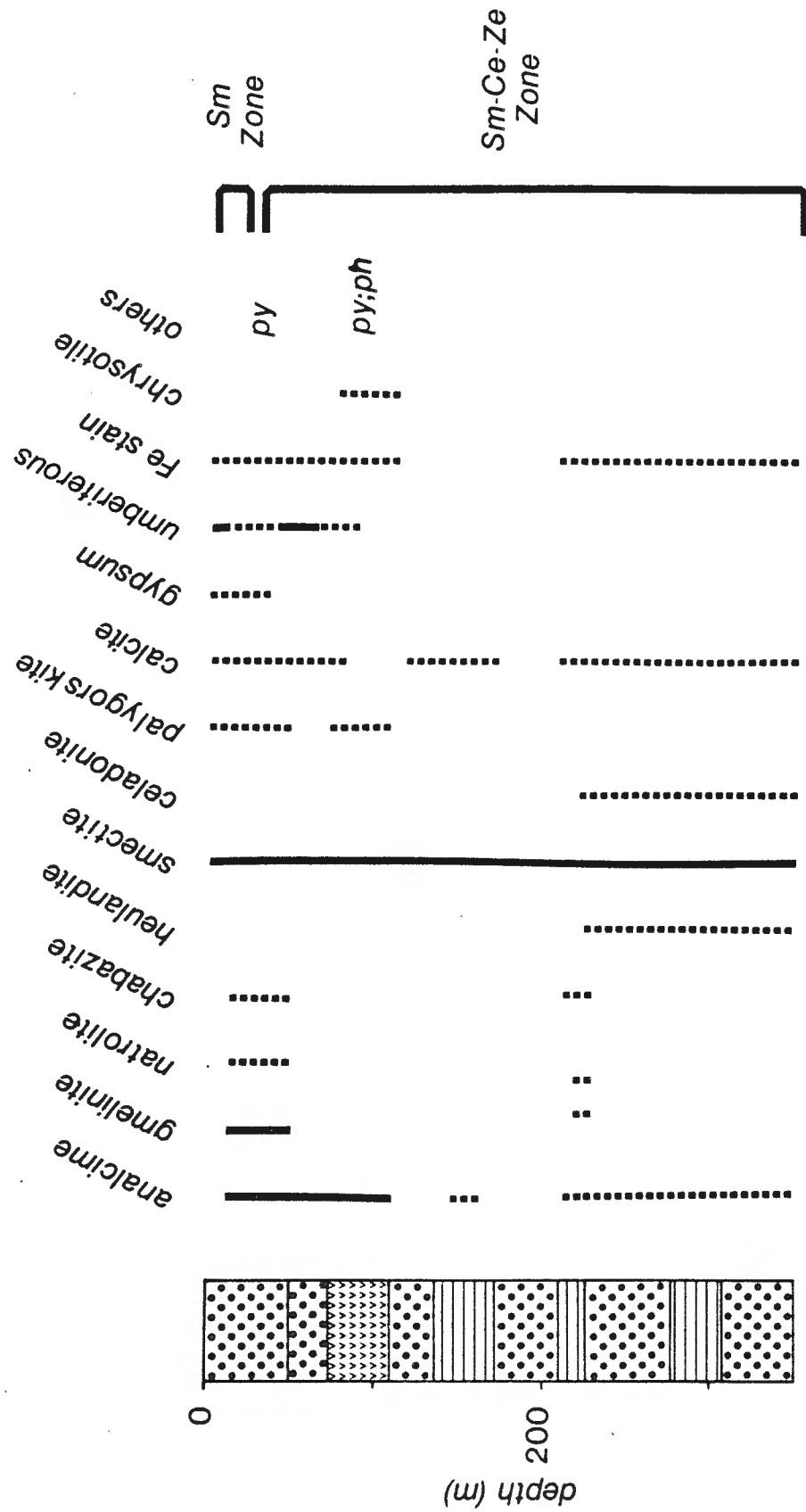
Sm
Zone

Sm-Ce-Ze
Zone

py

py;ph

others
chrysotile
Fe stain
umberiferous
gypsum
calcite
palygorskite
celadonite
smectite
heulandite
chabazite
natrolite
gmelinite
analcime

depth (m)

0

200

1. Smectite–Palygorskite–Calcite Zone (Sm–Pa–Ca Zone)

2. Smectite Zone (Sm Zone)

3. Smectite–Celadonite–Zeolite Zone (Sm–Ce–Ze Zone)

4. Laumontite–Smectite/Chlorite–Quartz Zone (La–Sm/Ch–Qz Zone)

5. Epidote–Chlorite–Quartz Zone (Ep–Ch–Qz Zone)

6. Sulfide–Chlorite–Quartz Zone (Su–Ch–Qz Zone)

Although minerals in these assemblages are abundant throughout each zone, they are not necessarily restricted to a particular zone. For example, palygorskite occurs in the Sm–Pa–Ca Zone as well as the Sm–Ce–Ze Zone. Within the former zone, however, it is ubiquitous whereas in the latter zone it only occurs sporadically. Because the secondary minerals were deposited sequentially, they do not represent equilibrium assemblages and should therefore not be considered metamorphic zones.

The field characteristics, alteration mineralogies, and depositional sequences of the secondary minerals in each of the alteration zones are described in the following section. The order in which these zones are presented generally reflects their stratigraphic position, starting at the top of the sequence. The boundaries between the zones are usually distinct, but are gradational in some areas. They also vary laterally and should not be interpreted as being depth–controlled. The spatial relationships within the field area are fully discussed in a subsequent section of the chapter.

3.2.1 Sm–Pa–Ca Zone

The Smectite–Palygorskite–Calcite Zone (Sm–Pa–Ca Zone) is characterized in the field by its red "oxidized" appearance, its

pervasive alteration, and the abundance of interpillow sediment. This zone is directly overlain by the marls and chalks of the Middle to Upper Lefkara Formation and is contained within lava Sequence III. Its lower boundary is generally sharp and lies between 50 - 250 m depth. In some locations, however, the transition from reddish-green, pervasively altered pillows into less pervasively altered greyish-green rocks is gradational over tens of metres. The lateral boundary of this zone with the Smectite Zone is sharp.

The rocks of this zone are chiefly pillowed lavas and breccias. Thick glassy margins are pervasively altered to green smectite and zeolites. Round to irregular glass spalls, elongate parallel to pillow margins, generally contain spherical phillipsite granules, and perlitic cracks are filled with phillipsite. These palagonitized spalls are contained within a green smectite-phillipsite-calcite-palygorskite matrix which is commonly stained with Fe oxide. Yellowish-brown, fine-grained pillow margins, 0.5 - 1.0 cm thick, are highly altered and crumbly. They grade into greyish-green to greenish-grey pillow interiors which are variably altered (Plate III-1A).

Pillow fragments and mini-pillows in breccia units have alteration assemblages similar to the coherent pillows (Plate III-1B). The matrix consists of hyaloclastite altered to bright green smectite, phillipsite, and analcime, and late-stage calcite and palygorskite. Autobrecciated flow tops are altered to the same assemblage as pillow margins although the color zonation is not as pronounced.

Alteration of the primary minerals in this zone is summarized in Table III-1. A box-like framework of goethite, whose interstices are filled with calcite, totally replaces olivine phenocrysts whereas red to

Plate III-1 A. Typical field appearance of the Sm-Pa-Ca Zone. Note iron

stained fracture surfaces, yellowish-brown chilled margins, and

greyish-green interiors. B. Close-up of pillow margins and

interpillow breccia. Matrix is composed of palygorskite + calcite.

Note the reddish-brown pseudomorphs after olivine in the left of

the photo. Photos taken in the Akaki River section.

TABLE III-1 SUMMARY OF PRIMARY MINERAL ALTERATION

Alteration Zone	Phenocrysts	Groundmass	Glassy Margins
Sm-Pa-Ca	oliv → goethite + calc (T) cpx → smec (F-M) spinel (F)	cpx → smec (S) plag → smec (S-M) plag → K-spar (T) Ti-mag → maghemite (S-M) mesostasis → smec, calc(M-T)	smec ± phil (T)
Sm	oliv → goethite + tr calc (T) cpx → smec (F-M) Ti-mag → maghemite (F-S)	cpx → smec (F-M) plag → smec (S-M) Ti-mag → maghemite (F-S) mesostasis → smec (T)	smec (S-T)
Sm-Ce-Ze	oliv → goethite + calc (T) oliv → serpentine* (S-T) cpx → smec (F-S) plag → smec, calc, celad (F-M) spinel (F) Ti-mag	cpx → smec (S-M) plag → smec, calc, celad (S-M) Ti-mag → maghemite (S-M) mesostasis → smec, celad, calc (M-T)	pillows: smec ± phil ± anal (S-T) flows: smec ± celad ± heul (S-T) hyal: smec ± phil ± heul (S-T)
La-Sm/Ch-Qz	cpx → smec, smec/chl (S-M) plag → albite (T) oxides	plag → smec (M) plag → albite, K-spar (T) cpx → smec, smec/chl (S-M) Ti-mag mesostasis → smec, smec/chl qtz, pyrite	smec + smectite/chlorite ± laum (S-T)
Ep-Ch-Qz	cpx → chl (S-M) plag → albite (T) plag → calc, epi, chl (M-T)	cpx → chl (S-M) plag → albite (T) plag → epi + chl (M-T) Ti-mag → sphene (S-M) mesostasis → chl, qtz, epi, pyrite	chl + qtz ± epi (S-T)

* occurs in picritic units in the Margi area; F fresh, S slightly altered, M moderately altered, T totally altered; oliv=olivine, cpx=clinopyroxene, plag=plagioclase, Ti-mag=titanomagnetite, smec=smectite, calc=calcite, anal=analcime, phil=phillipsite, celad=celadonite, laum=laumontite, chl=chlorite, smec/chl=mixed layer smectite/chlorite, epi=epidote, qtz=quartz

opaque spinel inclusions remain fresh. Clinopyroxene is partly altered along grain boundaries and fractures to smectite. Red staining adjacent to titanomagnetite indicates that the opaque minerals have expelled iron and are cation deficient (Hall et al. in press).

Original groundmass textures are preserved but may be obscured by the reddish-brown, fibrous to amorphous smectite which replaces the mesostasis. Plagioclase microlites commonly have a cloudy appearance and are partially replaced by smectite.

Reddish-brown segregation vesicles give the rocks their spotty appearance. The mesostasis within the segregation vesicles is extensively altered to reddish-brown smectite whereas variolitic plagioclase is only partially altered. Spherical voids within the segregation vesicles are commonly filled with calcite although many remain open.

Radial fractures within pillows are generally lined with pale green smectite and filled with smectite, calcite, and palygorskite, in varying proportions. Fracture surfaces and fillings are commonly stained with Fe oxide. Analcime and rare adularia locally fill fractures, which were re-opened and filled with calcite.

Two stages of crack and fracture filling have been recognised in the rocks of this zone. During the first stage, several generations of secondary minerals were deposited. Cross-cutting relations of veins and depositional sequences within filled voids, observed on a hand specimen scale, allow the following generalizations to be made:

1. Smectite, mixed with Fe-rich phases, was the first phase to form - it lines vesicles, vugs, cracks, and fractures.

2. Where present, zeolites and adularia commonly line voids and project

inward towards open cavities. In many cases these minerals fill the remaining space and are mixed with calcite.

3. Several generations of calcite deposition occurred, with later veins cross-cutting or re-opening earlier ones (Figure III-5). Successive layers of euhedral crystals, mantled by a light dusting of smectite, indicate several stages of growth.

Composite veins of buff to white palygorskite and calcite, commonly containing thin zeolite-rich zones, were deposited during the latest stage of crack and fracture filling (Figure III-6). In outcrop, they form vertical to near-vertical veins which cross-cut and bend around individual pillows and fill interstices. On a hand specimen scale, these late veins cut across and re-open the earlier veins (Table III-2).

3.2.2 Smectite Zone

The Smectite Zone (Sm Zone) is restricted to the extrusive sequence immediately below the umbers of the Perapedhi Formation. Pillows in this zone typically have crumbly grey interiors and fresh glassy margins. It is only within this zone that fresh glass is preserved so close to the sediment/lava boundary. Although the pervasiveness of alteration is similar to that in the Sm-Pa-Ca Zone, rocks of the Sm Zone are not pervasively oxidized. The thickness of the Sm Zone varies from a few metres to tens of metres.

Preservation of glassy pillow rinds is common throughout the Sm Zone although cracks and surfaces are partially altered to smectite (Plates III-2 & III-3). Hyaloclastite matrices in brecciated zones underlying the umbers are totally altered to smectite with minor

Figure III-5. A. Calcite stringers with inclusions of basalt fragments
crosscut chilled pillow margin (Sample CY-1:58.50 m). B. Two
generations of calcite veining crosscut a pillow margin (Sample
CY-1:180.85 m). Abbreviations as in Table III-1.

A.

B.

green smec
brown zone
calc
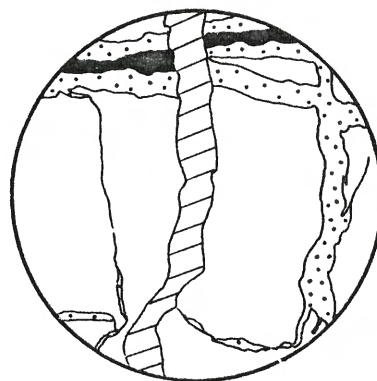
calc
pink calc
yellow calc

0 1 2 3 cm

Figure III-6. A. A late-stage, 1.0 - 1.5 cm thick palygorskite + calcite vein cross-cuts a heterolithic breccia. Glass spalls and basalt fragments are in a calcite + smectite matrix (Sample CY-1:25.95 m). B. A composite vein with a palygorskite + calcite rim and a pink zeolite + calcite centre crosscuts an earlier analcime + calcite vein system (Sample CY-1:104.70 m).

Abbreviations as in Table III-1.

A.
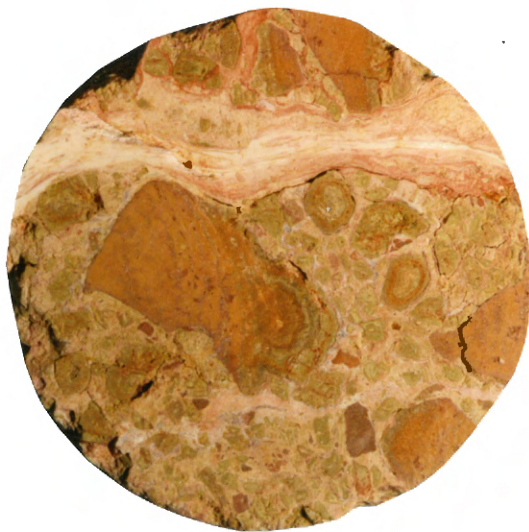
paly + calc

calc + minor smec

B.
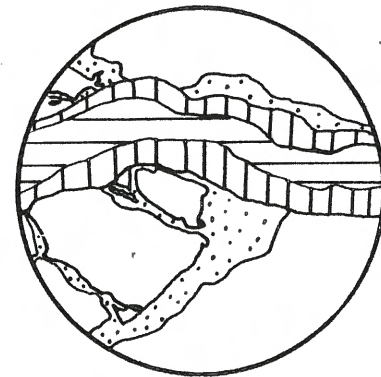
0   1   2   3 cm

anal + calc

paly + calc

calc + anal +
chab + trace phil

57

TABLE III-2   SUMMARY OF VEIN DEPOSITION IN THE Sm-Pa-Ca ZONE OF CY-1

DEPTH (m)	LITHOLOGY	VEIN SETS [*] Early	Late
25.95	heterolithic breccia	smec → smec + calc → calc	paly + calc
76.10	spars. ol phyric lower pillow margin	1. smec → calc + minor phil 2. smec → phil + minor calc 3. smec → calc + phil + smec	
102.9	centre spars ol-cpx phyric flow	yellow calc → milky calc	1. anal + calc + tr phil 2. anal + calc + chab
104.7	centre spars ol-cpx phyric flow	calc	paly + calc + minor anal anal + chab + calc + phil
112.0	spars ol-cpx phyric flow top	smec → calc 1-2 mm thick smec rich halo	
141.52	upper aphyric pillow margin	1. clear to milky calcite 2. green smec → calc + smec 3. Fe oxide + smec	
180.85	spars ol phyric lower pillow margin	clear calc → pink calc	yellowish brown calc

[*] order of deposition is listed from rim to centre; numbers indicate oldest to youngest veins; phil=phillipsite, anal=analcime, calc=calcite, chab=chabazite, paly=palygorskite, smec=smectite.

Plate III-2 Lava-Perapedhi Formation boundary along the easternmost

    tributary of the Pediaeos River. The umbers accumulated in small

    hollows. Note the preservation of fresh glassy rinds on grey,

    highly altered pillows.

Plate III-3. Example of the typical lithologies and alteration beneath

   fault-bounded umber deposits. Exposed section is located midway

   between the villages of Kambia and Analiondas. Grey pillows on the

   left hand side of the plate are underlain by, and in fault contact

   with, breccia.

heulandite and/or phillipsite. Vesicles in both breccia fragments and coherent pillows are partially filled with fibrous green smectite. Calcite-filled vesicles are locally present.

Yellowish-brown to dark brown umberiferous sediment, white to buff palygorskite, and calcite-rich sediment locally fill interpillow voids, form discrete horizons within the lava pile, or cross-cut the pillow pile in vertical to near vertical veins. These veins generally terminate within the lower half of the umber layer.

Alteration of olivine differs in this zone from that in the Sm-Pa-Ca Zone, as the interstices of the goethite framework are open. The groundmass adjacent to titanomagnetite lacks Fe-staining which suggests that the opaque mineral is only slightly altered to maghemite (B. Fisher, pers. comm., 1986). Groundmass textures are preserved and smectite totally replaces the mesostasis.

3.2.3 Smectite-Celadonite-Zeolite Zone

The Smectite-Celadonite-Zeolite Zone (Sm-Ce-Ze Zone) dominates the extrusive sequence and the upper portion of the Basal Group. Greyish-green to greenish-brown lavas are less pervasively altered than in the Sm-Pa-Ca and Sm Zones. This zone is characterized by significant variations in the intensity of alteration between, and within, individual lithologic units, distinctive assemblages of secondary minerals for each of the main cooling-unit types, and random preservation of fresh glass.

Greyish-green to greyish-brown pillows and pillow breccias generally lack the pronounced color zonation within pillow margins and along fractures seen in the Sm-Pa-Ca Zone. Chilled margins are pale

green where the pillows are highly altered, whereas the margins of relatively fresh pillows are dark green to black. Glassy margins are altered to smectite $\pm$ phillipsite $\pm$ analcime. Where both zeolites are present, phillipsite is the earliest phase to form (Plate III-4A). Interpillow sediment, variably altered hyaloclastite, or breccia fill the pillow interstices.

Smectite-lined vesicles are partly to totally filled with calcite, smectite, and/or mixtures of one or more zeolites. Where more than one of these phases is present, zeolites extend inwards from the vesicle walls and calcite or smectite fills the interior. Within a single pillow, individual vesicles may be filled with calcite and zeolites whereas others remain open.

Radial fractures are lined with smectite and are locally filled with smectite, calcite, and assemblages of analcime, phillipsite, chabazite, gmelinite, and natrolite, in varying proportions (Plate III-4B). Where pillows are adjacent to sills, dykes or massive flows, celadonite and, rarely, heulandite may line fracture surfaces.

Hyaloclastites are variably altered to smectite and heulandite with minor celadonite and rare phillipsite. Where associated with heulandite, phillipsite is the earliest zeolite to form. Narrow zeolite and sepiolite stringers form irregular networks within hyaloclastite units.

The degree of alteration within the massive and sheet flows is quite variable. Most flows are relatively fresh with minor surficial celadonite and/or hematite staining (Plate III-5A). Zones of intense alteration locally occur along flow margins and to a lesser extent along joint surfaces. These zones consist of celadonite mixed with

Plate III-4. Typical mineral assemblages in pillowed lavas of the Sm-Ce-Ze Zone. A. Pillow margins and interpillow breccias are altered to phillipsite (P), analcime (A), and smectite. B. Radial fractures are lined with clay and filled with analcime. Photos taken in the Akaki River section.

A
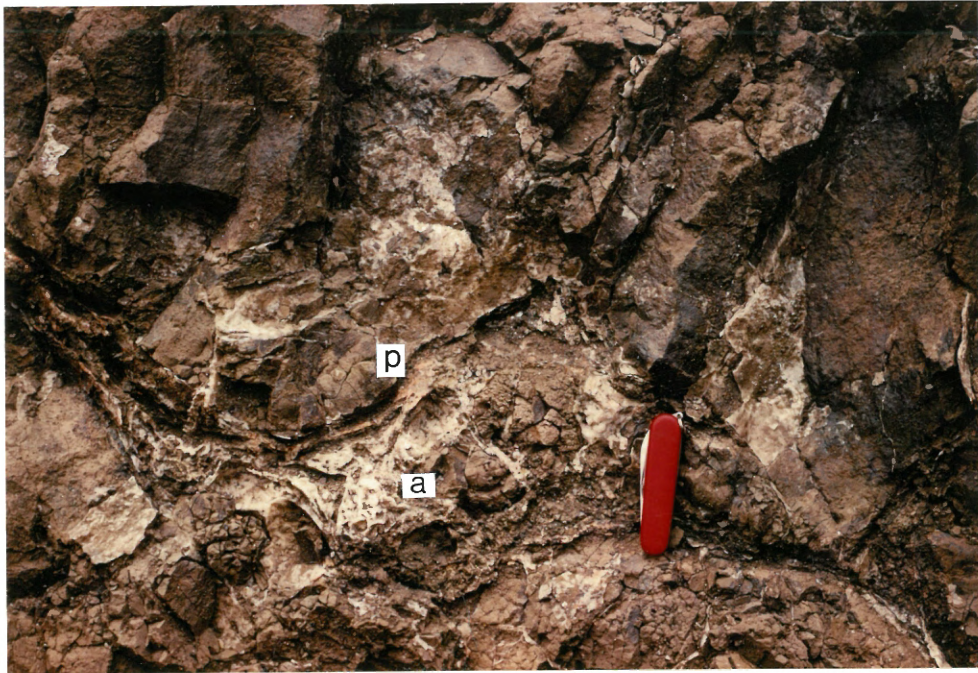
B

Plate III-5. Typical mineral assemblages in massive and thin flows of

the Sm-Ce-Ze Zone. A. Celadonite stained massive flow. Note that

the margins are more highly altered than the interiors. Photo

taken in the Pediaeos River section. B. Celadonitized flow margin

contains celadonite with lesser smectite, heulandite, mordenite,

and calcite (Sample CY-1a:49.80 m).

A

B

CY-1a   49.80 m

0   5   10 cm
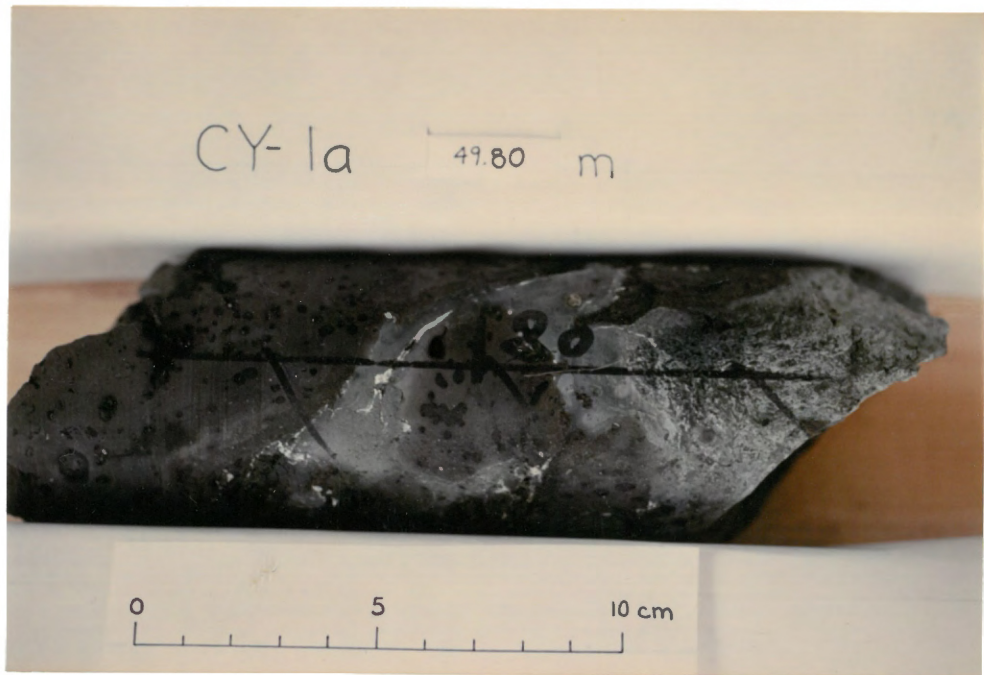
heulandite, mordenite and calcite (Plate III-5B) and may contain massive jasper nodules.

Brecciated flow tops are variably altered to smectite, celadonite, heulandite, mordenite, and chalcedony (Plate III-6). Where heulandite and mordenite occur together, heulandite clusters radiate outward from a clay-lined surface and are overlain by mordenite. Jasper-rich flow tops are common in Sequence I lavas, especially in the eastern part of the study area. Mordenite, quartz, opal, and goethite are the typical mineral assemblage in these cm- to tens of cm-thick zones.

Ovoid, clay-lined vugs are open or partially filled with the celadonite-zeolite assemblage described above, chalcedonic silica, or calcite rhombs. Smectite, celadonite, single zeolite phases, or calcite totally or partially fill clay-lined spherical and pipe vesicles.

Joint surfaces of flows, lined with mixtures of celadonite and smectite, are thinly coated with platy-brown sepiolite, calcite rhombs, or rarely bluish-white opal or pyrite. Hematite locally stains fracture surfaces and penetrates inward along flow margins which haven't been "celadonitized". The irregularity of the stain in Figure III-7 suggests that the staining is not strictly fracture- or surface-controlled. Concentric clay and Fe-oxide rich rings are generally parallel to the outer 3 - 10 cm of columnar joints. These rings are 2 - 3 mm wide and are spaced 5 - 20 mm apart. Alteration of the groundmass is more pervasive within these rings.

Discontinuous stringers of smectite and celadonite, with or without zeolite or calcite, form within individual flow units. In some cases these stringers appear to replace aphanitic or glassy patches

Plate III-6. Brecciated flow top is altered to celadonite, smectite, heulandite, and mordenite. Note that the glassy rind is only partially altered. (Sample CY-1a:31.30 m).

CY-1a   31.30   m

0   5   10 cm
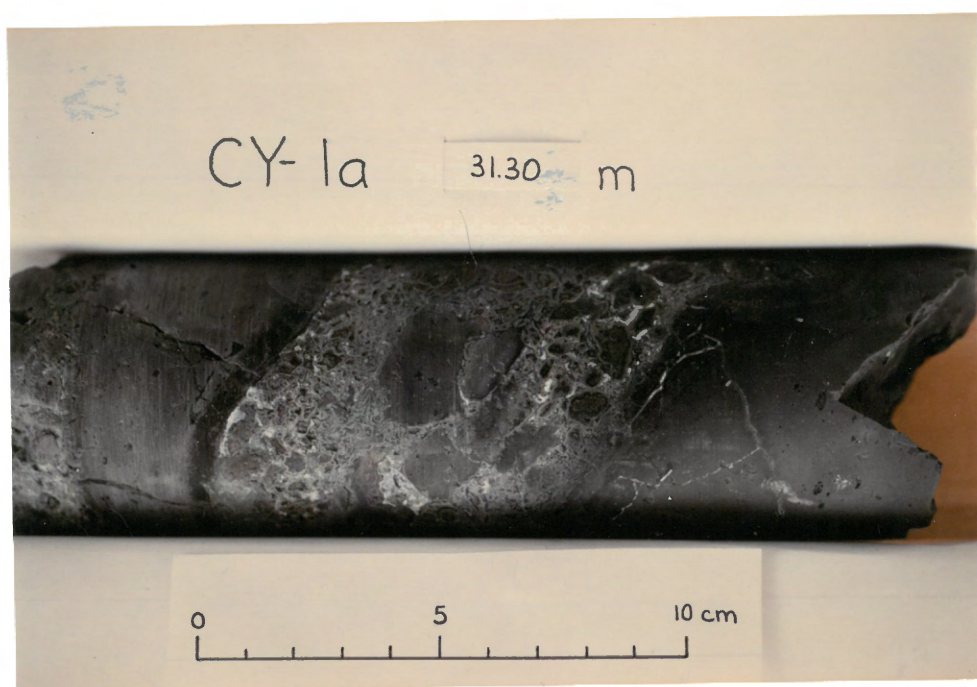
Figure III-7. A dark red, 1 - 2 mm thick line marks the inner edge of a
hematite-stained lower flow boundary (Sample CY-1:387.42 m).
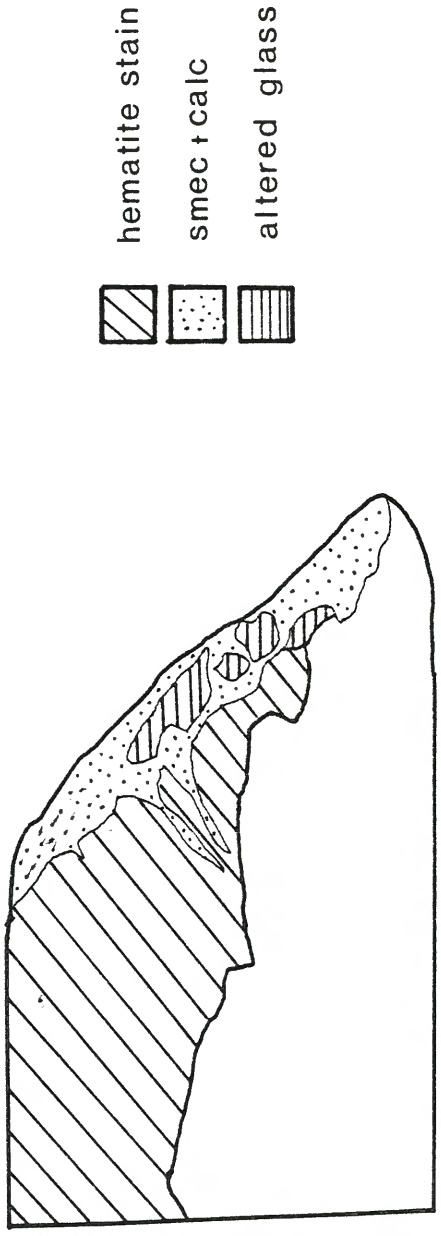
hematite stain

smec + calc

altered glass

0   1   2   3 cm
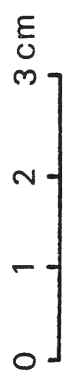
within the crystalline unit whereas in others they fill cracks.
Stringers generally lack obvious halos in the adjacent groundmass.
Where flow tops are replaced by jasper, jasper stringers penetrate into
the flow interior.

The alteration of the primary minerals in both pillows and flows
is similar to that in the Sm-Pa-Ca and Sm Zones with two notable
exceptions (Table III-1). Olivine phenocrysts in picritic pillows and
flows are slightly to totally altered to serpentine whereas in the other
lithologies, olivine is altered to goethite and calcite.
Titanomagnetite is less altered than in the Sm-Pa-Ca Zone (Hall et al.
in press).

Primary igneous textures are preserved and pale brown to
yellowish-green smectite replaces the mesostasis. Celadonite and quartz
are also part of the groundmass alteration assemblage in flow units.
Alteration within segregation vesicles and veins is similar to that in
the Sm-Pa-Ca Zone. Miarolitic voids, most common in thick flow units,
are variably filled with clay minerals.

The diversity and discontinuous nature of early vein systems in
each of the cooling-unit types reflects the heterogeneous style of
alteration characteristic of this zone. The following generalizations
may be made:

1. In all cooling units, smectite is the first phase to form, lining
cracks, fractures, vesicles, and vugs (Figure III-8).

2. Assemblages of analcime, phillipsite, gmelinite, natrolite, and
chabazite fill fractures and cracks in pillowed units. Where analcime
and phillipsite occur together, phillipsite is the first phase to form.

3. Assemblages of celadonite, mordenite, heulandite, and silica replace

Figure III-8. Analcime + calcite fill re-opened smectite-filled
    fracture (Sample CY-1:256.20 m).

smec

anal + calc

0   1   2   3 cm

glassy zones and fill fractures and cracks in massive and sheet flows. Where heulandite and mordenite occur together, heulandite is generally the first phase to form (Figure III-9).

4. Calcite is associated with zeolites in both cooling-unit types and commonly is the latest phase to form. Successive layers of euhedral crystals mantled by a light dusting of clay indicate several stages of growth.

The latest stage of crack and fracture filling occurs in both pillows and flows and is restricted to the upper few hundred metres of the Sm-Ce-Ze Zone. Vertical to near vertical veins of palygorskite and calcite cross-cut and bend around pillow margins and trend parallel to joint surfaces in flows (Plate III-7). Veins and stringers of gypsum, up to 5 cm wide, are found in the Sm-Ce-Ze Zone of the CY-1 drillcore. They generally re-open pre-existing veins and fill clay-lined fractures (Figure III-1Ø).

At different stratigraphic levels within this zone, two types of resistant vertical vein systems which range in width from < Ø.5 to 2 m cut across the pillow pile. The first vein system consists of hematite-stained basalt fragments in a vuggy calcite matrix and the second contains several <1- to 3-cm-thick calcite veins which both parallel and cross-cut one another. Oxidation halos extend from both vein systems into the adjacent lava pile for 1 - 1.5 m.

3.2.4 Laumontite-Smectite/Chlorite-Quartz Zone

The Laumontite-Smectite/Chlorite-Quartz Zone (La-Sm/Ch-Qz Zone) is the most difficult zone to define because its characteristic secondary minerals are common in both the overlying Sm-Ce-Ze or

Figure III-9. A. Schematic cross-section of the core in Plate III-5.

The "celadonitized" zone is rimmed by narrow celadonite + smectite

rich zones (Sample CY-la:45.80 m). B. Altered basalt fragments are

sequentially rimmed with celadonite followed by heulandite $\pm$

mordenite. A celadonite and smectite mixture with minor heulandite

and mordenite comprises the matrix (Sample CY-la:31.30 m).
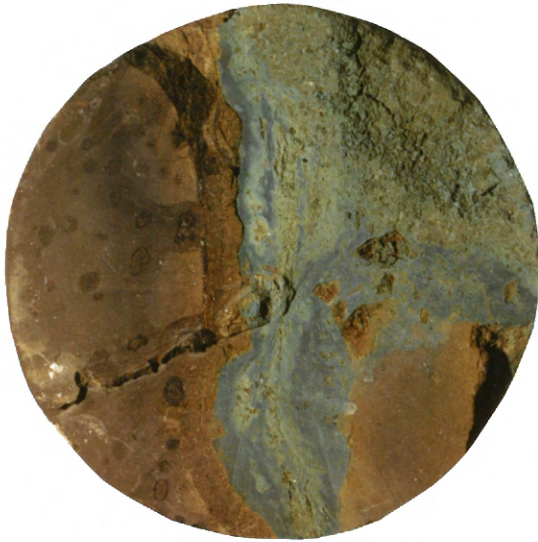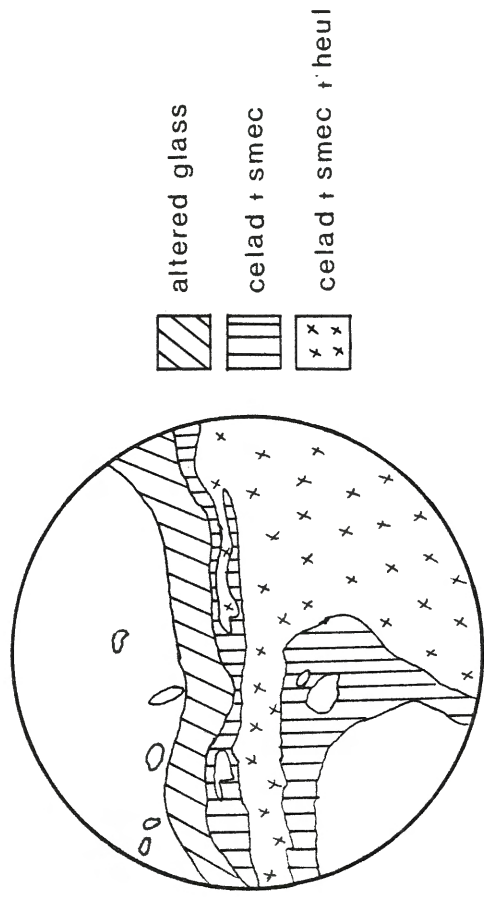
altered glass

celad + smec

celad + smec + heul

A.

B.

0 1 2 3 cm

Plate III-7. Late-stage vertical to near-vertical, white to buff

   palygorskite + calcite veins bend around and cross-cut the pillow

   pile. Photo taken in the Akaki River section.

Figure III-1Ø. A smectite-lined calcite vein within a thick flow is re-opened and filled with gypsum (Sample CY-1:27Ø.6Ø m).
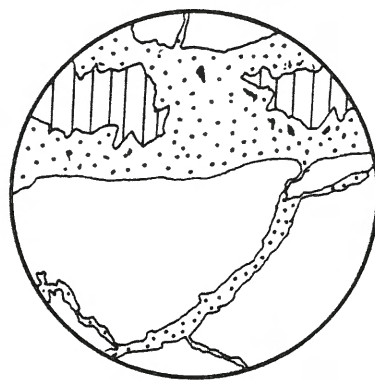
gypsum
calc

0   1   2   3 cm

TABLE III-3 SUMMARY OF VEIN DEPOSITION IN THE Sm-Ce-Ze ZONE

SAMPLE #	LITHOLOGY	DEPOSITIONAL SEQUENCE[*]
CY-1 270.6	grey spars phyric thick flow	smectite → calcite → gypsum
Cy-1 253.15	aphryic pillow rim	1. smec + fe oxide → smec 2. smec → calc → anal
CY-1 256.2	aphyric pillow centre	smectite → calcite
CY-1a 41.45		smec → celad → zeo
CY-1a 145.30	aphyric flow	smec → phil → anal → smec
CY-1a 155.85	thick flow	smec → calc + ? halo
KG83223 Margi	thick picritic flow	calc → calc + chrysotile → calc
KG82468 Akaki	aphyric pillow margin	celad → +/- heul → mord

[*] order of deposition is listed from rim to centre; number indicates order of deposition from oldest to youngest; abbreviations as in Table III-1; celad=celadonite, mord=mordenite; qtz=quartz

underlying Ep-Ch-Qz Zones. The upper boundary of the La-Sm/Ch-Qz Zone is marked by the first appearance of laumontite whereas the lower boundary is defined by the dominance of chlorite-quartz-pyrite in the groundmass and the first appearance of epidote. This lower boundary in the CY-la drillcore is also marked by the disappearance of laumontite. Late-stage veins of laumontite, however, are locally abundant in the Ep-Ch-Qz Zone in other areas.

The thickness and depth at which the La-Sm/Ch-Qz Zone occurs are variable. It may be completely contained within Sequence I lavas or the sheeted dyke complex, although it is generally located at the lava-dyke transition. The best documentation of this zone is found in the CY-la drillcore. The following observations are primarily from this section.

The rocks in this zone are uniformly altered and fresh glassy rinds are rare. Light to dark green pillow and flow margins and glassy brecciated zones are variably altered to smectite or mixtures of smectite-chlorite and laumontite (Plate III-8A). Heulandite, mordenite, and celadonite with smectite locally replace glassy zones in the upper tens of metres.

Ovoid, clay-lined vugs are either open or partially to totally filled with assemblges of quartz, laumontite, calcite, pyrite, and clay minerals (Plate III-8B). Prismatic quartz radiates inward from the vug walls whereas laumontite fills the interstices. Where present, calcite is the latest phase to form and locally appears to replace the laumontite. Vesicles are sporadically filled with mixtures of gmelinite, chabazite, and calcite.

Smectite, smectite-chlorite mixtures, or, rarely, chlorite line fractures and cracks which are locally filled with assemblages of

Plate III-8.   Typical mineral assemblages in the La-Sm/Ch-Qz Zone.   A.

Glassy matrix in breccia zone is altered to smectite + laumontite;

vesicles in basalt fragments are filled with laumontite (Sample

CY-1a:217.73 m).   B. Laumontite-filled vugs in pillow screens

within the Basal Group. Photo taken 1 km south of Kilrou along the

Nicosia-Apliki highway.

A

B
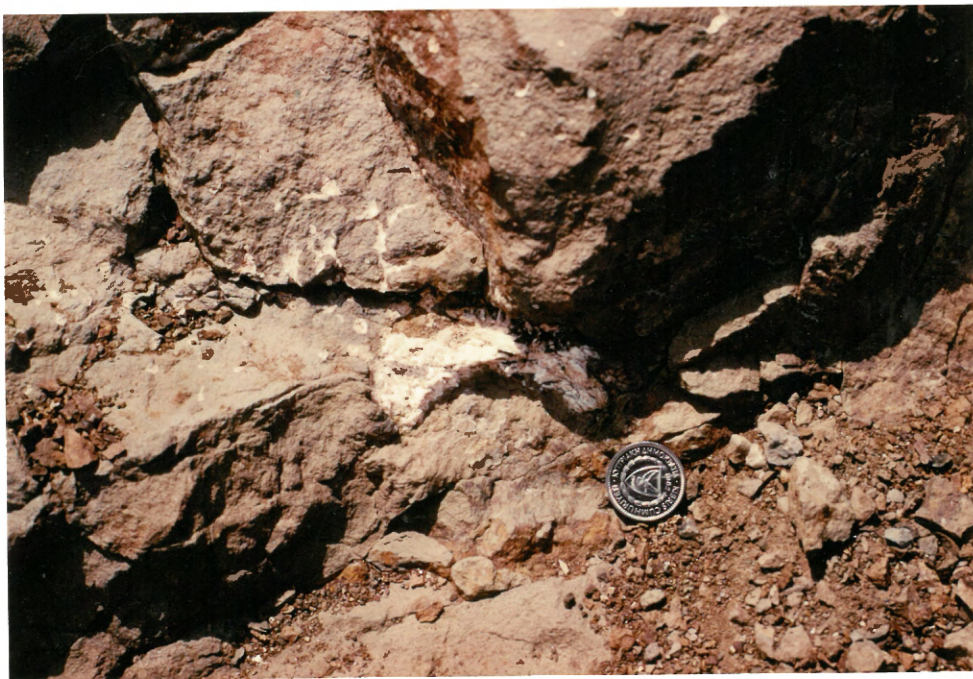
pyrite, calcite, laumontite, analcime, and quartz (Table III-4). Light grey, 1 - 3 mm thick, halos commonly rim narrow pyrite + quartz + chlorite stringers (Plate III-9). The groundmass within these halos is rich in quartz and very fine-grained pyrite. Analcime is restricted to the upper half of the zone.

Primary igneous textures are well preserved. Plagioclase and clinopyroxene phenocrysts are partially altered to the groundmass clay minerals (Table III-1). The mesostasis is uniformily altered to orange-brown smectite or light green mixed-layer smectite-chlorite with minor quartz and pyrite. Plagioclase microlites are altered to albite, clay minerals, or, rarely, K-feldspar.

3.2.5 Epidote-Chlorite-Quartz Zone

The Epidote-Chlorite-Quartz Zone (Ep-Ch-Qz Zone) is primarily contained within the Basal Group and the Sheeted Dyke Complex although it does extend upward into the overlying lavas in some areas. It is also found in areas immediatelely below the Su-Ch-Qz Zone (massive sulfide deposits) (Adamides 1984; Constantinou & Govett 1973).

The light grey to light green rocks in this zone are uniformly altered. The mesostasis is completely recrystallized to chlorite + quartz $\pm$ pyrite $\pm$ epidote. Where present, pyrite is disseminated throughout the groundmass whereas epidote is often concentrated in irregular patches. The distribution of this very fine- to fine-grained epidote does not appear to be fracture- or crack-controlled. The rocks in this zone locally have a distinctive, irregular, mauve to light green zonation which reflects the relative proportions of quartz (mauve) and chlorite (green) in the groundmass (Plate III-1Ø).

TABLE III-4 SUMMARY OF VEIN DEPOSITION IN THE La-Sm/Ch-Qz ZONE OF CY-1A

DEPTH (m)	LITHOLOGY	DEPOSITIONAL SEQUENCE[*]
229.00	cpx-plag phyric dyke	1. f.g. anal →m.g. anal + smec 2. smec→ anal →calc →anal 3. smec→ f.g. anal + smec →m.g. anal
233.05	m.g. aphyric flow	smec →laum →laum + anal →calc
237.00	f.g. aphyric flow	smec→ anal→ calc + minor anal→ smec
269.85	v.f.g. aphyric dyke	pyrite + minor chl + qtz 2 cm thick, 1-2 mm grey halo
293.00	chilled dyke? margin	1. laum + qtz + m.g. pyrite 2. laum + qtz + f.g. pyrite 3. laum + qtz + ? 1-2 mm thick pyrite halo

[*] order of deposition is listed from rim to centre; numbers indicate oldest to youngest veins; abbreviations as in Table III-1; chl=chlorite, laum=laumontite, qtz=quartz

Plate III-9. Light grey, 1 - 3 mm thick, halos rim pyrite + quartz + chlorite veins (Sample CY-1a:293.00 m).

CY-1a   293.0   m

293|00

0   5   10 cm

Plate III-10. Irregular mauve to light green zonation within a massive

flow. Vugs are rimmed with chlorite and lined with assemblages of

quartz, epidote, and calcite (Sample CY-1a:475.80 m).

93

CY-1a   475.80 m

180

0 · · · · 5 · · · · 10 cm
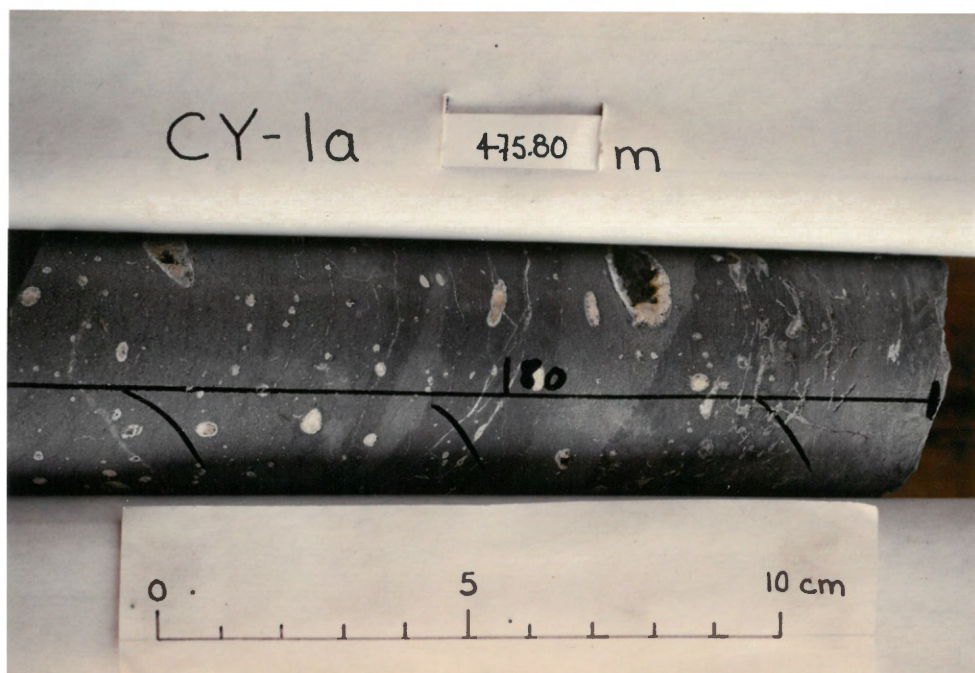
Flow and dyke margins are completely altered to chlorite, quartz, and epidote assemblages; no fresh glass is preserved. The initial brecciated texture is preserved whereas the fragments are completely recrystallized. Discontinuous, angular, jasper-rich zones appear to overprint earlier quartz + chlorite + epidote assemblages.

Epidosites which contain dominantly epidote with minor quartz, calcite, and jasper are erratically distributed (Plate III-11). These irregular zones range from cms to tens of cms in size and appear to fill voids and to replace the surrounding groundmass.

Igneous textures are generally preserved although in areas of most intense alteration, as in the epidosites, they are obliterated. Textures in segregation vesicles are obscured as the groundmass is completely altered to very fine-grained epidote, chlorite, and quartz. Plagioclase microlites are altered to mixtures of epidote and chlorite or replaced by albite; clinopyroxene is partly altered to chlorite. Titanomagnetite is locally replaced by sphene.

Chlorite-lined vesicles and vugs are rimmed with quartz and filled with assemblages of epidote, pyrite, calcite, chlorite, and prehnite (Table III-5). Laumontite locally overprints epidote. The age relationship of this laumontite and the laumontite from the La-Sm/Ch-Qz Zone, however, is not known.

Veins are much less abundant than in the overlying zones. Fractures and cracks are lined with mixtures of chlorite, albite, pyrite, and quartz and are locally coated with Fe-stained calcite (Table III-5). Epidote overprinted by laumontite was locally observed in field exposures. Narrow pyrite and quartz stringers are rimmed by light green, chlorite-rich halos. The areas between these halos, where quartz

Plate III-11 A. The groundmass surrounding medium to coarse grained

calcite + epidote-filled vug is totally replaced by epidote +

quartz (Sample CY-1a:495.80 m). B. Epidotized zone within

intrusive unit is cross-cut by quartz + pyrite + epidote veins

which are rimmed by jasper (Sample CY-1a:570.80 m). C. Coarse

grained epidote + calcite + jasper-filled vug (Sample

CY-1a:517.32 m).

A

B

C

CY-1a   517.32 m

0   5   10 cm
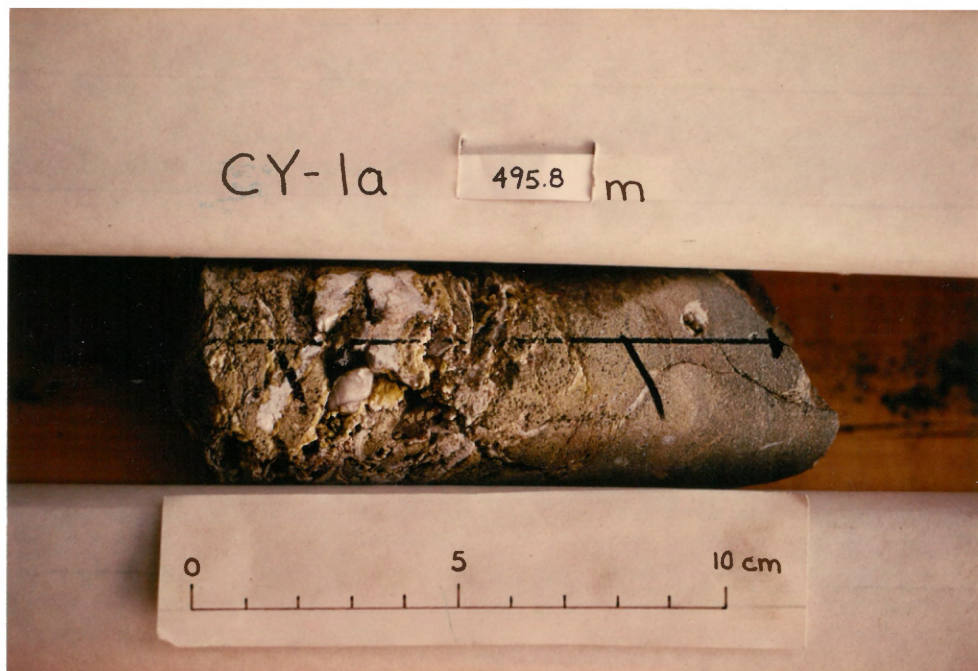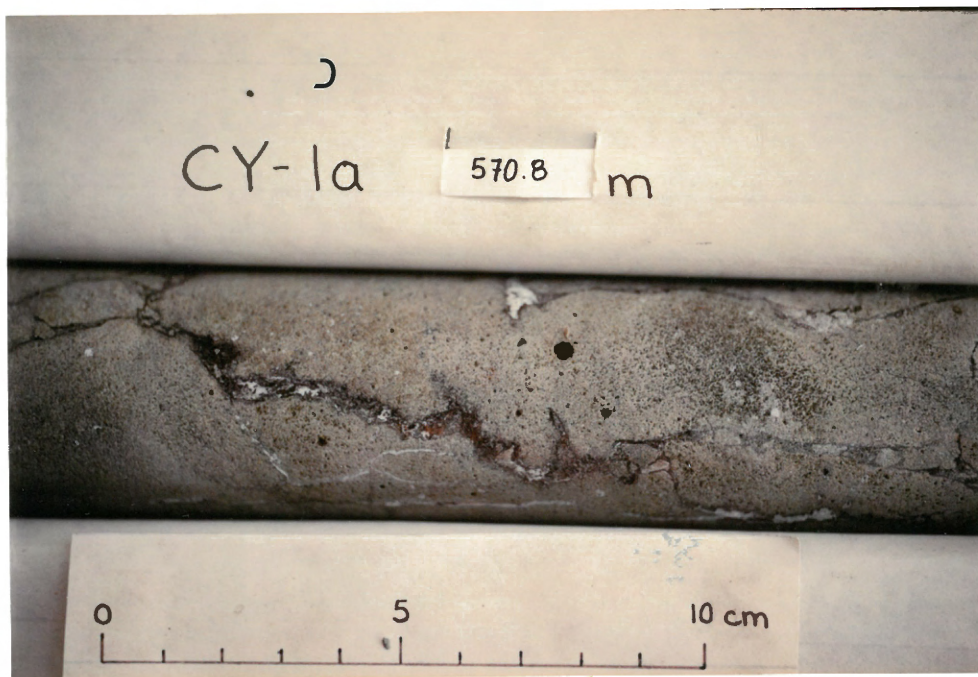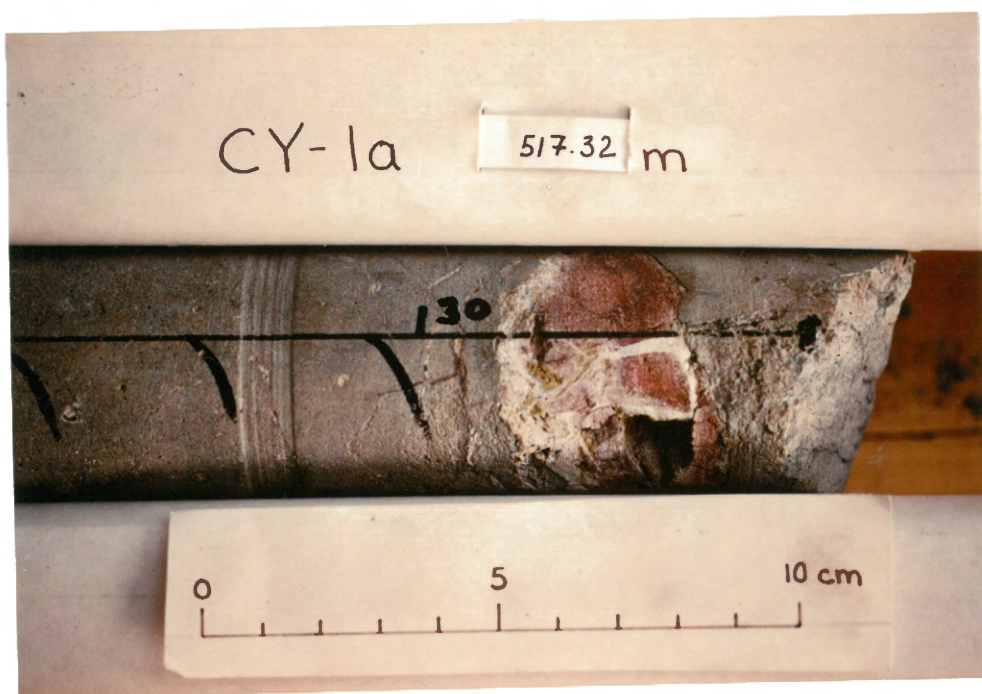
TABLE III-5 SUMMARY OF VEIN AND VUG DEPOSITION IN THE Ep-Ch-Qz ZONE OF CY-la

DEPTH (m)	LITHOLOGY	DEPOSITIONAL SEQUENCE
339.00	f.g. aphyric massive unit (dyke)	vugs: 1. quartz $\rightarrow$ epidote + chlorite 2. quartz $\rightarrow$ prenhite
367.25	v.f.g. aphyric brecciated flow top	veins: 1. chlorite $\rightarrow$ quartz + chlorite + epidote 2. fe oxide overprints #1
446.78	f.g. aphyric dyke	veins: 1. chlorite $\rightarrow$ epidote $\rightarrow$ calcite 2. quartz $\rightarrow$ calcite
571.92	f.g. aphyric brecciated flow	veins: 1. chlorite $\rightarrow$ quartz +chlorite + epidote 2. Fe oxide overprints #1 and groundmass
629.	f.g. aphyric flow	vugs: 1. epidote + quartz $\rightarrow$ epidote + pyrite 2. quartz $\rightarrow$ epidote + pyrite $\rightarrow$ calcite

* order is listed from rim to centre; numbers indicate oldest to youngest veins; abbreviations as in Table III-1.

is more abundant, are mauve; thus, the rocks have an irregular surficial pattern. Randomly distributed pyrite veins, 10 - 15 mm wide, are not rimmed by halos.

3.2.6 Sulfide-Chlorite-Quartz Zone

The massive sulfide deposits and their underlying stockwork zones comprise the Sulfide-Chlorite-Quartz Zone (Su-Ch-Qz Zone). These deposits are spatially restricted and occur at all levels within the extrusive sequence, ranging from the Basal Group-lava contact (Kokkinopezoula) to the top of the volcanic pile (Skouriotissa) (Figure II-4), (Constantinou 1976). Post-hydrothermal dykes cross-cut this zone in many locations suggesting that the deposits are synvolcanic (Conatantinou 1976). Well-bedded ochreous sediment overlies many of these zones.

Comprehensive study of this high temperature zone has been, and currently is, the focus of many investigations and is not within the scope of this thesis.

3.3 SPATIAL DISTRIBUTION OF THE ALTERATION ZONES

Detailed and reconnaissance mapping in the study area has clearly shown that there are significant lateral and vertical variations in the thickness and distribution of the alteration zones (Figure III-11). To describe these regional variations, the top of the extrusive sequence has been used as a datum and all cited depths are relative to this.

The Sm Zone underlies the discontinuously distributed umbers of the Perapedhi Formation. Its lower boundary with the Sm-Ce-Ze Zone is generally sharp whilst lateral boundaries with either the Sm-Pa-Ca or
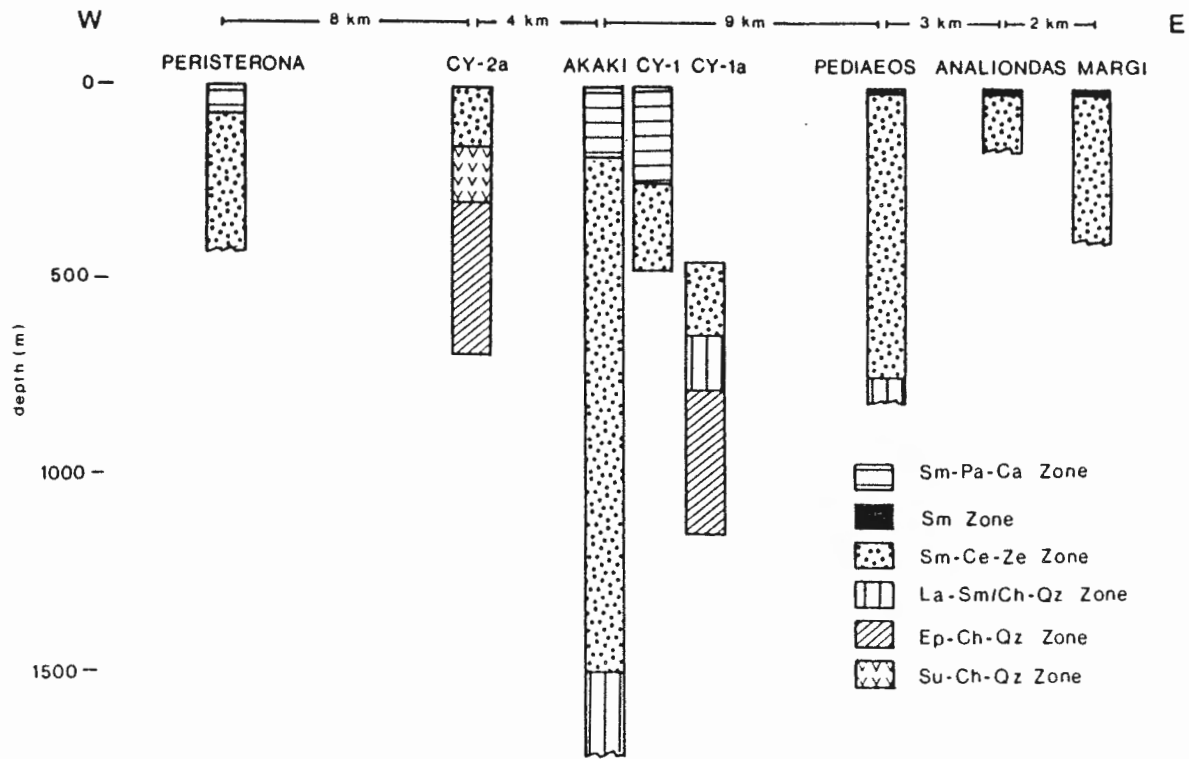
Figure III-11.   Distribution of the alteration zones within the field
area. The top of the extrusive sequence was used as the datum.

Sm-Ce-Ze Zones are generally ambiguous due to the discontinuity of field exposures. The Sm-Pa-Ca Zone occurs in the intervening areas along the sediment-lava interface where the lavas are overlain by the Lefkara Formation. Its lower boundary is generally gradational over tens of metres.

The Sm-Ce-Ze Zone is laterally continuous across the study area although its thickness varies significantly. The Sm-Ce-Ze Zone is 1200 - 1500 m thick in the Akaki River section whereas in the drillcore that samples the same stratigraphic sequence only tens to hundreds of metres to the north-west it is only 550 m thick. West of the Akaki River, the Sm-Ce-Ze Zone overlying the Agrokipia "B" deposit (CY-2a) is 150 m thick (Cann et al. in press; Herzig & Friedrich, in press; Sunkel et al. in press; Adamides 1984; Douma & Robinson 1984; Constantinou & Govette 1973). Farther to the west, in the Peristerona area, the actual thickness of this zone is not known but the presence of epidote-filled vesicles within the extrusive sequence indicates that its lower boundary is above the lava-dyke transition (Adamides, pers. comm., 1983). The area between the Akaki and Peristerona River sections, exclusive of the CY-2a drillcore, has not been mapped. Previous work indicates that below the Sm-Pa-Ca and Sm Zones, the Sm-Ce-Ze Zone is present everywhere except in the rocks which immediately underlie the Su-Ch-Qz Zones of the Kokkinopezula and Kokkinoyia ore deposits, situated west of Mitsero (Figure II-4). The basal lava sequence which surrounds the Kokkinopezula mine belongs to the Sm-Ce-Ze Zone (Adamides 1984). The Su-Ch-Qz Zone of the Kokkinoyia mine, contained within Sequence III lavas, is laterally bounded by the Sm-Ce-Ze Zone and overlain by the Sm-Pa-Ca Zone (Constantinou & Govett 1973).

East of the Akaki River section, the upper boundary of the Sm-Ce-Ze Zone has been well established whereas its lower boundary is generally at the lava-dyke transition. Outside of the Margi area and Pediaeos River section, reconnaissance mapping and other studies have shown that the extrusive sequence is dominated by the Sm-Ce-Ze Zone (Lewczuk, unpublished report, 1986; Mehegan, unpublished data, 1985). Localized zones of mineralization, generally associated with faults, are present throughout this area.

The La-Sm/Ch-Qz Zone is best documented in the CY-1a drillcore where it is 125 m thick. Based on both the CY-1 and CY-1a drillcores, the upper boundary of this zone is at 650 m depth whereas in the Akaki River section, its upper boundary occurs at approximately 1400 - 1600 m depth. The distribution and thickness of the La-Sm/Ch-Qz Zone outside the Malounda area has not been mapped in detail.

The Ep-Ch-Qz Zone characteristically is contained within the Basal Group although it does extend upward into the extrusive sequence, as seen in the CY-1a drillcore and in the Peristerona area. This zone also underlies the Su-Ch-Qz Zones which are generally contained within the extrusive sequence. In these occurrences, the La-Sm/Ch-Qz Zone is absent. Although the Ep-Ch-Qz Zone is laterally continuous throughout the study area, its upper boundary varies from 300 m depth beneath the Agrokipia "B" deposit to > 1800 m depth in the Akaki River section. The lower boundary has not been mapped in the study area.

3.4 ALTERATION ZONES IN "IN SITU" OCEANIC CRUST

Alteration zones have been defined on many scales for "in situ"

oceanic crust drilled by the DSDP. Poor recovery, shallow penetration, and variable styles of alteration in the recovered samples have led many investigators to define their alteration zones on the basis of variations in color and mineralogy on a hand specimen scale (e.g. Bohlke et al. 1981; Cann 1979; Bass 1976). Two areas drilled during successive legs, however, provide an excellent opportunity for direct comparison on a larger scale with the alteration zones defined for the Troodos ophiolite.

3.4.1 DSDP Sites 417 and 418

During Legs 51-53, two sites were drilled in 119 Ma crust south of the Bermuda Rise. The lithologies and intensity of alteration of the rocks recovered at each of these Sites are significantly different.

The pervasively altered pillows, breccias, and hyaloclastites of Hole 417A display strong color zonation, from yellowish-brown to light grey (Alt & Honnorez 1984). The abundance of Fe-rich phases often gives the rocks an "oxidized" appearance. Smectite, zeolites, calcite, mixtures of celadonite-smectite, and orthoclase are common throughout the core, although the zeolites are more concentrated in the lower half. Plagioclase phenocrysts are partially altered to either K-feldspar or smectite and titanomagnetite is totally altered to maghemite (Donnelly et al. 1979a). In contrast, the light grey pillows, massive flows, and minor breccias of Hole 417D, drilled only 450 m away, are much less pervasively altered. Fresh glass is locally preserved and plagioclase remains unaltered. The same secondary minerals occur in the Hole 417D samples but are signifiantly less abundant. The rocks also lack the "oxidized" appearance of those from Hole 417A.

The alteration of the pillows and massive flows of Hole 418A, drilled 7.5 km south of Site 417, is very similar in intensity and mineralogy to Hole 417D (Donnelly et al. 1979a; Humphris et al. 1979; Robinson 1977).

Holes 417D and 418A are overlain by Albian to Cenomanian sediments whereas the lavas of Hole 417A are not. Lack of evidence for an erosional period led the shipboard crew to conclude that the lavas of Hole 417A formed a topographic high that was exposed at the seafloor for a 10-20 million year period (Shipboard Scientific Crew, Legs 51, 52 & 53, 1979a). It has been suggested that the origin of this topographic high was either constructional (Donnelly et al. 1979a) or tectonic (Bleil et al. 1977).

The alteration patterns described for these cores are analogous to the characteristics of the alteration zones contained within the upper 500 m of Troodos ophiolite, particularily the Sm-Pa-Ca and Sm-Ce-Ze Zones. Hole 417A and the upper few metres of Hole 417D are very similar to the Sm-Pa-Ca Zone with one notable exception. These DSDP cores lack the pervasive, late-stage palygorskite-calcite veining which is ubiquitous in the Sm-Pa-Ca Zone and common in the Sm-Ce-Ze and Sm Zones. The remainder of Hole 417D and Hole 418A is analogous to the Sm-Ce-Ze Zone. Although the alteration assemblages common to distinct cooling-unit types have not been noted and palygorskite veining is also absent, the appearance of the rocks, the secondary mineral assemblage, and the erratic variations in the intensity of alteration are very similar.

Thus, it is evident that the Sm-Pa-Ca and Sm-Ce-Ze Zones mapped within the upper 500 m of the ophiolite are analogous to the alteration

zones described for the same depth interval in "in situ" oceanic crust. More importantly, the areal distribution and lateral variation in the thickness of these zones described in Section 3.3, suggests that the large difference in the "pervasiveness" of alteration described for Holes 417A and 417D, drilled only 450 m apart, may be a common feature of "in situ" crust.

3.4.2 DSDP Hole 504B

Hole 504B is the deepest basement hole drilled during the DSDP, penetrating 1075.5 m of oceanic basement. It was drilled 200 km south of the Costa Rica Rift in 5.9 Ma-crust during DSDP Legs 69, 70, and 83. The hole penetrated an upper 572-m-thick zone of pillows, massive flows, and breccias, a 209-m-thick transition zone with pillows, dykes, and massive units, and a lower 295-m-thick zone of dykes and massive lavas interpreted as a sheeted dyke complex (Shipborad Scientific Crew, Leg 83, 1985; Adamson 1985; Shipboard Scientific Crew, Legs 69 & 70, 1983). The aphyric to moderately plagioclase-olivine-clinopyroxene-phyric lavas are relatively homogeneous and generally primitive in composition (Kempton et al. 1985; Emmermman 1985).

Four alteration zones have been distinguished based on the distribution of secondary minerals and the appearance of the rocks in hand sample (Alt et al. 1985; Honnorez et al. 1983). The Upper Alteration Zone (0 - 320 m) is characterized by the presence of reddish-brown halos around cracks and veins whereas the rock away from these halos is light grey. The abundance of Fe-rich phases locally give the rocks an "oxidized" appearance. Olivine is partly to totally altered to clay minerals, plagioclase is locally altered and

titanomagnetite is moderately maghematized (Perchesky et al. 1983).
Zeolites, calcite, and saponite commonly fill voids. A Zeolite Zone
overprints the Upper Alteration Zone between 254 and 289 m. Thick
zeolite veins with saponite, celadonite, and calcite- and
zeolite-cemented breccias are rimmed by light grey halos.

The light grey rocks in the Lower Alteration Zone (324-624 m) are
more uniform in appearance than the overlying zones. Plagioclase is
commonly slightly replaced by saponite or rarely albite and calcite;
clinopyroxene remains fresh. Void-filling zeolites and calcite are not
abundant in this zone. Secondary pyrite is common and becomes more
abundant towards the base. Glassy rinds are partially altered above
518 m, whereas below this depth they are totally altered.

Zeolite and greenschist facies mineral assemblages characterize the
Lithologic Transition Zone and the Sheeted Dyke Section (624 - 1075.5 m)
(Alt et al. 1985). A mineralized stockwork zone, containing pyrite,
chalcopyrite, and sphalerite with minor galena, occurs in the upper 30 m
of the Lithologic Transition Zone (Honnorez et al. 1985). The lavas in
a 70-m-thick interval immediately below the stockwork zone are locally
silicified. In the remainder of the core, the intensity of alteration
is variable. Light green to grey alteration halos are common and
primary minerals are more extensively altered than in the overlying
zones. Four stages of crack and fracture filling have been identified
(listed from oldest to youngest): chlorite and mixed-layer clay
minerals; quartz, epidote, and sulfides; anhydrite; and zeolites,
calcite, and prehnite.

The characteristics of the alteration zones defined for Hole 504B
as well as their thickness and depth distribution are directly

comparable to the alteration zones mapped in the upper 1500 m of the Troodos ophiolite. The Upper Alteration Zone of Hole 504B and the Sm-Pa-Ca Zone are similar in mineralogy, appearance, and thickness. As in Holes 417A and 417D, the "in situ" zone lacks the pervasive palygorskite-calcite veining characteristic of the Sm-Pa-Ca Zone. The lower tens of metres of the Upper Alteration Zone and the upper half of the Lower Alteration Zone are analogous to the Sm-Ce-Ze Zone. Notable differences are the lack of mineral associations with respect to cooling-unit type and the decrease in the abundance of zeolites with increasing depth at Hole 504B. The extrusive sequence in the Troodos ophiolite lacks a distinct later period of pervasive zeolite deposition characteristic of the Zeolite Zone of Hole 504B and the rocks in the Ep-Ch-Qz Zone are only locally overprinted by laumontite. The presence of mixed-layer clays and an increase in the abundance of quartz in the lower 150 m of the Lower Alteration Zone in 504B suggests that this depth interval may be equivalent to the La-Sm/Ch-Qz Zone. Laumontite, however, is not resticted to this zone and is locally abundant in the rocks equivalent to the Ep-Ch-Qz Zone.

The mineralogical and textural features of the stockwork-like zone in Hole 504B are comparable to the Su-Ch-Qz Zone. A zone with greenschist facies mineral assemblages is present below both the stockwork zone of Hole 504B and the Su-Ch-Qz Zones. The secondary mineral assemblages, the variation in the intensity of alteration, and the sequence of secondary mineral deposition are remarkably similar. However, rocks from the Ep-Ch-Qz Zones studied in the Troodos ophiolite lack amphibole whereas rocks from the equivalent zone in Hole 504B contain amphibole.

The depth distribution of alteration zones between Hole 504B and the upper 1500 m of the Troodos ophiolite are analogous. The thickness of the equivalent Sm-Ce-Ze Zone in Hole 504B is thinner than its average thickness in the Troodos ophiolite but is similar to those zones overlying the mineralized Su-Ch-Qz Zones. This implies that the alteration zones defined for the Troodos ophiolite are representative of the alteration zones in "in situ" crust. Therefore, the areal distribution of these zones in Troodos provides valuable insights into the spatial relationships of alteration zones in the oceanic crust.

3.5 ALTERATION ZONES WITHIN OPHIOLITES

In most ophiolites, the original ocean floor alteration pattern has been overprinted by a later, commonly higher grade, metamorphism which occurred during their transportation and subsequent emplacement. Therefore, very few are appropriate for study of low temperature alteration processes.

Investigators of the ophiolites with preserved "in situ" alteration patterns have distinguished regional metamorphic zones or facies. Although the characteristic secondary minerals are implied to be equilibrium asemblages, disequilibrium textures and late-stage void-filling phases are common, primary textures are typically preserved, and recrystallization is generally incomplete. Two ophiolites which have not been overprinted by a later regional metamorphism are the Sarmiento and Del Puerto complexes. The stratigraphy of both has been subdivided into regional, equilibrium metamorphic facies and zones (Figure III-12) (Evarts & Schiffman 1983; Stern & Elthon 1979; Elthon & Stern 1978).

Sarmiento

Del Puerto

thickness (m)

Ze	zeolites ± smectite ± calcite ± quartz ± sulphides ± albite ± sphene
Gr	chlorite, epidote, sphene Na-plag ± quartz ± calcite ± biotite
Am	actinolite/tremolite, Ca-plag, sphene ± biotite ± calcite

Ze	laumontite, heulandite
Pu	pumpellyite, prehnite, corrensite, sphene, albite quartz
Ep	epidote, chlorite, sphene, quartz, albite
Am	amphibole, epidote, Ca-plag, ± chlorite
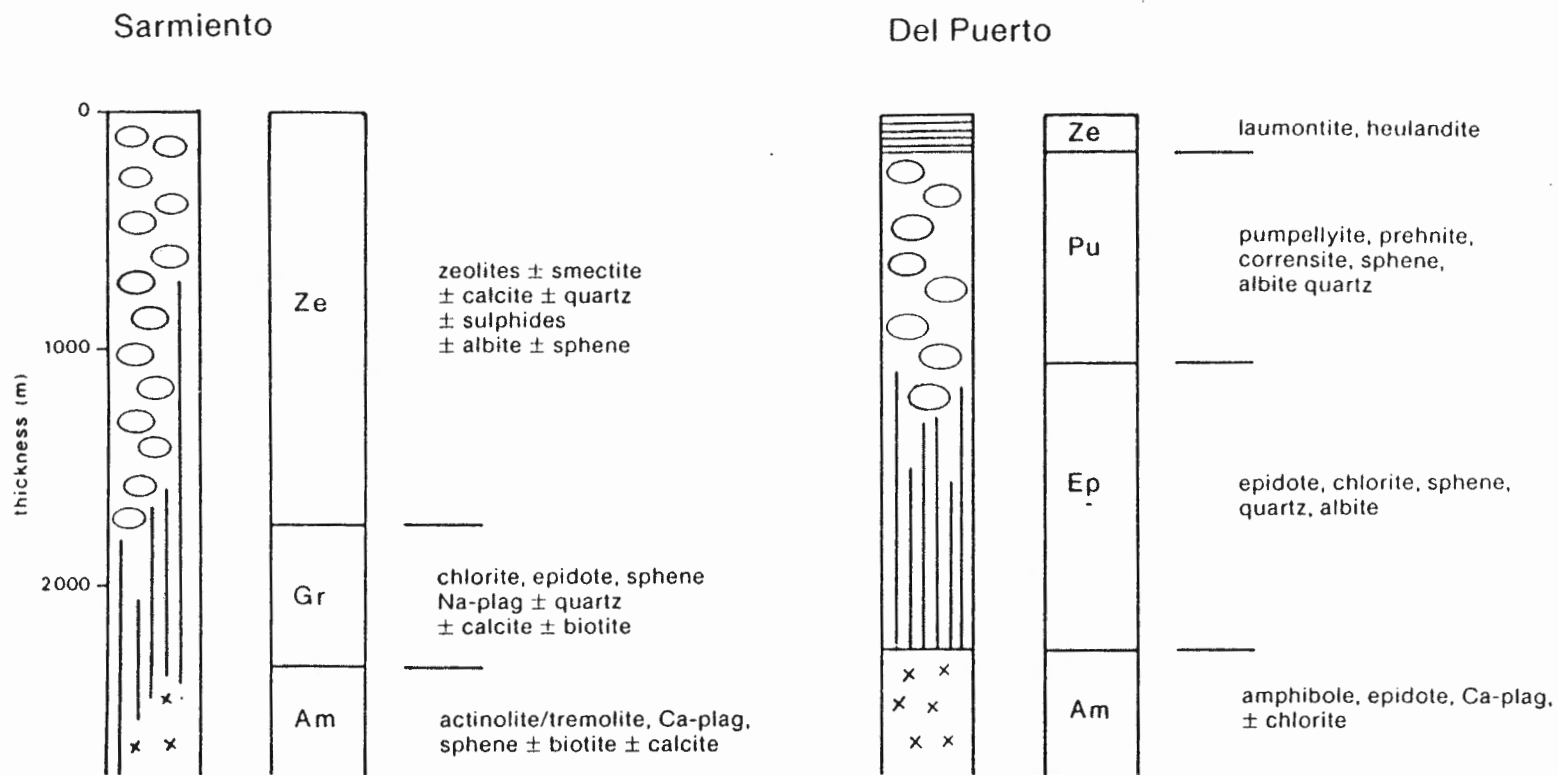
Figure III-12. Lithologies and metamorphic zones in the upper 2000 m of the Sarmiento and Del Puerto ophiolite complexes (modified after Elthon & Stern 1978; 1979; Evarts & Schiffmann 1983, respectively).

The Sarmiento Ophiolite Complex is part of a series of discontinuous exposures of Mesozoic mafic complexes in the southern Andes. The igneous succession has been subdivided into four regional metamorphic facies: zeolite, greenschist, lower amphibolite, and upper amphibolite (Stern & Elthon 1979; Elthon & Stern 1978). These facies are laterally continuous and their boundaries trend subparallel to the stratigraphy. The mineral assemblages, host lithologies, and stratigraphic position of the zeolite facies are most analogous to the Sm-Ce-Ze and La-Sm/Ch-Qz Zones of the Troodos ophiolite. However, greenschist facies minerals have also been recognised within the zeolite facies rocks. The greenschist facies is similarily analogous to the Ep-Ch-Qz Zone of Troodos (Figure III-12). Although variation in the thickness of these facies is implied, it is not possible to make a comparison of the scale of the lateral variation with the Troodos ophiolite.

The Del Puerto Ophiolite is part of the Jurassic Coast Range Belt in California. Four regional metamorphic zones have been defined by the first appearance of an index mineral: zeolite, pumpellyite, epidote, and amphibole (Evarts & Schiffman 1983). These zones are laterally continuous and trend subparallel to the igneous stratigraphy. The epidote zone, which is the only metamorphic zone that resembles the alteration zones of the Troodos ophiolite, has similar mineralogy, host lithologies, and stratigraphic position to the Ep-Ch-Qz Zone. The zeolite and pumpellyite zones contained within the overlying volcaniclastic sediments and extrusive sequence have distinctly different characteristics from the alteration zones that occur at an equivalent stratigraphic level in the Troodos ophiolite. It is

therefore impossible to compare the spatial distribution of the metamorphic zones and facies with the alteration zones defined for the Troodos ophiolite.

The East Taiwan ophiolite (Liou & Ernst 1979; Liou 1979) and the Semail ophiolite of Oman (Alabaster & Pearce 1985; Alabaster et al. 1980) also lack a later regional metamorphic overprint. The degree and grade of metamorphism and the distribution of metamorphic zones is similar to those described for the Sarmiento ophiolite.

The minerals that characterize the alteration zones of the Troodos ophiolite do not represent equilibrium assemblages whereas it has been implied that the minerals that define the metamorphic zones of the other ophiolites are. The grade of metamorphism in the other ophiolites is generally higher in the upper 1000 to 1500 m than in the Troodos ophiolite. Below this level, the rocks in Troodos and the other ophiolites are altered to greenschist facies mineral assemblages.

3.6 SUMMARY

Six regional alteration zones have been defined for the upper 1500 m of the Troodos ophiolite and their spatial relationships have been mapped in the study area. These non-equilibrium, non-genetic zones, named for their most abundant secondary phases, vary significantly in vertical and lateral extent on the scale of tens to hundreds of metres.

Visual estimates indicate that there is no systematic increase in the intensity of alteration with increasing depth (Figure III-13). Outside of the mineralized Su-Ch-Qz Zones, alteration is most pervasive in the Sm-Pa-Ca and Sm Zones. The Sm-Ce-Ze Zone is characterized by
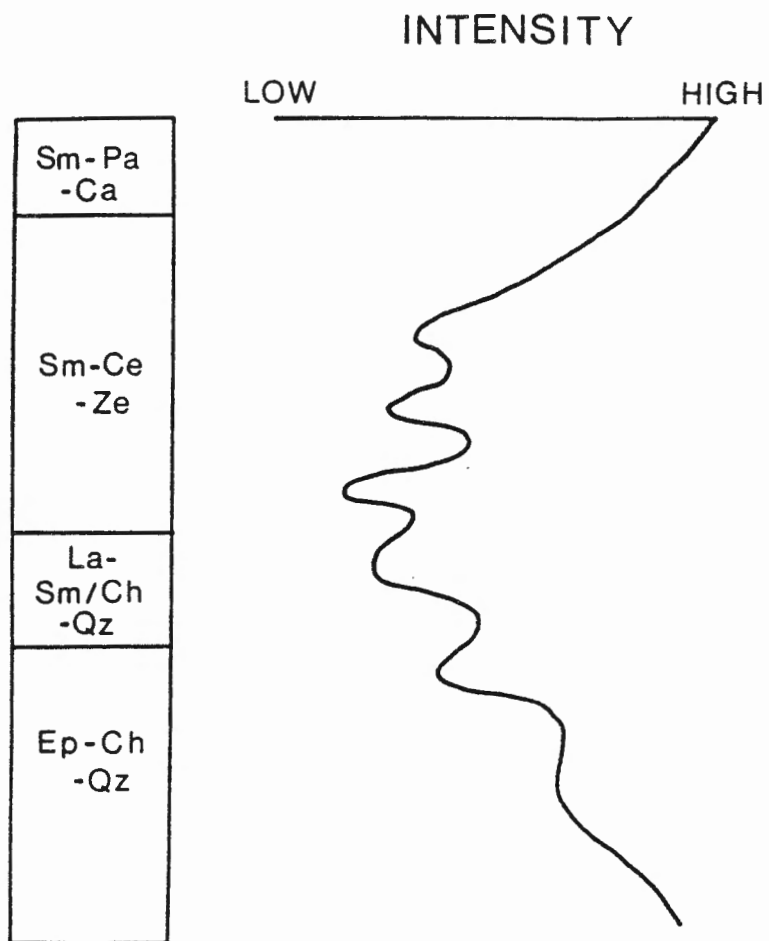
Figure III-13. Schematic diagram illustrating a visual estimate of the intensity of alteration in the most common alteration zones in the study area.

significant variation in the intensity of alteration. Apparent changes in the distribution of secondary mineral assemblages with depth merely reflect a change of the dominant cooling-unit type, from pillows to massive and sheet flows. The La-Sm/Ch-Qz and Ep-Ch-Qz Zones are characterized by more uniform alteration, although there are localized zones of more pervasive alteration. Regional reconnaissance surveys indicate that the study area is representative of the alteration along the northern flank of the ophiolite.

The Sm Zone is restricted to the lavas immediately below the synvolcanic umbers of the Perapedhi Formation. In the intervening areas, the Sm-Pa-Ca Zone is overlain by Maastrichtian to Miocene sediments. Assuming that there was no period of erosion, the lavas in these intervening areas were exposed to seawater for a few to tens of million years. Thus, the sedimentary cover and the duration of exposure to seawater influenced the alteration in the upper few hundred metres.

The characteristics, thickness, and stratigraphic position of the alteration zones defined for the Troodos ophiolite are analogous to those outlined for "in situ" oceanic crust as is the areal distribution of the Sm-Pa-Ca and Sm-Ce-Ze Zones. Comparison of the distribution of the other zones, however, is not possible as only one deep basement hole has been drilled to date.

Alteration and metamorphic zones analogous to the Sm-Pa-Ca and Sm-Ce-Ze Zones have not been recognised in other ophiolites which are generally altered to a higher grade. Zones analogous to the Ep-Ch-Qz Zone, however, are commonly present at the same stratigraphic level.

CHAPTER IV

SECONDARY MINERALS: OCCURRENCE AND COMPOSITION

4.1 INTRODUCTION

In the previous chapter, six alteration zones were defined for
the study area primarily on the basis of the distribution of secondary
mineral assemblages. Within these zones, it was possible to distinguish
consistent mineral associations and depositional sequences.

The purpose of this chapter is to document the compositional
trends of individual mineral groups and to elaborate upon the previously
described depositional sequences within single alteration zones or
between zones. This documentation is essential to unravel the
alteration history of the ophiolite because these secondary minerals
record the interaction between seawater and rock through time.

The heterogeneous distribution and variability of assemblages,
particularly in the Sm-Pa-Ca and Sm-Ce-Ze Zones, necessitated the
collection of numerous samples from each of the field areas and from the
CY-1 and CY-1a drillcores. Phases in over 700 samples were identified
by x-ray diffractometry (Appendix II) and their compositions were
obtained by microprobe. Paragenetic relations were determined
macroscopically and through the examination of 300 thin sections.

In the following sections, the occurrence and composition of each
mineralogic group of secondary phases are described and the paragenetic
relations and mineral associations are discussed. The alteration of
both the primary minerals and volcanic glass is then discussed.
Generalized mineral formulas for the common secondary minerals are
listed in Table IV-1.

114

TABLE IV-1.   GENERALIZED SECONDARY MINERAL FORMULAS[1]

analcime	$Na(AlSi_2O_6) \cdot H_2O$
natrolite	$Na_2(Al_2Si_3O_{10}) \cdot 2H_2O$
phillipsite	$(1/2Ca,Na,K)_3(Al_3Si_5O_{16}) \cdot 6H_2O$
gmelinite	$(Na_2,Ca)(Al_2Si_4O_{12}) \cdot 6H_2O$
chabazite, gmelinite	$(Na_2,Ca)(Al_2Si_4O_{12}) \cdot 6H_2O)$
clinoptilolite/ heulandite	$(Ca,Na_2,K_2)(Al_2Si_7O_{18}) \cdot 6H_2O$
mordenite	$(Na_2,K_2,Ca)(Al_2Si_{10}O_{24}) \cdot 7H_2O$
laumontite	$Ca(Al_2Si_4O_{12}) \cdot 4H_2O$
epidote	$CaFeAl_2O\ OH(Si_2O_7)(SiO_4)$
prehnite	$Ca_2Al(AlSi_3O_{10})\ (OH)_2$
smectite	$(1/2Ca,Na)_{0.7}(Al,Mg,Fe)_4(Si,Al)_8O_{20}(OH)_4 \cdot nH_2O$
celadonite	$K(Fe,Al,Mg)(Si_4O_{10})(OH)_2$
chlorite	$(MgAlFe)_{12}((SiAl)_8O_{20})(OH)_{16}$
palygorskite	$Si_8Mg_5O_{20}(OH)_2(OH_2)_4 \cdot 4H_2O$
sepiolite	$Si_{12}Mg_8O_{30}OH_4(OH_2)_4 \cdot 8H_2O$

[1] from Deer et al. (1963).

4.2 CLAY MINERALS

Clay minerals, by far the most abundant secondary phases, replace the primary minerals and mesostasis and line or fill vesicles, vugs, and fractures. Several clay mineral varieties have been identified on the basis of their composition, calculated structural formula, and crystal structure.

4.2.1 Smectite

Smectite is the most abundant secondary mineral in the study area, being a characteristic mineral in four out of six of the alteration zones. It is a 2:1 layer silicate, identified by its broad basal peak at 16 Å and the subsequent shift to 18 Å upon treatment with ethylene glycol (Brindley & Brown 1980). Two types of smectite have been distinguished on the basis of calculated structural formulas: saponite and Al-saponite (Appendix I). Representative microprobe analyses and calculated mineral formulas are listed in Table IV-2.

Saponite, a trioctahedral smectite, is characterized by its octahedral occupancy of 6 (Ross & Hendricks 1945). It is generally orange-brown to brown with 1st to 2nd order birefringence.

A plot of the molar proportions of Al_2O_3-FeO-MgO shows that the saponites are generally Mg-rich with low Al_2O_3 contents (Figure IV-1). Within individual samples, FeO/(FeO+MgO) ranges from 0.2 to 0.8. Saponites from the Akaki and Pediaeos River sections and the CY-1 and CY-1a drillcores trend towards slightly higher FeO contents and the range of FeO/(FeO+MgO) narrows with increasing depth (Figure IV-2). The MnO content of saponite is generally < 0.5 wt.% (Figure IV-3).

TABLE IV-2   REPRESENTATIVE SAPONITE AND AL-SAPONITE ANALYSES

	1	2	3	4	5	6	7	8	9
SiO_2	42.51	43.65	46.94	38.32	42.70	55.54	42.09	55.86	47.71
TiO_2	0.13	0.21	-	0.06	0.06	0.48	0.06	-	0.11
Al_2O_3*3	10.01	16.94	8.86	7.91	10.73	13.74	8.67	17.77	15.88
FeO*	12.60	11.93	6.75	22.21	14.84	12.48	16.60	10.74	14.39
MnO	0.18	0.04	0.08	0.02	0.08	0.04	0.08	0.11	0.18
MgO	19.68	7.72	21.40	10.56	14.21	7.70	16.97	5.71	8.77
CaO	0.98	0.50	1.38	2.40	1.39	1.61	0.92	0.78	0.76
Na_2O	0.63	-	0.07	0.09	0.02	0.15	1.68	0.59	0.46
K_2O	1.16	3.71	0.17	1.57	4.14	2.77	1.82	2.00	3.02
Total	87.70	84.66	85.57	83.12	88.09	94.47	88.81	93.45	91.10

Cation Proportions on the basis of 22 (O, OH)

	1	2	3	4	5	6	7	8	9
Si	6.43	6.76	6.94	6.55	6.60	7.56	6.47	7.49	6.90
Al^{iv}	1.57	1.24	1.08	1.45	1.40	0.44	1.53	0.51	1.10
total	8.00	8.00	8.00	8.00	8.00	8.00	8.00	8.00	8.00
Al^{vi}	0.22	1.85	0.48	0.14	0.56	1.76	0.04	2.30	1.61
Fe	1.60	1.55	0.83	3.17	1.92	1.42	2.14	1.20	1.74
Mg	4.44	1.78	4.72	2.69	3.28	1.56	3.89	1.14	1.89
Mn	0.02	0.01	0.01	-	0.01	-	0.01	0.01	0.01
Ti	-	0.02	-	0.01	0.01	0.05	0.02	0.01	1.02
total	6.31	5.21	6.04	6.02	5.80	4.79	6.17	4.69	5.27
Ca	0.16	0.08	0.22	0.44	0.23	0.23	0.15	0.11	0.12
Na	0.18	-	0.02	0.03	0.01	0.04	0.54	0.15	0.13
K	0.22	0.73	0.03	0.34	0.82	0.48	0.33	0.34	0.56
total	0.56	0.81	0.27	0.81	1.06	0.75	1.02	0.06	0.81

- not detected; * Total iron as FeO; 1 KG:83:012, or-br saponite, gm; 2 KG:83:018, pale yel Al-saponite, gm; 3 KG:83:022, or-br saponite, vein; 4 KG:83:176, or-br Fe-rich saponite, gm; 5 KG:84:029, or-br saponite, gm; 6 KG:84:061, pale br Al-saponite, gm; 7 CY-1a 158.05 m, br saponite, gm; 8 CY-1 72.75 m, yel-gr Al-saponite, vesicle; 9 CY-1 75.25 m, yel-gr Al-saponite, gm.
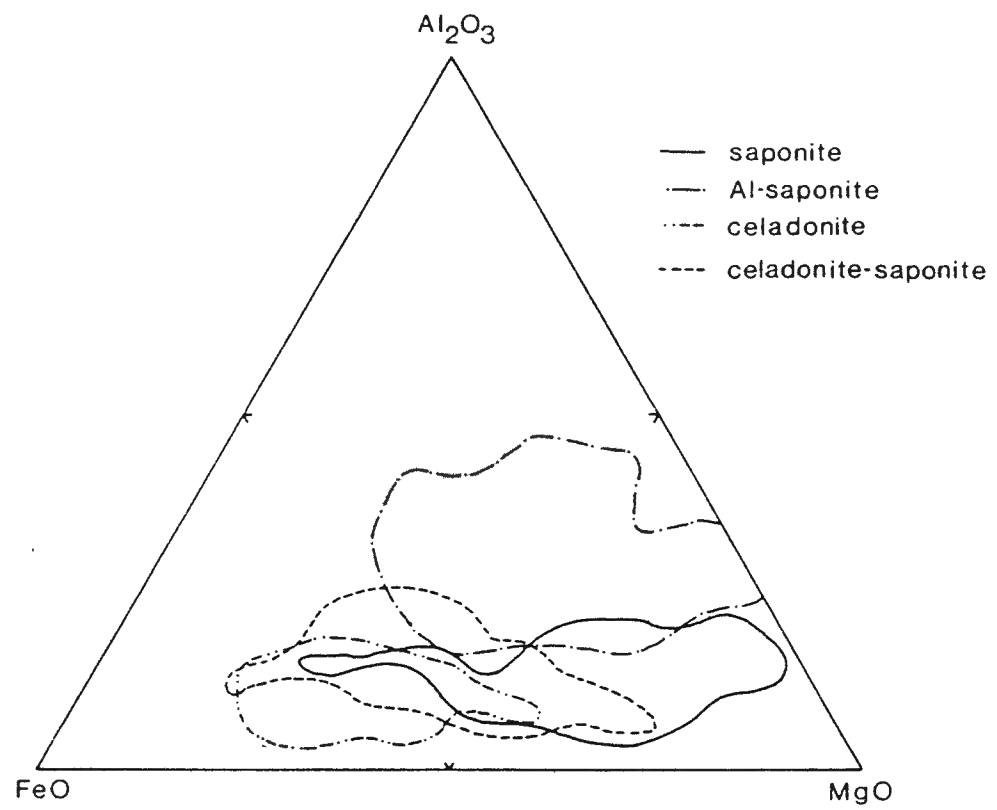
Figure IV-1.   Molar Al_2O_3-FeO-MgO (AFM) proportions of saponite, Al-saponite, celadonite, and celadonite-saponite from all field areas.

Figure IV-2.   Variation in the FeO/(FeO+MgO) (wt%) for clay minerals

   versus depth: A. CY-1 drillcore, B. Pediaeos River section, C.

   CY-1a drillcore.

   Symbols: ● saponite; ○ Al-saponite; ■ celadonite;

   □ celadonite-saponite; ▲ chlorite; △ smectite-chlorite.

C.

FeO/FeO + MgO

depth (m)

- saponite
- Al-saponite
- celadonite
- celadonite-saponite
- chlorite
- smectite-chlorite
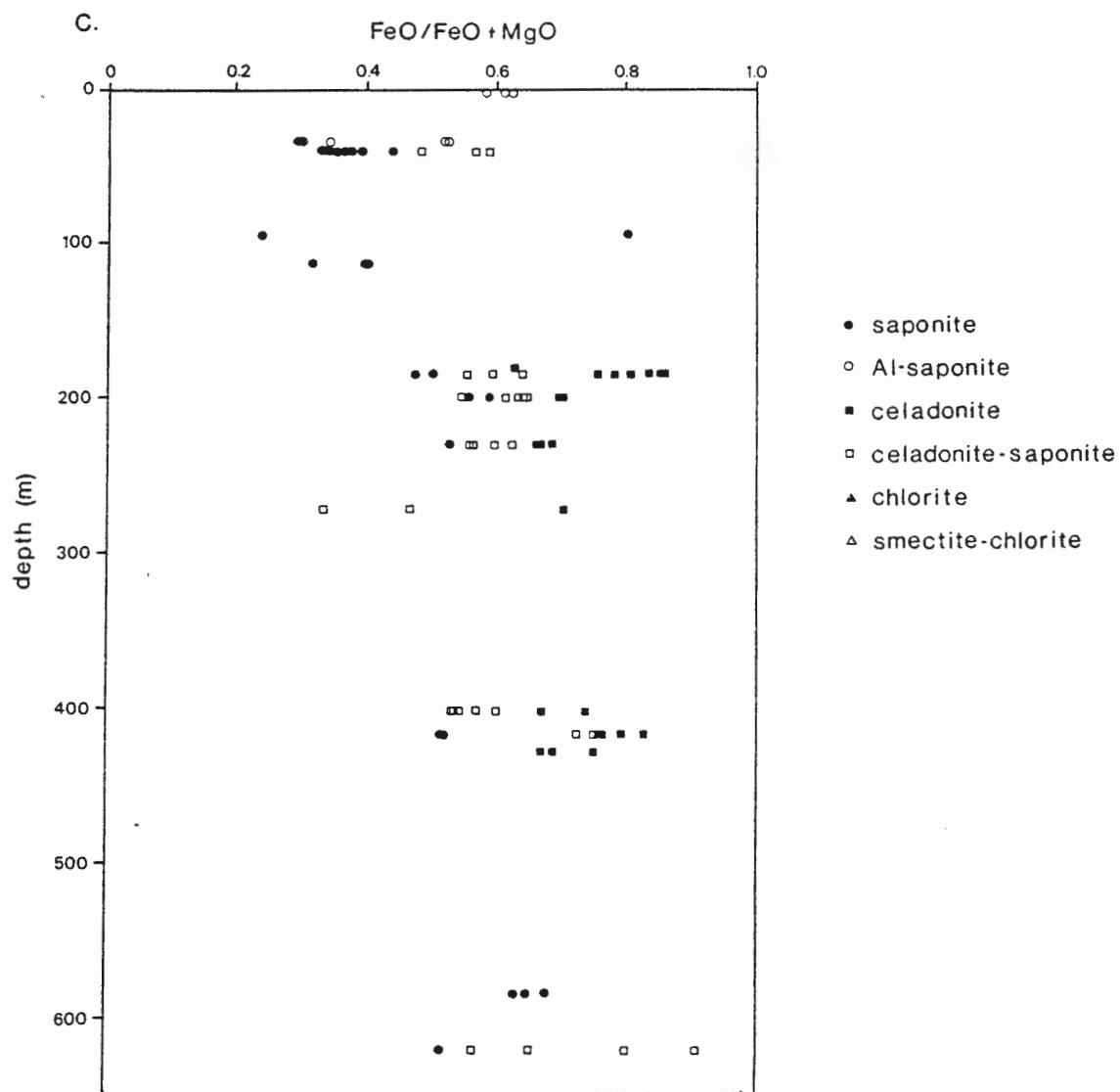
Figure IV-3. Variation in the MnO content (wt%) of clay minerals from
the CY-1a drillcore. Symbols as in Figure IV-2.
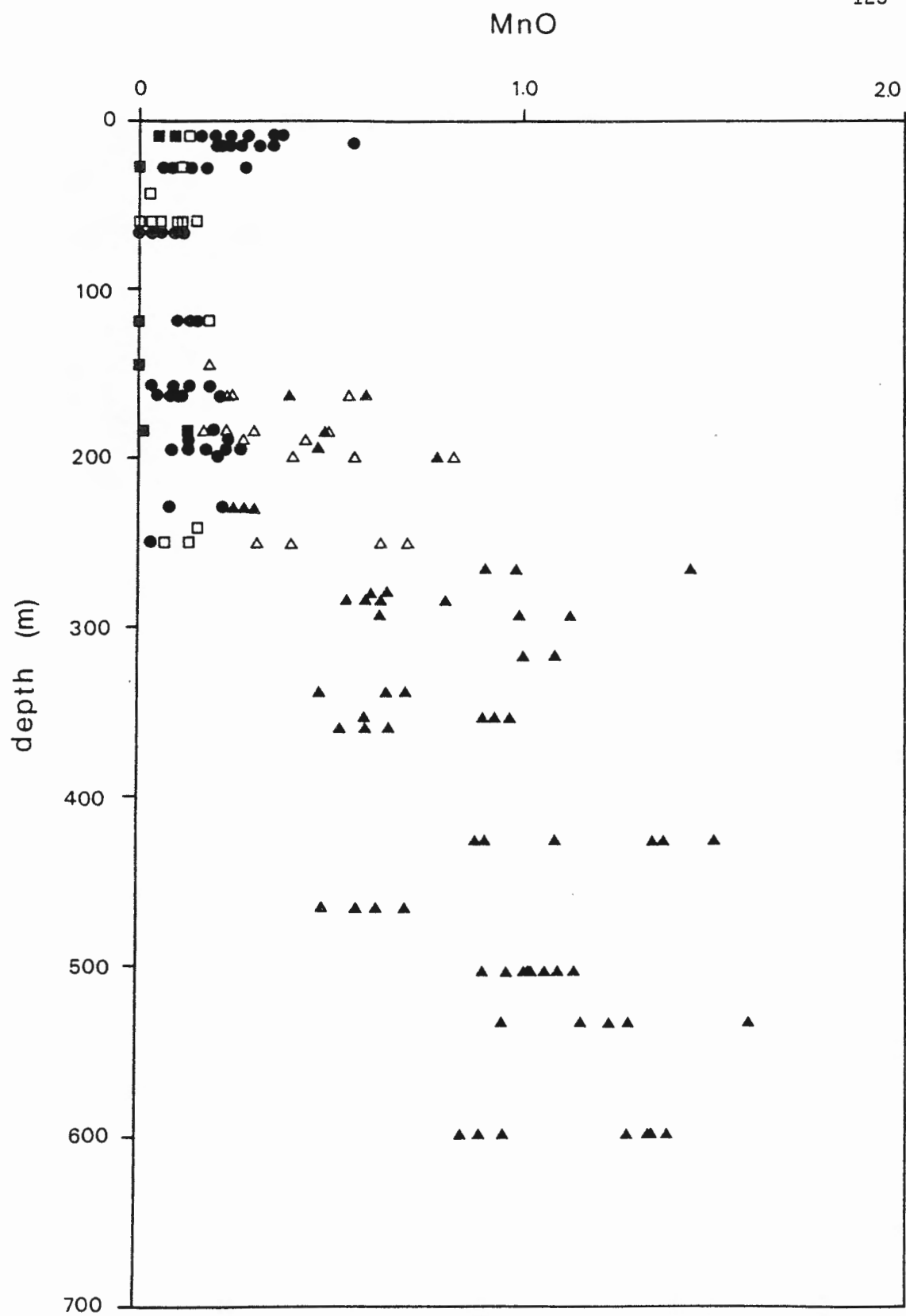
Groundmass varieties are fibrous, finely crystalline, radiating, or globular. Saponite that fills voids is usually fibrous to platy and radiates out from the wall of the cavity. Saponite is abundant throughout the Sm-Pa-Ca, Sm-Ce-Ze, Sm, and La-Sm/Ch-Qz Zones. In the latter zone it is commonly interstratified with chlorite. This interlayering is discussed further in the section 4.2.3.

The octahedral occupancy of Al-saponite ranges from 4.4 − 5.3 indicating either that its structure is intermediate or that it is a mixture of dioctahedral and trioctahedral smectite (Alt & Honnorez 1984). Al-saponite is pale yellow to pale brown with 1st order birefringence and has the same range in habit as saponite.

A molar Al_2O_3-FeO-MgO plot indicates that Al-saponites are more aluminous and slightly more Fe-rich than saponite (Figure IV-1) which suggests that substitution of Al^{3+} for Mg^{2+} in the octahedral site in saponite could result in an intermediate structure (Alt & Honnorez 1984). It is also possible that Al-saponite may be a mixture of beidellite, an Al-rich, dioctahedral smectite, with saponite. The compositional and structural continuity between saponite and Al-saponite illustrated in Figure IV-1 and the absence of pure beidellite, however, make the former explanation preferable. More detailed XRD studies using non-oriented powdered mounts are required to differentiate between these possibilities. The FeO/(FeO+MgO) ratios of Al-saponites are variable within individual samples; however, there are no consistent compositional trends with depth (Figure IV-2). The MnO content of Al-saponite is similar to saponite.

Al-saponite is generally restricted to the upper 500 m of the studied stratigraphic sections and is most abundant in the Sm-Pa-Ca

Zone.

Nontronite, a dioctahedral smectite, has been identified in the Sm-Pa-Ca Zone of CY-1 by x-ray analyses (Elsbree 1985). Calculated structural formulas from this study did not confirm its presence; however, low-K celadonite may in fact be nontronite.

4.2.2 Celadonite

Celadonite, an Fe-rich dioctahedral mica, is commonly identified in the field by its distinctive bluish-green color. X-ray analyses of celadonite indicate that most samples are intimate mixtures of celadonite and smectite (Appendix II). The observed d-spacings of pure celadonites correspond closely to those of Wise & Eugster (1964).

Representative analyses of celadonite are shown in Table IV-3. For comparison, the average and range in composition of celadonites from the study of Buckley et al. (1978) are shown. It is obvious that celadonites from the present study differ from pure celadonite reported in the literature in two ways. First, in many samples celadonite has excess Si in the tetrahedral site. This may be attributed to the close association of celadonite with amorphous or cryptocrystalline silica. Second, octahedral totals generally range from 4.0 to 5.6, indicating that they are not true dioctahedral clays. A mixture of celadonite with trioctahedral saponite would result in an octahedral total intermediate between diocthedral and triocthedral. Further support for this mixture is the systematic decrease in K_2O content with increasing octahedral totals and thus smectite component (Figure IV-4). The proportions of celadonite and saponite may be quite variable within a single sample as seen in Figure IV-4 where the K_2O and octahedral totals of sample

TABLE IV-3   REPRESENTATIVE CELADONITE & CELADONITE-SAPONITE ANALYSES

	1	2	3	4	5	6	7	
SiO_2	55.85	49.57	52.32	55.80	52.46	52.59	52.55	(56.05–47.23)
TiO_2	0.16	0.23	0.11	–	0.21	0.11	0.14	(0.58–0)
Al_2O_3	2.32	8.14	6.16	0.77	5.55	6.60	3.90	(6.88–0.82)
FeO*	17.72	13.64	16.83	20.01	20.52	17.35	17.20	(22.08–12.42)
MgO	6.18	10.59	6.64	6.13	4.38	10.80	6.34	(9.00–4.28)
CaO	–	0.43	0.17	0.07	0.42	0.60	0.21	(0.68–0.04)
Na_2O	0.10	1.35	0.13	0.04	0.12	0.45	0.15	(0.81–0)
K_2O	9.44	2.37	8.41	8.80	5.80	5.48	9.07	(10.28–7.69)
Total	91.77	86.32	90.77	91.62	89.46	93.98	89.42	

Cation Proportions on the basis of 22 (O, OH)

	1	2	3	4	5	6	7	
Si	8.38	7.55	7.92	8.49	8.07	7.60	7.92	(8.18–7.66)
Al^{iv}	–	0.45	0.08	–	–	0.40	0.10	(0.34–0)
total	8.38	8.00	8.00	8.49	8.07	8.00	8.02	
Al^{vi}	0.41	1.01	1.02	0.14	1.01	0.72	0.58	(1.16–0.04)
Fe	2.24	1.74	2.13	1.39	2.64	2.10	1.40	(2.16–0.09)
Mg	1.40	2.40	1.50	2.55	1.00	2.33	2.00	(2.54–1.42)
Ti	0.02	0.03	0.01	–	0.02	0.01	0.00	(0.02–0)
total	4.10	5.22	4.66	4.08	4.66	5.16	3.98	
Ca	–	0.07	0.03	0.01	0.07	0.09	0.06	(0.20–0)
Na	0.03	0.04	0.04	0.02	0.04	0.13	0.02	(0.10–0)
K	1.82	0.46	1.62	1.71	1.14	1.01	1.75	(1.94–1.46)
total	1.85	0.93	1.69	1.73	1.25	1.23	1.83	

– not detected; * Total iron as FeO; 1 CY-1a 8.78 m, celadonite, vesc; 2 CY-1a 49.57 m, celadonite-saponite, gm, or-br; 3 CY-1a 52.32 m, celadonite-saponite, vein, gr; 4 KG:82:165, celadonite, gm; 5 KG:82:156, celadonite, gm; 6 CY-1 203.95 m, celadonite-saponite, gm; 7 average and range of 13 celadonites from Buckley et al. (1978).

Figure IV-4. Relationship between K_2O (wt%) and octahedral totals for celadonite and celadonite-saponite. Sample KG:83:127 (diamond symbol) illustrates the variation within a single sample.

KG:83:127

K_2O
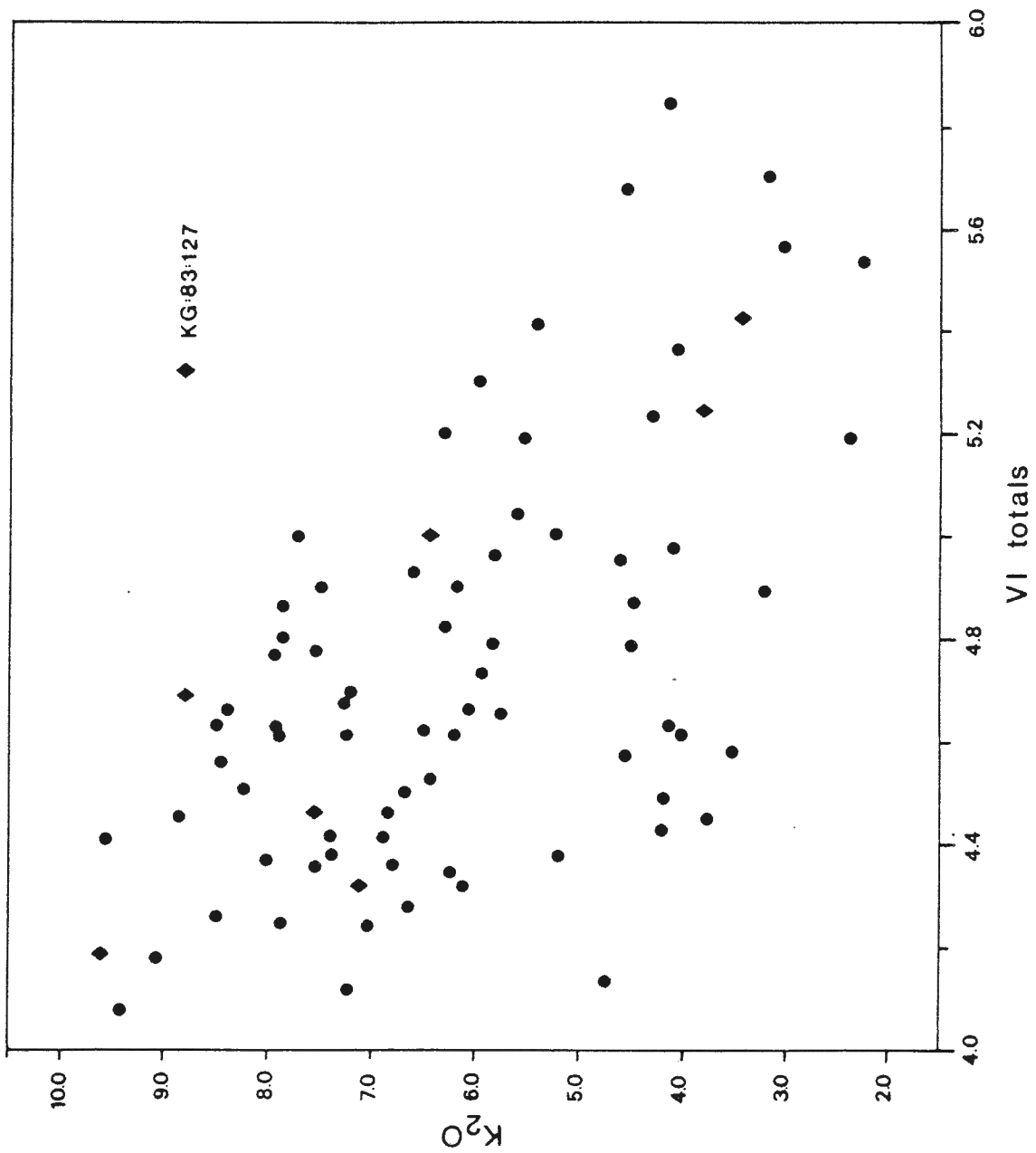
VI totals

KG:83:127 vary from 9.6 – 3.45 wt % and 4.19 – 5.42, respectively. An increase in FeO and K_2O contents characterizes the transition from saponite through celadonite-smectite to celadonite (Figure IV-5). High octahedral totals reported for celadonites from DSDP Leg 37 were also attributed to saponite interlayering (Andrews 1980).

Petrographically identified celadonite has therefore been subdivided into two clay types: celadonite and celadonite-saponite, the latter type being a mixture, in varying proportions, of saponite and celadonite. This should not be considered a strict subdivision, however, as the composition and structure are continuous between the two end member components (Table IV-3).

Celadonite and celadonite-saponite form fibrous or cryptocrystalline masses filling voids and replacing glass in massive and sheet flows in the Sm-Ce-Ze Zone and sporadically in the upper portion of the La-Sm/Ch-Qz Zone. Where mixed with chalcedony or quartz, celadonite has a splintery fracture whereas softer, darker varieties often have a waxy texture. In crystalline flow interiors, celadonite is generally restricted to 1-10-mm-wide alteration fronts which are parallel to fracture surfaces. Concentrations of dark orange clays which mark the outer boundaries of these halos may be mixtures of Fe-hydroxide with saponite or celadonite. Similar halos are common in samples from "in situ" oceanic crust and are believed to represent the earliest stage of alteration (Honnorez, pers. comm., 1985). Celadonite also occurs in irregular patches throughout the groundmass in some flow units.

Figure IV-5. Relationship between K_2O and $FeO/(FeO+MgO)$ (wt%) of clay
minerals: A. Pediaeos River section, B. CY-1 and CY-1a. Symbols as
in Figure IV-2.
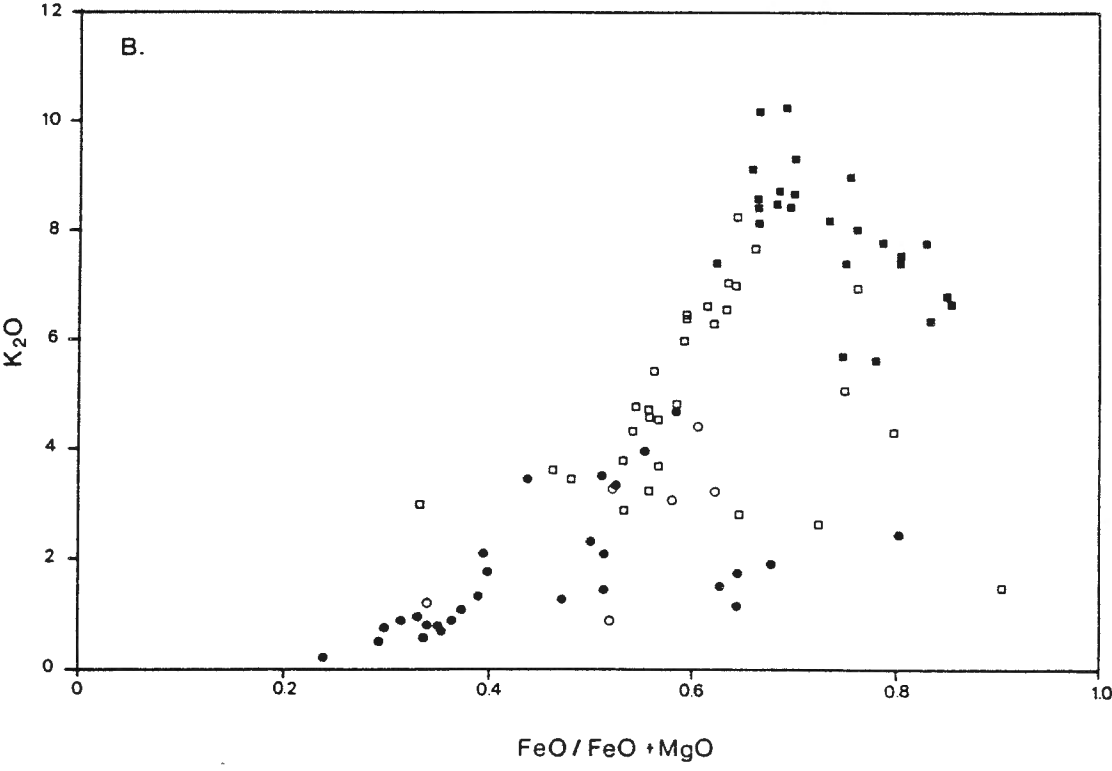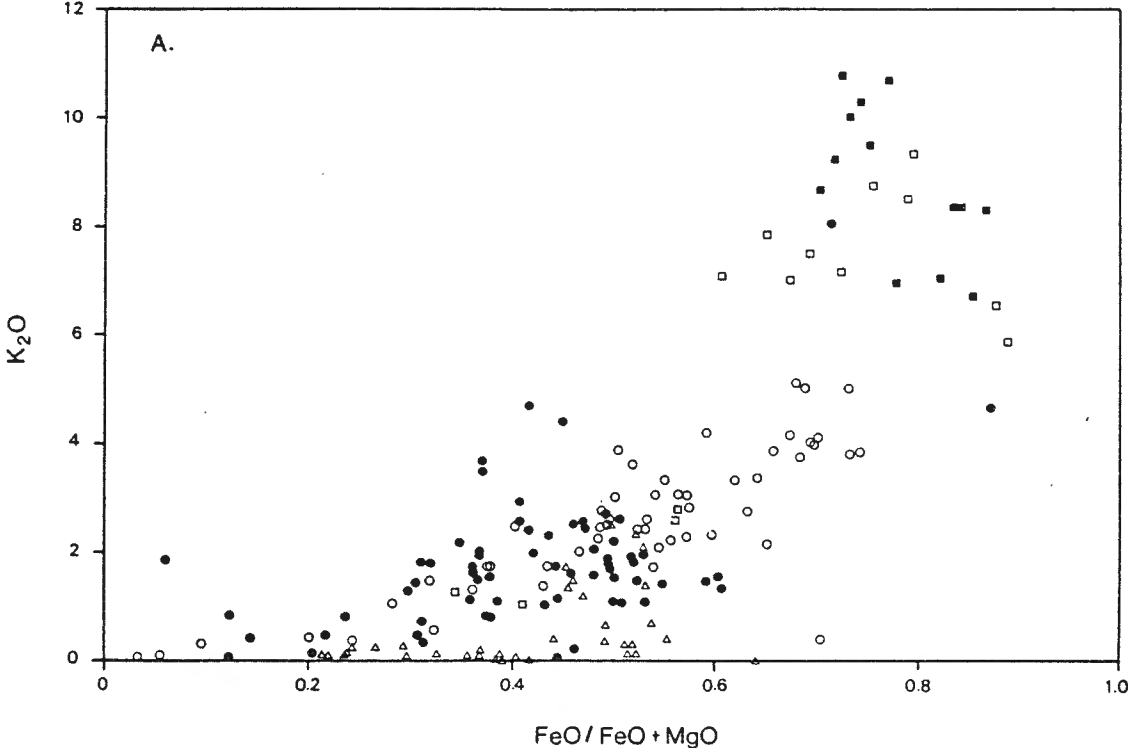
4.2.3 Chlorite

Trioctahedral chlorite has been identified by x-ray peaks at 14.2 and 7.1 A that do not shift after treatment with ethylene glycol (Brindley and Brown 1980). In thin section, chlorite is generally cryptocrystalline to fibrous and pale green. Most chlorites have anomalous blue interference colors although a few display 1st order birefringence.

The majority of chlorites are ferroan clinochlores although there are a few occurrences of magnesian chamosites (Bayliss 1975). Chlorites are slightly more Fe-rich than saponites from this study (Figure IV-6) and show a slight tendency toward increasing Fe content with increasing depth (Figure IV-2c). Within indivudual samples, there is very little variation in $FeO/(FeO+MgO)$ (Figure IV-2c). Chlorite contains up to 1.5 wt% MnO, with individual samples varying by up to 1 % (Figure IV-3). The compositions of void-filling and groundmass-replacing phases are indistinguishable (Table IV-4).

Chlorite is a characteristic mineral of the Ep-Ch-Qz Zone and is sporadically distributed in the Sm-Ce-Ze and La-Sm/Ch-Qz Zones. Chlorite has also been identified in a few samples from the Sm-Pa-Ca Zone of CY-1 (Chudeyev et al. in press; Elsbree 1985).

Physical and structural mixtures of smectite and chlorite have been identified by x-ray analyses and calculated structural formulas. The proportion of these mixtures varies from smectite with minor chlorite to chlorite with minor smectite although mixtures dominated by smectite are most common. Identification of these mixed-layer clays is based upon the common basal 001 and 002 reflections at 14 and 7 Å of
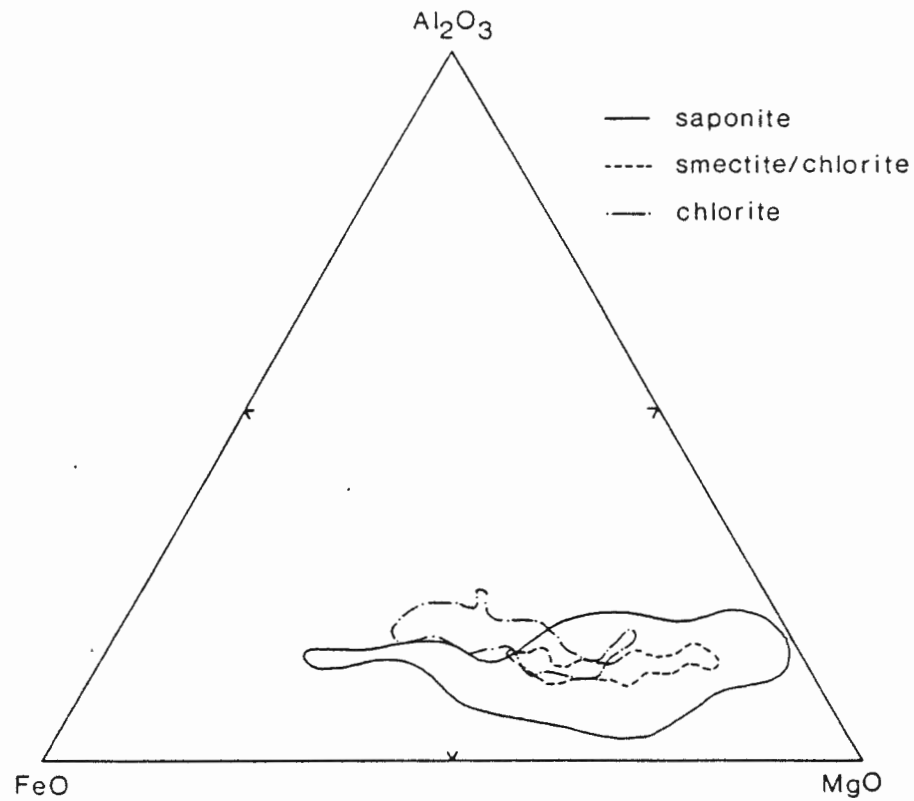
Figure IV-6. Molar AFM proportions of chlorite, smectite/chlorite, and saponite from all field areas. Symbols as in Figure IV-2.

TABLE IV-4   REPRESENTATIVE CHLORITE ANALYSES

	1	2	3	4	5	6
SiO_2	27.37	27.05	28.82	25.97	26.76	27.59
TiO_2	--	--	0.02	--	--	--
Al_2O_3	17.87	16.64	17.38	20.31	18.60	17.84
FeO^*	25.10	30.52	23.47	24.45	23.31	23.36
MnO	0.86	0.42	0.46	1.10	1.16	0.59
MgO	15.98	13.13	17.36	13.82	17.05	16.97
CaO	0.08	0.13	0.15	0.09	0.02	0.05
Na_2O	0.18	--	0.03	0.32	0.02	0.07
K_2O	0.01	0.05	0.02	--	--	--
Total	87.45	87.94	87.71	86.06	86.92	86.47
Cation Proportions on the basis of 28 (O, OH)						
Si	5.80	5.87	6.00	5.58	5.66	5.84
Al^{iv}	2.20	2.12	2.00	2.42	2.34	2.16
total	8.00	8.00	8.00	8.00	8.00	8.00
Al^{vi}	2.26	2.13	2.26	2.73	2.30	2.29
Fe	4.45	5.53	4.09	4.40	4.12	4.14
Mg	5.05	4.24	5.39	4.43	5.38	5.36
Mn	0.15	0.08	0.08	0.20	0.21	0.11
Ca	0.02	--	0.03	0.02	--	0.01
Na	0.07	--	0.01	0.13	0.01	0.03
K	--	0.01	0.01	--	--	--
Total	12.00	12.01	11.87	11.91	12.02	11.94

- not detected; * Total iron as FeO; 1 CY-la 266.60 m, gm; 2 CY-la 464.00 m, gm; 3 CY-la 360.08 m, ves; 4 CY-la 598.15 m, gm; 5 CY-la 598.15 m, ves; 6 CY-la 466.78, gm.

smectite and chlorite, respectively. The 002 peak is most intense for chlorite; the 001 peak is most intense for smectite. Treatment with ethylene glycol further differentiates the two minerals as smectite is an expandable clay mineral and chlorite is not. The proportion of each clay mineral in the mixtures is therefore estimated by comparing the 001 and 002 peak intensities and their shift towards larger d-spacings after treatment with ethylene glycol.

Several varieties of mixed-layer clays have been identified in the rocks from DSDP Hole 504B based upon the relative proportions of smectite and chlorite (Alt 1984). A similar approach has been used to identify four varieties of mixed-layer smectite-chlorite which fill voids or replace glassy margins (Appendix II). In other sections of this thesis, these varieties are not differentiated and are referred to collectively as smectite-chlorite.

It was not possible to characterize the optical properties of each variety. Groundmass-replacing smectite-chlorite is usually indistinguishable from co-existing saponite or celadonite-saponite in thin section. Void-filling phases, however, are commonly fibrous to platy and pale green to brownish-green with 1st to 2nd order birefringence.

Mixtures of smectite and chlorite are also distinguished by calculated structural formulas. For a basis of comparison, structural formulas were calculated for chlorite on the basis of 22 (O, OH). The resulting octahedral total for chlorite is approximately 7.8 whereas the octahedral total of saponite is 6.0. Thus, samples with octahedral totals intermediate between saponite and chlorite are deemed to be mixtures of the two minerals. Mixed-layer smectite-chlorite is present

in samples between 130 m and 350 m depth in the CY-la drillcore where it replaces the groundmass and lines cavities. This interval corresponds to the general depth range for smectite-chlorite outlined by XRD (Figure IV-7).

Distinguishing clay types purely on the basis of structural formulas must be viewed with caution, particularily for samples which are dominated by the smectite component. Mg in excess of that required to satisfy the octahedral sites of 6 possibly should be assigned to the interlayer position (Andrews 1980).

In most cases mineral analyses were not obtained from the same samples used for the XRD study so the composition of each variety has not been characterized. An increase in Al_2O_3 and FeO and a decrease in SiO_2 and MgO characterize the compositional transition from saponite to chlorite (Figure IV-6). Within individual thin sections, smectite-chlorite mixtures are slightly more Fe-rich than co-existing saponites. It is notable that the compositions of smectite-chlorite in the Sm-Pa-Ca Zone in the Cy-1 drillcore are more magnesian than those sampled lower in the lava sequence in the CY-la drillcore. The MnO contents of smectite-chlorite are intermediate between saponite and chlorite (Figure IV-3, Table IV-5).

Smectite-chlorite mixtures are found primarily in the La-Sm/Ch-Qz Zone but also toward the base and top of the over- and underlying zones, respectively. The distribution of smectite-chlorite identified by calculated structural formulas and the different varieties identified by x-ray analysis in the CY-la drillcore is summarized in Figure IV-7. Smectite-chlorite mixtures have also been documented for the Sm-Pa-Ca Zone of CY-1 (this study; Chudeyev et al. in press; Elsbree 1985) and

TABLE IV-5   REPRESENTATIVE SMECTITE-CHLORITE ANALYSES

	1	2	3	4	5	6	7	8
SiO_2	45.70	38.11	35.15	39.19	32.87	33.98	34.75	27.37
Al_2O_3	7.00	9.47	10.9	11.77	12.83	12.50	12.32	17.87
FeO^*	11.21	17.66	19.40	19.12	21.35	8.08	26.01	25.10
MnO	0.14	0.24	0.26	0.28	0.61	0.23	0.30	0.86
MgO	20.08	18.31	17.45	16.88	18.22	26.01	23.91	15.98
CaO	0.97	1.18	0.46	0.34	0.45	0.32	0.51	0.08
Na_2O	0.45	1.08	0.77	0.68	0.79	0.09	1.49	0.18
K_2O	0.98	0.33	1.21	1.89	0.63	0.09	0.07	0.01
Total	86.60	86.14	85.38	89.87	87.14	81.30	86.56	86.14

Cation Proportions on the basis of 22 (O, OH)

	1	2	3	4	5	6	7	8
Si	6.91	6.09	5.75	6.03	5.33	5.48	5.45	4.56
Al^{iv}	1.09	1.78	2.11	1.97	2.45	2.28	2.28	3.44
total	8.00	7.87	7.86	8.00	7.78	7.86	7.73	8.00
Al^{vi}	0.16	—	—	0.17	—	—	—	0.07
Fe	1.42	2.36	2.72	2.65	2.90	1.09	1.73	3.49
Mg	4.53	4.36	4.25	3.87	4.41	6.26	5.59	3.97
Mn	0.02	0.03	0.04	0.04	0.08	0.03	0.04	0.12
total	6.16	6.75	7.01	6.73	7.39	7.38	7.76	7.65
Ca	0.16	0.20	0.08	0.06	0.08	0.06	0.09	0.01
Na	0.13	0.33	0.24	0.06	0.08	0.03	0.45	0.06
K	0.19	0.07	0.25	0.37	0.13	0.02	0.01	—
total	0.48	0.60	0.57	0.49	0.29	0.11	0.55	0.07

— not detected; * Total iron as FeO; [1] CY-la 8.78 m, saponite; [2] CY-la 188.75 m, smectite-chlorite; [3] CY-la 182.95 m, smectite-chlorite; [4] CY-la 250.20 m, smectite-chlorite; [5] CY-la 250.20 m, smectite-chlorite; [6] CY-1 141.52 m, smectite-chlorite; [7] CY-1 254.30 m, smectite-chlorite; [8] CY-la 266.00 m, chlorite.

Figure IV-7. Distribution of smectite/chlorite mixtures in the CY-1a

drillcore, identified by x-ray diffraction. 1 - identified by

calculated structural formulas.
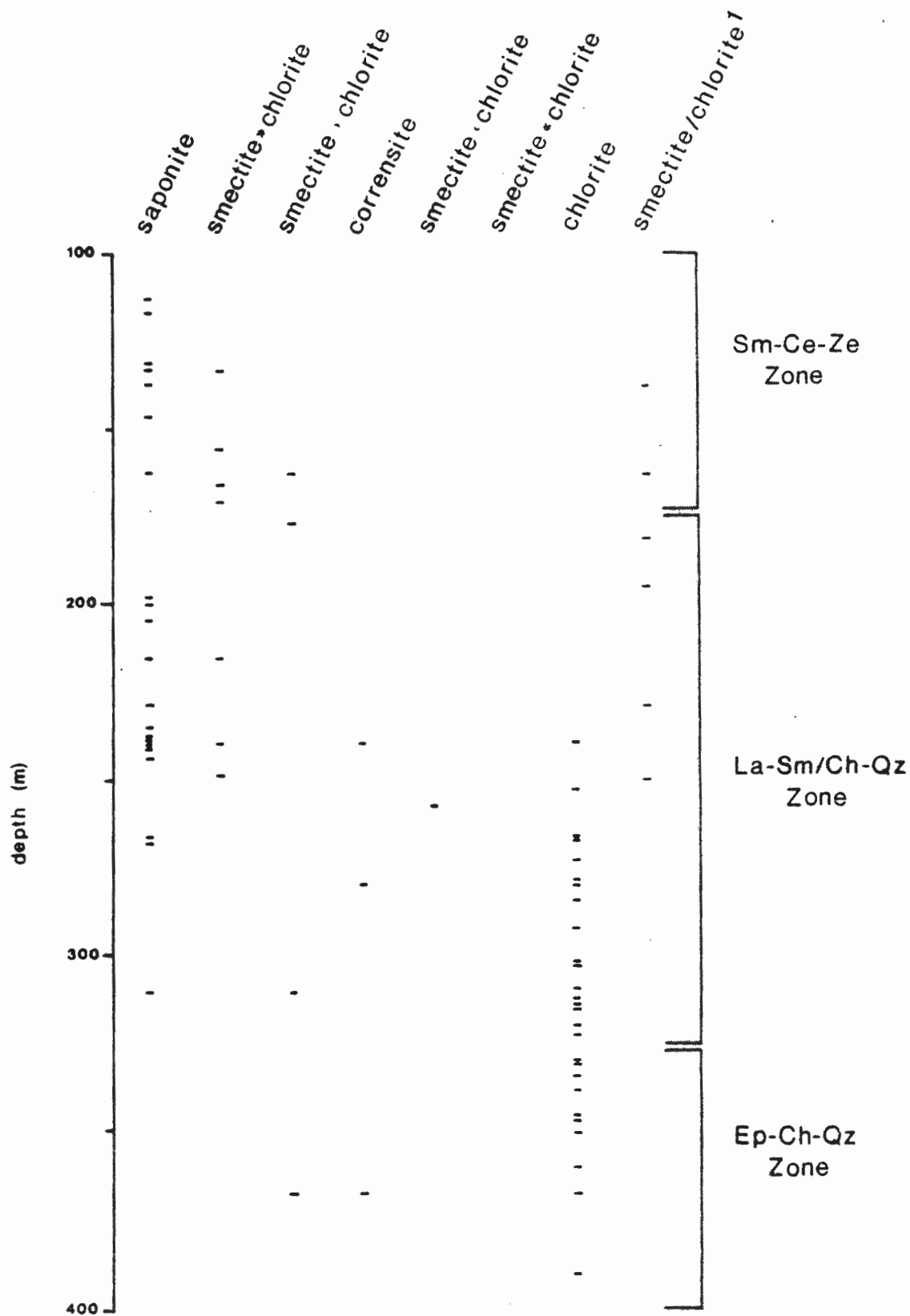
the Sm-Ce-Ze Zone in the Margi area.

4.2.4 Palygorskite, Sepiolite

Palygorskite and sepiolite, both fibrous, magnesian chain
phyllosilicates, occur only as void-filling phases. Palygorskite is
recognised by XRD on the basis of the 10.4, 6.4, and 4 Å peaks which
remain unchanged after treatment with ethylene glycol (Brindley & Brown
1980). This fibrous to platy clay is generally intimately mixed with
calcite. It forms in late-stage veins throughout the Sm-Pa-Ca Zone and
locally in the Sm and Sm-Ce-Ze Zones.

Sepiolite, a platy brown clay, is identified by its 12.1, 4.5,
and 4.3 Å peaks which also do not shift after glycolation (Brindley &
Brown 1980). It forms a thin veneer along cooling surfaces,
particularily in flows but also in pillows and hyaloclastites. It is
present throughout the Sm-Ce-Ze and La-Sm/Ch-Qz Zones and sporadically
in the others.

4.2.5 Zoning in Clay Mineral Aggregates

In the previous sections, the regional distribution and
compositional variation of each variety of clay mineral have been
described. Small scale variations in composition and/or clay type have
also been recognised within vesicles and vugs and in patches of clays
replacing the mesostasis or filling miarolitic voids. Changes in color
and habit across such clay-rich zones generally accompany these
variations.

Celadonite followed by celadonite-smectite followed by saponite
is the characteristic sequence for clay mineral deposition within the

Sm-Ce-Ze Zone (Plate IV-1). The absence of one of these clay minerals is common and reverse ordering occurs in a few samples. It is evident from Table IV-6 that a gradual decrease in Al/Si and Fe/Mg ratios and in the abundance of exchangeable cations accompanies the change in clay types (Table IV-6, analyses 1 - 6). Where saponite occurs alone, it is generally more magnesian toward the core of amygdules or patches in the groundmass with little change in its Al/Si ratio (Table IV-6, analyses 7 & 8).

The depositional relationship between coexisting Al-saponite and saponite was not evident from the studied samples. Within individual samples, no compositional change was observed. Smectite-chlorite in the Sm-Pa-Ca Zone is the last phase to be deposited (Table IV-6, analyses 9 & 10).

Saponite is generally followed by smectite-chlorite in the La-Sm/Ch-Qz Zone. An increase in the Al/Si ratio is the most distinctive compositional change which accompanies this zonation. In many samples, the progressive deposition of smectite-chlorite mixtures with an increasing chlorite component is suggested by an increase in both the octahedral totals and the Al/Si ratios in the last phase to be deposited (Table IV-6, anaylses 11 & 12).

In summary, the characteristic depositional zonations in the clay minerals are:

1. celadonite ⟶ celadonite-smectite ⟶ saponite

2. saponite ⟶ more Mg-rich saponite

3. saponite ⟶ smectite-chlorite

4. smectite-chlorite ⟶ smectite-chlorite with a greater chlorite component

Plate IV-1 A. Typical clay zonation replacing mesostasis in an aphyric

massive flow. Olive-green celadonite-saponite rims orange-brown

saponite (Sample KG:83:060)

B. Platy, green smectite/chlorite (s/c) vesicle filling rimmed by

orange-brown saponite (sa), mesostasis is altered to orange-brown

to yellowish-green saponite (Sample CY-la:182.95 m).

A
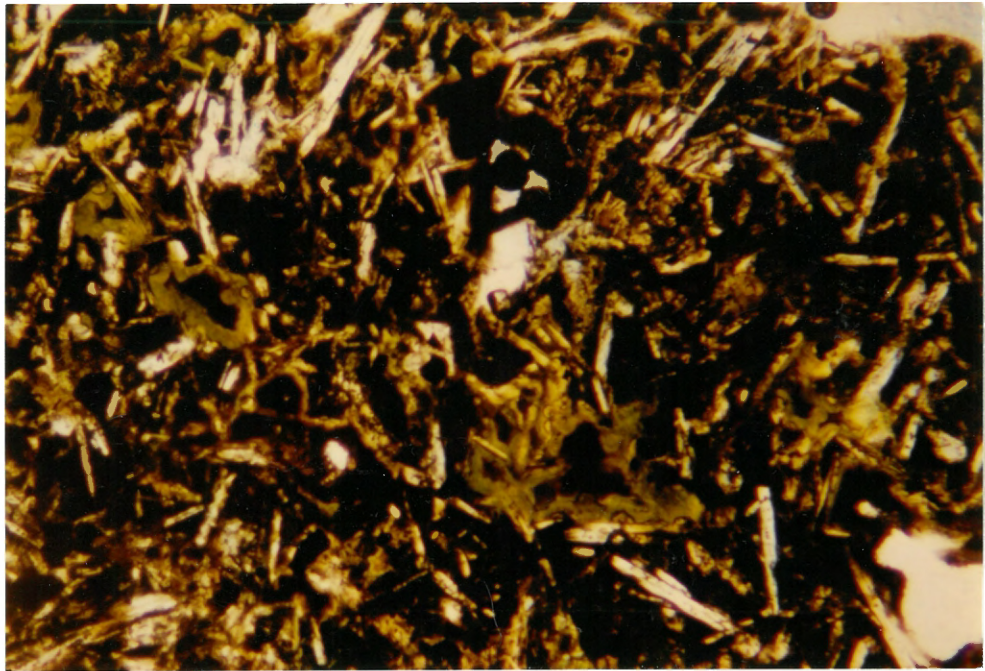
B
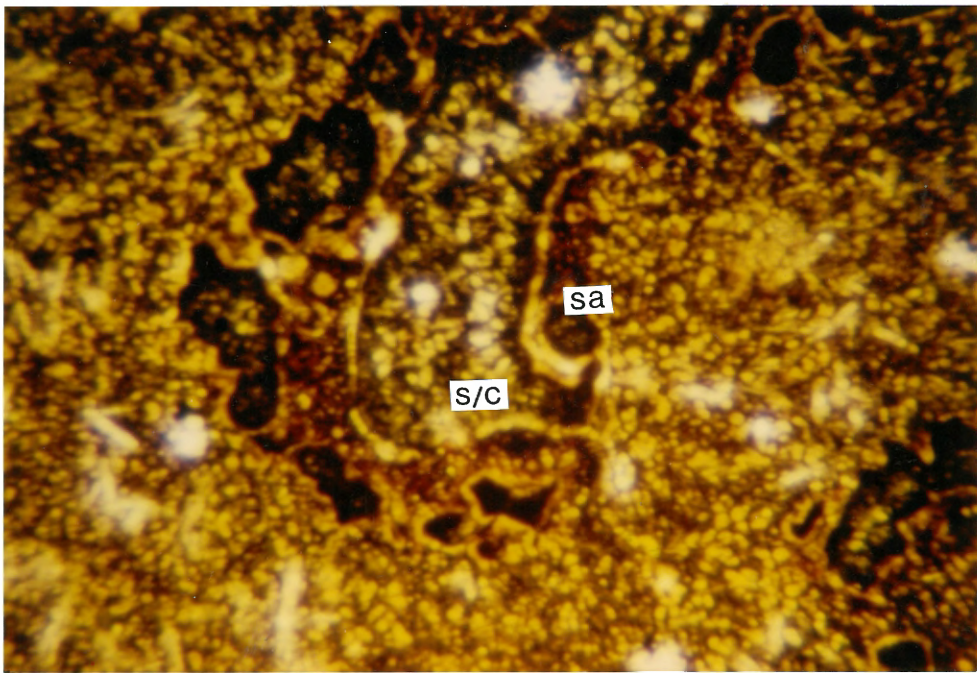
TABLE IV-6   TYPICAL CLAY ZONATION

	1 R	2 M	3 C	4 R	5 M	6 C
SiO_2	55.02	42.86	46.61	56.21	49.92	48.09
TiO_2	0.26	0.10	0.10	0.20	–	0.04
Al_2O_3	3.02	3.59	3.43	7.82	5.30	5.08
FeO^*	17.20	15.51	14.84	17.59	17.01	16.54
MnO	0.05	0.13	0.08	–	0.05	0.06
MgO	8.86	12.11	11.75	5.49	16.08	15.77
CaO	0.46	0.82	0.61	1.52	2.66	1.04
Na_2O	0.01	0.25	0.03	0.48	0.06	0.12
K_2O	8.50	4.32	3.71	6.63	1.92	3.14
Total	93.52	79.72	81.23	95.95	93.00	89.91

Cation Proportions on the basis of 22 (O, OH)

Si	8.11	7.41	7.74	7.94	7.25	7.25
Al^{iv}	–	0.59	0.26	0.06	0.75	0.75
Total	8.11	8.00	8.00	8.00	8.00	8.00
Al^{vi}	0.52	0.14	0.41	1.24	0.16	0.15
Fe	2.12	2.24	2.06	2.08	2.06	2.09
Mg	1.95	3.12	2.91	1.16	3.48	3.55
Ti	0.03	0.01	0.01	0.02	–	–
Mn	0.01	0.02	0.02	–	0.01	0.01
Total	4.67	5.53	5.41	4.52	5.71	5.80
Ca	0.07	0.15	0.11	0.23	0.41	0.17
Na	–	0.08	0.01	0.13	0.02	0.04
K	1.60	0.95	0.79	1.19	0.36	0.60
Total	1.67	1.18	0.91	1.55	0.79	0.81
Al/Si	0.06	0.10	0.09	0.16	0.12	0.12
Fe/Mg	1.08	0.72	0.71	1.79	0.59	0.59

– not detected; * Total iron as FeO; R – rim; M –
middle; C – core; 1 celadonite, 2, 3 or-br
celadonite-saponite (KG:83:085, gm); 4 light gr
celadonite-saponite, 5 gr saponite, 6 or-br
saponite (KG:83:131, vesicle).

TABLE IV-6   (Continued)

	7 R	8 C	9 R	10 C	11 R	12 C
SiO_2	46.48	44.79	37.66	50.98	37.69	31.63
TiO_2	0.10	0.04	0.07	0.11	0.02	0.03
Al_2O_3	4.76	4.88	12.12	5.49	10.06	12.98
FeO^*	11.11	9.45	10.45	18.74	16.93	21.34
MnO	0.11	0.02	0.29	0.03	0.20	0.43
MgO	16.71	20.50	25.20	7.48	16.97	19.90
CaO	1.69	1.23	0.43	0.39	0.17	0.18
Na_2O	—	0.04	0.16	0.22	0.99	0.14
K_2O	1.45	0.71	0.23	5.50	2.15	0.16
Total	84.47	81.72	86.73	89.35	85.28	86.86

Cation Proportions on the basis of 22 (O, OH)

	7 R	8 C	9 R	10 C	11 R	12 C
Si	7.38	7.11	5.75	7.85	6.13	5.17
Al^{iv}	0.62	0.89	2.18	0.15	1.87	2.50
Total	8.00	8.00	7.93	8.00	8.00	7.67
Al^{vi}	0.27	0.02	—	0.85	0.06	—
Fe	1.48	1.25	1.33	2.41	2.30	2.95
Mg	3.95	4.85	5.73	1.72	4.11	4.85
Ti	0.01	—	0.01	0.01	—	—
Mn	0.01	—	0.04	—	0.03	0.06
Total	5.73	6.12	7.07	4.99	6.44	7.89
Ca	0.29	0.21	0.07	0.06	0.03	0.03
Na	—	0.01	0.05	0.07	0.31	0.03
K	0.29	0.14	0.04	1.08	0.45	0.04
Total	0.58	0.36	0.16	1.21	0.79	0.10
Al/Si	0.12	0.13	0.31	0.13	0.31	0.48
Fe/Mg	.037	0.26	0.23	1.40	0.56	0.61

— not detected; * Total iron as FeO; R - rim; M -
middle; C - core; 7 yel-gr saponite, 8 yel-br
saponite (KG:83:033, gm); 9 br smectite-chlorite,
10 yel-gr celadonite-saponite (CY-1 203.95 m, gm),
11 light gr smectite-chlorite, 12 yel-gr
smectite-chlorite (CY-1a 182.95 m, gm).

4.3 ZEOLITES

Zeolites form distinctive assemblages with other secondary minerals throughout the extrusive sequence. They have been identified petrographically and on the basis of their XRD patterns and compositions.

In the Sm-Ce-Ze Zone, clear, well-formed trapezohedral crystals of analcime, commonly accompanied by radiating aggregates of phillipsite, line fractures and vesicles and replace glassy pillow margins. Phillipsite is generally the earliest of these two phases to form. Radiating prisms of natrolite are commonly associated with analcime and occur chiefly in vesicles and vugs. Hexagonal clusters of pinkish-orange gmelinite are intimately mixed with assemblages of chabazite, phillipsite, and analcime. Analcime also forms as a single phase in the Sm-Pa-Ca Zone and in the lower portion of the Sm-Ce-Ze Zone and is associated with laumontite in the La-Sm/Ch-Qz Zone where it is the earliest phase to form.

Analcime is uniform in composition with only minor substitution of Ca and K for Na whereas phillipsite is Na- and K-rich with minor Ca (Figure IV-8, Tables IV-7 & IV-8, analyses 3 & 4). Natrolite analyses are close to the ideal formula with minor substitution of Ca for Na (Figure IV-8, Table IV-8, analyses 1-3). Gmelinite is Na-rich while chabazite is Ca and Na-rich (Table IV-8, analyses 6, 7, & 8, respectively). With the exception of natrolite, the Si content of all these phases is slightly higher than usual (Bohlke et al. 1980; Deer et al. 1962). Low Na contents for many of the Na-rich zeolites may be due to volatilization of alkalis during microprobe analyses.
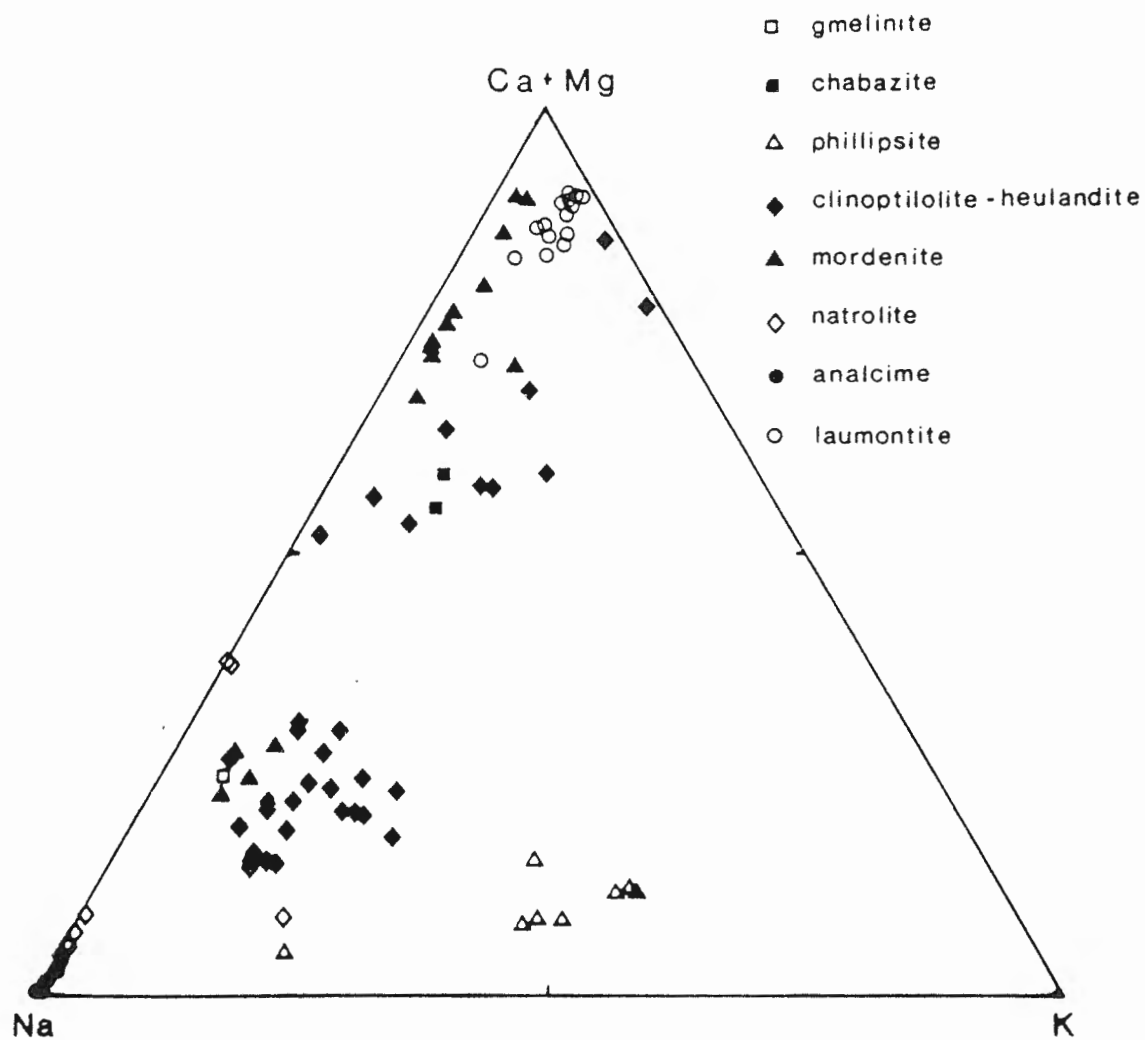
Figure IV-8. Molar Na-K-Ca+Mg proportions in zeolites from all field areas.

TABLE IV-7 REPRESENTATIVE ANALCIME ANALYSES

	1	2	3	4	5	6	7	8
SiO_2	55.86	59.36	61.73	58.39	61.30	55.33	61.37	59.97
Al_2O_3	23.20	22.61	22.95	23.44	22.50	23.24	21.52	22.91
FeO^{*}	0.47	0.01	0.09	–	–	–	–	0.09
MgO	0.31	–	–	–	–	–	–	0.02
CaO	0.01	–	0.04	–	–	–	–	–
Na_2O	11.48	12.54	9.90	9.10	9.88	11.65	8.28	7.44
K_2O	0.08	0.01	0.03	0.02	0.04	–	–	0.02
Total	91.41	94.51	94.64	90.95	93.72	90.22	91.17	90.45

Cation Proportions on the basis of 7 (O, OH)								
Si	2.37	2.43	2.49	2.45	2.50	2.38	2.54	2.50
Al	1.16	1.09	1.09	1.16	1.08	1.18	1.05	1.13
Fe	0.02	–	–	–	–	–	–	–
Mg	0.02	–	–	–	–	–	–	–
Ca	–	–	–	–	–	–	–	–
Na	0.95	1.00	0.77	0.74	0.78	0.97	0.67	0.60
K	–	–	–	–	–	–	–	–
Total	4.53	4.52	4.35	4.35	4.36	4.53	4.26	4.23
Al/Si	0.46	0.45	0.44	0.47	0.43	0.50	0.41	0.45

– not detected; * Total iron as FeO; 1 CY-1a 243.30 m; 2 KG:82:076; 3 KG:82:108; 4 KG:83; 5 CY-1a 229.0 m; 6 CY-1a 138.0 m; 7 CY-1a 164.0 m; 8 CY-1a 8.78 m.

TABLE IV-8   REPRESENTATIVE ZEOLITE ANALYSES

	1	2	3	4	5	6	7	8
SiO_2	47.54	49.73	47.73	57.59	62.26	50.16	52.26	53.22
Al_2O_3*	28.77	26.43	24.64	22.24	19.96	18.64	19.29	19.39
FeO*	0.16	0.04	0.62	0.08	0.15	0.04	0.47	0.96
MgO	–	0.02	0.52	–	–	0.06	0.17	0.05
CaO	0.61	0.21	0.48	0.96	0.24	3.63	2.62	4.63
Na_2O	9.22	7.68	1.81	2.93	5.11	11.20	5.25	2.63
K_2O	–	0.03	4.25	4.28	2.52	1.46	1.23	1.36
Total	86.30	83.70	80.12	88.20	92.13	85.27	81.37	82.37

Cation Proportions

	1	2	3	4	5	6	7	8
Si	24.43	25.75	26.12	11.43	12.18	16.15	25.43	25.53
Al	17.43	16.29	15.89	5.20	4.26	7.07	11.06	10.96
Fe	0.07	0.02	0.28	0.01	0.02	0.01	0.19	0.39
Mg	–	0.02	0.42	–	–	0.03	0.12	0.04
Ca	0.34	0.12	0.28	0.20	0.05	1.25	1.37	2.38
Na	9.19	7.79	4.51	1.13	1.79	6.99	4.95	2.45
K	–	0.02	1.26	1.08	0.58	0.60	0.76	0.83
O	80	80	80	32	32	48	72	72

– not detected; Total iron as FeO; 1 natrolite (KG:83:012); 2 natrolite (CY-1a 14.96 m); 3 natrolite (CY-1a 14.96 m); 4 phillipsite (CY-1 87.40 m); 5 phillipsite (KG:83:190); 6 gmelinite (KG:83:204); 7, 8 chabazite (KG:83:204).

Yellowish-green rosettes of tabular clinoptilolite and heulandite line the edges of fractures and vesicles in massive and sheet flows and are the alteration products of fresh glass in hyaloclastite-rich zones. Clay inclusions are common in these minerals and partial replacement by calcite is locally evident. Clinoptilolite was distinguished from heulandite by its larger molar Si/Al ratio (8.5 - 10 compared to 6) (Mumpton 1960), higher (Na+K)/Ca, and the constancy of the 020 peak upon heating (Boles 1972) (Figure IV-8, Table IV-9). Ca-rich heulandite has only been identified in the Pediaeos River section whereas clinoptilolite is dominant in the remaining areas. Both species occur chiefly in the Sm-Ce-Ze Zone and in the upper part of the La-Sm/Ch-Qz Zone. These minerals are referred to collectively in the rest of this thesis as clinoptilolite.

Fibrous mordenite is typically associated with clinoptilolite in vesicles and in glassy margins where it is the last of the two phases to form. Mixing with quartz, particularly in the La-Sm/Ch-Qz Zone, resulted in higher Si contents than reported in the literature (Deer et al. 1962). Samples from CY-1a are Na+K-rich whereas Ca is the dominant cation in the samples from the Pediaeos and Akaki River sections (Figure IV-8, Table IV-10).

Laumontite is the most common zeolite in the La-Sm/Ch-Qz Zone where pinkish-white prisms primarily fill voids and replace glassy margins. It is commonly associated with quartz, either intermixed or the latest of the two phases to form. XRD analyses indicate that many samples are actually leonhardite, a partially dehydrated variety of laumontite (Coombs 1952). A small change in cleavage angle gives the leonhardite samples a friable texture. Laumontite compositions are

TABLE IV-9   REPRESENTATIVE CLINOPTILOLITE-HEULANDITE ANALYSES

	1	2	3	4	5	6	7	8	9	10
SiO_2	63.99	60.33	62.92	62.41	61.13	66.35	66.52	64.60	63.03	68.17
Al_2O_3*	11.26	12.30	12.75	12.00	12.50	13.59	13.09	11.79	11.37	12.34
FeO	0.06	0.01	0.04	0.12	0.04	0.03	0.13	0.19	0.04	0.06
MgO	0.05	0.17	0.19	0.11	0.23	0.20	0.09	0.18	0.11	0.01
CaO	1.96	2.42	1.50	2.20	1.97	2.90	2.89	3.06	4.92	1.29
Na_2O	7.32	3.85	4.20	4.85	6.55	3.77	1.54	3.30	0.10	3.50
K_2O	0.98	1.60	1.81	1.32	1.77	1.87	1.24	1.10	0.66	1.16
Total	85.62	80.68	83.41	83.01	84.19	88.71	85.50	84.22	80.27	86.53

Cation Proportions on the basis of 72 (O, OH)										
Si	29.19	28.94	29.13	29.13	28.52	28.95	29.59	29.50	29.81	29.97
Al	6.05	6.95	6.96	6.60	6.87	6.99	6.86	6.35	6.34	6.39
Fe	0.02	–	0.02	0.05	0.02	0.01	0.05	0.07	0.02	0.02
Mg	0.03	0.12	0.13	0.08	0.16	0.13	0.06	0.12	0.08	0.01
Ca	0.96	1.24	0.74	1.10	0.98	1.36	1.38	1.50	2.49	0.61
Na	6.47	3.58	3.77	4.39	5.93	3.19	1.31	2.92	0.09	2.98
K	0.57	0.98	1.07	0.79	1.05	1.04	0.70	0.64	0.40	0.65
Total	43.29	41.36	41.82	42.14	43.53	41.67	39.26	41.10	38.87	40.63
Si/Al	8.00	8.36	8.38	8.87	8.77	8.30	8.65	9.45	9.41	9.38

– not detected; * Total iron as FeO; 1 KG:82:156; 2 CY-1a 182.95 m; 3 CY-1a 31.35 m; 4 CY-1a 250.20 m; 5 CY-1a 182.95 m; 6 KG:83:085; 7 KG:83:085; 8 KG:83:166; 9 KG:82:168; 10 KG:82:153.

TABLE IV-10   REPRESENTATIVE MORDENITE ANALYSES

	1	2	3	4	5	6
SiO_2	67.46	70.76	77.30	69.10	66.25	71.59
Al_2O_3*	10.10	10.86	12.11	11.99	9.36	11.62
FeO*	0.15	0.19	0.04	0.06	–	0.07
MgO	0.05	0.06	0.03	0.29	0.04	–
CaO	3.51	3.40	3.52	3.47	1.62	1.76
Na_2O	1.17	0.96	0.28	0.93	4.84	4.70
K_2O	0.09	0.09	0.18	0.90	0.98	0.62
Total	82.53	86.32	93.46	86.86	83.16	90.40
Cation Proportions on the basis of 48 (O, OH)						
Si	20.50	20.49	20.58	20.08	20.36	20.14
Al	3.62	3.72	3.80	4.11	3.39	3.85
Fe	0.04	0.05	0.01	0.01	–	0.02
Ca	1.14	1.06	1.00	1.08	0.53	0.53
Na	0.69	0.54	0.14	0.52	2.88	2.56??
K	0.03	0.03	0.06	0.33	0.38	0.22
Total	26.06	25.92	25.60	26.13	27.54	26.79

– not detected; * Total iron as FeO; 1, 2 KG:82:497; 3 KG:83:176; 4 KG:83:166; 5 CY-1a 43.45 m; 6 CY-1a 163.50 m.

close to the ideal formula with minor subsitution of Na and K for Ca

(Figure IV-8, Table IV-11).

4.4 CARBONATES

Calcite is common throughout the Sm-Pa-Ca Zone and is locally
abundant in the other alteration zones. Generally the latest phase to
be deposited in primary cavities, calcite also forms irregular patches
in the groundmass and replaces phenocrysts. Many calcites have
undergone several stages of growth indicated by successive layers of
euhedral crystals, commonly mantled by a clay mineral.

Calcite is commonly pure in composition with < 1 mole % $MgCO_3$
(Table IV-12). Manganiferous calcite, containing up to 3.5 wt % MnO, is
present throughout the Sm-Pa-Ca, Sm-Ce-Ze, La-Sm/Ch-Qz, and Ep-Ch-Qz
Zones but is most common in Sm-Ce-Ze Zones where the lavas are overlain
by umbers. It is also abundant in samples from CY-1a. Both
manganiferous and pure calcites occur within the same veins and vesicles
(Figure IV-9).

Aragonite was identified at one locality in the La-Sm/Ch-Qz Zone.
Coarse grained aggregates of columnar calcite, sporadically distributed
throughout the lava sequence, may be pseudomorphs after aragonite.

4.5 SILICA

Secondary jasper, chalcedony, opal-C, opal-CT, and clear
colorless quartz form chiefly in the voids of massive flows and dykes.
Jasper, an intimate mixture of quartz and hematite, is commonly
associated with celadonite in zones of intense alteration within massive
flows. Clear, colorless chalcedony and quartz line or fill vesicles,

TABLE IV-11   REPRESENTATIVE LAUMONTITE ANALYSES

	1	2	3	4	5
SiO_2	52.07	56.85	50.29	51.91	54.91
Al_2O_3*	20.13	20.19	19.96	19.71	20.51
FeO	–	0.62	0.10	0.07	–
MgO	–	0.05	–	–	–
CaO	8.23	6.95	8.36	8.01	7.75
Na_2O	0.24	1.90	0.79	0.68	0.34
K_2O	1.13	1.06	0.90	0.98	0.97
Total	81.80	86.62	80.40	80.55	83.73

Cation Proportions on the basis of 48 (O, OH)

	1	2	3	4	5
Si	16.71	17.18	16.51	16.77	16.60
Al	7.61	7.19	7.72	7.50	7.54
Fe	–	0.16	0.03	0.02	–
MgO	–	0.02	–	–	–
Ca	2.83	1.93	2.94	2.77	2.59
Na	0.15	1.11	0.50	0.43	0.21
K	0.46	0.41	0.38	0.40	0.39
Total	27.76	28.00	28.08	27.89	27.33

– not detected; * Total iron as FeO; 1 CY-la
241.4 m, ves; 2 CY-la 241.4 m, gm; 3 CY-la 293.0
m, vein; 4 CY-la 280.7 m, gm; 5 CY-la 266.6 m,
ves.

TABLE IV-12   REPRESENTATIVE CALCITE ANALYSES

	1	2	3	4	5	6
FeO[*]	–	–	–	0.02	0.06	–
MnO	0.02	1.23	2.49	–	–	0.28
MgO	–	0.23	0.05	0.99	1.37	0.28
CaO	64.79	61.44	61.82	59.61	54.54	61.07
Total	64.86	62.90	64.38	60.62	55.97	61.07

– not detected; [*] Total iron as Fe_2O_3; 1, 2 CY-1a 145.30 m; 3 KG:83:012; 4 KG:83:10; 5 KG:82:008; 6 KG:83:076.

Figure IV-9. Variation in MnO content (wt%) in carbonates with depth in
the CY-1 and CY-1a drillcores.
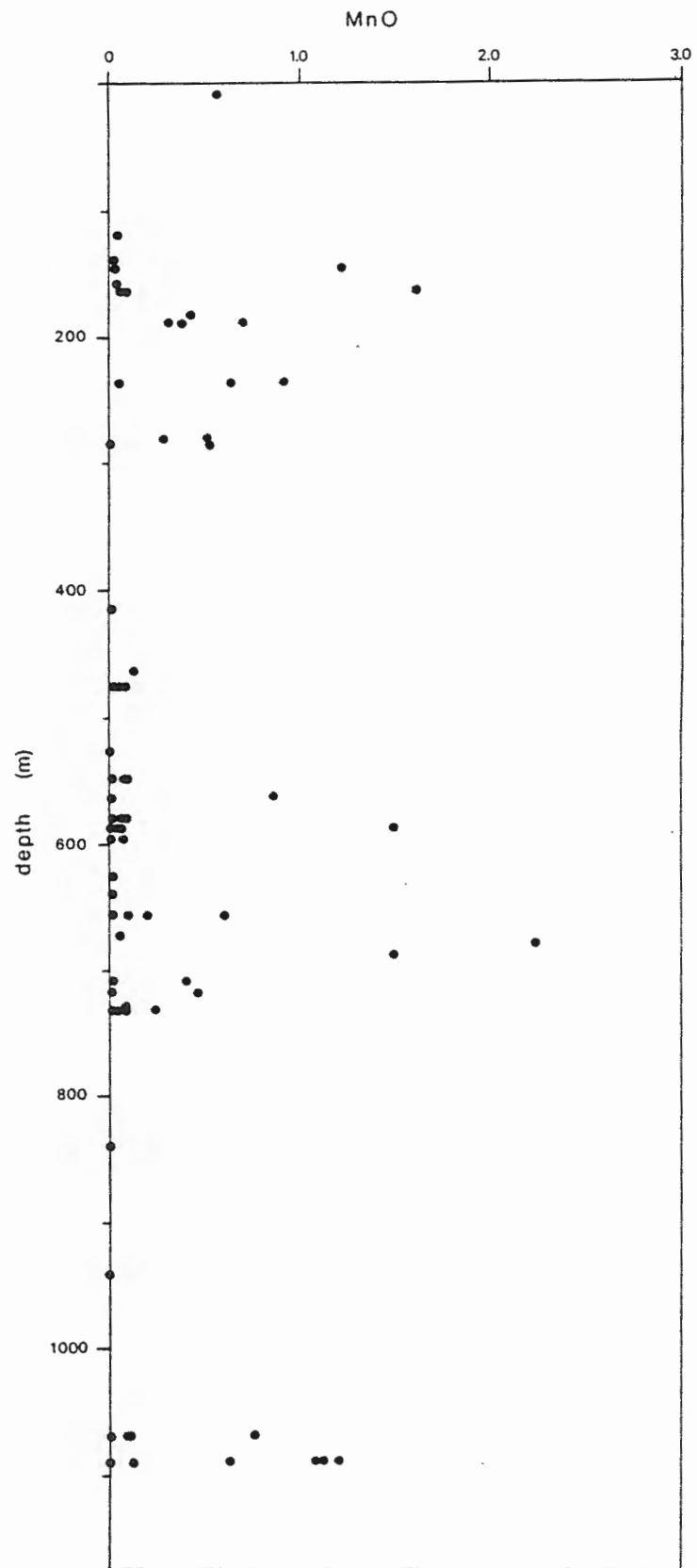
vugs, and fractures, particularly in the Sm-Ce-Ze Zone of the Sequence I lavas and in the La-Sm/Ch-Qz Zone. Late-stage, fine-grained silica is typically present in calcite veins in the Sm-Ce-Ze and La-Sm/Ch-Qz Zones. White to bluish opal-C and opal-CT (classification after Jones & Segnit 1971) form very thin layers on fracture and cooling-joint surfaces in massive and sheet flows. Quartz is abundant in the groundmass throughout the La-Sm/Ch-Qz and Ep-Ch-Qz Zones.

4.6 EPIDOTE

Yellowish-green, blocky to radiating epidote is a common void-filling phase whereas granular epidote is locally distributed in the groundmass of rocks from the Ep-Ch-Qz Zone. It is associated with quartz and chlorite, either mixed or as the latest phase to form. Analysed epidotes are uniform in composition with a narrow range in pistacite component, from 18 to 30 ($Fe/Fe+Al^{iv}$). No difference between groundmass and void-filling phases were observed (Figure IV-10, Table IV-13).

4.7   OTHER MINERALS

4.7.1 Adularia

Adularia, a K-feldspar, lines fractures and vesicles in the Sm-Pa-Ca Zone. A few anhedral grains, which resemble quartz and analcime, were identified by microprobe.

4.7.2 Prehnite

Prehnite has been identified in two samples from the CY-1a drillcore. In these samples, tabular grains with 2nd order

Figure IV-1Ø. Fe/(Fe+Al^{iv}) contents of groundmass-replacing and

void-filling epidote.
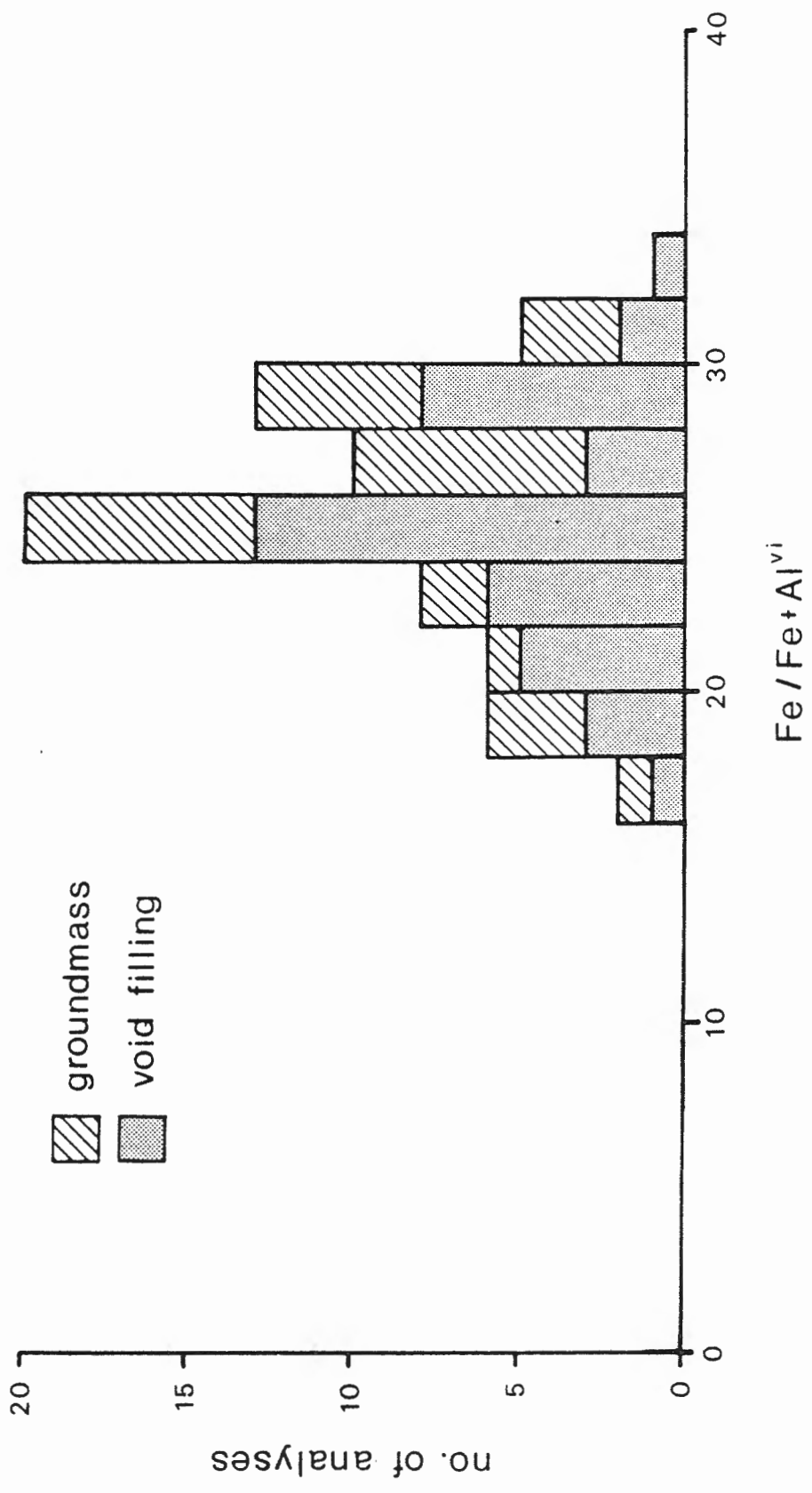
TABLE IV-13   REPRESENTATIVE EPIDOTE ANALYSES

	1	2	3	4	5	6
SiO_2	37.81	38.08	37.54	36.43	37.32	38.79
Al_2O_3*	25.17	24.38	21.36	22.62	25.24	22.91
Fe_2O_3	8.87	9.43	12.56	11.18	8.95	10.71
MnO	0.17	0.18	0.17	0.16	0.27	0.20
MgO	-	-	-	0.04	0.03	0.05
CaO	24.46	24.05	25.16	25.45	25.35	23.34
Total	96.48	96.12	96.79	95.88	97.16	96.00

Cation Proportions on the basis of 12.5 (O, OH)

	1	2	3	4	5	6
Si	3.07	3.11	3.11	3.04	3.02	3.18
Al^{iv}	-	-	-	-	-	-
Total	3.07	3.11	3.11	3.04	3.02	3.18
Al^{vi}	2.41	2.34	2.08	2.23	2.41	2.22
Fe	0.60	0.64	0.87	0.78	0.61	0.73
Total	3.01	2.99	2.97	3.01	3.02	2.95
Mn	0.01	0.01	0.01	0.01	0.02	0.01
Ca	2.14	2.10	2.23	2.28	2.20	2.05
Total	2.15	2.11	2.24	2.29	2.22	2.06
$\frac{Fe}{Fe+Al^{iv}}$	0.20	0.22	0.30	0.26	0.20	0.25

- not detected; * Total iron as Fe_2O_3; 1 CY-1a 632.25 m, vesicle; 2 CY-1a 632.25 m, gm; 3 CY-1a 632.25 m, ves; 4 CY-1a 446.78 m, vein; 5 CY-1a 571.92 m, gm; 6 CY-1a 339.26 m, ves.

birefringence are associated with quartz. A few occurrences in the groundmass have been identified petrographically (Table IV-14).

4.7.3 Fe-hydroxides and oxides

Fe-hydroxides and oxides are present in every alteration zone in the study area but are most abundant in the Sm-Pa-Ca Zone where they give the rocks their characteristic "oxidized" appearance. These phases were identified visually as poor crystallinity prevented XRD identification in most cases. Microprobe analyses indicate that they are intimately mixed with clay minerals (Table IV-15, analyses 1 & 2).

Fe-hydroxides line the margins of vesicles and veins and form irregular patches within the groundmass of many samples, giving the rocks a spotty appearance. Narrow alteration fronts, which are parallel to the outer surface of cooling-units or fractures, are dominantly goethite mixed with clay minerals. Surficial hematite staining on pillows and flows is sporadic throughout the lava sequence where it is commonly associated with celadonite in flow units, and with both celadonite and saponite in the matrix of brecciated units.

4.7.4 Mn oxides

Mn oxides are restricted to the Sm-Pa-Ca and Sm Zones and in the upper part of the Sm-Ce-Ze Zone. Soft, powdery pyrolusite is generally associated with calcite and earthy hematite in late-stage veins in the Margi area. Dendritic Mn oxide commonly forms on the surface of palygorskite and calcite veins.

4.7.5 Sulfides and sulfates

TABLE IV-14   REPRESENTATIVE PREHNITE ANALYSES

	1	2	3
SiO_2	43.46	43.74	43.61
Al_2O_3*	20.14	20.97	20.32
Fe_2O_3	4.44	4.62	4.22
MnO	0.04	0.03	0.08
MgO	-	-	-
CaO	26.48	26.04	26.19
Total	94.66	94.92	94.34

Cation Proportions on the basis
of 11 (O, OH)

	1	2	3
Si	3.09	3.08	3.11
Al	1.69	1.74	1.65
Fe	0.26	0.24	0.26
Mn	-	-	-
Ca	2.02	1.97	2.03
Na	0.01	-	-
Total	7.07	7.03	7.00

- not detected; * Total iron as Fe_2O_3; 1,2 CY-1a 360.08 m, ves; 3 CY-1a 339.26 m, ves.

TABLE IV-15 REPRESENTATIVE ANALYSES OF CLAY MINERALS
REPLACING OLIVINE

	1	2	3	4	5	6	7	8
SiO_2	14.25	11.39	45.95	51.56	54.54	47.99	39.78	44.98
TiO_2	0.04	1.37	–	–	0.02	0.15	0.17	–
Al_2O_3	5.15	4.45	9.70	7.52	12.05	15.59	12.56	12.59
FeO^{*}	57.44	56.62	7.73	20.70	8.92	10.75	13.13	1.14
MnO	0.19	0.33	0.21	0.07	0.15	–	0.06	–
MgO	2.62	1.86	21.47	7.39	12.07	11.40	20.55	24.75
CaO	0.72	0.82	0.86	0.74	2.63	1.30	1.65	2.48
Na_2O	–	0.05	0.08	0.14	0.13	–	–	–
K_2O	0.08	0.09	0.32	4.63	1.17	0.88	–	–
Total	79.77	76.98	86.32	92.75	91.60	88.06	87.90	85.94

Cation Proportions on the basis of 22 (O, OH)								
Si			6.79	7.63	7.51	6.96	6.02	6.48
Al^{iv}			1.21	0.37	0.49	1.04	1.98	1.52
Total			8.00	8.00	8.00	8.00	8.00	8.00
Al^{vi}			0.48	0.94	1.47	1.62	0.26	0.62
Fe			0.96	2.56	1.03	1.30	1.66	0.14
Mg			4.73	1.63	2.48	2.46	4.63	5.31
Mn			0.03	0.01	0.02	–	0.01	–
Total			6.20	5.14	5.00	5.38	6.55	6.07
Ca			0.14	0.12	0.39	0.20	0.27	0.38
Na			0.02	0.04	0.02	–	–	–
K			0.06	0.87	0.21	0.16	–	–
Total			0.22	0.99	0.62	0.38	0.27	0.38

– not detected; [*] Total iron as FeO; 1 KG:82:062, goethite; 2
KG:83:241, goethite; 3 KG:83022, saponite; 4 KG:83:022,
celadonite-saponite; 5 KG:83:033, Al-saponite; 6 KG:83:033,
Al-saponite; 7 KG:82:008, smectite-chlorite; 8 KG:83:008,
saponite.

Pyrite is the only secondary sulfide identified in this study.
It is most common in the La-Sm/Ch-Qz and Ep-Ch-Qz Zones where it is
associated with quartz, chlorite, and epidote in the groundmass and with
quartz, albite, and chlorite or smectite/chlorite on fracture surfaces.
Veins of euhedral to subhedral pyrite, up to 2 cm wide, cut the massive
units in the Ep-Ch-Qz Zone of CY-1a and are locally abundant in field
exposures.

Pyrite with lesser amounts of marcasite and chalcopyrite is
common in all Su-Ch-Qz Zones whereas sphalerite and pyrrhotite are only
present in some deposits (Constantinou 1980).

Gypsum is the only sulfate identified outside the Su-Ch-Qz Zones.
In field exposures, it is primarily associated with gossans whereas in
the Sm-Ce-Ze Zone of CY-1 it forms clear, massive crystals in
late-stage veins.

4.8 ALTERATION OF PRIMARY MINERALS

Olivine is partly to totally replaced by an assemblage of clay
minerals, calcite, and goethite (Plate IV-2). All of the clay mineral
varieties defined in section 4.2, with the exception of chlorite,
replace olivine (Table IV-15). The clay minerals present in the
alteration assemblages are compositionally similar to co-existing
groundmass clays. In the Margi area, olivine is locally altered to a
serpentine group mineral (Table IV-15, analyses 9 & 10). The
distribution of these alteration assemblages is discussed in Chapter
III, and summarized in Table III-1.

Plagioclase is variably altered in all zones except in the
Ep-Ch-Qz Zone where it is completely replaced by albite. In the

Plate IV-2. Primary mineral alteration in an olivine- and

clinopyroxene-phyric pillow. Olivine phenocryst (ol) is altered to

goethite, smectite, and calcite; fresh clinopyroxene (cp); fresh

spinel inclusion (sp); mesostasis is altered to smectite and

calcite (Sample KG:82:008).
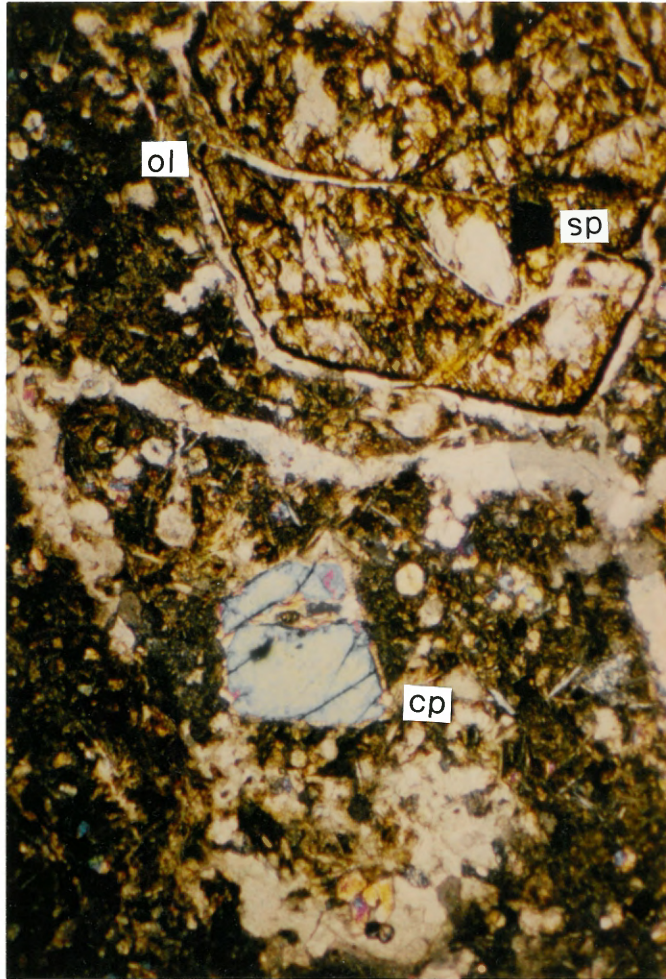
Sm-Pa-Ca, Sm-Ce-Ze, and La-Sm/Ch-Qz Zones, plagioclase may be partly altered to calcite, groundmass clays, or totally replaced by K-feldspar. In addition, plagioclase is locally albitized in the La-Sm/Ch-Qz Zone. There is no consistent pattern in the distribution of these types of alteration. For example, within one thin section, K-feldspar, plagioclase partly replaced by smectite, and fresh plagioclase may be present.

Clinopyroxene remains essentially fresh in all the alteration zones. Celadonite or saponite locally line fractures and coat grain boundaries.

4.9 ALTERATION OF VOLCANIC GLASS

Fresh volcanic glass is present throughout the extrusive sequence and the Basal Group and is only absent in the Sm-Pa-Ca Zone. The degree of preservation of glass is quite variable within a single outcrop, from slightly altered with a thin clay coating to totally replaced by authigenic minerals.

Field studies have shown that the glassy margins of pillows and flows within the Sm-Ce-Ze and Sm Zones are replaced by different assemblages of secondary minerals. Distinction between cooling-unit types was not observed in the remaining zones.

Glassy pillow margins are initially altered to palagonite (residual glass) whereas cracks and vesicles are lined with smectite and phillipsite (Plate IV-3a). As alteration progresses, palagonite is replaced "in situ" by the same authigenic minerals until there is no longer evidence of the residual glass. In many locations, analcime is also associated with glassy pillow margins where it fills intergranular

169

Plate IV-3. A. Glassy pillow margin altered to orange-brown palagonite

(pa) and phillipsite (ph) (Sample CY-1:213.2 m).

B. Glassy massive flow margin altered to celadonite (ce),

clinoptilolite (C), and saponite (Sample KG:83:Ø85).
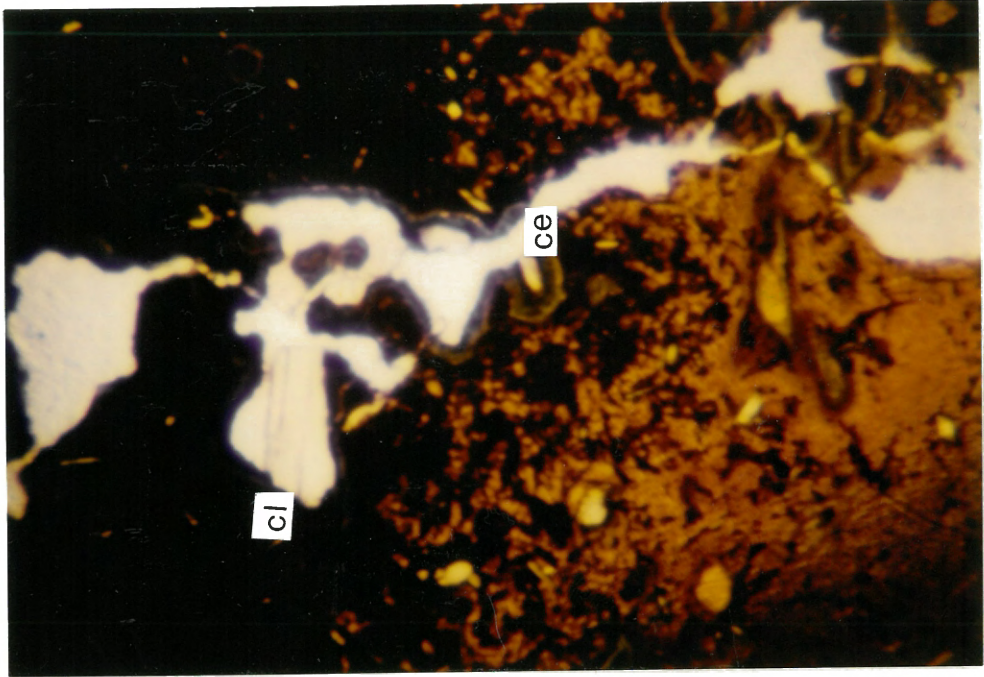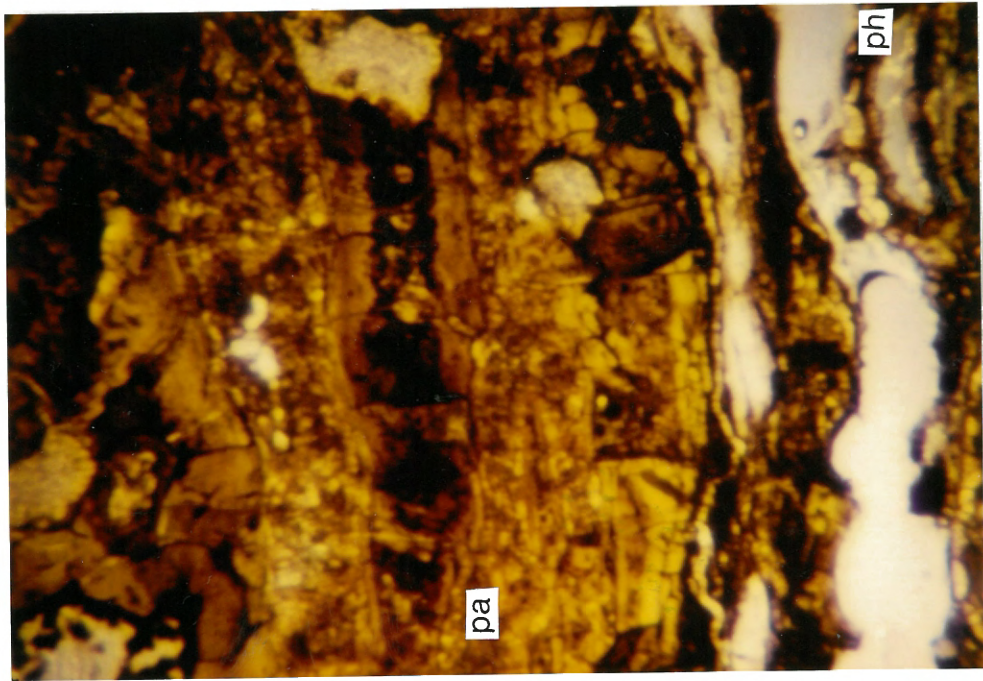
voids. Where associated with phillipsite, it is the latest phase to form. The typical paragentic sequence of secondary minerals replacing glassy pillow margins is, from oldest to youngest:

palagonite $\longrightarrow$ smectite $\longrightarrow$ phillipsite $\longrightarrow$ analcime

In a few cases, a thin layer of Fe-hydroxide separates the palagonite and smectite.

Glassy margins of massive flows are progressively altered in the same stages as pillows but with a different authigenic mineral assemblage (Plate IV-3b). The characteristic paragenetic sequence of secondary minerals replacing glassy flow margins is, from oldest to youngest:

palagonite $\longrightarrow$ celadonite $\longrightarrow$ smectite $\longrightarrow$ heulandite $\longrightarrow$ mordenite

As with the pillowed units, Fe-hydroxide is locally present.

The alteration of glass fragments in hyaloclastite units produces mixtures of smectite, clinoptilolite, celadonite, and phillipsite, in decreasing abundance. It was not possible to determine the depositional relationship between phillipsite and heulandite.

Several glass-palagonite and palagonite-clay pairs, listed in Table IV-16, illustrate the change in composition associated with the palagonization of volcanic glass. Direct comparison of weight percentages shows that CaO, TiO_2, Al_2O_3, and Na_2O are consistently lost from the glass whereas MgO and K_2O are added. These trends may be misleading, however, as the complete alteration assemblage, which includes zeolites, has not been considered and, most importantly, the compositions were not normalized to correct for the effects of dilution and accumulation.

TABLE IV-16   COMPOSITION OF GLASS AND ITS ALTERATION PRODUCTS

	1	2	3	4	5	6	7	8	9	10	11
SiO_2	49.69	50.62	40.47	54.51	63.48	55.79	57.27	51.17	56.32	47.69	44.91
TiO_2	0.65	0.20	–	0.54	0.40	1.11	0.05	0.02	0.63	0.77	0.68
Al_2O_3	16.59	16.27	14.78	15.27	17.56	14.20	5.07	5.14	15.40	14.87	13.98
FeO*3	11.07	12.09	12.65	7.69	4.85	12.94	16.71	19.31	7.72	9.53	9.33
MgO	11.68	9.32	21.86	7.02	7.06	3.66	7.63	11.60	5.96	7.95	7.16
CaO	0.66	0.79	0.63	11.03	1.27	8.38	0.60	0.91	9.50	10.98	11.11
Na_2O	0.71	0.79	0.38	0.18	0.61	2.37	0.03	0.22	1.06	1.24	1.12
K_2O	2.09	2.84	0.10	0.16	0.52	0.34	7.92	4.97	0.21	0.33	0.44
Total	93.30	92.99	91.14	98.19	95.96	98.96	95.36	93.38	97.05	93.61	88.95

– not detected; [*] Total iron as FeO; 1 pale gr palagonite, rim, 2 or-br saponite, mid, 3 br saponite, core (CY-1 213.2 m, vesic); 4 glass, 5 or-br palagonite, (CY-1 435.85 m); 6 palagonite, rim, 7 celadonite, mid, 8 saponite ?, core (KG:83:085); 9 palagonite, core, 10 colorless palagonite, mid, 11 or-br palagonite, rim (KG:83:033).

4.10 SUMMARY

In this chapter, the composition and occurrence of each of the secondary minerals was described. The following is a summary of these observations:

1.   Zeolites and carbonates primarily fill open spaces, often forming beautiful aggregates of crystals in vesicles and vugs whereas clay minerals most commonly replace the mesostasis. Other minerals, like epidote and quartz, occur in both.

2.   Six varieties of clay minerals were defined on the basis of their composition and structure: saponite, Al-saponite, celadonite, celadonite-saponite, chlorite, and smectite-chlorite. However, the boundaries between saponite and Al-saponite, celadonite and celadonite-saponite, and smectite-chlorite are gradational.

3.   Typical depositional sequences for the clay minerals are:

i.   celadonite $\longrightarrow$ celadonite-saponite $\longrightarrow$ saponite

ii.   saponite $\longrightarrow$ more Mg-rich saponite

iii.   saponite $\longrightarrow$ smectite-chlorite

iv.   smectite-chlorite $\longrightarrow$ smectite-chlorite with a greater chlorite component

4.   Compositions of the zeolites are constant with the exception of clinoptilolite and mordenite which are more calcic in samples from the Pediaeos River section.

5.   Typical depositional sequences in the alteration zones are:

i.   Sm-Pa-Ca, Sm-Ce-Ze, and Sm Zones

        celadonite $\longrightarrow$ saponite $\longrightarrow$ zeolite $\longrightarrow$ carbonate

ii.   La-Sm/Ch-Qz Zone

        saponite or smectite-chlorite $\longrightarrow$ quartz $\longrightarrow$ laumontite

iii. Ep–Ch–Qz Zone

chlorite $\longrightarrow$ quartz $\longrightarrow$ epidote $\longrightarrow$ calcite

CHAPTER V

ALTERATION GEOCHEMISTRY

5.1 INTRODUCTION

This chapter documents the effect of alteration on bulk rock compositions in each of the alteration zones represented in the CY-1 and CY-1a drillcores. Two approaches may be used to determine which elements are locally redistributed during alteration and which are lost from or added to the rocks. First, co-variance of bulk rock compositions with indices of alteration and indicators of differentiation provides qualitative estimates of element mobility (summarized in Honnorez 1981). Second, a comparison of fresh and altered bulk rock compositions that corrects for the effects of dilution and the passive accumulation of immobile elements provides a semi-quantitative estimate of elemental flux (Thompson 1983; Colman 1982).

Two sets of samples have been used to estimate the mobility of elements in each of the alteration zones in this study. The first set includes 347 samples from the CY-1 and CY-1a drillcores which were collected for the ICRDG. Because these samples were chosen to study primary compositional variations within the drilled rocks, they are biased toward fresher samples. Major and trace element analyses were performed at Memorial University, the Geological Survey of Canada, and the Open University (Appendix I) using standard XRF, AA and wet chemical techniques. The second set includes 12 samples from four pillows and massive flows collected from the Akaki River section. This data set has been supplemented by data from five cooling-units from CY-1 (Auclair et

175

al. in press).

In the following sections, the qualitative and semi-quantitative estimates of element mobility for the two data sets are presented and compared. The mineralogical expression of the compositional trends for each alteration zone is described. The results are compared with element mobilities determined for "in situ" oceanic crust and other ophiolites.

5.2 PREVIOUS STUDIES

The use of whole rock compositions to deduce the petrogenesis and tectonic setting of the Troodos ophiolite has been hotly debated during the past 15 years (Rautenschlein et al. 1985; Thy et al. 1985; Mehegan & Robinson 1985; Malpas & Langdon 1984; Robinson et al. 1983; Gass 1980; Kay & Senechal 1976; Smewing et al. 1975; Gass & Smewing 1973; Pearce 1975; Pearce & Cann 1973; Miyashiro 1973; Moores & Vine 1971). Despite this intense discussion, there have been comparatively few attempts to study the mobilization of elements during alteration.

In his discussion of the tectonic setting of Troodos, Miyashiro (1973) assumed that most elements were mobile during alteration in the UPL whereas only the alkali elements were mobile in the LPL. In contrast, Smewing et al. (1975) assumed that SiO_2 was enriched during alteration while MgO was depleted and TiO_2, Y, Zr, Hf, and Ce were unaffected. Kay & Senechal (1976) assumed that the major elements were mobile but were unable to find fresh rocks to model the effects of metamorphism. They also suggested that Rb, Ba, Sr, and Ni were affected by metamorphism.

Estimates of element mobility were made by Smewing (1975) through

direct comparisons between fresh and altered samples. The small data set, consisting of 5 fresh samples and 33 altered samples from throughout the ophiolite, made these estimates purely qualitative considering the diversity of rock compositions documented for the massif.

Adamides (1984) also calculated elemental fluxes on a regional scale. Through comparisons of fresh and altered rock compositions and correlation of elements with Zr, an immobile element, he mapped enrichments and depletions in the rocks along the northern flank of the ophiolite on a kilometre scale.

5.3 BULK COMPOSITIONAL TRENDS

Variations in the major and trace element compositions of crystalline rock samples from the CY-1 and CY-1a drillcores with depth reflects both the variable primary composition and the effect of alteration (Appendix III). Composition versus depth plots provide a qualitative estimate of major, minor, and trace element mobility.

In the CY-1 drillcore, SiO_2, Al_2O_3, $Fe_2O_3^*$ (total Fe), MgO, MnO, TiO_2, and H_2O+ contents show no consistent trends toward enrichment or depletion with depth (Appendices III-1a, 1b, 1c, 1f, & 1g). Scatter in the data, particularly in the upper 75 - 100 m where picrites and olivine-phyric pillows are common, primarily reflects the variation in modal mineralogy (Figure II-7). In contrast, the $Fe_2O_3/(Fe_2O_3 + FeO)$ ratio of the rocks consistently decreases with depth indicating that the uppermost lavas are more oxidized (Appendix III-1e). The alkali and alkaline earth elements in the upper 300 m show consistent trends. K_2O, Sr and Rb are enriched and Na_2O is depleted relative to the samples from

below 300 m (Appendices III-1d & III-1h). CaO contents are quite variable in the upper 100 m, whereas below this depth they are constant (Appendix III-1c). The variation in CO_2 content with depth is similar to K_2O (Appendix III-1f). The transition elements Cu, Zn, Cr, Ni, V, Y, and Zr show no consistent variation with depth (Appendices III-1i, 1j, & 1k). Cr and Ni, compatible elements in olivine, show considerable scatter in the upper 100 m reflecting the variation in the modal abundance of olivine (Appendix III-1i).

In summary, variations in the composition of the CY-1 drillcore with depth suggest that the bulk rock compositions in the upper 300 m have been modified, with respect to the lower 200 m, as follows:

GAINS: K_2O, CaO, $Fe_2O_3/(Fe_2O_3 + FeO)$, CO_2, Sr, Rb, Ba

LOSSES: Na_2O, SiO_2

Below this depth, the concentration of all elements remains relatively constant. The depth of 300 m, which marks a change in element mobility, correlates well with the boundary between the upper Sm-Pa-Ca and lower Sm-Ce-Ze alteration zones in CY-1.

Samples from the upper 200 m of the CY-1a drillcore are similar in composition and mineralogy to the rocks from the lower 175 m of the CY-1 drillcore and show the same trends in element mobility. At depths greater than 200 m, these trends are not necessarily continuous.

Al_2O_3 and $Fe_2O_3{}^*$ show no consistent enrichment or depletion throughout the drillcore (Appendices III-2a & III-2c). SiO_2, MnO, and MgO are similarily consistent to approximately 350 m depth, below which, SiO_2 and MnO are slightly enriched and MgO is slightly depleted (Appendices III-2a, 2c, & 2g). CaO contents are constant to 150 m, decrease slightly over a 125-m-interval, and remain constant to the

bottom of the core (Appendix III-2c). K_2O, Rb, and Sr contents are consistent to a depth of 350 m, although slightly higher than in the samples from the lower 175 m of CY-1, below which K_2O and Rb are depleted and Sr shows considerable scatter (Appendices III-2d & III-2h). Na_2O is progressively enriched with depth in the drillcore (Appendix III-2d). Zn and Cu contents are comparable to the CY-1 samples to 200 m and 500 m depth, respectively (Appendix III-2i). Below these depths, they are enriched relative to the overlying rocks by factors up to 10. Cr and Ni contents are generally low throughout the core with a few scattered high values (Appendix III-2g). Pb is enriched relative to the CY-1 samples but shows no enrichment or depletion with depth (Appendix III-21).

In summary, the variation in composition of the CY-1a drillcore with depth suggests that bulk rock compositions have been modified as follows:

    0 - 200 m: GAINS: K_2O, Rb, Na_2O

                    NO LOSSES

  200 - 350 m: GAINS: K_2O, Na_2O, MnO, Ba, Rb, Zn

                    LOSSES: CaO, Sr

  350 - 700 m: GAINS: SiO_2, MnO, Na_2O, Cu, Zn

                    LOSSES: MgO, K_2O, CaO, Rb, V, Ba, Sr

The depth intervals which mark different element mobilities in the CY-1a drillcore correlate well with the boundaries between the alteration zones. The corresponding alteration zones with increasing depth in CY-1a are the Sm-Ce-Ze, La-Sm/Ch-Qz, and Ep-Ch-Qz Zones, respectively.

Qualitative estimates of the degree or intensity of alteration and element mobility during alteration correlate with the oxidation

state, H_2O+, and CO_2 content of a given sample with the weight % content of the remaining elements (Honnorez 1981). These estimates assume that increases in the $Fe_2O_3/(Fe_2O_3 + FeO)$ ratio, H_2O+, and CO_2 contents, relative to fresh rock, reflect an increase in the intensity of alteration and that elements which correlate with any of these parameters are mobile during alteration.

Correlation between the $Fe_2O_3/(Fe_2O_3 + FeO)$ ratios of the CY-1 samples with the other elements suggests that K_2O, Rb, Sr, Ba, and Na_2O were mobile during alteration (see Figure V-1 for K_2O, MgO, Na_2O, & Sr). Positive correlation with the $Fe_2O_3/(Fe_2O_3 + FeO)$ ratio indicates that K_2O, Rb, Ba, and, to a lesser extent, Sr were added to the rocks during an oxidizing stage of alteration whereas the negative correlation with Na_2O indicates that it was added to the rocks during a less oxidizing stage. These results are in agreement with the predictions from the CY-1 depth plots.

The negative correlation of both CaO and CO_2 with H_2O+ suggests that $CaCO_3$ was not precipitated during hydration (see Figure V-2 for K_2O, CaO, CO_2, & Sr). The remaining elements do not correlate with H_2O+ content (Figure V-2), suggesting that bulk rock H_2O+ contents are not as sensitive to alteration as the oxidation state.

In contrast, CO_2 contents of the CY-1 samples correlate well with the major elements (see Figure V-3 for SiO_2, Na_2O, CaO, & K_2O). The negative correlation of Al_2O_3, SiO_2, MgO, FeO, and Na_2O with CO_2 indicates that these elements were removed during a period of carbonate deposition. The remaining major, minor, and trace elements are independent of CO_2.

It was not possible to estimate element mobility using alteration

Figure V-1.   Sr, MgO, Na$_2$O, and K$_2$O versus Fe$_2$O$_3$/(Fe$_2$O$_3$ + FeO) in

samples from the CY-1 drillcore.   Major elements are in weight %;

trace elements are in ppm.
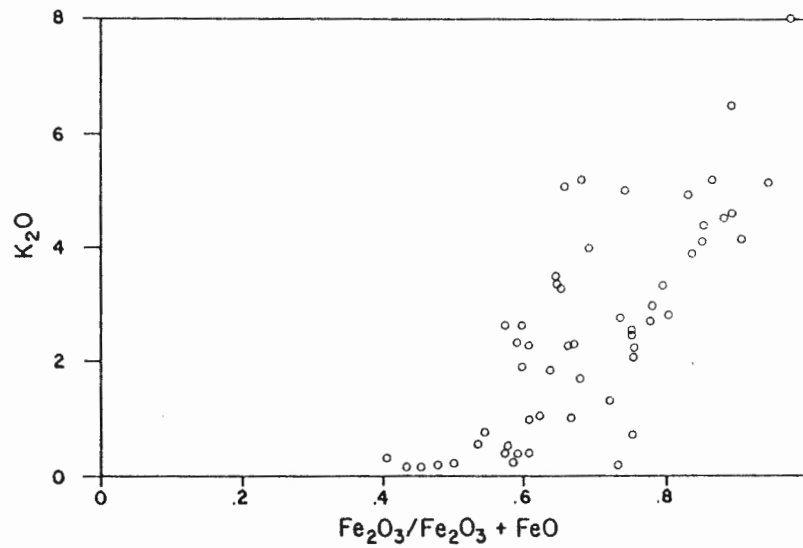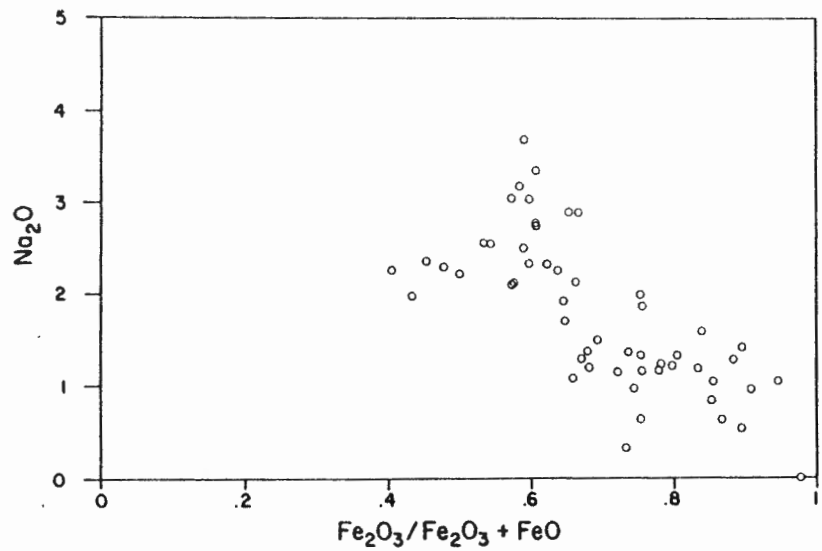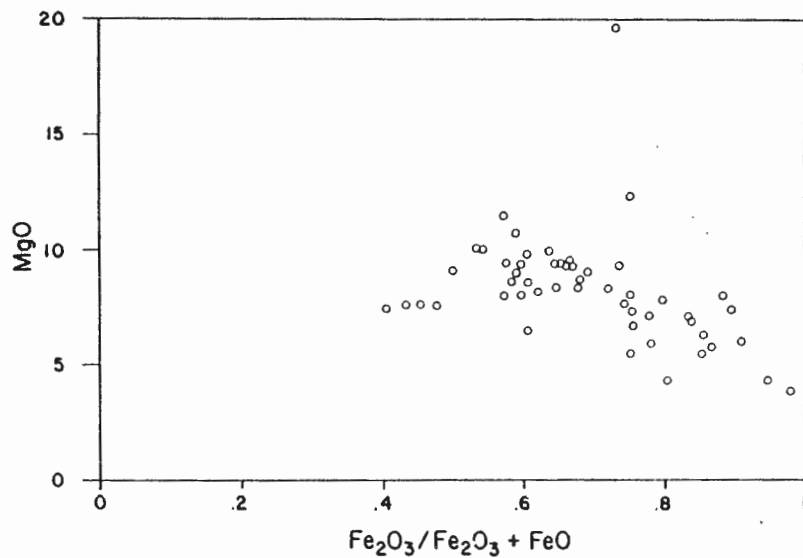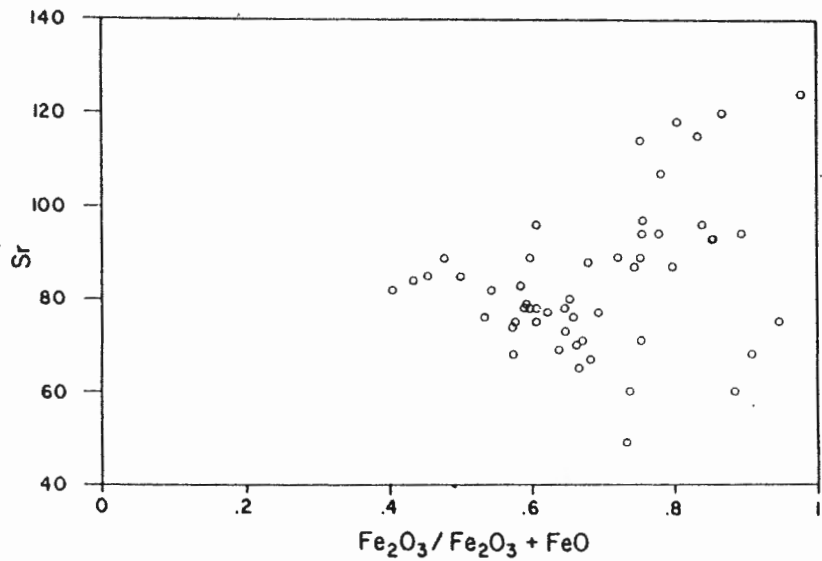
Figure V-2. Sr, K_2O, CaO, and CO_2 versus H_2O+ in samples from the CY-1 drillcore. Major elements are in weight %; trace elements are in ppm.
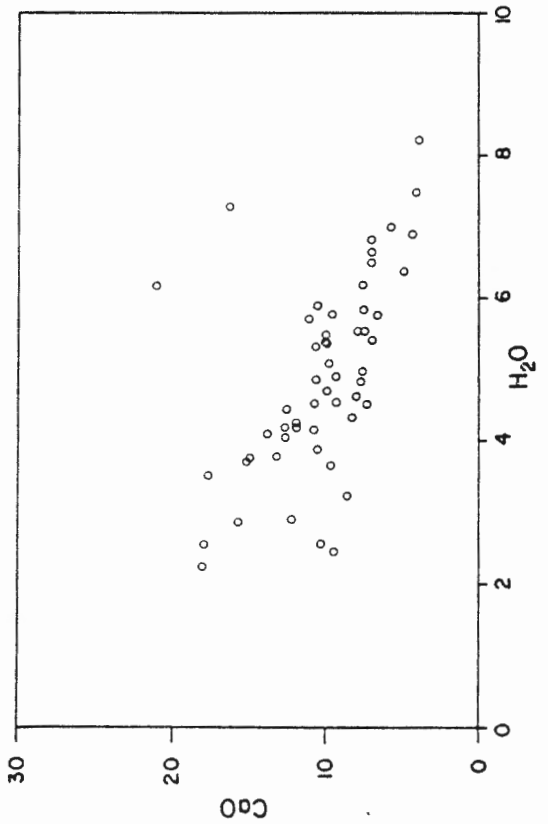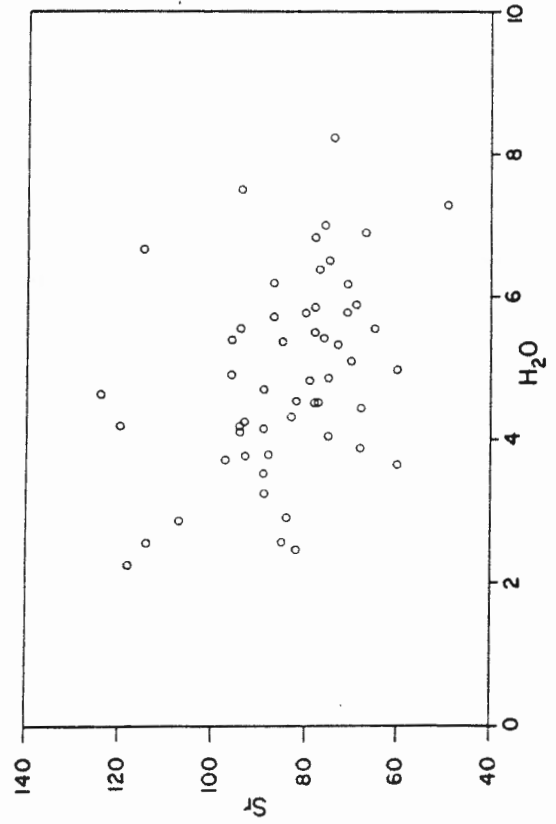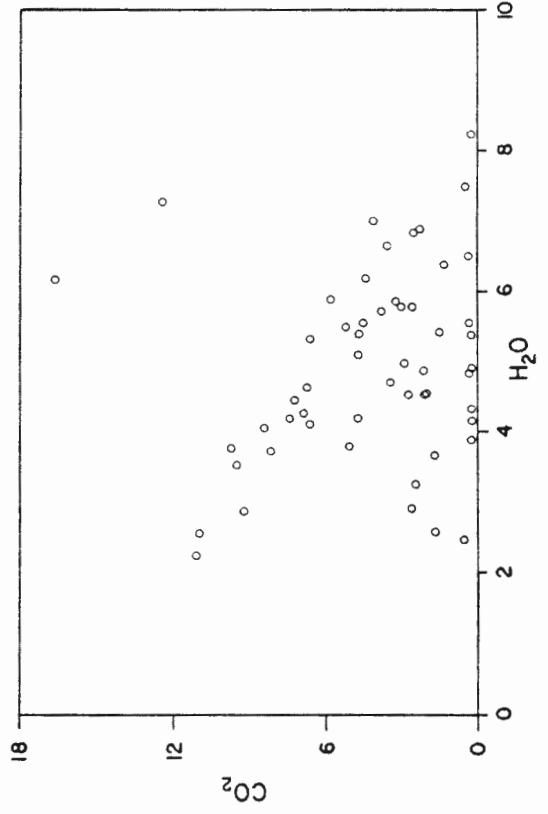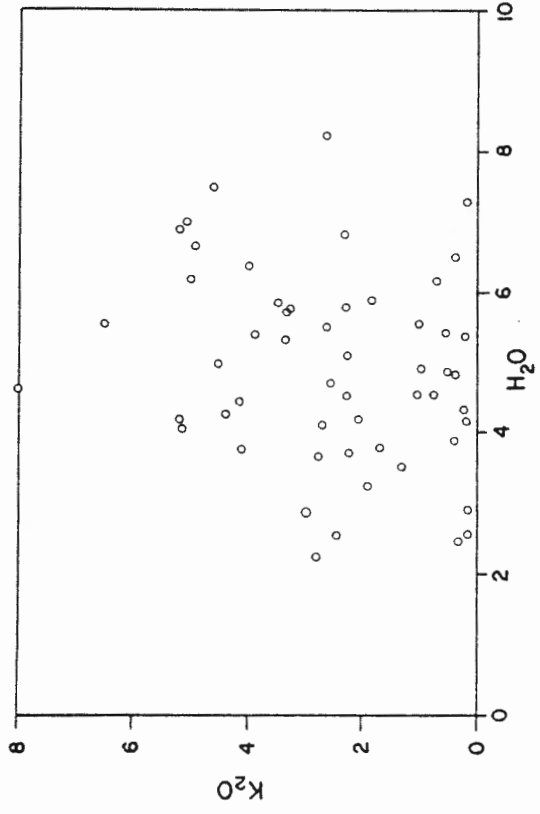
Figure V-3. SiO_2, Na_2O, CaO, and K_2O versus CO_2 in samples from the CY-1 drillcore. Major elements are in weight %.
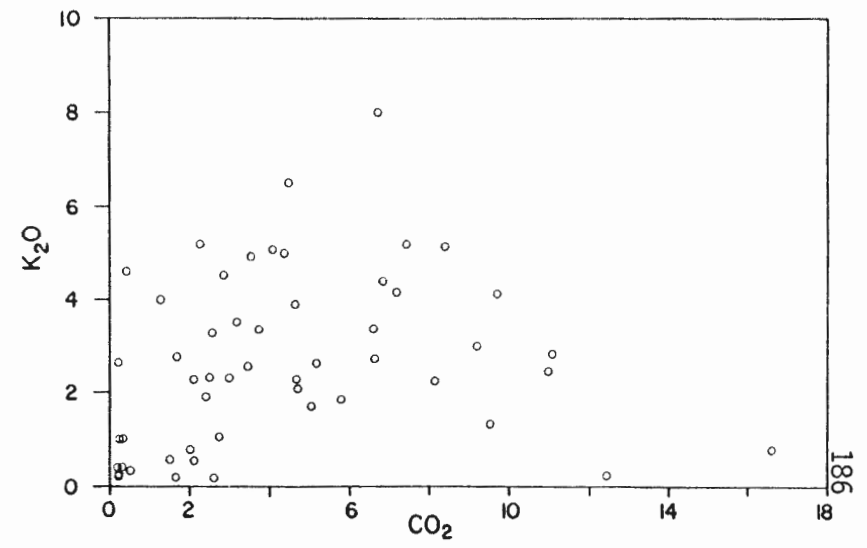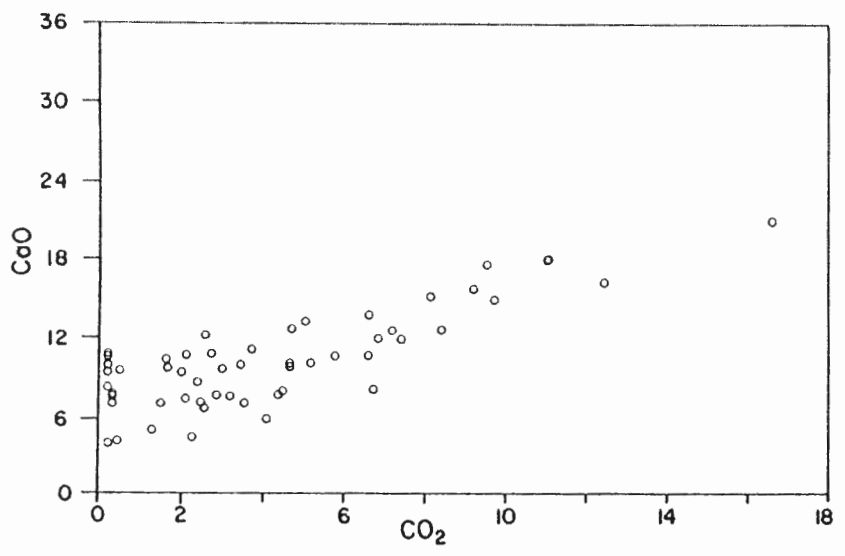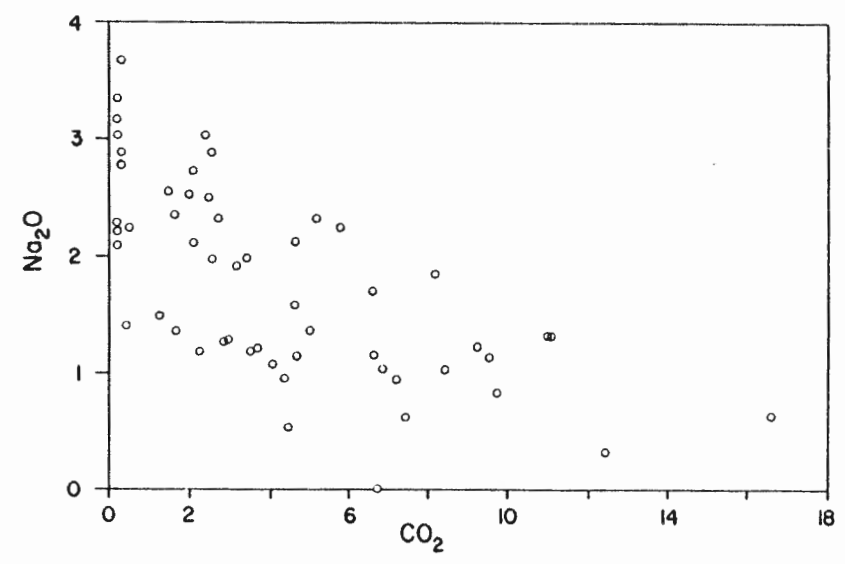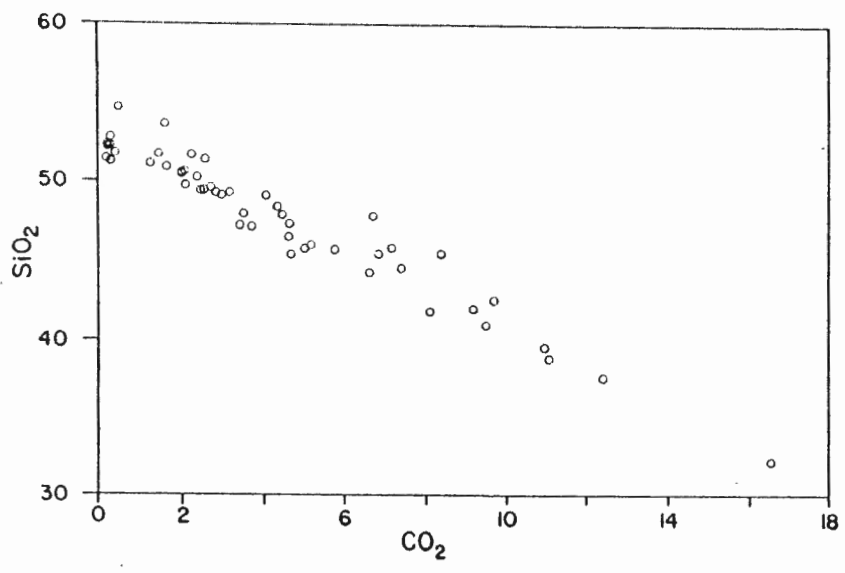
indices for the CY-1a samples because H_2O+, CO_2, Fe_2O_3, and FeO contents were not measured.

5.4 ELEMENTAL FLUXES

The most common approach to evaluate the mobility of elements in drilled and dredged oceanic rocks compares the composition of altered rocks to their unaltered equivalents. It is assumed that elements gained by the rock were removed from seawater and that elements lost from the rocks were taken up by seawater.

Semi-quantitative estimates of element mobility have been determined for the ICRDG samples from the CY-1 drillcore and for a set of samples from several cooling-units from CY-1 and the field. All samples belong to the high MgO-high SiO_2 geochemical suite and occur in either the Sm-Pa-Ca or Sm-Ce-Ze Zone. Elemental fluxes have not been calculated for samples from the CY-1a drillcore as appropriate fresh rock equivalents were not available.

In the following section, the flux calculations and their assumptions are described and the results of the calculations for each of the alteration zones are presented.

5.4.1 Theory and Assumptions

Most methods which calculate elemental fluxes assume that volume remains constant and/or that elements such as TiO_2, Al_2O_3, and FeO are immobile during alteration (Colman 1982; Hendricks & Whittig 1968; Gresens 1967; Barth 1948). The most common method employed in studies of altered oceanic rocks does not consider changes in volume. Fluxes are calculated assuming that either TiO_2 or Al_2O_3 are passively

accumulated during alteration due to the gains and losses of the other elements. The compositions of the altered samples are normalized to either constant TiO_2 or Al_2O_3 and compared with their unaltered equivalents. These results are often converted to a constant volume using density data for both the altered and unaltered rocks (Thompson 1983; Humphris & Thompson 1978).

In this study, elemental fluxes for each sample were calculated twice, correcting first for the accumulation of TiO_2 and second for Al_2O_3. The following formula was used:

$$(F)^*C_n^A - C_n^F = \text{flux (g/100g)} \qquad (5.1)$$

Where F is the ratio of weight % TiO_2 or Al_2O_3 in the fresh rock to that in the altered sample; C_n is the concentration of element n in weight % of the fresh (F) and altered (A) samples (Colman 1982). The compositions of all samples were first normalized to 100 % on a volatile-free basis. No correction for volume change was made.

This method was chosen for several reasons. First, it has been demonstrated that TiO_2 is immobile during alteration (see previous section). This assumption is further supported by the absence of Ti-rich secondary phases in the alteration assemblages of all the alteration zones. It has also been demonstrated in previous studies that Al_2O_3 is immobile (Alt & Emmerman 1985; Humphris & Thompson 1978). The presence of aluminous phases such as clays and zeolites, however, suggests that local mobilization did occur. Second, the preservation of igneous textures and the partial replacement of phenocrysts suggests that no significant change in volume occurred during alteration. The

author does acknowledge, however, that small-scale volume changes may be important. Third, the formula listed above is the most common method used in studies of "in situ" oceanic rocks and therefore permits direct comparison with the results of this study.

5.4.2 Definition of Unaltered Fresh Rock

The most difficult task in calculating compositional changes due to alteration is choosing the "fresh", unaltered equivalent of an altered rock. The presence of fresh glass throughout the entire extrusive sequence of the Troodos ophiolite makes this task appear easy. Studies of whole rock – glass pairs have shown, however, that glass compositions are not representative of crystalline pillow interiors as crystal accumulation significantly modifies initial liquid compositions (c.f. Staudigel et al. 1979), (Appendix III-1).

For this study, a suite of petrographically "fresh" bulk rock samples was chosen to represent the original lava compositions of the high MgO – high SiO_2 suite (Bailey 1984; Mehegan, unpublished data, 1985). The TiO_2 content of this suite of "fresh" rocks was used to delineate several compositional groups which represent the range in composition of the CY-1 samples (Appendix IV). TiO_2 was chosen for two reasons. First, it is an incompatible element in basic rocks and thus is concentrated in the liquid phase. Although most samples contain trace amounts of titanomagnetite, the high correlation between TiO_2 and Zr in the suite of "fresh" rocks indicates that the TiO_2 contents of the Troodos lavas were not affected by crystal accumulation. Second, several studies of variably altered oceanic rocks have shown that TiO_2 is not affected by low temperature alteration (Colman 1982; Finlow-Bates

& Stumpft 1981; Pearce & Norry 1979; Wood et al. 1979; Floyd &

Winchester 1978; Smith & Smith 1976; Pearce & Cann 1973; Cann 1970).

Caution must be used, however, as gains and losses of more mobile

elements in a sample result in the passive accumulation of TiO_2. Thus,

the TiO_2 content of the altered rock may no longer reflect its original

concentration.

5.4.3 Variation In Elemental Fluxes With Depth In CY-1

Elemental fluxes calculated for the CY-1 samples using the TiO_2

and Al_2O_3 correction factors are consistent in magnitude and direction.

The minor variation in the TiO_2 and Al_2O_3 fluxes with depth supports the

assumption that these elements are immobile during alteration. The

magnitude of the Al_2O_3 fluxes, calculated using the TiO_2 correction

factor, also indicates that the choice of standards based on the TiO_2

content of each sample was reasonable.

It is evident that SiO_2 is consistently lost from the samples

above 275 m depth with the magnitude of the flux decreasing with

increasing depth, from 12 to <5 g/100g. Below this depth, the SiO_2 flux

has no consistent trend. The $Fe_2O_3^T$ flux has no consistent trend in

either magnitude or direction with depth (Figure V-4). The Na_2O and MgO

fluxes are variable in the upper 200 m. Below this depth, Na_2O are

consistently added to the rocks whereas MgO has no consist trend

(Figures V-5 & V-6). In contrast, the rocks in the upper 300 m of CY-1

are enriched in K_2O relative to the fresh rock suites (Figure V-5). The

degree of enrichment decreases systematically with depth, from 5 to

<1 g/100g. Below 300 m, the enrichment is consistent. CaO fluxes are

Figure V-4. Variation in SiO_2, Al_2O_3, and FeO^* fluxes with depth in the

CY-1 drillcore. Fluxes are in g/100g.
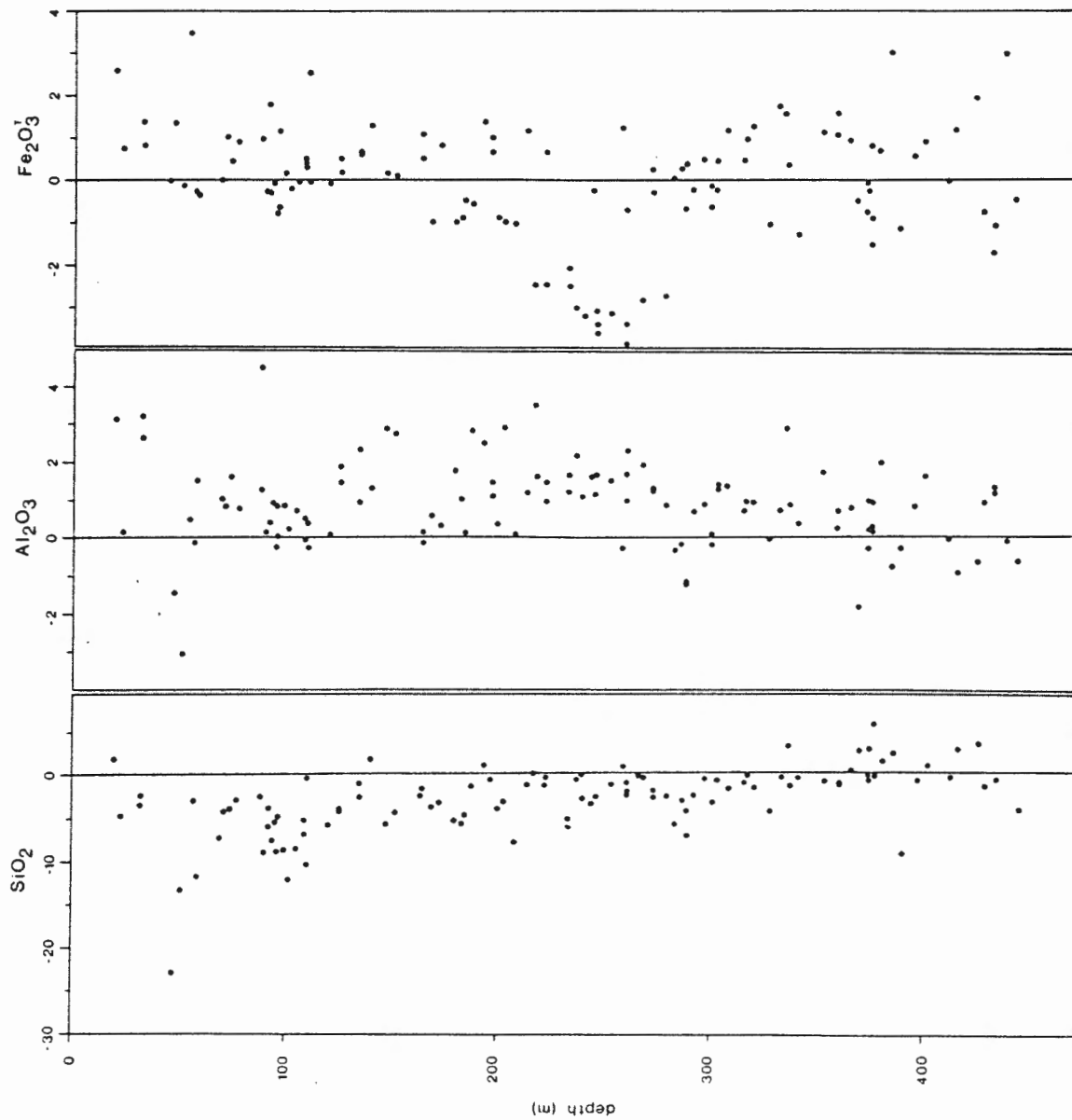
Figure V-5. Variation in CaO, Na_2O, and K_2O fluxes with depth in the CY-1 drillcore. Fluxes are in g/100g.

194
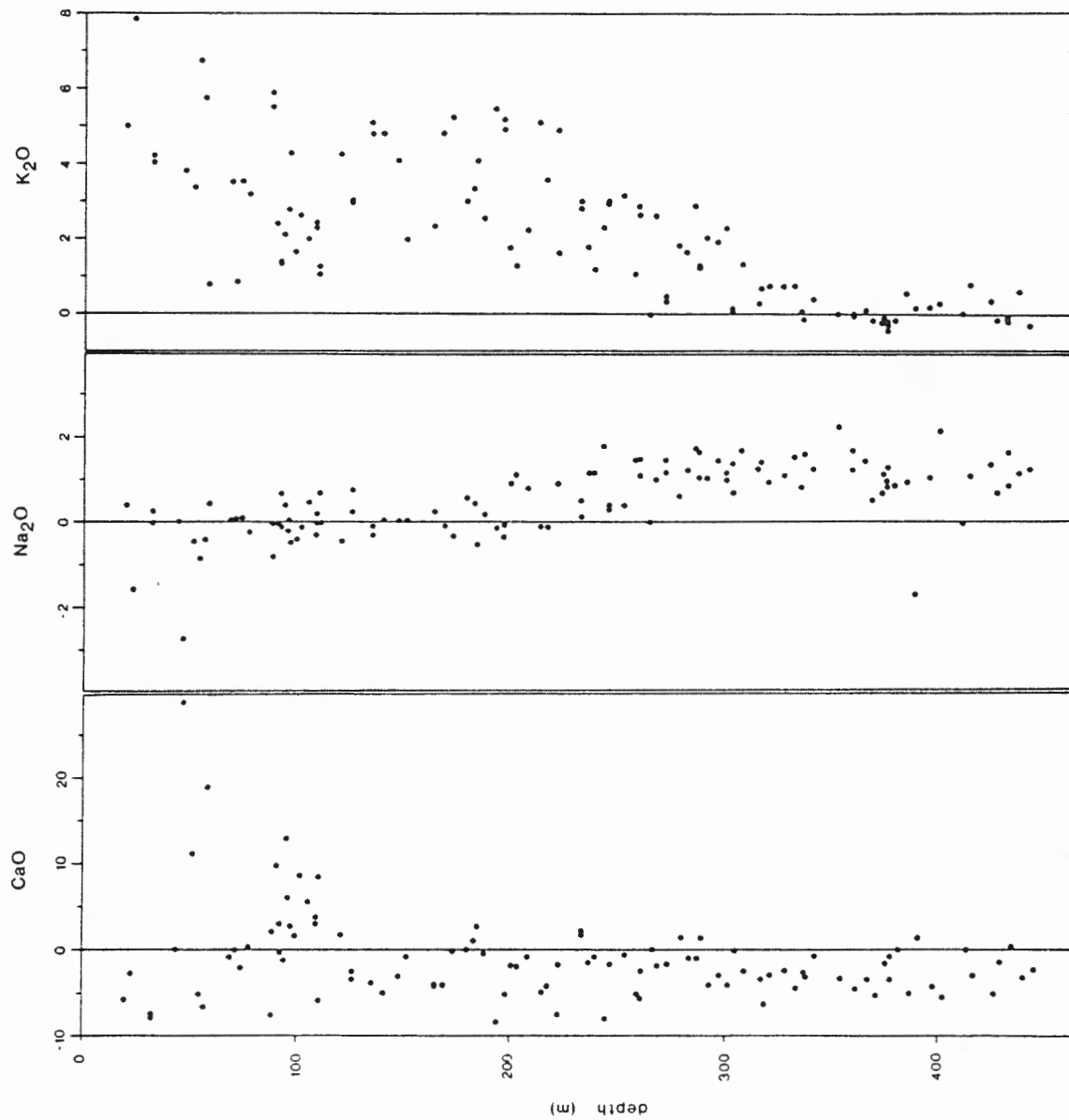
Figure V-6.   Variation in MgO, Rb, and Sr fluxes with depth in the CY-1

drillcore.   MgO fluxes are in g/1ØØg; Rb and Sr fluxes are in 10^{-4}

g/1ØØg.
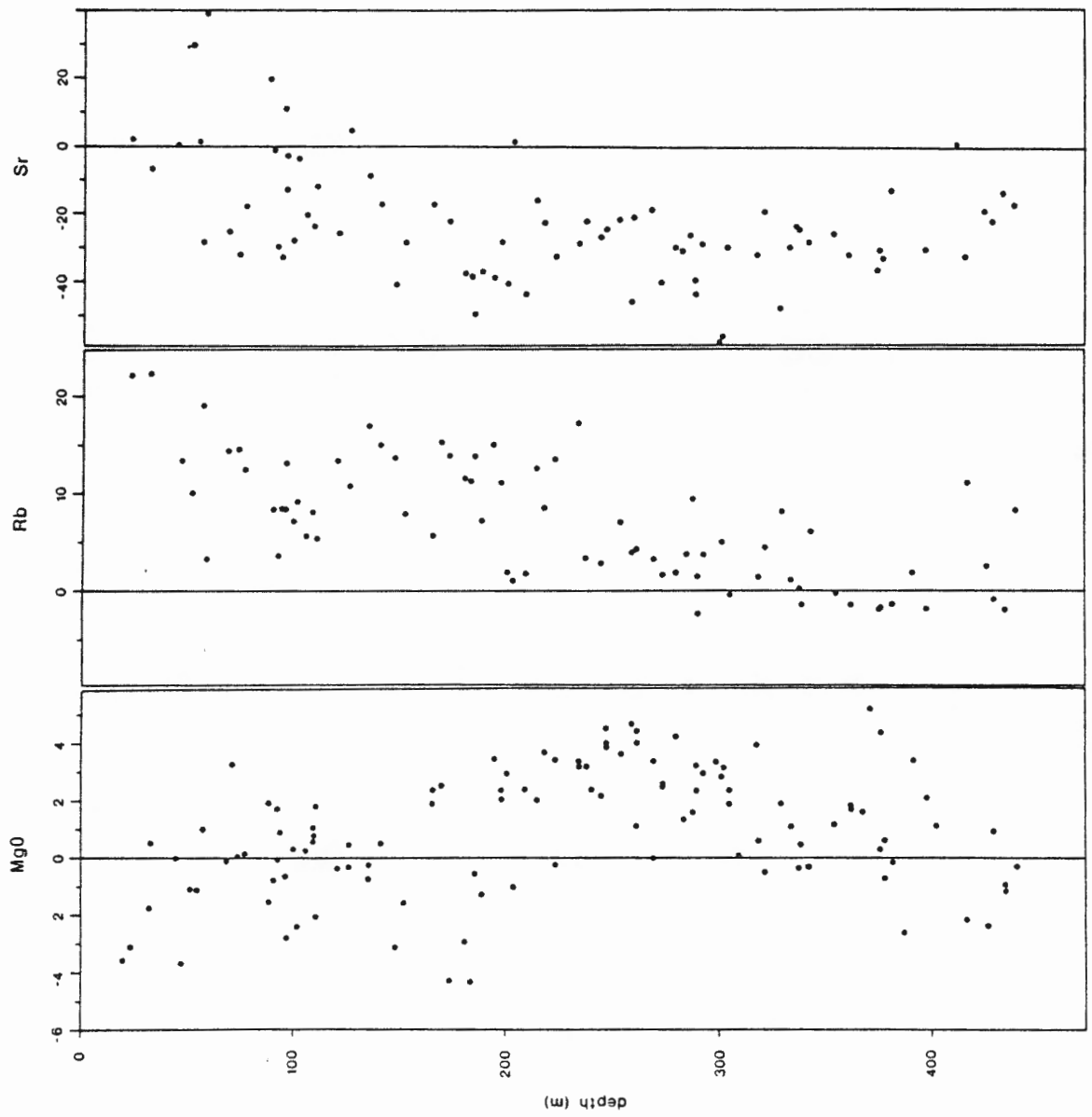
scattered around the zero reference line in the upper 110 m whereas below this depth CaO is consistently lost from the rocks (Figure V-5). MnO and P_2O_5 fluxes are small and have no consistent trend.

The alkali and alkaline earth elements are the most mobile trace elements (Figure V-6 & V-7). Rb is enriched (5 to 50 $\times 10^{-4}$ g/100g) in the upper 275 m of the CY-1 samples; below this depth there is no systematic trends in either magnitude or direction. Sr is consistently depleted throughout the core. Of the transition elements, Zr and Y are the least mobile showing minor scatter around the zero reference line (see Figure V-7 for Zr). V, Cu, and Zn are consistently depleted but show no systematic variation in magnitude with depth (see Figure V-7 for Zn).

The boundary between the Sm-Pa-Ca and Sm-Ce-Ze alteration zones in the CY-1 drillcore occurs at approximately 275 m depth. The average elemental fluxes and ranges for these zones are listed in Table V-1. It is apparent from the flux calculations that distinct compositional trends are associated with each zone (Table V-1). K_2O and Rb are enriched in the Sm-Pa-Ca Zone and Na_2O and MgO are enriched in the Sm-Ce-Ze Zone. SiO_2 and Al_2O_3 are more mobile in the Sm-Pa-Ca Zone and relatively unchanged in the Sm-Ce-Ze Zone. In contrast, CaO is relatively unchanged in the Sm-Pa-Ca Zone whereas it is depleted in the Sm-Ce-Ze Zone. With the exception of Rb, there is no significant change in the mobility of the trace elements in either zone.

5.4.4 Compositional Variation Within Individual Cooling-Units

Compositional variation within nine cooling-units sampled from the CY-1 drillcore and the Akaki River section has been determined.

Figure V-7. Variation in Ba, Zn, and Zr fluxes with depth in the CY-1 drillcore. Fluxes are in 10^{-4} g/100g.
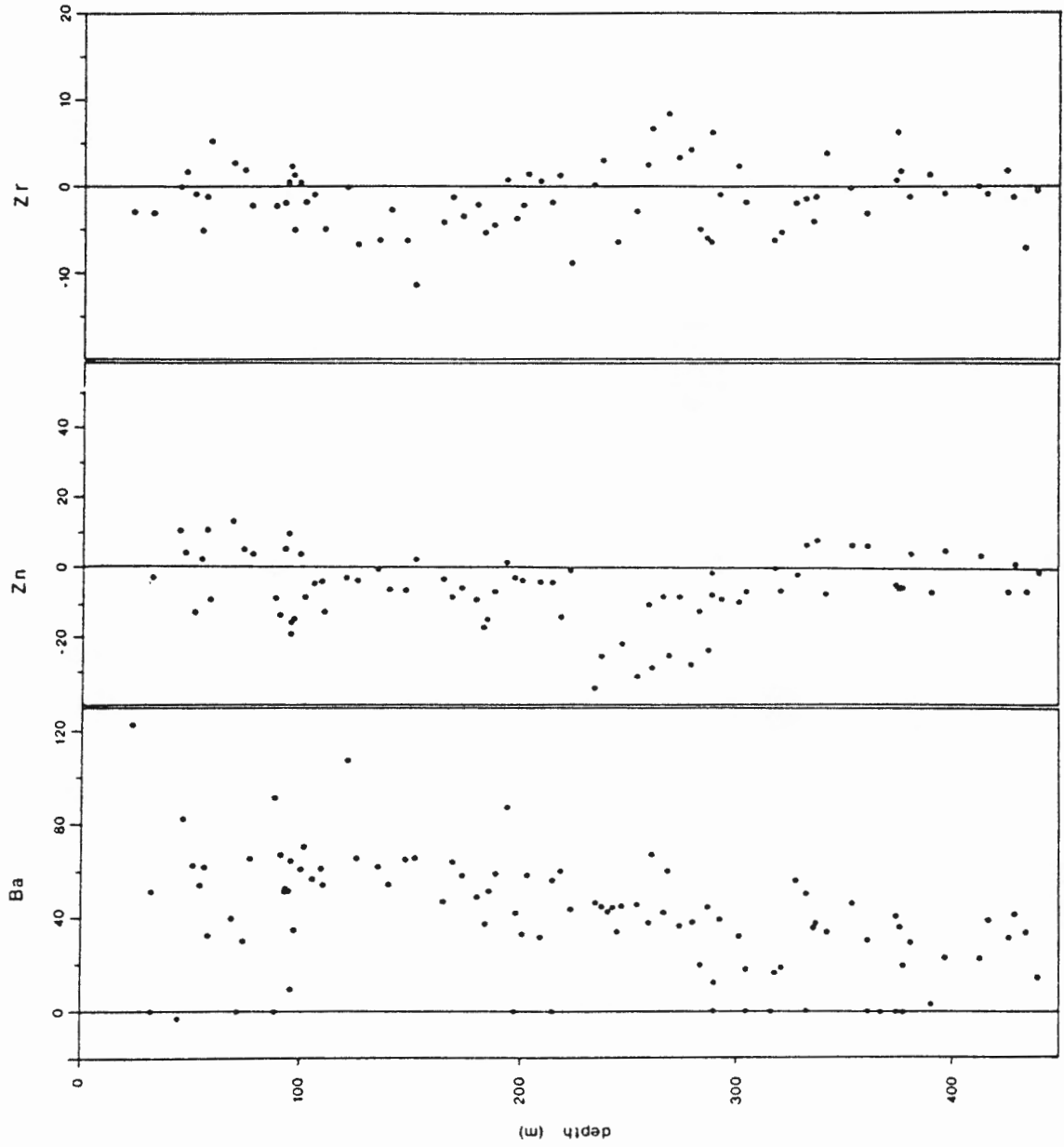
TABLE V-1   SUMMARY OF ELEMENTAL FLUXES FOR CY-1

	Sm-Pa-Ca Zone		Sm-Ce-Ze Zone	
	average	range	average	range
Majors (g/100g)				
SiO_2	-3.9	-22.0 - +2.0	-0.8	-9.0 - +3.8
Al_2O_3	+1.1	-3.8 - +4.5	+0.4	-4.0 - +2.9
FeO	-0.2	-3.8 - +3.5	+0.3	-2.7 - +3.0
MnO	n.c.		n.c.	
MgO	+0.7	-14.0 - +3.9	+1.3	-2.6 - +5.2
CaO	-0.3	-8.4 - +28.0	-2.4	-6.4 - +1.3
Na_2O	+0.2	-2.6 - +1.6	+1.1	-1.6 - +1.9
K_2O	+3.9	+0.1 - +7.8	+0.6	-0.3 - +2.9
P_2O_5	n.c.		n.c.	
		n=75		n=44
traces (10^{-4} g/100g)				
Rb	+20	-7 - +48	+4	-6 - +22
Sr	-16	-60 - +38	-27	-56 - -13
Y	-1	-10 - +7	+2	-7 - +8
Ba	+55	+9 - +120	+30	+3 - +54
Zr	-1	-11 - +8	-1	-6 - +6
V	-41	-149 - +41	-31	+21 - -72
Zn	-6	-35 - +51	-4	-28 - +8
Cu	-17	-261 - +204	-15	-240 - +50
		n=56		n=27

Calculated assuming constant TiO_2; n.c.=no change; FeO^* - Fe_2O_3 + FeO

These pillows and flows represent the style and intensity of alteration typical in the Sm-Pa-Ca and Sm-Ce-Ze Zones. Each unit was sampled along a cross-section from top to bottom at 5 - 50 cm intervals. In most cases it was not possible to sample the outer chilled margin. Major, minor, and trace elements analyses were performed at St.Mary's University, Dalhousie University, and Universite de Montreal (Auclair et al. in press) (Appendix I).

Elemental fluxes were calculated using equation (5.1). The TiO_2 content of the sample from the core of each cooling-unit was used to choose its "fresh rock" equivalent. This "fresh rock" was then used for the flux calculations of the other samples from that cooling-unit. This approach assumes that TiO_2 is homogeneously distributed throughout the unit and that the core of each cooling-unit is the least altered. To check this assumption, the TiO_2 content of every sample from a few cooling-units was used to choose the standard for that sample. The direction of the fluxes from the latter calculation is in agreement with the former calculation; there is minor variation in the magnitude. The resultant fluxes using the TiO_2 and Al_2O_3 correction factors are similar in both magnitude and direction.

In addition, the variation in Fe_2O_3, FeO, H_2O+, CO_2, and S contents across each cooling-unit was determined.

In the following section, the results of these calculations are discussed for each alteration zone. Descriptions of the cooling-units are summarized in Appendices V-1 and V-2.

5.4.4.1 Sm-Pa-Ca Zone

There is considerable variation in elemental fluxes both within

and between the pillows from the Sm-Pa-Ca Zone (pillows 5, 6, & 7). The magnitude and direction of SiO_2, Al_2O_3, FeO^T, Na_2O, H_2O+, CO_2, CaO, and Sr fluxes in pillows 5, 6, and 7 have no consistent trends (see Figure V-8 for compositional variation in pillows 5 & 6). K_2O, Rb, Ba, and H_2O+ are consistently enriched the in pillows whereas MgO is depleted. The margins of the pillows are more depleted in MgO and enriched in Fe_2O_3 and H_2O+ relative to their cores.

5.4.4.2 Sm-Ce-Ze Zone

There are no consistent trends in either magnitude or direction of the Al_2O_3, CaO, Na_2O, Ba, Sr, Y, and Zr fluxes and H_2O+ and CO_2 contents in the pillows from the Sm-Ce-Ze Zone (pillows 2, 3, & 8)(see Figure V-9 for compositional variation in pillow 2 & flow 1). SiO_2, FeO^T, Cu, and Zn are consistently depleted whereas MgO, K_2O, and Rb are consistently enriched. SiO_2 and Sr fluxes are greater in the margins of the pillows relative to their cores whereas Cu, Zn and S have the opposite trend.

The flows in the Sm-Ce-Ze Zone (flows 1 & 9) have no consistent trends in the magnitude or direction of the SiO_2, Al_2O_3, Na_2O, CaO, K_2O, Zr, Y, Cu, and Zn fluxes (Figure V-9). Ba is consistently enriched while MgO is consistently depleted.

Bulk rock compositions of pillows have been modified to a greater degree than flows in the Sm-Ce-Ze Zone. The outer margins of pillows have been modified more than their cores. This trend is not evident within the flow units.

Figure V-8. Variation in bulk rock compositions across pillows 6 (A)
and 5 (B) from the Sm-Pa-Ca Zone. Major element fluxes are in
$g/100g$; trace elements are in 10^{-4} $g/100g$. Fluxes were calculated
assuming TiO_2 was immobile. The sample within each cooling-unit
used as the "core" in the calculations is indicated by the shaded
bar. The vertical scale is the thickness of the pillow, from top
to bottom (m); the horizontal scales for the elemental fluxes are
different for each pillow.
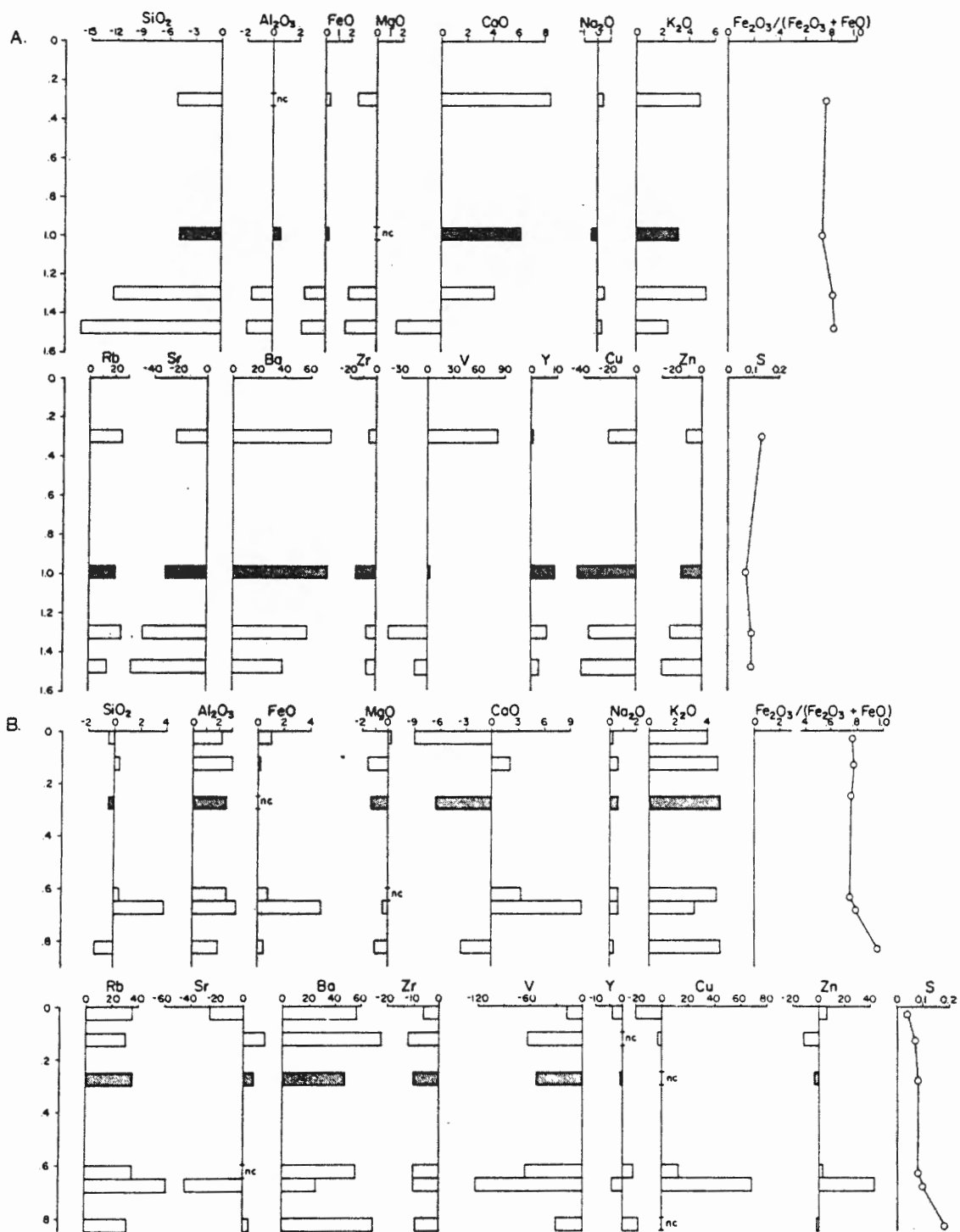
Figure V-9. Variation in bulk rock compositions across pillow 2 (A) and
flow 1 (B) from the Sm-Ce-Ze Zone. Major element fluxes are in
$g/100g$; trace elements are in 10^{-4} $g/100g$. Fluxes were calculated
assuming TiO_2 was immobile. The sample within each cooling-unit
used as the "core" in the calculations is indicated by the shaded
bar. The vertical scale is the thickness of the coooling-unit,
from top to bottom (m); the horizontal scales for the elemental
fluxes are different for each cooling-unit.
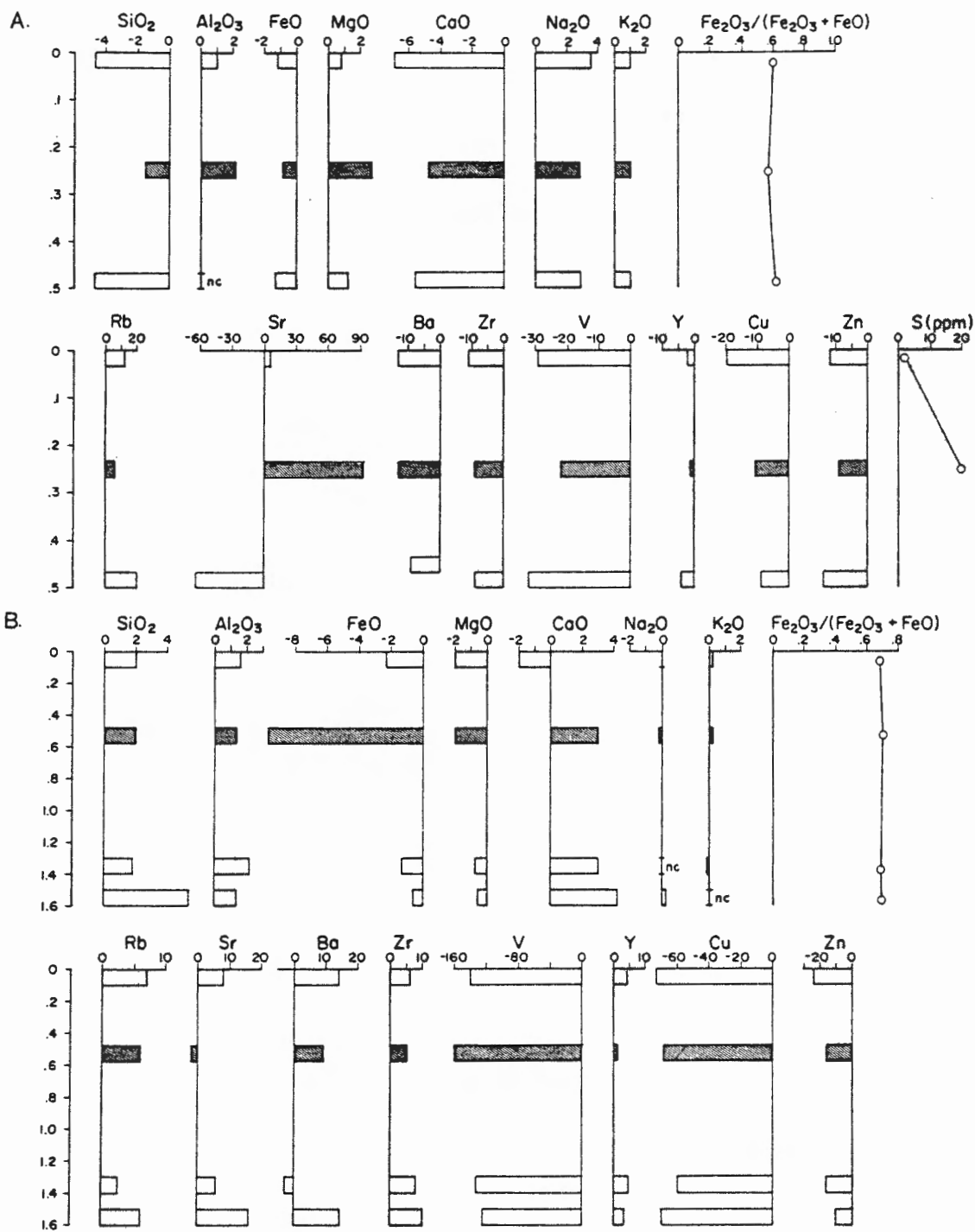
5.4.4.3 Comparison of results

Elemental fluxes calculated for the nine cooling-units fall within the range of elemental fluxes for the ICRDG samples from each of the alteration zones in the CY-1 drillcore. This suggests that the ICRDG samples which were collected with a bias towards "freshness" are not fresh and are representative of the alteration geochemistry in both alteration zones.

5.5 ELEMENT MOBILITY IN CY-la

It was not possible to calculate elemental fluxes for the samples from the CY-la drillcore because fresh rock equivalents which span the range in primary composition are not available. It has been possible, however, to make more critical estimates of element mobility than those obtained from depth plots. The approach used evaluates the effects of differentiation through correlation of each element with indicators of differentiation, such as Zr and MgO. Elements which diverge from expected differentiation trends are deemed to be mobile. Such estimates are insensitive to the effects of dilution and enrichment. This approach is complicated by the presence of two geochemical suites in the CY-la samples which have different, and often overlapping, trends.

The co-variance of SiO_2, Al_2O_3, $Fe_2O_3^T$, and MgO with Zr in all samples from CY-la closely follows the fractionation trends of the two geochemical suites (see Figures V-10 & V-11 for SiO_2, MgO, & $Fe_2O_3^T$) (Mehegan, unpublished data, 1986; Bailey 1984; Robinson et al. 1983). The strong correlation of TiO_2, Y, and, to a lesser extent, V with Zr indicates that they are also immobile.

The alkali and alkaline earth elements are mobile in all the

Figure V-1Ø. SiO$_2$, K$_2$O, MgO, and Rb contents versus Zr in samples from the CY-la drillcore. Major elements are in weight %; trace elements are in ppm. Open circles = Ep-Ch-Qz Zone; closed circles = Sm-Ce-Ze Zone; open triangles = La-Sm/Ch-Qz Zone.
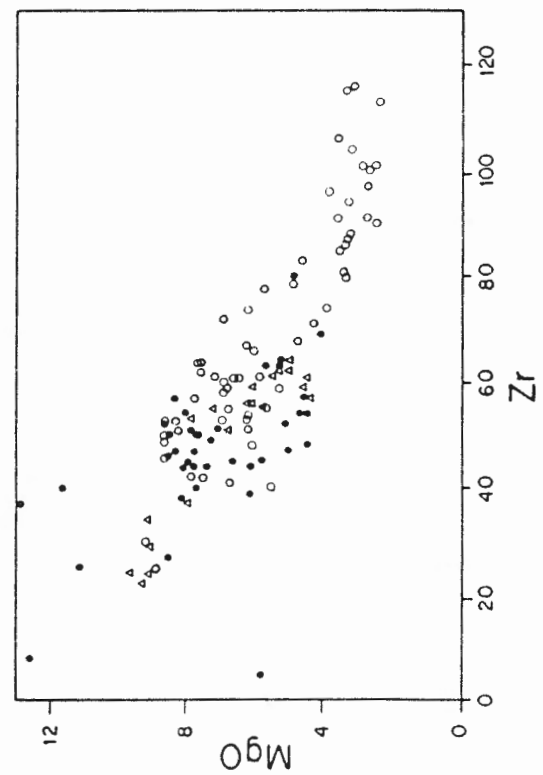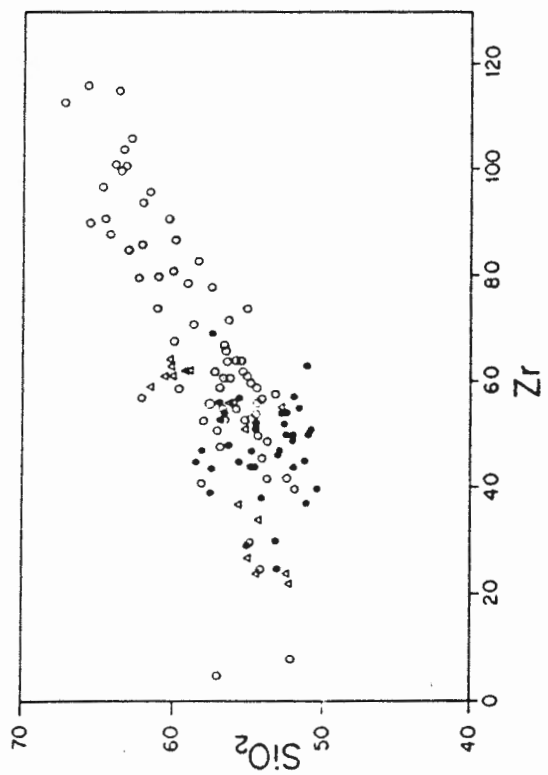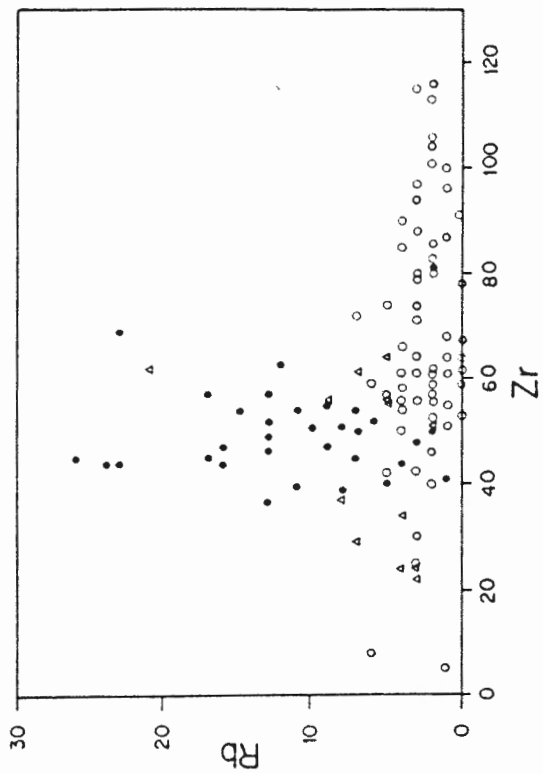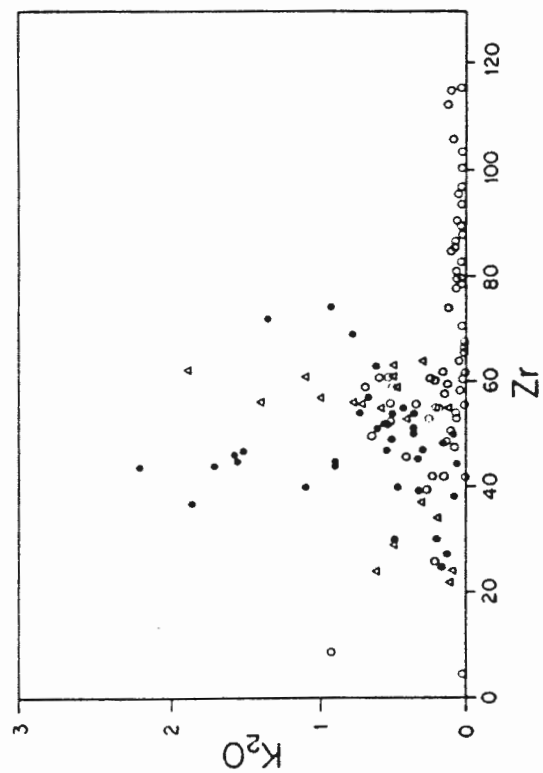
Figure V-11. CaO, Na$_2$O, and Fe$_2$O$_3$[*] contents versus Zr and CaO versus

Na$_2$O in samples from the CY-1a drillcore. Major elements are in

weight %; trace elements are in ppm. Open circles = Ep-Ch-Qz Zone;

closed circles = Sm-Ce-Ze Zone; open triangles = La-Sm/Ch-Qz Zone.
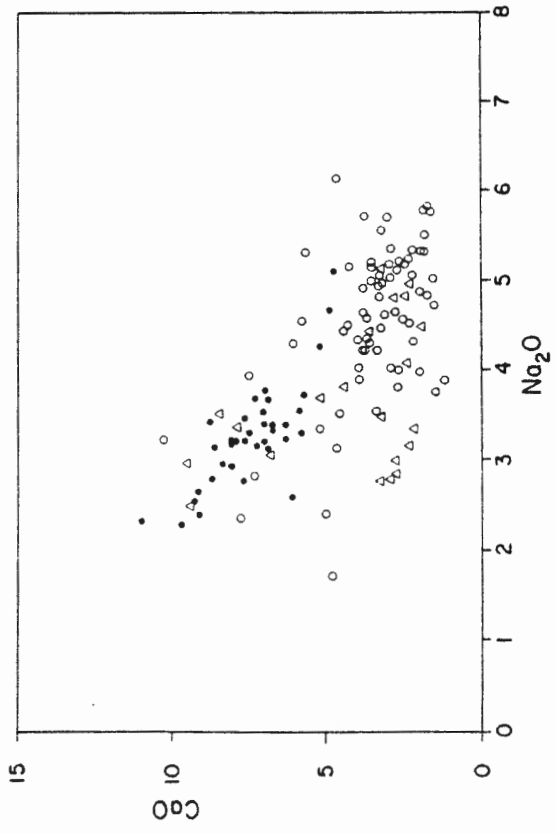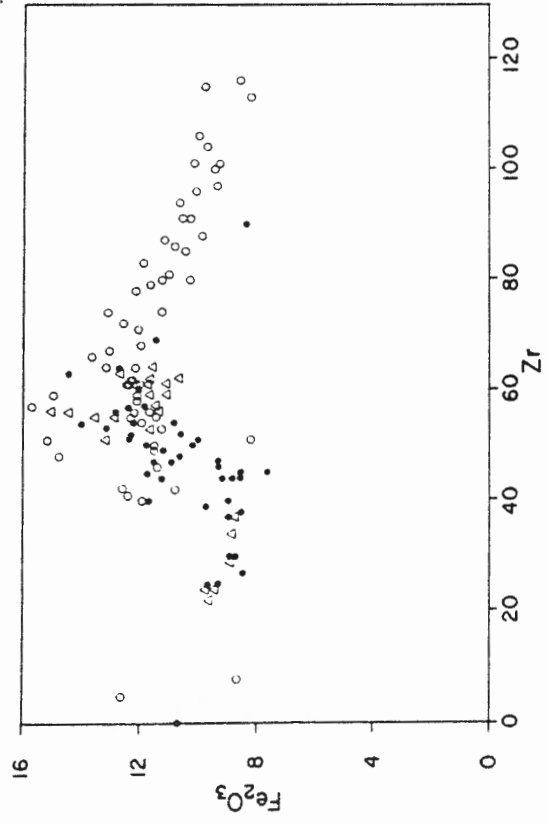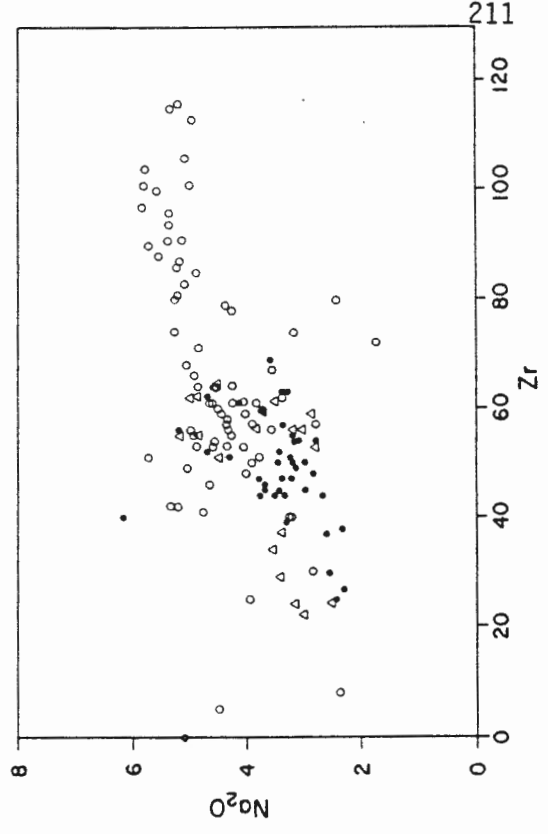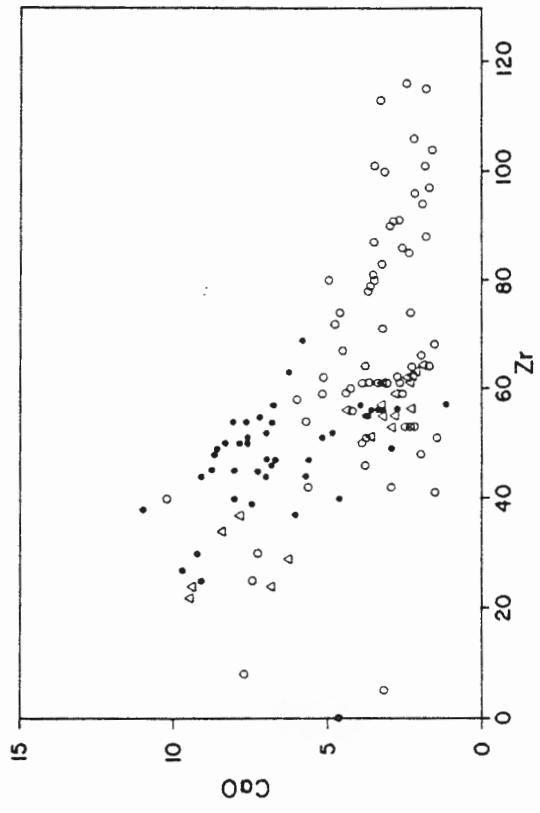
alteration zones in CY-1a. K_2O, Rb, and Ba are enriched in the Sm-Ce-Ze and La-Sm/Ch-Qz Zones and depleted in the Ep-Ch-Qz Zone (see Figure V-10 for Rb). Na_2O and CaO have opposing trends. Na_2O is consistently enriched in the La-Sm/Ch-Qz and Ep-Ch-Qz Zones whereas CaO is depleted (Figure V-11). In the Sm-Ce-Ze and La-Sm/Ch-Qz Zones there is a sympathetic variation between Na_2O and CaO whereas in the Ep-Ch-Qz Zone, the depletion of CaO is greater than the enrichment of Na_2O (Figure V-11). Sr contents have a trend similar, albeit more scattered, to CaO.

5.6 CORRELATION OF MINERALOGICAL AND COMPOSITIONAL TRENDS

Compositional trends documented in Sections 5.3 to 5.5 reflect both the secondary mineralogy of the rocks and the degree of alteration of the primary minerals, mesostasis, and volcanic glass in each of the alteration zones. Because the samples from CY-1 and CY-1a were collected to study primary compositional variations, void-filling phases were avoided. Therefore, the influence of these phases on the bulk rock composition cannot be determined.

The almost ubiquitous replacement of plagioclase by K-feldspar, the presence of void-filling adularia, and the scattered distribution of celadonite-saponite reflect the addition of K_2O in the Sm-Pa-Ca Zone. The replacement of plagioclase by K-feldspar releases Al_2O_3, CaO, and Na_2O. The immobility of Al_2O_3 indicated by the flux calculations suggests that the excess Al may be incorporated into Al-saponite which is common in this zone, wherea CaO may be incorporated into carbonates and Na_2O is lost from the rocks. The erratic, high CaO and CO_2 contents of some samples from this zone reflect the erratic distribution of calcite in the groundmass. The breakdown of olivine to clay minerals,

goethite, and calcite has no apparent influence upon the bulk rock composition. The Fe_2O_3 contents of the CY-1 drillore are greatest in the Sm-Pa-Ca Zone where goethite and other Fe-hydroxides are abundant.

The scatter in the K_2O content of samples from the Sm-Ce-Ze Zone reflects the heterogeneous distribution of celadonite and the random replacement of plagioclase by K-feldspar. The CaO released by the breakdown of plagioclase is not incorporated into any groundmass-replacing secondary phase and is apparently lost from the rocks. Locally abundant Ca-rich zeolites, such as heulandite and mordenite, may incorporate some of the released CaO. Groundmass-replacing analcime and, rarely, clinoptilolite, may contribute to the Na_2O enrichment of this zone. No other groundmass-replacing secondary phases contains significant Na_2O. The scattered albitization of plagioclase in the La-Sm/Ch-Qz Zone and the complete albitization of plagioclase in the Ep-Ch-Qz Zone contribute to the addition of Na_2O and the depletion of CaO in these zones. In addition, analcime is locally present in the groundmass in the La-Sm/Ch-Qz Zone. Void-filling laumontite and epidote, both Ca-rich phases, are locally abundant in the La-Sm/Ch-Qz and Ep-Ch-Qz Zones, respectively, suggesting that some of the Ca leached from the rocks is locally redistributed. Epidote is also locally abundant in the groundmass which may account for the scatter in the CaO contents in the Ep-Ch-Qz Zone.

Mn-rich chlorite and, to a lesser extent, Mn-rich smectite/chlorite contribute to the enrichment of MnO in the La-Sm/Ch-Qz and Ep-Ch-Qz Zones (Figure IV-3). Void-filling, manganiferous carbonate also occurs sporadically throughout these zones (Figure IV-9). The

FeO/(FeO + MgO) ratios of saponite, smectite/chlorite, and chlorite closely reflect the bulk rock compositional trends (Figure IV-6).

It is evident, therefore, that the composition of groundmass-replacing secondary minerals and the breakdown of primary minerals account for most of the geochemical trends in the CY-1 and Cy-1a drillcores.

5.7 COMPOSITIONAL TRENDS IN "IN SITU" OCEANIC CRUST

Elemental fluxes and estimates of elemental mobility have been determined for rocks recovered at DSDP Sites 417A, 418, and 504 (Alt et al. 1986; Honnorez et al. 1983; Thompson 1983; Staudigel & Hart 1979; Humphris et al. 1979; Donnelly et al. 1979b). In the following section, the element mobilities for the alteration zones in the drillcores outlined in Section 3.4 are compared to the equivalent alteration zones in the CY-1 and CY-1a drillcores.

Elemental fluxes and qualitative estimates of element mobility for Holes 417A, 417D, and 418A were compiled and summarized in Thompson (1983). Flux calculations in this review followed the method described in Section 5.4.1 with an additional factor to correct for changes in density. This factor has been removed for comparison with the results from this study.

Elemental fluxes for the Sm-Pa-Ca and Sm-Ce-Ze Zones of the CY-1 drillcore are remarkably similar, in both direction and magnitude, to their equivalent zones in the Holes 417A and 418D drillcores, respectively, with one notable difference (Table V-2). CaO is enriched in the Sm-Pa-Ca Zone of Hole 417A but is slightly depleted in CY-1. The degree of preservation of plagioclase may contribute to this difference.

In the samples from Hole 417A, plagioclase remains fresh whereas in CY-1 it is almost completely replaced by K-feldspar. In addition, the bias towards fresher samples in the CY-1 sample set has removed the influence of the abundant void-filling carbonate on the bulk rock composition. In contrast, the samples used in the calculations of Thompson (1983) were collected to represent the average degree and style of alteration of the drillcore and are therefore more representative of the alteration geochemistry.

Qualitative estimates of element mobility for each alteration zone in Site 504B are remarkably similar to those in the CY-1 and CY-1a drillcores (Tables V-2 and V-3).

5.8 COMPOSITIONAL TRENDS IN OTHER OPHIOLITES

Qualitative estimates of element mobility in rocks from the zeolite and greenschist facies of the Sarmiento ophiolite, described in Section 3.5, are similar to those of the Sm-Ce-Ze and Ep-Ch-Qz Zones with one notable exception. SiO_2 is consistently added to the rocks of the Sarmiento ophiolite in both facies whereas it is depleted in the Sm-Pa-Ca and Sm-Ce-Ze Zones of CY-1 and immobile in the equivalent alteration zones of CY-1a. The lack of unaltered rocks in the Sarmiento ophiolite precluded the possibility of flux calculations.

The effect of metamorphism on bulk rock composition the Del Puerto, East Taiwan, and Semail ophiolites has not been determined.

5.9 SUMMARY

Qualitative and semi-quantitative estimates of element mobility have shown that each of the alteration zones represented in the CY-1 and

TABLE V-2   COMPARISION OF ELEMENTAL FLUXES IN THE CY-1
DRILLCORE WITH IN SITU OCEANIC STUDIES

	Sm-Pa-Ca Zone	417A[1]	504B[2] UPA	Sm-Ce-Ze Zone	418A[1]	504B[2] LPA
	Majors (g/100g)					
SiO_2	-3.9	-0.5	-	-0.8	-4.5	nc
Al_2O_3	+1.1	+0.9	nc	+0.4	-1.4	-
FeO	-0.2	+0.9	nc	+0.3	-0.5	nc
MgO	+0.7	-1.0	nc	+1.3	-1.3	+
CaO	-0.3	+3.6	nc	-2.4	-0.8	-
Na_2O	+0.2	-0.2	nc	+1.1	+0.3	nc
K_2O	+3.9	+1.7	+	+0.6	+0.5	nc
$\dfrac{Fe_2O_3}{FeO+Fe_2O_3}$	+	+	+	nc	nc	nc
	traces (10^{-4} g/100g)					
Rb	+20	+24		+4	+3	
Ba	+55	+62		+30	+6	
Sr	-16			-27	+12	
Y	-1			+2	+2	
Zr	-1			-1	+1	

[1] from Thompson (1983), [2] from Honnorez et al. (1983).
nc = no change; - = depletion; + = enrichment
UPA = Upper Pillow Alteration Zone; LPA = Lower Pillow Alteration Zone

TABLE V-3 COMPARISION OF ELEMENTAL MOBILITY IN THE CY-1A
DRILLCORE WITH SITE 504B

	Sm–Ce–Ze Zone	504B[1] LPA	La–Sm/Ch–Qz Zone	504B LPA*	Ep–Ch–Qz Zone	504B[1] TZD
SiO_2	nc	nc	nc	nc	nc	–
Al_2O_3	nc	vc	nc	vc	nc	vc
FeO	nc	+	nc	nc	nc	nc
MgO	nc	nc	nc	nc	nc	vc
MnO	nc	nc	+	nc	+	+
CaO	–	nc	—	–	—	–
Na_2O	+	nc	++	+	++	+
K_2O	++	++	+	+	–	nc
TiO_2	nc	nc	nc	nc	nc	vc

[1] modified from Alt et al. (in press) and Honnorez et al. (1983).
nc = no change; vc = variable change; – = minor depletion; — =
depletion; + = minor enrichment; ++ = enrichment. LPA = Lower
Pillow Alteration Zone; LPA* = Lower 150 m of the Lower Pillow
Alteration Zone; TZD = Transition Zone and Dyke Section.

CY-1a drillcores has a distinctive compositional signature (Table V-4). The greatest modification of bulk rock composition occurs in the most pervasively altered Sm-Pa-Ca and Ep-Ch-Qz Zones.

Elemental fluxes in individual cooling-units from the Sm-Pa-Ca and Sm-Ce-Ze Zones are within the range of the fluxes calculated for the ICRDG samples. This suggests that the ICRDG samples, even though collected with a bias towards "freshness", are representative of the alteration geochemistry. Bulk rock compositions of pillows are modified to a greater degree than those of massive flows and the outer margins of pillows have been modified more than their cores.

The composition of the secondary phases in each alteration zone closely reflects bulk rock compositional trends. The degree of alteration of the primary phases, particularly plagioclase, strongly influences compositional trends. Variation in Cr and Ni contents closely reflects the distribution of olivine but not the intensity of alteration. The transition elements TiO_2, Y, Zr, and V are immobile in all alteration zones. Rb, Ba, and Sr closely follow the trend of K_2O.

Co-variance of bulk rock compositions with indices of alteration suggest that the rocks from the CY-1 drillcore have undergone three stages of alteration:

1. a "less" oxidizing stage during which Na_2O was leached

2. an oxidizing stage during which the rocks were oxidized and K_2O, Rb, Ba, and Sr were added to the rocks.

3. a carbonatization stage during which the rocks were partially replaced by carbonate.

The mobility of elements in each alteration zone is remarkably similar to that characterized for equivalent zones of "in situ" oceanic

TABLE V-4 Summary of Element Mobility in the Alteration
Zones of CY-1 and CY-1a

	GAINS	LOSSES
Sm-Pa-Ca Zone[1]	K_2O Fe_2O_3 H_2O+ CO_2 Rb Ba	SiO_2 Sr
Sm-Ce-Ze Zone[1]	Na_2O K_2O MgO H_2O Rb Ba	SiO_2 CaO Sr
La-Sm/Ch-Qz Zone[2]	Na_2O MnO Zn K_2O Ba	CaO Sr Rb
Ep-Ch-Qz Zone[2]	Na_2O MnO Zn Cu	K_2O CaO Rb Sr

[1] from flux calculations
[2] from qualitative estimates

crust (Tables V-2 and V-3).

CHAPTER VI

ALTERATION STAGES

6.1 INTRODUCTION

In an open hydrothermal system, the rate of fluid flow and the
rate of reaction of that fluid with the rock through which it passes
influences the composition of the solution, the bulk composition of the
altered rock, and the nature of the secondary mineral assemblages (Mottl
& Seyfried 1980). Physical parameters such as temperature, differential
pressure, permeability, and the surface area available for reaction
determine the relative rates of fluid flow versus reaction. In a fossil
hydrothermal system it is difficult to separate the cause and effect of
these variables.

Altered bulk rock compositions, secondary mineral assemblages,
and the compositions of the secondary minerals are the products of the
physical and chemical conditions that prevailed at the time of
alteration. Because the compositions of both the unaltered and altered
rock, unaltered seawater, and the secondary phases are known, it has
been possible to infer which chemical components were added or lost from
both the rock and seawater to produce the secondary minerals. Such mass
balances, however, provide no insights into the physical and chemical
conditions during the formation of these secondary phases. It is only
possible to deduce these conditions by comparison with experimental
studies and studies of natural occurrences where some physical
parameters are known.

The rate of flow in an open system is a function of permeability,
on both a cooling-unit and formation scale. Permeability is a very

221

poorly constrained variable because very few measurements have been made in "in situ" oceanic crust. In addition to direct measurements, permeability may also be inferred from "in situ" resistivity measurements (Anderson et al. 1985). Estimates may be made from the number of fractures, the degree to which they are interconnected, and how much they are filled with secondary minerals. Estimates may also be made from the distribution of the various cooling-units. This approach has been taken for the CY-1 and CY-1a drillcores and is discussed in Section 6.3.

Water/rock ratios provide estimates of fluid flow that are independent of permeability measurements. Such ratios are used as both qualitative and quantitative variables depending upon the point of view of the investigator. For natural hydrothermal systems, water/rock ratio is defined as the total mass of water that has passed through the system, integrated through time, divided by the total mass of rock within the system (Mottl 1983). On a smaller, hand specimen scale, the water/rock ratio is defined as a measure of the change in bulk chemistry of a rock during alteration (Humphris & Thompson 1978; Spooner et al. 1977b). Water/rock ratios in experimental studies are the ratio of initial masses of seawater to rock in the experimental charge. It is this latter definition which provides the most quantitative estimate and is the most commonly quoted value.

A less quantitative but more realistic estimate of fluid flow combines experimentally-measured water/rock ratios and reaction rates and their effect upon seawater composition to define seawater-dominated and rock-dominated conditions (Mottl & Seyfried 1980). Under seawater-dominated conditions, the solution maintain high concentrations

of MgO, SiO$_2$, and metals and low pH whereas under rock-dominated conditions, the solution has low concentrations of MgO, SiO$_2$, and metals, and near neutral pH. In natural hydrothermal systems, seawater-dominated conditions are favored by high permeability, high flow rates (water/rock ratios $\geq$ 50), and/or slow reaction rates. Slow reaction rates occur where fractures are lined with "MgO-saturated" clay minerals and where seawater volume/rock surface area ratios are high. Reaction rates would also be slower at low temperatures and for crystalline versus glassy rocks. In contrast, rock-dominated conditions are favored by low permeability, low flow rates (water/rock ratios < 50) and faster reaction rates. In an open system, it is probable that rock-dominated and seawater-dominated conditions exist at the same time in different areas and in the same areas at different times.

Temperatures outlined for each stage of alteration in Section 6.4 represent the range over which the characteristic secondary minerals are stable. The thermal stability fields for each mineral have been determined experimentally (e.g. Liou 1971a&b) and have been inferred from natural environments such as geothermal systems (e.g. Iceland, Kristmannsdottir 1975) and burial metamorphic terrains (e.g. New Zealand, Boles & Coombs 1977). In most cases, temperature estimates from the natural environments are lower than experimental results. Stable isotopic studies have also provided temperature estimates for many minerals sampled from DSDP drillcores. Where possible, temperatures derived from oceanic studies or geothermal systems were used. Otherwise, experimental temperatures were used.

The composition of the solution (Eh, pH, alkali ratios, element activites) during each stage of alteration and, more specifically, at

the time each secondary mineral precipitated is not known and may only
be inferred from experiments which simulate the physical conditions of
alteration. The chemical conditions which favor the formation of the
various secondary minerals have been experimentally derived.
Correlation of these chemical conditions with the assemblages of
secondary minerals provides additional constraints on the composition of
the solution.

It is the purpose of this chapter to outline the progressive
stages of alteration for each zone, to describe the physical and
chemical conditions prevalent during each stage, and to propose a
general scheme for alteration in the extrusive sequence. First the
conclusions from experimental studies under various alteration
conditions are reviewed, permeability versus water/rock ratio is
discussed, and the petrographic basis for the alteration stages is
reviewed.

6.2 REVIEW OF EXPERIMENTAL STUDIES

Experiments where seawater reacts with powders of crystalline and
glassy mid-ocean ridge basalts have been successful in duplicating the
composition of high-temperature effluent of natural hydrothermal systems
and the compositions of altered oceanic rocks, but have been less
successful in reproducing secondary mineral assemblages. A wide range
of conditions has been used - temperatures range from $70 - 500^{\circ}C$,
pressures from $1 - 1000$ bars, and water/rock mass ratios from $1 - 125$
(Mottl 1983). Most of these experiments were performed at temperatures
greater than $150^{\circ}C$ and under seawater-dominated conditions.
Significantly, evidence from submarine metabasalts (e.g. Humphris &

Thompson 1978) and from hot-spring solutions (e.g. Edmond et al. 1979) suggests that most natural hydrothermal systems are rock-dominated.

At temperatures of >70 - 500°C, Mg is quantitatively removed from seawater as a $Mg(OH)_2$ component and is incorporated into smectite, chlorite, or amphibole, leaving behind H^+ in seawater, thus lowering its pH (Bischoff & Dickson 1975). A decrease in the pH of seawater would occur, even if Mg removal was slow, in response to the formation of a $Mg-OH-SO_4$ phase when seawater is heated to temperatures > 200°C (Bischoff & Seyfried 1978). Removal of Mg from seawater is balanced in terms of electrical charge by the leaching of Ca from the rock (Seyfried & Bischoff 1981; Mottl & Holland 1978). At water/rock ratios <10, Na is removed from seawater whereas at higher water/rock ratios, Na is leached from the rocks along with Ca.

At low temperatures, the compositions of the solutions and the altered rocks are less dependent upon the behavior of MgO and removal of MgO is favored by alkaline and oxygen-depleted solutions (Seyfried et al. 1978).

Experimental results for seawater-dominated (water/rock ratios > 50) and rock-dominated conditions (water/rock ratios < 50) for temperatures of 70° C and 150-360°C are summarized in Table VI-1.

6.3 PERMEABILITY OF THE EXTRUSIVE SEQUENCE AND THE SHEETED DYKE COMPLEX

No quantitative measurement of permeability exists for the Troodos ophiolite. In fact, permeability has only been measured in two of the DSDP Sites that penetrated basement, Sites 395 and 504 (Anderson et al. 1985; Becker 1985; Hickman et al. 1984). Therefore, our knowledge of the permeability of the oceanic crust and how it varies

TABLE VI-1 SUMMARY OF EXPERIMENTAL RESULTS[*]

	ROCK-DOMINATED TEMP: 70°	ROCK DOMINATED TEMP: 150-350°	SEAWATER-DOMINATED TEMP: 150-350°
Mg	minor removal from seawater	completely removed from seawater	no change in seawater, enriched in rock
pH	slight decrease	near neutral	acidic
Ca	removed from rock, enriched in seawater	removed from rock, half ppt as anhydrite	removed from rock, steady state lower than rock-dominated
Na	removed from seawater	W/R <10: removed from seawater W/R >10: leached from rock	
K	removed from seawater, enriched in rocks	removed from rock	removed from rock
metals		low concentrations in seawater, minor removal in rocks	high concentrations in seawater, leached from rock
SiO_2	removed from rock	removed from rock, near qtz saturation	removed from rock, at qtz saturation
SO_4^{2-}	unchanged in seawater	removed from seawater	removed from seawater
products	none detected	smec, smec/chl, qtz, pyrite, truscottite, wairakite,anhydrite	smec/chl, smec, qtz, anhydrite

[*] summarized from Rosenbauer & Bischoff (1983); steady-state conditions.

with age is very poorly constrained.

In a qualitative sense, fissure permeability is a function of the number of fractures, their connectivity, and the extent of filling by secondary minerals. It is obvious from field exposures of the Troodos ophiolite that pillows and breccias are more fractured than flows and dykes suggesting that the distribution of these cooling-units controls permeability.

A plot of the volume percent of each type of cooling-unit throughout the CY-1 and CY-1a drillcores versus depth shows that pillows and breccias are most abundant in the upper one hundred metres of CY-1 whereas the proportion of pillows to massive or sheet flows below this depth is approximately 1:1 (Figure VI-1). Massive flows and pillows with minor dykes comprise the upper 200 m of CY-1a whereas the proportion of flows to dykes below this depth is approximately 1:1 (Figure VI-1). The distribution of cooling-units with depth in the Akaki and Pediaeos River sections is similar to that in the drillcores (Figures II-6 & II-9). This stratification, combined with the observation that the distribution of cooling-units controls permeability, suggests that permeability decreases with increasing depth in the extrusive sequence and the sheeted dyke complex.

A similar trend of decreasing permeability and apparent bulk porosity with increasing depth was directly directly at DSDP Hole 504B (Anderson et al. 1985; Becker 1985). Permeability decreased from 10^{-13} - 10^{-15} m^2 in the upper 250 m where pillows, flows, and breccias are most abundant, to 10^{-17} m^2 in the lower 680 m (Figure VI-2). Over this 680-m-thick interval, the proportion of cooling-units is constant to the lowermost 230 m, where massive units (undifferentiated flows and dykes)

Figure VI-1. Volume % of cooling-units versus depth for the CY-1 and

CY-1a drillcores (summarized from Douma & Robinson 1984; Horne &

Robinson 1986). Basement depth refers to the additive depth of

CY-1 and CY-1a, where the upper 475 m comprises CY-1 and the lower

700 m comprises CY-1a. No correction for stratigraphic overlap

between CY-1 and CY-1a was made. Recovery of CY-1 and CY-1a

drillcores was 92% and 95%, respectively.
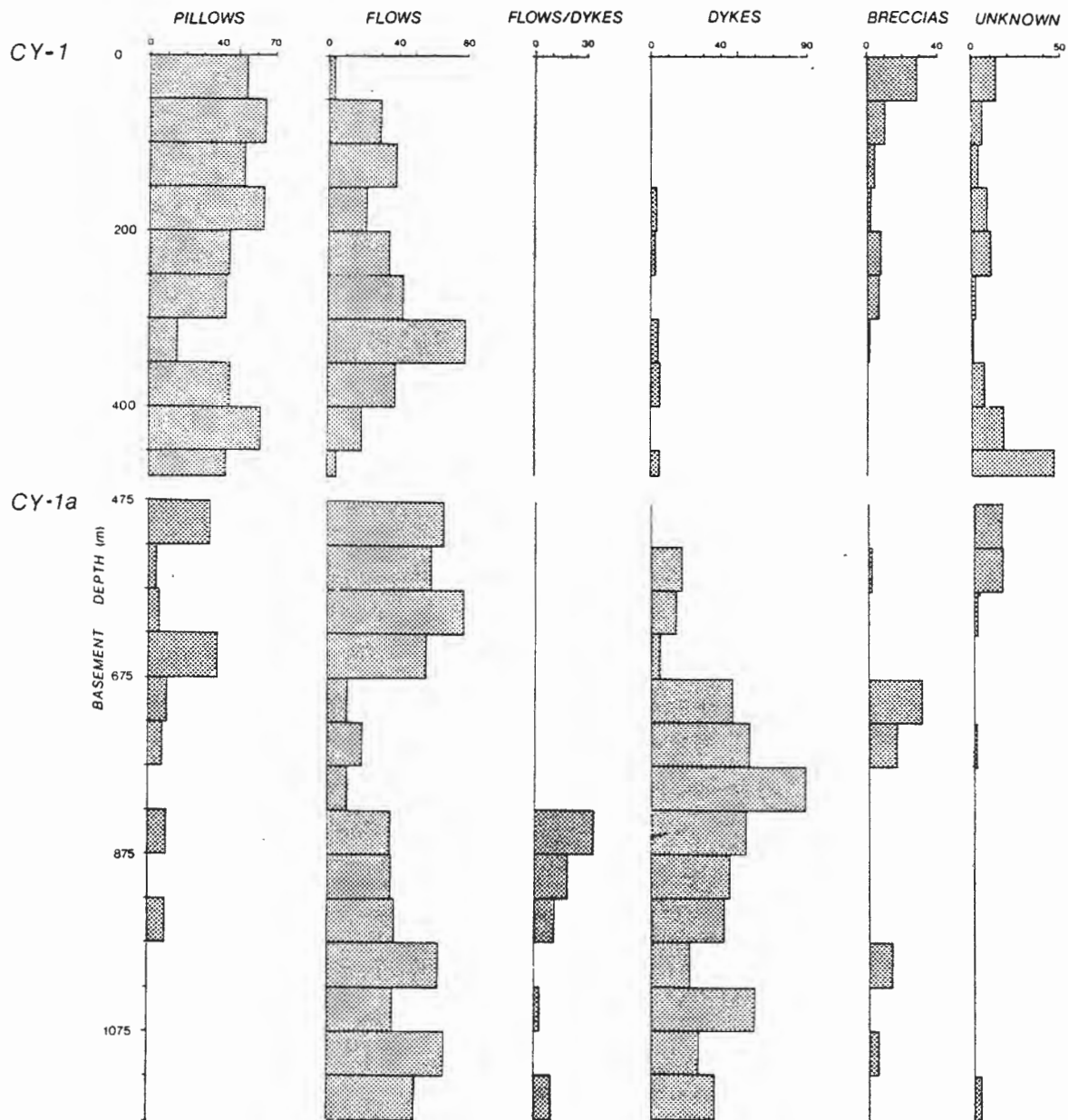
Figure VI-2. Volume % of cooling units, apparent bulk porosity, and

permeability versus depth for DSDP Site 504B (Note: 0 m basement

depth is equivalent to the sediment/lava boundary at 275 m below

mean sea level; recovery averaged 20%; Shipboard Scientific Crew,

Legs 69, 70, & 83, 1983 & 1985). Apparent bulk porosity was

calculated from measured resistivities (Becker 1985). Bulk

permeability measurements were averaged over the interval

indicated by the vertical lines (Anderson et al. 1985).
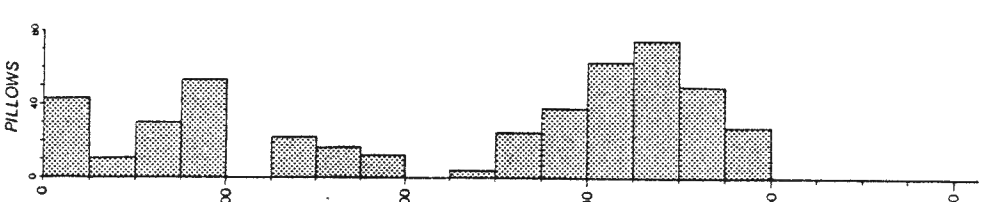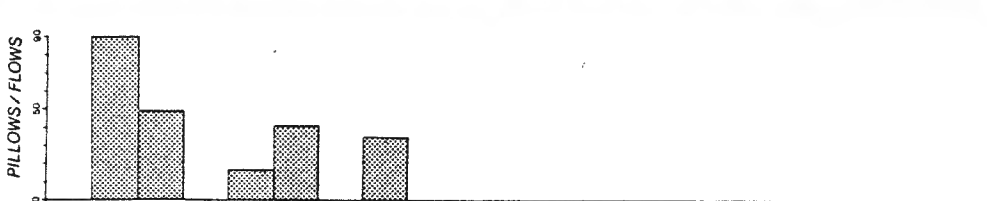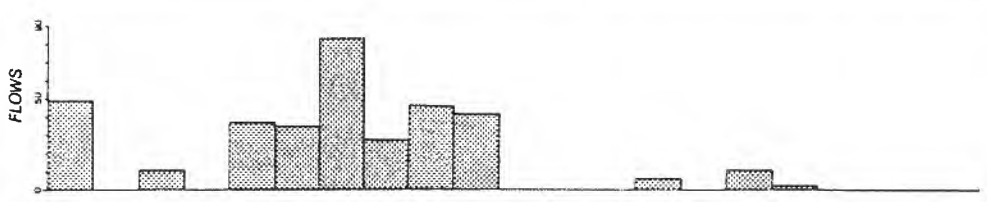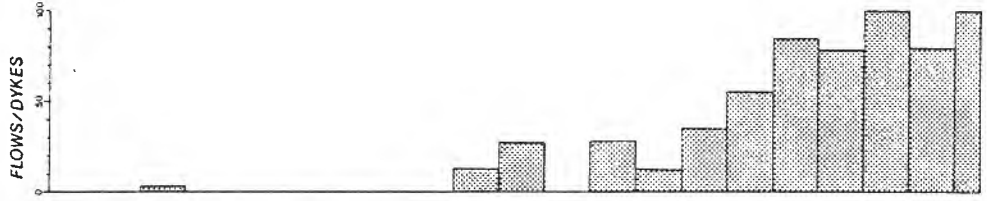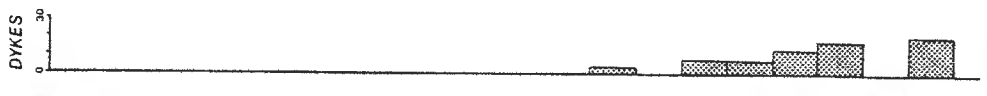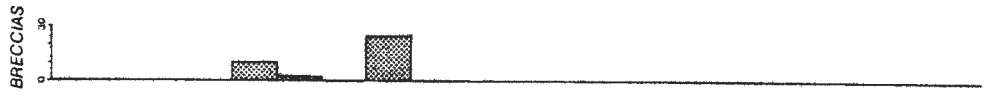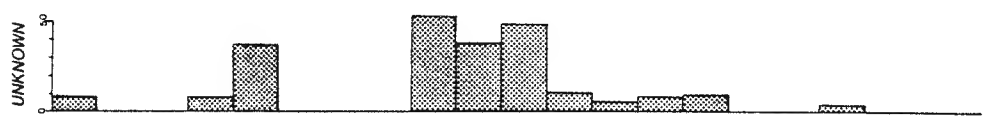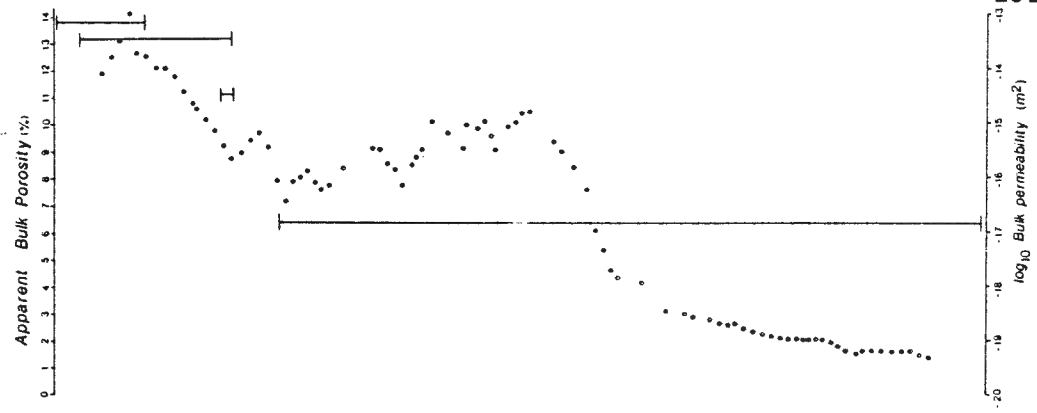
became most abundant. Because the rocks sampled at Hole 504B have been altered, the measured permeability does not represent the initial permeability and is a minimum value. It is possible to conclude, however, that at Hole 504B the decrease in permeability corresponds to an increase in the abundance of massive units.

Permeability measurements at Site 395A support the correlation of low permeability with massive units (Hickman et al. 1984). Permeabilities of 3 to 9 x 10^{-18} m^2 were measured in the lowermost 80 m, an interval composed of massive dolerites.

Apparent bulk porosities, which reflect some combination of pore, crack, and fracture porosities, are calculated from measured "in situ" resistivities and provide further evidence for permeability stratification at Site 504B (Figure VI-2), (Becker 1985). Bulk porosities are consistently high in the upper 650 m where pillows, flows, and breccias are most abundant. A sharp decrease over the next 100-m-thick interval is not marked by a change in lithology. Undifferentiated flows and dykes comprise the lower 300 m where bulk porosities are consistently low (Figure VI-2).

At Hole 504B, decreases in permeability and bulk porosity correspond to systematic changes in lithology, from pillows, flows, and breccias to flows and dykes with depth (Figure VI-2). It may be be inferred, therefore, that the permeability of the CY-1 and CY-1a drillcores and the extrusive sequence in general also decreases with increasing depth, in response to the distribution of cooling-units. This lithologic stratification suggests that there may be an upper "permeable layer" and a lower "less permeable layer" whose boundary is marked by a change in the dominant lithologic type. Considerable

lateral variation in lithologic type is a characteristic feature of the
igneous succession suggesting that permeability in these layers is
heterogeneous.

This model for permeability stratification does not consider the
distribution of faults or fissures. These structural features may be a
more important mechanism for bringing large volumes of seawater deep
into the oceanic crust than migration through the lava pile. In the
intervening areas, however, it is reasonable to assume that lithologic
variation controls the movement of seawater.

Permeability also changes through time due to compaction of the
crust and the sealing of fractures by the deposition of secondary
minerals. It is possible to estimate the extent of fracture-filling
during each stage of alteration from the secondary mineral assemblages
and, from that, infer the resultant change in permeability. The effect
of compaction, however, is unknown.

6.4 ALTERATION STAGES

Consistent depositional sequences of secondary minerals and bulk
rock compositional trends have been documented for each alteration zone.
From these sequences, several stages of alteration have been recognized
which record progressive changes in physical and chemical conditions
during and after crustal formation. Evidence for an early deuteric
stage of alteration during construction and cooling of the extrusive
sequence has been largely obscured by later alteration. It is also
difficult to distinguish alteration which resulted from interaction of
seawater and host rock during construction of the lava pile from the
later alteration. Rocks recovered from the upper tens of metres of

young oceanic crust (<10,000 years), however, are remarkably fresh, suggesting that alteration during crustal accretion is minimal (Leg 106 Scientific Party, in press).

The stages for each alteration zone are described in the following section. The boundaries separating these stages do not necessarily represent a significant change in alteration conditions but, rather, mark a change in the style of alteration, for example, from dominantly groundmass-replacing to void-filling.

6.4.1 Sm-Pa-Ca Zone

Four stages of alteration have been identified in the Sm-Pa-Ca Zone (Table VI-2).

High bulk rock Fe_2O_3 contents and the pervasive distribution of Fe-hydroxides indicate that oxidizing conditions dominated the first stage of alteration. K_2O, Rb, Sr, and Ba were added to the rocks and FeO was oxidized whereas Na_2O was depleted.

Fe-hydroxides mixed with smectite are most abundant in the outer margins of pillows and breccia fragments whereas their interiors are dominated by smectite. The oxidation of basaltic Fe and the formation of Fe-hydroxides reflects low pH conditions whereas the formation of saponite reflects more alkaline environments (Alt & Honnorez 1984; Seyfried et al. 1978). Therefore, seawater became more alkaline and less oxygenated as it migrated inward from the margin of cooling units. Such conditions would favor the replacement of plagioclase by K-feldspar (Alt & Honnorez 1984). Olivine is replaced dominantly by Fe-hydroxides and Mg-saponites indicating that alteration occurred during an oxidizing stage.

TABLE VI-2 SUMMARY OF ALTERATION STAGES

Alteration Zone	Stage[*]	Mineralogy	Composition
Sm–Pa–Ca	1	Fe-hydroxides, K-feldspar, Al-saponite	$+Fe_2O_3$, K_2O +Ba, Sr, Rb $-SiO_2$??
	2	analcime	??
	3	calcite	$+CO_2$
	4	palygorskite, calcite	??
Sm	1	saponite	??
	2	palygorskite, Mn-sediments	??
Sm–Ce–Ze	1	saponite, celadonite Fe-hydroxides	?? ??
	2	saponite, celadonite Fe-hydroxides	$+K_2O$, Rb, Ba, Na_2O $-CaO$, SiO_2, Sr
	3	zeolites	??
	4	calcite	??
	5	palygorskite, calcite, gypsum,	??
La–Sm/Ch–Qz	1	saponite, smectite/chlorite, albite, K-feldspar	$+Na_2O$, MnO, Zn $-CaO$, Sr
	2	laumontite, quartz, analcime	??
	3	calcite	??
Ep–Ch–Qz	1	chlorite, quartz, pyrite, albite, epidote	$+Na_2O$, MnO, Cu $-CaO$, K_2O, Rb
	2	epidote, quartz, pyrite	??
	3	calcite	??
	4	zeolites	??

[*] stages are listed from oldest to youngest

Al-saponites are consistently more Fe-rich than coexisting saponites and closely resemble the bulk rock compositions. Their dominance over the other clay types in this zone indicates conditions were too acidic for Mg-saponite formation and that sufficient SiO_2, K_2O or FeO was not available for celadonite formation.

The bulk rock enrichment of K_2O and Rb and oxidation of FeO indicate that the rocks were altered at high water/rock ratios by oxygenated seawater. The high permeability of this zone (Figure VI-1) further supports high water/rock ratios, however, it is not possible to determine if rock-dominated or seawater-dominated conditions prevailed. The maintenance of lower pH by the oxidation of host rock Fe prevented widespread formation of Mg-saponite and thus, MgO enrichment. Negative correlation between Na_2O and $Fe_2O_3/(Fe_2O_3 + FeO)$ contents suggests that Na_2O may have been leached from the rocks during a less oxidizing phase of alteration.

Analcime and adularia were locally deposited on fracture surfaces during the second stage of alteration. The presence of both minerals indicates more alkaline conditions and local variations in seawater Na/K ratios.

The association of smectite, phillipsite, Fe-hydroxides, and K-feldspar and the alteration of titanomagnetite to maghemite (Hall et al. in press) indicate temperatures <50°C (Table VI-3).

Pervasive calcite deposition and subsequent enrichment of bulk rock CaO and CO_2 contents occurred during the third stage of alteration. Mg/Ca ratios of the calcites, from 0 to 0.02, indicate that the seawater was depleted in MgO because the $MgCO_3$ content of calcite which precipitates from normal seawater is 8 mole % (Mucci & Morse 1983).

TABLE VI-3   TEMPERATURE RANGES FOR CHARACTERISTIC
             SECONDARY MINERALS

Mineral	Temperature $^\circ$C	Reference
analcime	<100 - 200	8, 9
phillipsite	<50	4, 15
K-feldspar	<50 - 140	4, 10
clinoptilolite	<50	17
mordenite	<100 - 120	2, 3
celadonite	<40	4, 5, 6, 12
saponite	<50 - 200	1, 4, 11, 12
laumontite	<100 - 200	1, 2, 7, 9
albite	>140	10, 11
smectite/chlorite	200 - 280	1, 9
chlorite	>230	1, 13, 16
epidote	>250	1, 16
prehnite	>250	16

1   Kristmannsdottir (1975)
2   Palmason et al. (1979)
3   Kristmannsdottir & Tomasson (1978)
4   Bohlke et al. (1984)
5   Kastner & Gieskes (1976)
6   Stakes & O'Neil (1982)
7   Liou (1971a)
8   Liou (1971b)
9   Iijima & Utada (1971)
10   Munha et al. (1980)
11   Honnorez et al. (1983)
12   Seyfried et al. (1978)
13   Friedrichsen (1985)
14   Hoffman & Hower (1979)
15   Honnorez (1978)
16   Liou et al. (1985)
17   Barrows (1980)

Temperatures calculated from oxygen isotopic data range from $5 - 14^{\circ}C$ (Table VI-4), comparable to Cretaceous bottom seawater ($5 - 15^{\circ}C$, Brass et al. 1982). Carbon isotopic data indicate the carbonates were precipitated from solutions with an inorganic carbon component (Table VI-4)(Muehlenbachs 1979).

Palygorskite and a later generation of calcite were deposited in all remaining voids during the fourth stage of alteration, greatly reducing the bulk permeability of this zone. Their common association with Fe-hydroxides and low-SiO_2 zeolites, such as analcime and chabazite, suggests that palygorskite precipitated from oxidized, highly alkaline seawater enriched in MgO and SiO_2 (Donahoe & Liou 1985; Surham & Sheppard 1978; Couture 1977).

6.4.2 Sm Zone

Two stages of alteration have been identified in the Sm Zone (Table VI-2).

Crystalline pillow interiors were pervasively altered to smectite during the first stage of alteration whereas glassy pillow margins were generally preserved. The deposition of synvolcanic umbers directly on top of the volcanic rocks restricted the penetration of seawater into the upper few metres of the lava pile, producing rock-dominated conditions. The absence of Fe-hydroxides indicates that anoxic conditions prevailed.

Veins of palygorskite and Mn-rich sediment mixed with calcite were deposited during the second stage of alteration. Termination of many of these veins in the overlying umbers suggests that they formed during the waning stages of volcanism (Boyle & Robertson 1984). The age

TABLE VI-4   OXYGEN AND CARBON ISOTOPIC DATA AND CALCULATED TEMPERATURES
OF FORMATION OF CALCITES FROM CY-1 AND CY-1a DRILLCORES

DEPTH (m)	ALTERATION ZONE	$^{13}C_{PDB}$	$^{18}O_{PDB}$	$^{18}O_{SMOW}$	TEMPERATURE ^{O}C 1	2
CY-1						
58.35	Sm-Pa-Ca	2.3	0.62	31.50	9.3	5.3
86.30	Sm-Pa-Ca	1.8	-0.41	30.43	13.7	9.6
123.30	Sm-Pa-Ca	2.0	0.63	31.54	9.2	5.3
291.00	Sm-Ce-Ze	2.7	-0.47	30.37	14.0	9.8
299.05	Sm-Ce-Ze	2.8	0.01	30.87	11.8	7.8
410.43	Sm-Ce-Ze	2.4	-1.36	29.46	16.1	13.6
CY-1a						
36.35	Sm-Ce-Ze	1.2	-4.38	26.34	32.8	27.8
138.75	Sm-Ce-Ze	0.8	-5.89	24.79	41.1	35.6
242.09	La-Sm/Ch-Qz	-0.9	-7.85	22.77	53.0	46.9
314.05	La-Sm/Ch-Qz	1.7	-12.13	18.36	84.6	76.6
434.00	Ep-Ch-Qz	0.9	-10.34	20.20	70.3	63.2
518.00	Ep-Ch-Qz	3.0	-12.09	18.40	84.2	76.3
617.00	Ep-Ch-Qz	3.3	-12.65	17.82	89.0	80.8
390.00	Ep-Ch-Qz	1.4	-10.66	19.87	72.7	65.5
406.00	Ep-Ch-Qz	2.7	-12.62	17.85	88.8	80.6

1 present seawater value
2 Cretaceous seawater value (Savin 1977)

relationship of this palygorskite and the palygorskite in the Sm-Pa-Ca
Zone is not known.

Sparse calcite lines fractures and fills vesicles in the Sm Zone.
Its relationship to Stage 2 is not known. Oxygen and carbon isotopic
data from one sample (KG:83:017) indicate that the calcite precipitated
from normal seawater at temperatures between 6 and $10^{\circ}C$ (Table VI-5).

6.4.3 Sm-Ce-Ze Zone

Five stages of alteration have been outlined for the Sm-Ce-Ze
Zone (Table VI-2).

The earliest stage of alteration is evident primarily in massive
flows and pillows that have not been pervasively altered. Mixtures of
celadonite, celadonite-saponite, saponite, and Fe-hydroxides are
concentrated in 1-10-mm-wide zones which are parallel to fracture or
cooling surfaces. Similar zones, termed "black halos", have been
described for samples from DSDP cores where they are interpreted as the
first stage of alteration (Honnorez et al. 1983; Honnorez 1981; Bohlke
et al. 1980; Humphris et al. 1979). It was not possible to determine
the age relationship between these celadonite-rich zones and the clay
minerals in the adjacent groundmass in the Troodos samples. Their
assignment to the first stage of alteration is based solely upon their
similarity to the black halos.

Stage 2 alteration is characterized by the replacement of both
the mesostasis and volcanic glass to differing degrees by saponite and
celadonite and the local replacement of plagioclase by K-feldspar. Bulk
rock compositions are enriched in K_2O, Rb, and Ba and, to a lesser
extent, Na_2O, and are depleted in CaO and SiO_2. Host rock Fe is

TABLE VI-5   OXYGEN AND CARBON ISOTOPIC DATA AND CALCULATED TEMPERATURES
OF FORMATION OF CALCITES FROM THE PEDIAEOS AND
AKAKI RIVER SECTIONS

SAMPLE #	ALTERATION ZONE	$^{13}C_{PDB}$	$^{18}O_{PDB}$	$^{18}O_{SMOW}$	TEMPERATURE ^{O}C	
					1	2
KG82255	Sm-Ce-Ze	1.83	-4.43	26.30	33.0	28.0
KG82360	Sm-Ce-Ze	2.87	-3.65	27.10	29.0	24.1
KG82383	Sm-Ce-Ze	2.5	-1.92	28.80	20.5	16.4
KG83012	Sm-Ce-Ze	2.73	0.05	30.91	11.7	7.6
KG83017	Sm	1.97	0.24	31.11	10.9	6.9
KG83032	Sm-Ce-Ze	2.88	0.02	30.88	11.8	7.7
KG83093	Sm-Ce-Ze	0.78	-3.15	27.62	26.4	21.7
KG83089	Sm-Ce-Ze	1.42	-1.91	28.89	20.5	16.0
KG83147	Sm-Ce-Ze	-13.49	-5.61	25.08	39.5	34.1
KG83063	Sm-Ce-Ze	2.92	-0.01	30.85	11.9	7.9

1   $^{18}O_{sw}=0^{O}/\infty$, present seawater value
2   $^{18}O_{sw}=-1^{O}/\infty$, Cretaceous seawater value (Savin 1977)

partially oxidized.

Stable isotopic and experimental studies of celadonite indicate that it generally forms at temperatures < 40°C whereas saponite forms at temperatures <50 - 200°C (Table VI-3). The replacement of plagioclase by K-feldspar at normal seawater Na/K ratios indicates temperatures <140°C (Munha et al. 1980). Oxygen isotopic data of chalcedonic quartz associated with celadonite indicate temperatures of 20°C (Heaton & Shepperd 1977). Therefore, the prevailing temperature during Stage 2 was probably <50°C.

The widespread distribution of celadonite $\pm$ Fe-hydroxides/oxides indicates that oxidizing conditions prevailed locally during the second stage of alteration (Wise & Eugster 1964). Calculations by Seyfried et al. (1978) indicate that basaltic SiO_2 and FeO coupled with seawater K_2O and MgO are adequate for celadonite formation. Thus, no external source of SiO_2 or FeO is required. Their calculations also show that local depletion of K_2O, MgO, or SiO_2 in seawater would produce Fe-hydroxides in place of celadonite. Oxidation of host rock FeO and some removal of MgO from seawater would generate H^+ and thus lower the pH of the seawater (Seyfried et al. 1978).

The formation of saponite is favored by a less oxidizing environment (Andrews 1980; Seyfried et al. 1978; Bass 1976). The formation of MgO-rich saponite, common in the Sm-Ce-Ze Zone, at low temperatures is favored by alkaline conditions (pH >8.5) (Drever 1974). Such conditions may be produced by silicate hydrolysis reactions under rock-dominated conditions (Seyfried et al. 1978).

Progressive zonation from celadonite to Mg-rich, K-poor saponites in single samples and the tendency for saponites to become more Fe-rich

with depth suggest that seawater becomes less oxidizing and more alkaline through time and with depth in the extrusive sequence due to continued reaction with the rocks (Andrews 1980; Seyfried et al. 1978). These clay mineral zonations also indicate that conditions changed from seawater-dominated to rock-dominated in response to decrease in permeability.

Zones of intense alteration along flow margins and joint surfaces of massive flows, with mixtures of celadonite, saponite, jasper or chalcedony, clinoptilolite, and mordenite, are locally distributed throughout the Sm-Ce-Ze Zone. This assemblage of secondary minerals is also common in rocks adjacent to intrusive bodies. These observations suggest that margins of intrusive units and flows were more permeable and have been altered at higher water/rock ratios than the surrounding rock, perhaps under seawater-dominated conditions. Such high water/rock ratios would be required to maintain the high O_2, SiO_2, and H^+ concentrations in seawater necessary for celadonite formation.

The third stage of alteration is characterized by the scattered distribution of zeolites filling open spaces or re-opened clay-filled cracks and fractures. Temperatures for the characteristic zeolites in this zone range from $0 - 100^{\circ}C$ (Table VI-3).

Conditions changed progressively from Stage 2 to Stage 3. Permeability was reduced by the deposition of clay minerals during the second stage of alteration, therefore, seawater became more alkaline, MgO-poor, and SiO_2-enriched, conditions which favor zeolite deposition (Alt & Honnorez 1984; Hay 1966). Clay minerals locally mantle the zeolites indicating that there were local fluctuations in pH and SiO_2 activity. The boundary between these stages, therefore, is not distinct

and reflects primarily a change in the style of alteration, from groundmass-replacing to void-filling.

A characteristic feature of the Sm-Ce-Ze Zone is the association of specific zeolites with either pillows or flow units. The formation of each of these zeolite groups is favored by different Si/Al ratios and pH (Donahoe & Liou 1985; Surham & Sheppard 1978; Hay 1966). Phillipsite and other SiO_2-undersaturated zeolites, such as chabazite, gmelinite, and natrolite, precipitate from fluids with lower Si activities and higher pH than the SiO_2-saturated zeolites, such as clinoptilolite and mordenite (Iijima 1974; Mariner & Surdam 1970). This suggests that the zeolites associated with pillows precipitated from solutions with higher pH and lower SiO_2 activity than the solutions that precipitated the zeolites associated with flows. This is consistent with observed association of SiO_2-saturated zeolites with jasper, opal, or chalcedony.

The conditions necessary for zeolite formation are consistent with the conditions inferred for the formation of the clays associated with pillows and massive flows. The formation of celadonite at high water/rock ratios (seawater-dominated?) lowers the pH and increases the activity of SiO_2 in seawater. As the water/rock ratio decreases due to reduced permeability, the pH of the solution increases, but high SiO_2 activities are maintained, thus favoring the formation of zeolites with high Si/Al ratios. In contrast, saponite formation is favored by more alkaline conditions. It should be noted that many other variables, such as alkali ratios, would affect these assemblages. The consistency of assemblages and associations, however, suggests that permeability and thus water/rock ratios are the dominant influences.

Consistent depositional sequences have also been observed for

each zeolite assemblage. In pillow units where phillipsite and analcime occur together, phillipsite is always the first phase to form. The formation of analcime at the expense of phillipsite is favored by a lowering of the seawater Na/K ratio (Holler & Wirsching 1978; Honnorez 1978), which may also be attributed to the formation of K-feldspar or celadonite (Alt & Honnorez 1984). In flow units, clinoptilolite forms before mordenite; the precipitation of mordenite occurs at the expense of clinoptilolite at increasing temperatures (Hawkins et al. 1978). In experimental studies, phillipsite is commonly the precursor of clinoptilolite (Hawkins et al. 1978).

Deposition of calcite dominates the fourth stage of alteration. Several stages of growth are commonly evident but do not reflect any change in seawater composition. Low Mg/Ca ratios indicate that calcite was deposited from MgO-depleted seawater. Temperatures ranging from 10 to 41°C are consistent with those outlined for Stages 2 and 3 and are higher than those in the overlying zones (Tables VI-4 & VI-5). Carbon isotopic data indicate that all but one of the analysed carbonates precipitated from solutions with an inorganic carbon component (Tables VI-4 & VI-5). The d ^{13}C (PDB) value of sample KG83147 from the Pediaeos River section is -13.9°/oo. This low value suggests that the calcite precipitated from a solution with both a normal seawater (0°/oo) and organic carbon (-25°/oo) component. Mixing of these two sources indicates that either calcite was deposited from seawater with an organic component or that the carbonate precipitated from normal seawater, was subsequently dissolved, and redeposited from a solution, such as meteoric water, with an organic component. Partial replacement of the Ca-rich zeolites by calcite is common in this zone, indicating an

increase in CO_2 activity (Liou et al. 1985; Mehegan et al. 1982).

Veins of palygorskite/calcite and gypsum were deposited during
the fifth stage of alteration in the upper few hundred metres of the
Sm-Ce-Ze Zone. These veins generally re-open clay- or zeolite-filled
fractures.

6.4.4 La-Sm/Ch-Qz Zone

Three stages of alteration have been outlined for the La-Sm/Ch-Qz
Zone (Table VI-2).

The first stage is characterized by the replacement of the
mesostasis and glassy margins by saponite, celadonite,
smectite/chlorite, and quartz and by the partial replacement of
plagioclase by K-feldspar or albite. Na_2O, MnO, and Zn are added to the
rocks; CaO and Sr are depleted.

The coexistence of saponite, celadonite, and smectite/chlorite in
the upper half of this zone, coupled with the disappearance of
celadonite and increased abundance of smectite/chlorite and chlorite in
the lower half, marks a sharp increase in temperature from <100 to
>230°C (Table VI-3). The replacement of plagioclase by K-feldspar at
normal Na/K ratios is favored at a temperature <140°C and by albite at a
temperature >140°C (Munha et al. 1980). The presence of both K-feldspar
and albite suggests that the temperature was around 140°C.

The distribution of the clay minerals also reflects the decrease
in permeability and thus water/rock ratio across this zone (Figure
VI-1). In samples where saponite and smectite/chlorite coexist,
saponite is generally more MgO-rich and the earliest phase to form.
This suggests that the solutions became slightly depleted in MgO during

saponite deposition, as would be the case under rock-dominated conditions.

Laumontite, analcime, albite, quartz, and pyrite were deposited in fractures and vesicles during the second stage of alteration. The solutions compositions that favor the deposition of these void-filling phases are CaO- and SiO_2-enriched and alkaline. As in the Sm-Ce-Ze Zone, the deposition of zeolites does not necassarily imply a separate alteration stage but rather that the solutions compositions have evolved under rock-dominated conditions.

Laumontite and albite are both stable at temperatures $>100^{\circ}C$ whereas analcime is stable at temperatures $<100^{\circ}C$ (Table VI-3). The zonation of these minerals, with analcime concentrated in the upper half of the zone and laumontite being most abundant in the lower half, suggests that the temperature gradient evident during Stage 1 was maintained, although at slightly lower temperatures.

Calcite was deposited during the third stage of alteration. As in the Sm-Ce-Ze Zone, low Mg/Ca ratios suggest that calcite precipitated from solutions depleted in MgO. Temperatures were lower during this stage than during earlier stages, ranging from $50 - 80^{\circ}C$ (Table VI-4). Carbon isotopic data indicate that calcite precipitated from solutions with an inorganic carbon component (Table IV-4) (Muehlenbachs 1979).

6.4.5 Ep-Ch-Qz Zone

The rocks in the Ep-Ch-Qz Zone have undergone three successive stages of alteration (Table VI-2).

During the first stage of alteration, chlorite + quartz + pyrite $\pm$ epidote replaced the mesostasis and glassy margins of cooling-units,

and plagioclase was albitized. Bulk rock compositions were enriched in Na_2O, MnO, Cu, and Zn and depleted in CaO, K_2O, and Rb. The abundance of quartz in the groundmass does not reflect a bulk increase in SiO_2 contents (Figure IV-10) but rather excess SiO_2 released during the formation of chlorite (Mottl 1983).

The dominance of chlorite and quartz and the scattered distribution of epidote indicates that temperatures were 180 - >250°C during the first stage of alteration (Table VI-3).

Chlorite compositions are slightly more Fe-rich than chlorite from typical dredged (Humphris & Thompson 1978) and drilled (Alt et al. 1985) metabasalts and from those produced experimentally (Mottl 1983), whereas they fall within the Mg-rich end of greenstone breccias with quartz-chlorite-pyrite veins (Delaney et al. 1980) (Figure VI-3). Enrichment in whole-rock MgO contents and the concomitant MgO-rich chlorite in the typical metabasalts resulted from interaction between relatively unmodified seawater and basalt under seawater-dominated conditions (Mottl 1983; Humphris & Thompson 1978; Alt et al. 1986). The chlorites from the Ep-Ch-Qz Zone probably formed from slightly MgO-depleted solutions under rock-dominated conditions. The higher MgO contents of the smectite/chlorites from the more permeable La-Sm/Ch-Qz Zone suggest that as the solution moved deeper it became MgO-depleted (Figure VI-3).

Comparison of compositional trends in the Ep-Ch-Qz Zone with experimental studies suggests two different solution sources. The lack of MgO enrichment, the consistent enrichment of Na_2O, and the lack of FeO depletion in the rocks suggest that the rocks were altered under rock-dominated conditions (Mottl 1983; Seyfried & Mottl 1982; Mottl &
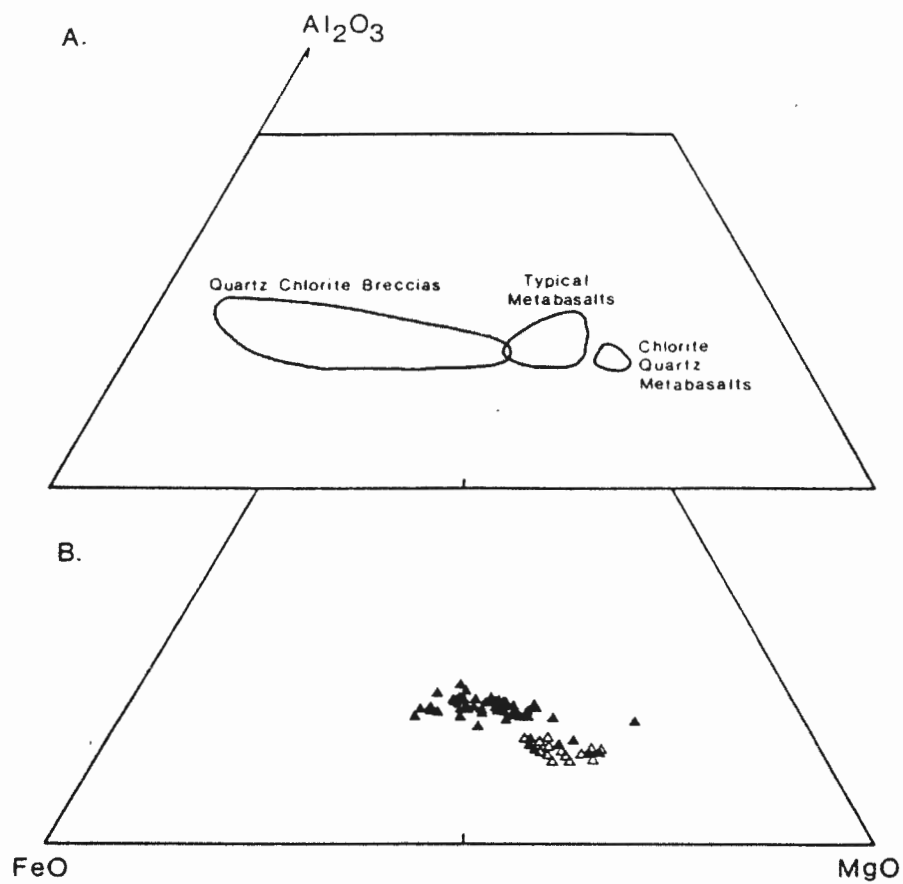
Figure VI-3. A. Molar proportions of chlorites from "in situ" oceanic

metabasalts (modified after Mottl 1983).

B. Molar AFM proportions of chlorite and smectite/chlorite from

CY-la.

Closed triangles are chlorite; open triangles are

smectite/chlorite.

Seyfried 1980; Mottl & Holland 1978; Hajash 1975). Experiments under rock-dominated conditions, however, also predict minor depletion in the metal concentrations of the altered rocks whereas MnO, Zn, and Cu are enriched in these rocks. Alternatively, the enrichment of Zn, MnO, and, to a lesser extent, Cu and the lack of MgO enrichment could result from reaction with soltuions enriched in metals and depleted in MgO, the seawater having reacted with rocks elsewhere at temperatures >400°C under rock-dominated conditions (Rosenbauer & Bischoff 1983). At temperatures greater than 400°C, the pH of seawater is more dependent upon temperature than MgO removal, therefore, at high temperatures seawater may become metal-enriched under rock-dominated conditions. The physical mixing of such "evolved seawater" enriched in metals and depleted in MgO with downwelling solutions would increase the pH of seawater by dilution, lowering the solubility of the metals. In other words, downwelling solutions that has reacted under rock-dominated conditions may have mixed with ascending "evolved seawater".

Deposition of epidote, quartz, pyrite, and rare prehnite in fractures and vesicles and the formation of epidosites in permeable zones during Stage 2 may also have resulted from the mixing of ascending and descending solutions. Co-precipitation of these void-filling phases suggests that solutions were CaO-, SiO_2-, and metal-enriched and MgO-depleted, indistinguishable from the metal-enriched "evolved" fluid envisioned for Stage 1. Similar compositions of both void-filling and groundmass-replacing epidotes (Figure IV-10) suggest that they were precipitated from similar fluids at similar temperatures (Liou et al. 1985). In addition, the "evolved seawater" could provide the FeO and SiO_2 necessary to form these phases (Mottl 1983).

The common association of epidote and hematite in the epidosites suggests that the solutions were locally oxidizing. The restriction of epidosites to permeable zones suggests that the "evolved" seawater may have mixed with more oxygenated seawater.

Localized deposition of calcite occurred during the third stage of alteration. Oxygen isotopic data indicate that the calcite precipitated at temperatures between 60 and 90°C (Table VI-4), significantly less than Stages 1 and 2. Low Mg/Ca ratios, from 0 to 0.02, indicate that the fluids were depleted in MgO, because the MgCO$_3$ content of calcite that precipitates from normal seawater is 8 mole % at 25°C (Mucci and Morse 1983) and at higher temperatures, Mg incorporation is enhanced (Table VI-4) (Fuchtbauer & Hardie 1976). Carbon isotopic data indicate that calcite precipited from solutions with an inorganic carbon component (Table VI-4)(Muehlenbachs 1979).

6.5 SUMMARY OF ALTERATION STAGES

Correlation of the alteration stages outlined for each alteration zone indicates that different physical and chemical conditions prevailed at different depths in the extrusive sequence at different times. The numerous alteration stages described in detail in section 6.4 have been condensed into a general alteration scheme with four alteration stages. Each stage represents simultaneous, similar conditions or progressive changes in conditions between alteration zones. The depositional relationships of the characteristic secondary minerals from each stage are summarized in Figure VI-4 and the inferred conditions for each stage are summarized in Table VI-6.

Figure VI-4. Schematic diagram illustrating the change in secondary

mineralogy with time for each alteration stage (numbered 1 to 4).

The associated alteration zones are indicated on the left side of

the diagram. Solid lines indicate that the phase is abundant;

dashed lines indicate that the phase is less abundant.

Time →

1 2 3 4

palygorskite
gypsum
calcite

Sm-Pa-Ca Zone
Fe hydroxides
saponite
analcime
adularia

Sm-Ce-Ze Zone
saponite
celadonite
Fe hydroxides
phillipsite
analcime
clinophilolite
mordenite

La-Sm/Ch-Qz Zone
laumontite
quartz
pyrite
smectite/chlorite

Ep-Ch-Qz Zone
epidote
quartz
pyrite
chlorite
hematite
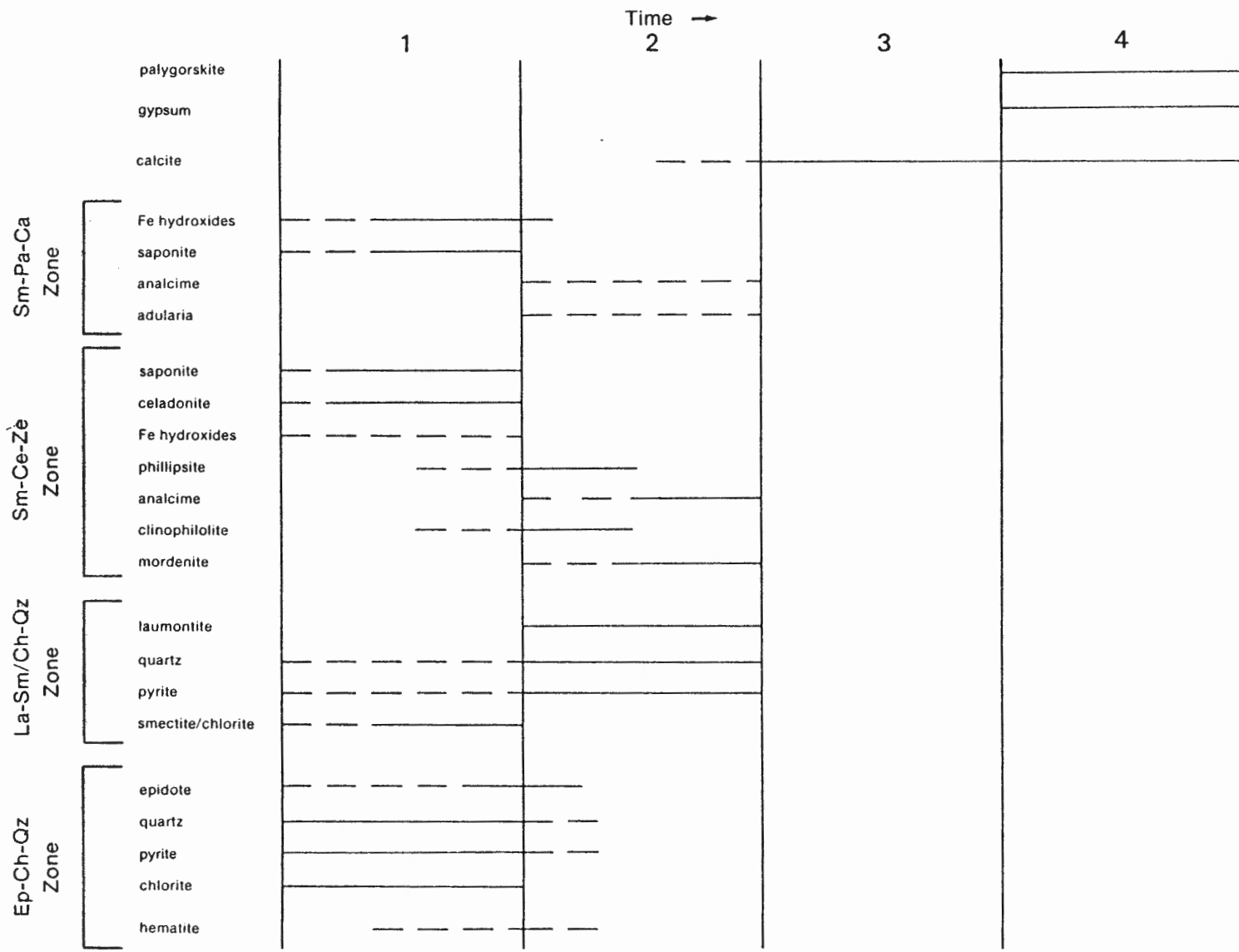
TABLE VI-6   PHYSICAL AND CHEMICAL CONDITIONS IN EACH ALTERATION ZONE DURING EACH STAGE

Alteration Zone		1	2	3	4
Sm-Pa-Ca[*]	temperature	<50	<50	<10	<25
	permeability	high	high	low	low
	water/rock	high	high	moderate	low
	fluid	high O_2,	alkaline	MgO-depleted	??
	composition	low-pH			
Sm	temperature	<50		6-10	<25
	permeability	high		high	high
	water/rock	low			??
	fluid	less O_2			
	composition				
Sm-Ce-Ze	temperature	<50-100	<50-100	10-41	<25
	permeability	high-moderate	high-moderate	high-moderate	high-moderate
	water/rock	moderate	moderate	moderate	moderate
	fluid	high-moderate	alkaline	MgO-depleted	??
	composition	O_2, variable pH			
La-Sm/Ch-Qz	temperature	100-250	100	50-80	
	permeability	moderate-low	moderate-low	moderate-low	
	water/rock	moderate-low	moderate-low	moderate-low	
	fluid	MgO-depleted,	$CaO-SiO_2$-rich,	MgO-depleted	
	composition	moderate-low O_2,	alkaline		
		variable pH			
Ep-Ch-Qz	temperature	>250	>250	60-90	
	permeability	low	low	low	
	water/rock	low	low	low	
	fluid	MgO-depleted,	$CaO-SiO_2-$	MgO-depleted	
	composition	$CaO-K_2O$-rich,	metal-rich		
		near neutral pH			

[*] Stage 1 is not necessarily synchronous with Stage 1 in the other zones.

During and after crustal construction, seawater at ambient
seafloor temperatures migrated downwards into the upper permeable layer
of the extrusive sequence. Temperatures less than $100^{\circ}C$ prevailed as
the seawater reacted with the rocks under both seawater- and
rock-dominated conditions. The deposition of clay minerals along
fractures and cracks reduced the permeability and thus limited the
access of seawater to the rocks.

A thermal gradient, imposed from deeper levels of the crust, was
depressed in this permeable zone by the circulation of cold seawater.
In the transition zone, where permeability decreased and thus the volume
of seawater passing through the rocks decreased, there was a sharp
increase in temperature, from < 100 to $> 200^{\circ}C$. This promoted the rapid
removal of MgO from seawater under rock-dominated conditions. In the
"less permeable" layer where dykes and flows are most abundant, the
thermal gradient was less steep than in the transition zone (Figure
VI-5). Solutions in this layer were slightly alkaline, depleted in MgO,
partially depleted in Na_2O, enriched in CaO and K_2O, and slightly
enriched in metals.

An increase in bulk rock Zn, MnO, and, to a lesser extent, Cu
contents indicates that the downwelling, slightly depleted seawater may
have mixed with more evolved solutions, possibly coming from deeper
crustal levels. The zonation of Zn and Cu enrichment, with Zn being
enriched at shallower levels than Cu suggests that rocks from the
La-Sm/Ch-Qz and Ep-Ch-Qz Zones of CY-la were in the periphery of a zone
of upwelling (Alt et al. 1986; Franklin et al. 1981). The deposition of
epidote, quartz, and pyrite from solutions similar in composition to

Figure VI-5. Schematic thermal gradients for each stage of alteration.
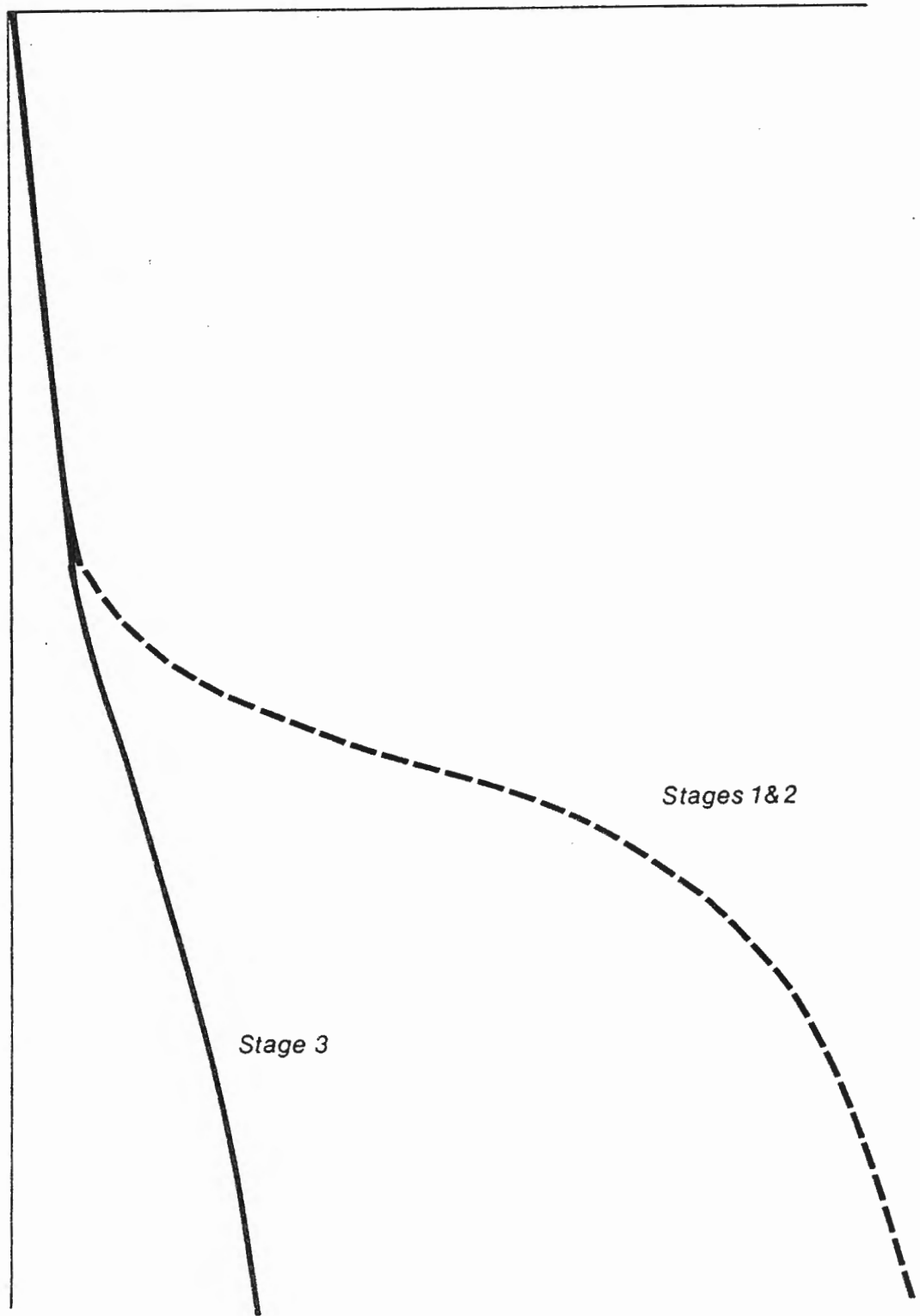
that envisioned for the "evolved" seawater suggests that the enrichment of the rocks in metals and the precipitation of these phases were synchronous.

At all levels in the extrusive sequence, continued reaction of seawater during stage 1 gradually sealed cracks and fractures, decreasing intraformational permeability.

6.5.2 Stage 2

Cold seawater continued to migrate downward during Stage 2; however, reduced permeability within individual cooling-units limited reaction with the rocks and restricted the deposition of secondary minerals to open cavities. Under rock-dominated conditions, solutions became more alkaline and less oxygenated than during Stage 1. Localized changes in alkali ratios, SiO_2 activity, and the pH of the solutions resulted in the deposition of zeolites. Solutions in the transition zone was enriched in CaO, K_2O, and SiO_2 and depleted in MgO due to continued reaction under rock-dominated conditions.

The distribution of zeolites and the local preservation of volcanic glass suggests that there were preferred paths of fluid flow in the permeable layer and transition zone. The lateral variability in permeability indicated by the distribution of cooling-units may have controlled the flow of seawater; therefore, some places became more altered than others. The formation of zeolites and the preservation of glass are favored by less permeable environments.

In the uppermost 100 - 200 m, interaction between the rocks and oxygenated, cold seawater continued oxidizing the lavas at high water/rock ratios.

6.5.3   Stage 3

Stage 3 marks an overall change in conditions. Calcite was deposited from MgO-depleted seawater at all levels in the igneous succession. The stepped temperature gradient of Stages 1 and 2 is greatly reduced (Figure VI-5).

The direction of the flow of the solutions is not known. Its composition indicates that it had previously reacted under conditions which would remove Mg from seawater, suggesting that it may have circulated through deeper levels or laterally. However, the pervasive deposition of calcite in the shallowest, most permeable zones suggests that the source of the solutions was above the lava pile.

6.5.4   Stage 4

Stage 4 was restricted to the upper few hundred metres of the lava pile. Palygorskite, calcite, and gypsum were deposited in re-opened fractures and cracks and in the remaining voids. Decrease in the intensity of Stage 4 veining with increasing depth in the volcanic sequence indicates that the depositing fluids migrated from the upper surface of the lava pile downwards.

6.6   SUMMARY

A general scheme for the alteration in the extrusive sequence outside of the Su-Ch-Qz Zones has been outlined (Figure VI-4, Table VI-5). Each stage correlates the progressive change in physical and chemical conditions with depth in the igneous succession. During Stages 1 and 2, a thermal gradient was imposed at depth in the crust and

seawater migrated down into the extrusive sequence. This flow of cold seawater effectively lowered the temperature throughout the "permeable" layer producing almost isothermal conditions. A sharp rise in temperature across the transition zone and in the lower "less permeable" layer corresponds to a decrease in permeability. The reduction in the volume of seawater flowing through the rocks in the "less permeable" layer allowed for the restoration of a near normal thermal gradient.

In the permeable layer, the rocks were oxidized, enriched in alkalis, slightly enriched in MgO, and locally depleted in CaO. As seawater passed through this layer, it became depleted in O_2, and slightly depleted in alkalis and MgO. In the "less permeable" layer, where temperatures were higher and reaction rates faster, CaO, K_2O, Sr, and Rb were leached from the rocks whereas Na_2O, MnO, Zn, and Cu were enriched. Rock-dominated conditions prevailed and seawater was depleted in MgO, enriched in CaO, K_2O, Rb, and Sr. Mixing of descending seawater under rock-dominated conditions with ascending "evolved" seawater enriched the rocks in metals and resulted in the precipitation of epidote, quartz, and pyrite in voids. Progressive deposition of secondary minerals reduced the permeability in both layers.

Calcite deposition from MgO-depleted seawater throughout the extrusive sequence and the sheeted dyke complex characterized Stage 3. The "evolved" nature of the seawater suggests that it may have circulated through deeper levels in the ophiolite. Pervasive palygorskite, calcite, and gypsum veining was restricted to the upper few hundred metres of the extrusive sequence, suggesting that the seawater originated from above the lava surface during Stage 4.

It is evident from this general alteration scheme that the

composition of the solutions and the degree of its interaction with the rock through which it passes is dependent upon temperature, permeability, and the resultant water/rock ratio. This interaction is reflected in secondary mineral assemblages, bulk compositional trends, and, on a regional scale, the spatial distribution of alteration zones (Figure III-12).

TIMING OF ALTERATION STAGES

7.1 INTRODUCTION

It is the purpose of this chapter to investigate the age relationships between alteration stages and the tectonic history of the ophiolite. Distinction of "in situ" alteration stages from those attributed to the emplacement of the ophiolite is essential to the development of a model for crustal aging which is meaningful for normal oceanic crust. An additional objective is to place some constraints upon the duration of each alteration stage attributed to "in situ" alteration and to compare the results with other models of crustal aging (c.f. Staudigel et al. 1981).

Eighteen void-filling zeolites, clay minerals, carbonates, and gypsum were analysed for $^{87}Sr/^{86}Sr$, K, Rb, and Sr at Lamont-Doherty Geological Observatory as part of a collaborative project with Hubert Staudigel (Appendix I, Tables VII-1 & VII-2). These samples include phases from both the Sm-Pa-Ca and Sm-Ce-Ze Zones and are representative of all stages of alteration (see Appendix VII for sample descriptions).

In the following chapter, the methods of isotopic dating commonly used for studies of secondary minerals from various DSDP sites are reviewed, the results of this study are presented, and constraints upon the timing and duration of each alteration stage are outlined. A discussion follows that relates the age and duration of the alteration stages to the tectonic evolution of the ophiolite.

262

TABLE VII-1   K, Rb, and Sr CONCENTRATIONS and $^{87}Sr/^{86}Sr$ OF
SECONDARY MINERALS FROM THE CY-1 DRILLCORE

DEPTH (m)	MINERAL	K (%)	Rb (ppm)	Sr (ppm)	$^{87}Rb/^{86}Sr$	$^{87}Sr/^{86}Sr$[a]
58.35	calcite	0.04089	0.83	128.1	0.01874	0.707513 ± 29
86.30	calcite	0.000469	n.d.	73.4	n.d.	0.707453 ± 36
86.30	smectite	0.2290	19.3	58.5	0.9541	0.708436 ± 34
123.65	calcite	0.00666	16.3	270.	0.1714	0.707784 ± 38
155.55	palygorskite	0.0586	1.23	36.28	0.09809	0.708121 ± 41
243.30	smectite	1.0400	51.6	22.67	6.577	0.713547 ± 45
291.85	calcite	0.001147	0.07	106.6	0.00190	0.707414 ± 64
293.35	analcime	0.0495	2.27	0.78	8.4252	0.711288 ± 36
293.35	phillipsite	1.6600	31.4	4.04	n.d.	n.d.
299.05	calcite	0.02518	0.64	117.5	0.1576	0.707268 ± 20
327.90	gypsum	0.000469	0.006	311	0.00006	0.708092 ± 52

[a] errors quoted as 2×10^{-6}
n.d. = not determined

TABLE VII-2 K, Rb, and Sr CONCENTRATIONS and $^{87}Sr/^{86}Sr$ OF
SECONDARY MINERALS FROM THE AKAKI AND PEDIAEOS RIVER SECTIONS[a]

SAMPLE#	MINERAL	K (%)	Rb (ppm)	Sr (ppm)	$^{87}Rb/^{86}Sr$	$^{87}Sr/^{86}Sr$[b]
KG82107	analcime	0.00942	1.56	1.403	4.3410	0.709502 + 50
KG82135	heulandite	0.795	4.39	1740	0.007298	0.707193 + 29
KG83203	gmelinite	0.64	2.58	3950	0.001370	0.707635 + 34
HSTR10	mordenite	0.086	1.87	40.96	0.135208	0.706746 + 34
HSTR8A	celadonite	5.96	193.2	2.154	268.3	1.053635 + 56
HSTR8N 106c	celadonite	7.661	211.	n.d.	n.d.	n.d.
HSTR8N 108	celadonite	7.339	210.	3.72	167.0	0.912836 + 48
HSTR8N 123	celadonite	6.49	209.	2.447	254.4	1.028669 + 41
HSTR9y	celadonite	n.d.	135.2	66.9	5.84	0.713921 + 44
HSTR9x	celadonite	3.68	110.7	132.9	2.41	0.709948 + 38
HSTR9xf	celadonite	3.72	109.4	142.57	2.22	0.709670 + 25
HSTR9xf 1	celadonite	3.33	111.3	53.15	6.06	0.713886 + 40
LAUM[c]	laumontite	n.d.	0.70	56	0.27189	0.707600 + 30

[a] data have previously been reported in Staudigel et al. (1986).
[b] errors quoted as 2 x 10^{-6}
[c] from Spooner et al. (1977a).
n.d. = not determined

7.2 BACKGROUND

The age of secondary mineral deposition in the oceanic crust may be determined by Rb/Sr and K/Ar systematics (c.f.Staudigel et al. 1986a). The duration of each stage of alteration may then be inferred by comparing the depositional age of the secondary minerals with the crustal age (Staudigel et al. in press; Staudigel et al. 1981; Richardson et al. 1980).

Rb/Sr compositions of the secondary phases may be used to obtain isotopic dates in two ways. First, isotopic compositions are plotted on a $^{87}Rb/^{86}Sr$ - $^{87}Sr/^{86}Sr$ isochron diagram. In interpreting the derived isochron, it is assumed that the secondary phases are co-genetic and that the Rb/Sr content of these phases has not been reset during a subsequent alteration event. The use of isochron diagrams is limited to phases that have a range of Rb/Sr ratios and has been most effective for clay minerals (Staudigel et al. 1986; Richardson et al. 1980; Staudigel & Hart 1979). An alternative method of dating, used primarily for low-Rb phases, compares the $^{87}Sr/^{86}Sr$ ratio of the secondary phase with the temporal variation in seawater $^{87}Sr/^{86}Sr$ (Staudigel et al. in press; Staudigel & Hart 1985). In using this method, it is assumed that the secondary phases precipitated from chemically and isotopically unmodified seawater and thus record the $^{87}Sr/^{86}Sr$ ratio of the seawater at the time of precipitation. Any contribution from the host rock, whose Sr content and $^{87}Sr/^{86}Sr$ ratios are significantly lower than seawater (98 ppm, 0.7035, Rautenschlein et al. 1985), would lower the $^{87}Sr/^{86}Sr$ ratio of seawater. Therefore, the $^{87}Sr/^{86}Sr$ of a phase that precipitated from the "modified" seawater would inherit a lower isotopic ratio and its age would be a maximum, rather than the true depositional

age.   266

7.3 ^{87}Rb - ^{87}Sr ISOCHRON DIAGRAM

Zeolite, carbonate, and clay mineral samples (except palygorskite) have been plotted on a $^{87}Rb/^{86}Sr$ - $^{87}Sr/^{86}Sr$ isochron diagram (Figure VII-1). The samples span a wide range in Rb/Sr ratios and are scattered around a straight line that may be interpreted as a 75.9 $\pm$ 0.2 Ma isochron (Figure II-1). It is evident that this isochron is dominated by the two celadonite samples, HSTR8 and HSTR9, that have a wide range in Rb/Sr ratios.

The scatter in the isochron diagram suggests that the secondary minerals were not co-genetic. To determine the influence of different depositional ages, isochron ages have been calculated for subsets of the data. Exclusion of the minerals deposited during Stages 3 and 4 (gypsum, palygorskite, calcite) results in an isochron age of 86.1 $\pm$ 0.4 Ma. Zeolites (except analcime) and carbonates, characterized by low Rb/Sr ratios, display a range in initial ratios, from 0.7067 - 0.7076 and 0.7072 - 0.7078, respectively, and include the initial ratio of the 86.4 Ma isochron (0.7071). This suggests that the seawater from which these phases precipitated was moderately heterogeneous in its $^{87}Sr/^{86}Sr$ ratio.

Further subdivision, to exclude the celadonite sample HSTR8 results in an age of 78.5 $\pm$ 0.6 Ma. Model ages for this sample range between 88.4 and 92.4 Ma. The high $^{87}Sr/\ ^{86}Sr$ ratios of the mineral separates of sample HSTR8 make the model fairly insensitive to the choice of initial ratios (host rock - 0.7030, Cretaceous seawater - 0.7075). These age data show that the two celadonite samples formed at

Figure VII-1. $^{87}Rb/^{86}Sr$ - $^{87}Sr/^{86}Sr$ isochron diagram for the zeolites,

carbonates, smectites, and celadonite. The 75.9 $\pm$ 0.2 Ma isochron

includes all the secondary phases except palygorskite and gypsum.

Error limits are included within the symbol for each sample.
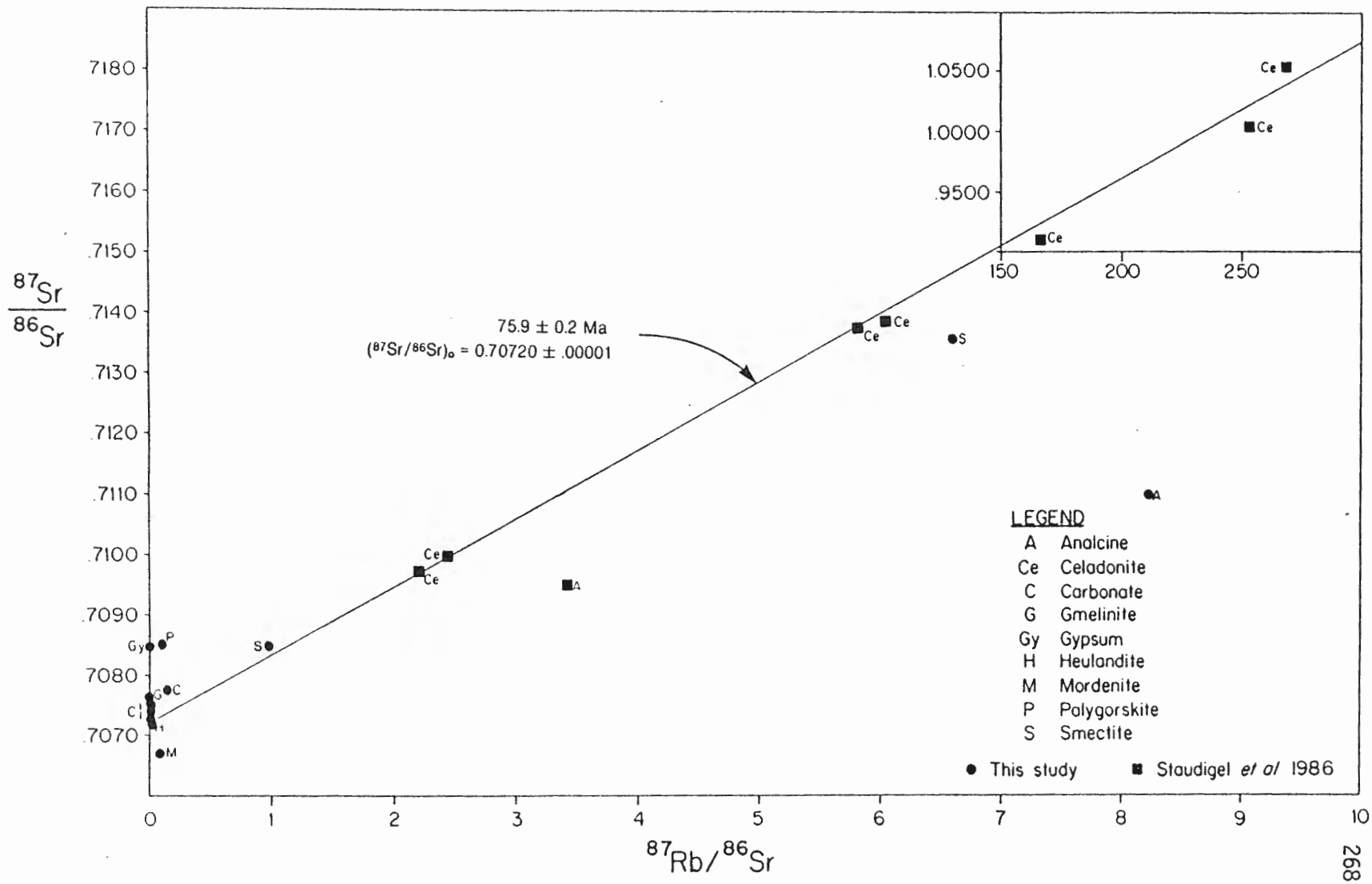
distinctly different times indicating that the 75.9 $\pm$ 0.2 Ma isochron that includes all the data is not appropriate.

A leaching experiment showed that 62.7% of the Sr and none of the Rb in celadonite sample HSTR9 are situated in exchangeable sites (Staudigel et al. 1986). The excellent agreement of the Rb/Sr systematics of leached and unleached fractions of sample HSTR9 indicates that there was no significant isotopic exchange of Sr or Rb in the exchangeable sites.

7.4 $^{87}Sr/^{86}Sr$ SEAWATER CURVE

The $^{87}Sr/^{86}Sr$ evolution curves for the zeolites, calcites, palygorskite, and gypsum have been plotted on the seawater curve of Hess et al. (1986) which illustrates the variation in seawater $^{87}Sr/^{86}Sr$ ratios during the past 100 million years (Figure VII-2). These phases were deposited in open spaces during either Stages 2, 3, or 4 in the upper 500 m of the extrusive sequence. It has been demonstrated in Chapter VI that the host rock contribution of chemical and isotopic components to seawater becomes progressively less from Stage 1 to Stage 4. Therefore, phases deposited during the later stages are most likely to record the unaltered seawater $^{87}Sr/^{86}Sr$ ratio and would be appropriate for dating by this method.

Zeolites were deposited during Stage 2. Their close association with clay minerals suggests that they were deposited from seawater that contains a host rock Sr component. The $^{87}Sr/^{86}Sr$ ratios of heulandite and laumontite fall below the seawater curve indicating that they were not deposited from unaltered seawater. The intersection of the gmelinite evolution curve with the seawater curve outlines a

Figure VII-2. $^{87}Sr/^{86}Sr$ ratios of secondary phases from Stages 2

through 4 and the temporal variation of seawater $^{87}Sr/^{86}Sr$ ratios

(modified after Hess et al. 1986). The shaded area includes the

range of values measured by Hess et al. 1986). The solid lines

are carbonates; long dashed lines are palygorskite and gypsum;

dashed lines are zeolites (A=analcime, G=gmeleinite, H=heulandite,

L=laumontite)
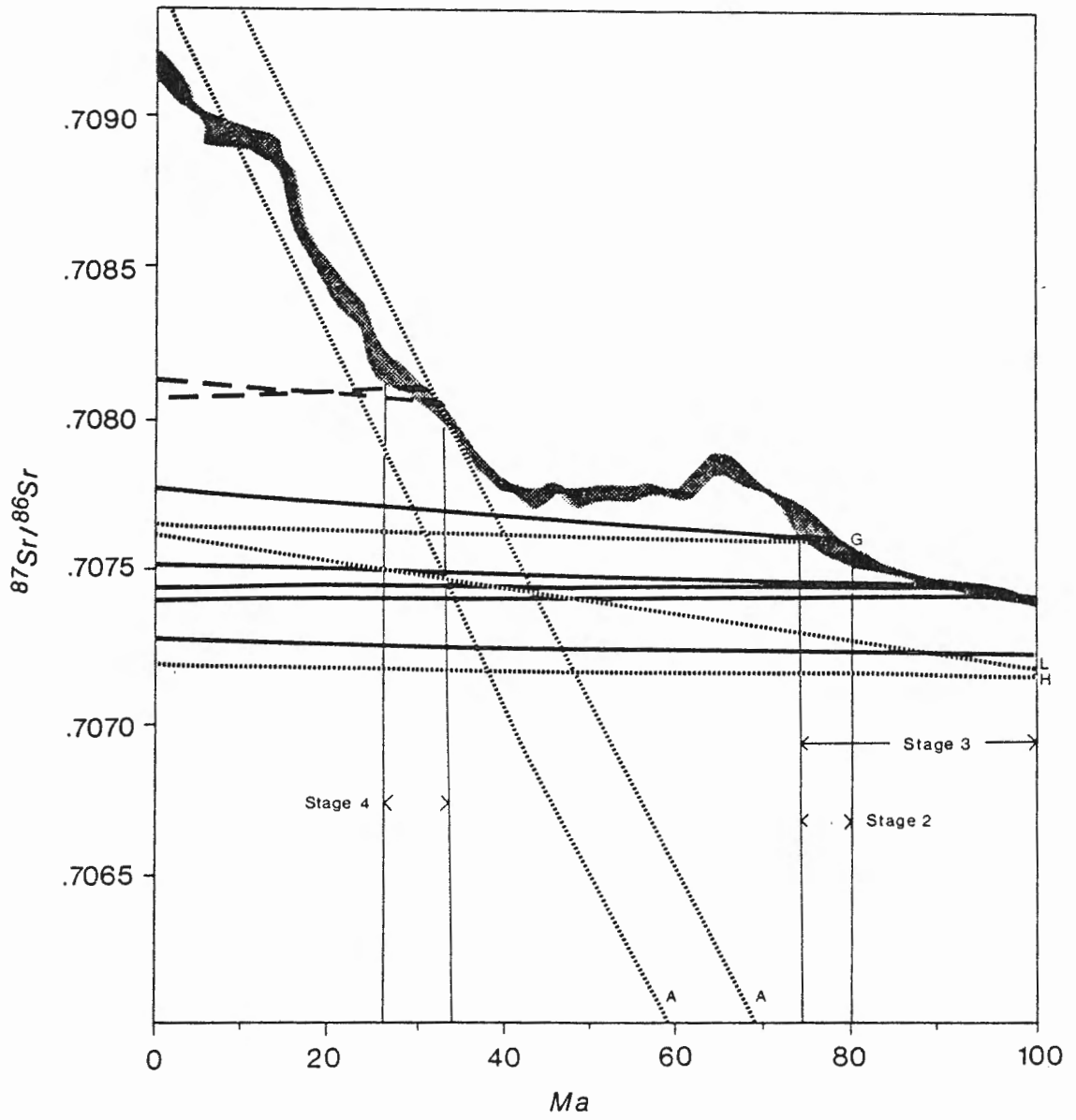
depositional age between 74 and 80 Ma. The $^{87}Sr/^{86}Sr$ ratios of both
analcime samples are significantly higher than the other zeolites. The
evolution curves of samples KG83107 and CY1:293.35 m indicate that they
could have precipitated between 32 and 90, and 10 and 65 Ma,
respectively. At ages less than 10 and 32 Ma, their ratios are greater
than the seawater values whereas at ages greater than 65 and 90 Ma,
their ratios are less than the host rock.

Four calcites from the upper 292 m of the CY-1 drillcore
intersect the seawater curve between 74 and 95 Ma whereas the calcite
from 299 m depth falls below the curve. The low MgO contents (<1 wt%)
of all samples and the low Sr contents (73 - 128 ppm) of four out of
five samples show that calcite did not precipitate from normal seawater.
Oxygen isotopic data indicate that the calcites precipitated at
temperatures between 5 and 16°C (Table VI-3). Calcite that precipitates
from normal seawater at 25° C contains 8 mole% $MgCO_3$ (Mucci & Morse
1983) and 300 - 500 ppm Sr, assuming a Sr/Ca partition coefficient of
0.035- 0.053 (Baker et al. 1982; Katz et al. 1972). Therefore, the four
calcite samples with low Sr contents give maximum ages. The calcite
with normal Sr contents (sample CY-1:123.65 m) intersects the curve
between 74 and 80 Ma, providing the most reliable age.

Comparison of the $^{87}Sr/^{86}Sr$ ratios of palygorskite and gypsum
with the seawater curve gives a depositional age of 28 to 32 Ma. This
indicates that Stage 4 was significantly later than Stages 1 - 3.

Because of the flat, sinusoidal character of the seawater curve
during the Cretaceous, the zeolites and calcites in this time interval
have a wide range of ages. The $^{87}Sr/^{86}Sr$ of seawater has continuously
increased since the Tertiary, therefore the ages of palygorskite and

gypsum are more tightly constrained.

In summary, zeolites were precipitated during Stage 2 from seawater whose isotopic composition may or may not have been modified. The maximum age for gmelinite is 74 to 80 Ma. The analcime samples KG83107 and CY1:293.35 m were deposited between 10 and 65, and 32 and 90 Ma, respectively. Only one of five analysed calcites precipitated from normal seawater during Stage 3. The age of this sample (CY-1:123.65 m) is between 74 and 80 Ma, indistinguishable from Stage 2 whereas the remaining calcites precipitated between 84 and 100 Ma. Palygorskite and gypsum precipitated during Stage 4 between 28 and 32 Ma.

It must be emphasized that the ages of the secondary minerals determined from the seawater curve, with the exception of calcite (sample CY-1:123.65 m), are maximum ages. At any time less than these maximum ages, the $^{87}Sr/^{86}Sr$ ratio of each phase falls between the $^{87}Sr/^{86}Sr$ ratios of seawater and the host rock (0.7030-0.7040). In other words, a mixture of host rock and seawater Sr, in various proportions, could produce the $^{87}Sr/^{86}Sr$ ratios of the secondary minerals, at any time from their maximum age to the present. Therefore, the outlined ages best indicate intervals of time during which the phases could not have formed rather than the actual depositional age.

Partition coefficients of Sr into the secondary minerals under a variety of conditions and seawater compositions are required before the seawater curve can be used as an effective, quantitative method of dating. At present, the seawater curve is useful primarily for dating carbonates.

7.5 K/Ar DATING

K/Ar ages have been determined for 2 unleached fractions of the celadonite sample HSTR9 and a leached and unleached fraction of the celadonite sample HSTR8. The ages of the two splits of sample HSTR9 are 79.8 $\pm$ 1.2 and 76.5 $\pm$ 0.4 Ma, nearly identical to the 78.5 $\pm$ 0.6 Ma isochron for sample HSTR9 + smectites + zeolites. The ages of the leached and unleached fractions of sample HSTR8 are 87.3 $\pm$ 0.8 and 87.0 $\pm$ 0.8 Ma, respectively, again in good agreement with the Rb/Sr model ages of HSTR8.

A leaching experiment showed that 4.2% of the K and 4.7% of the ^{40}Ar in sample HSTR8 are located in exchangable positions (Staudigel et al. 1986). The constancy of the K/^{40}Ar ratios in both fractions suggests that K/Ar systematics were not significantly affected by late-stage alteration processes. Slight differences in K/Ar ages of the two unleached fractions of sample HSTR9 may indicate minor loss of ^{40}Ar or, alternatively, slight age differences in a heterogeneous sample (Staudigel et al. 1986).

7.6 TIMING AND DURATION OF ALTERATION STAGES

Isotopic ages of the secondary minerals confirm that in the upper 500 m of the extrusive sequence, Stages 1 through 3 overlap in time and represent progressive changes in alteration conditions. Comparison of the depositional ages of the secondary phases with the 91.6 $\pm$ 1 Ma U-Pb age of zircons from the plagiogranites (for further discussion see Section 2.2.4) indicates that alteration took place from the time of

crustal accretion up to 17 Ma (Table VII-3).

The Turonian to Maastrichtian was a period of tectonic stability in the area which is now the northern flank of the ophiolite. Marls and chalks of the Lower Lefkara Formation were deposited in broad hollows on the seafloor (Robertson 1977; Robertson & Hudson 1974). This implies that the Troodos ophiolite was still "in situ" and that Stages 1 through 3 are representative of normal oceanic alteration processes. Models for the duration of alteration in normal oceanic crust suggest that it ceases within 13 $\pm$ 5 Ma of crustal accretion (c.f. Staudigel et al. 1986), consistent with the maximum duration outlined for Stages 1 to 3 (Table VII-3).

The last stage of alteration significantly postdates Stages 1 to 3 implying that palygorskite and gypsum were deposited during a separate period of seawater circulation in the upper 500 m of the extrusive sequence. By the Late Oligocene, gradual uplift of the ophiolite in the north produced a shallow, open-marine environment (Robertson 1977). Chalks and marls overlying the extrusive sequence were generally < 60 m thick (Figure II-5), probably not thick enough to prevent seawater penetration into the lava pile (Anderson & Hobart 1976). Gypsum and palygorskite may both have precipitated directly from normal seawater at ambient seawater temperatures (Couture 1977). Alternatively, the source of palygorskite and gypsum may have been the overlying sedimentary sequence rather than seawater. Palygorskite is a common constituent of the Lefkara Formation. Gypsum, however, is restricted to the Middle Miocene Pakhna Formation. This suggests that the age of these minerals must be less than the Middle Miocene. The emplacement of the Kyrenia Mountain Range from the north in the Late Miocene was accompanied by

TABLE VII-3 TIMING AND DURATION OF ALTERATION STAGES

STAGE	METHOD	MINERAL	AGE (Ma)	DURATION (Ma)
1	Rb/Sr	celadonite (HSTR8)	88.4–92.8	$\emptyset$ – 2.6
	Rb/Sr	celadonite (HSTR9)	78.5 $\pm$ $\emptyset$.6	9 – 13
	K/Ar	celadonite (HSTR8)	87.$\emptyset$ $\pm$ $\emptyset$.8 87.3 $\pm$ $\emptyset$.8	$\emptyset$ – 1.8
	K/Ar	celadonite (HSTR9)	79.8 $\pm$ 1.2 76.5 $\pm$ $\emptyset$.4	7 – 15
2	SWC*	zeolites	$\leq$78 – 82	6 – 13
3	SWC*	calcite (CY1:123.65 m)	74 – 8$\emptyset$	8 – 17
		remaining calcite	$\leq$84 – 95	$\emptyset$ – 7
4	SWC*	palygorskite, gypsum	$\leq$28 – 32	??

* seawater curve

deep faulting in the sediments and the Troodos basement (Robertson 1977; Moores 1960) which could provide a mechanism for seawater flow into the extrusive sequence. It is possible that sediments were dissolved and re-precipitated during this period of seawater circulation. There is no conclusive evidence, however, to clearly favor either of these explanations. Further dating may prove that in fact both are true.

7.7 SUMMARY

Isotopic ages of secondary minerals from all stages of alteration in the Sm-Pa-Ca and Sm-Ce-Ze Zones have been obtained using Rb/Sr and K/Ar systematics. Rb/Sr isochron and K/Ar dating methods proved to be most effective but their use is limited to phases with high Rb or K contents, primarily clay minerals. Comparison of the $^{87}Sr/^{86}Sr$ ratios of low-Rb phases with the seawater curve proved to be less effective. Only one calcite clearly precipitated from normal seawater, therefore the ages outlined for the remaining phases may only be treated as maximum ages.

Two periods of seawater circulation have been recognised in the upper 500 m of the ophiolite. The early period, which includes Stages 1 to 3, took place while the oceanic crust was "in situ" and lasted for at least 17 Ma after the time of crustal formation. This confirms that Stages 1 to 3 overlap and represent progressive changes in alteration conditions. Palygorskite and gypsum were deposited as either direct precipitates from seawater or as recycled sediments during the last period of seawater circulation. This period may record the emplacement of the Kyrenia range from the north.

CHAPTER VIII

EVOLUTION OF AXIAL HYDROTHERMAL SYSTEMS AND CRUSTAL AGING

8.1 INTRODUCTION

Models for the evolution of hydrothermal systems and the aging of

the oceanic crust rely upon regional geophysical surveys (e.g. seismic,

heat flow) and the petrology of drilled and dredged rocks. In most

cases, correlation of the results may only be inferred because the

studies were conducted in different areas. Only at drill sites may the

results from "in situ" geophysical measurements be combined with drilled

rocks to provide petrologic constraints for the regional geophysical

models. The DSDP has provided reasonable coverage of the upper few

hundred metres of the oceanic basement; however, samples from below this

depth have only been recovered at Site 504. Despite this gap in our

database, several mathematical models (e.g. Lister 1983; Fehn et al.

1983) and experimental studies (e.g. Mottl 1983) have successfully

duplicated the observed chemical and physical conditions of alteration,

especially those associated with the hydrothermal vents.

Currently, our best opportunity to develop a realistic model for

the aging of the oceanic crust combines studies of ophiolites and "in

situ" crust, with the mineralogical and chemical signatures of

alteration, which reflect the prevailing physical and chemical

conditions, being used as a basis of comparison.

A conceptual model for hydrothermal circulation and crustal aging

for the extrusive sequence of the Troodos ophiolite is presented in the

following sections. The development of a three-dimensional framework,

not available for "in situ" crust, was facilitated by the comparison of

278

excellent field exposures with drillcore. Comparative stratigraphic
sections indicate that the thickness and lithologic variation of the
extrusive sequence and dykes of the Troodos ophiolite are representative
of "in situ" crust (Figures VI-1 & VI-2). Because Troodos is a fossil
spreading centre(s), the circulation paths of seawater and the geometry
of the ridge may only be inferred. This model combines what is known
about the geometry of other ridge systems, the ore deposits, and the
altered rocks themselves.

8.2 CONSTRAINTS FROM THE GEOLOGIC SETTING

Although the actual structure of the spreading centre is not
known, excellent field exposures provide some insight into the geometry
of the ridge system and the style of intrusion. The important points
are:

1. The well-developed sheeted dyke complex indicates that the Troodos
ophiolite originated at a spreading axis or axes (Moores & Varga 1984;
Gass 1980; Moores & Vine 1971).

2. The sheeted dyke complex and the plutonic suite are complicated
zones of intrusion. The multiple gabbroic plutons and the complicated
intrusive relationships in the dykes indicate that intrusion was
episodic and that there was not a steady-state magma chamber (Baragar et
al. in press; Dunsworth & Calon 1984; Moores & Vine 1971). In addition,
the boundary between the gabbros and the dykes, with dykes intruding
gabbros, gabbros intruding dykes, and dykes rooted in gabbros, shows
that the site of intrusion shifted laterally along the ridge (Baragar et
al. in press).

3. Three north-northwest trending axial grabens have been proposed for

the ophiolite on the basis of coherent structural domains within the sheeted dyke complex (Ramsden & Moores 1985; Moores & Varga 1984). The location of the Skouriotissa ore deposit within the axis of the most westerly graben led Moores & Varga (1984) to suggest that these grabens represent fossil axial valleys. In addition, Schiffman et al. (1985) proposed that their boundaries controlled the location of fluid flow during hydrothermal circulation.

4. Both slow (Smewing et al. 1975; Moores & Vine 1971) and fast (Schmincke et al. 1983) spreading rates have been proposed for the construction of the Troodos ophiolite. The constant strike and dip of the extrusive sequence, indicative of eruption in fairly even terrain, suggests a fast spreading rate (Schmincke et al. 1983) whereas episodic magmatism, envisioned for the plutonic suite and sheeted dyke complex, has been proposed for slow spreading rates (e.g. Sleep 1983).

8.3 CONSTRAINTS FROM THE MASSIVE SULFIDE DEPOSITS

The massive sulfide deposits in the Troodos ophiolite are ancient analogues of present day "black smokers" (Oudin & Constantinou 1984). The identification of these "black smokers" at both fast (e.g. 21° N, East Pacific Rise, Edmond et al. 1979) and slow (e.g. 23° N, Mid-Atlantic Ridge, Leg 106 Scientific Party, in press) spreading centres suggests that hydrothermal systems are common features in the oceanic crust. Modern deposits similar in size to those in the Troodos ophiolite have been recognised at Middle Valley, Juan de Fuca Ridge (Davis, pers. comm., 1986) and associated with seamounts (Alt et al. in press). This may indicate that the physical and chemical conditions (i.e. flow rate, mechanism for preservation) necessary to accumulate

large deposits are not common in the oceanic crust (Strens & Cann 1982).
The field relations and metallogenesis of these deposits provide
constraints for the timing and pattern of seawater circulation during
crustal accretion. The important observations are:

5. The deposits are distributed in five mining districts, each
comprising four or more deposits (Constantinou 1980).

6. The ore deposits formed at all levels of the extrusive sequence,
from the transition zone between the dykes and lavas (Kokkinopezoula) to
the top of the lava pile (Skouriotissa). Late-stage dykes cut these
deposits suggesting that they formed prior to the cessation of volcanism
(Constantinou 1980).

7. Both exhalative and replacement deposits have been identified, the
exhalative deposits being by far the most abundant. The consistent
association of fractures and faults with the exhalative deposits
indicates that these structural features localized the upward flow of
hydrothermal fluids (Adamides 1984). In contrast, the replacement
deposits are generally smaller and are not fracture-controlled. This
suggests that the venting of the hydrothermal fluids at the seafloor
requires a means of channelizing the flow.

8. Most of the deposits have consistent mineralogic and chemical
trends. Cores of the stockwork zones are chloritic with no MgO
enrichment whereas their sericite-rich margins are enriched in K_2O
(Lydon 1984). The ore-depositing solutions, therefore, was MgO-poor and
metal-rich and probably evolved under rock-dominated conditions at
temperatures greater than $400^{\circ}C$ (Rosenbauer & Bischoff 1983). Similar
conditions have been inferred for the hydrothermal systems along the
East Pacific Rise where MgO-depleted seawater is actively precipitating

sulfides (e.g. Von Damm et al. 1985; Edmond et al. 1979).

8.4 CONSTRAINTS FROM ALTERED ROCKS

The mineralogical and chemical characteristics of the altered rocks provide valuable information about the physical and chemical conditions prevalent during alteration. The important conclusions are:

9. Permeability in the extrusive sequence is stratified with an upper "permeable" layer and a lower "less permeable" layer. Permeability in the "permeable" layer is not homogeneous because of lateral variation in lithologic types. In addition, permeability is generally greatest in the upper tens of metres of the "permeable" layer where breccias are most abundant. The sequential deposition of secondary minerals in voids indicates that permeability was reduced as alteration proceeded. The thickness of the "permeable" layer varies from 150 to 1400 m.

10. During construction, the intrusion of gabbroic plutons and the injection of dykes at the base of the extrusive sequence produced a steep thermal gradient. This gradient was effectively lowered in the "permeable" layer by the influx of cold seawater. The transition between the "permeable" and "less permeable" layers marks a sharp increase in temperature because of more restricted seawater flow. Therefore, the effective thermal gradient was stepped, with the uppermost zone being almost isothermal whereas below the step, the thermal gradient is more akin to the undisturbed gradient (Figure VI-5).

11. Pervasive alteration in the extrusive sequence is restricted to the uppermost Sm-Pa-Ca Zone where high permeabilities and low temperatures prevailed and the Ep-Ch-Qz Zone where low permeabilities and high temperatures prevailed. The intensity of alteration in the interval

separating these zones is variable because of variable permeability.

12. Rocks in the "permeable" layer, particularily in the uppermost 150 - 250 m, are oxidized and enriched in alkalis. MgO and CaO are locally enriched and depleted, respectively. There is no obvious enrichment in MgO in the "less permeable" layer. CaO and the alkalis are depleted whereas Na_2O is enriched. Variations in the metal content of this zone, from slightly depleted to enriched (this study; Baragar et al. in press) suggest that the rocks were altered under rock-dominated conditions and that ascending, "evolved seawater" locally mixed with descending seawater.

13. Sr, O, and H isotopic compositions of altered rocks confirm that the altering fluid was seawater and show that seawater penetrated down to the plutonic sequence, at 3 - 5 km depth (Chapman & Spooner 1977; Spooner et al. 1977b; Heaton & Shepperd 1977; Spooner et al. 1974). Oxidation profiles of the altered rocks indicate the downward flow of seawater in the recharge zones (Spooner et al. 1977b).

14. Four stages of alteration have been recognised. Stages 1 to 3 were gradational and were associated with hydrothermal alteration and crustal aging prior to the obduction of the ophiolite. Stage 4 was a separate, later alteration event. The sequence of secondary minerals deposited during these stages records progressive changes in the physical and chemical conditions.

15. Alteration associated with "in situ" processes continued from the time of crustal construction for at least 17 Ma. Therefore, only the earliest stage of alteration may be attributed to hydrothermal convection associated with the formation of the ore deposits.

8.5 HYDROTHERMAL CIRCULATION AND CRUSTAL AGING

Circulation of seawater in the oceanic crust is most vigorous during its constructional stage, when permeability is greatest and the injection of hot magma below the axial valleys produces a steep thermal gradient (Lister 1982). This "active", hydrothermal stage, with temperatures in discharge zones ranging from $250 - 350^{\circ}C$, probably lasts for hundreds of years. As the source of heat cools and/or the section moves off-axis and permeability decreases, seawater circulation is restricted to the "permeable" layer. This "passive" stage of circulation is driven by the conduction of heat upward from the underlying rocks. Temperatures are $<100^{\circ}C$ and circulation is much slower (Lister 1982). Active and passive circulation may coexist during the early stages of alteration whereas passive circulation may continue indefinitely. A schematic section perpendicular to the strike of a spreading axis illustrates the variable flow of seawater through the upper few kilometres of the oceanic crust as it moves away from the ridge axis (Figure VIII-1).

8.5.1 Hydrothermal Stage

Large-scale, ore-producing hydrothermal activity was restricted to the constructional stages of Troodos crustal evolution (Points 6 & 7). Permeability in the extrusive sequence was greatest during this early hydrothermal stage because reaction between the downwelling seawater and the lavas was only getting started and, therefore, the deposition of secondary minerals in fractures was minimal. The geographic and stratigraphic distribution of the ore bodies also suggests that the convection cells were not fixed with respect to a

Figure VIII-1. Schematic section perpendicular to a spreading centre. Outlined areas $A^1 - A^2$ and $B^1 - B^2$ are enlarged in Figures VIII-2 and VIII-3 respectively. Dark shaded areas represent sulfide mineralization; stipled areas represent sedimentary rocks; arrows indicate the flow of seawater.
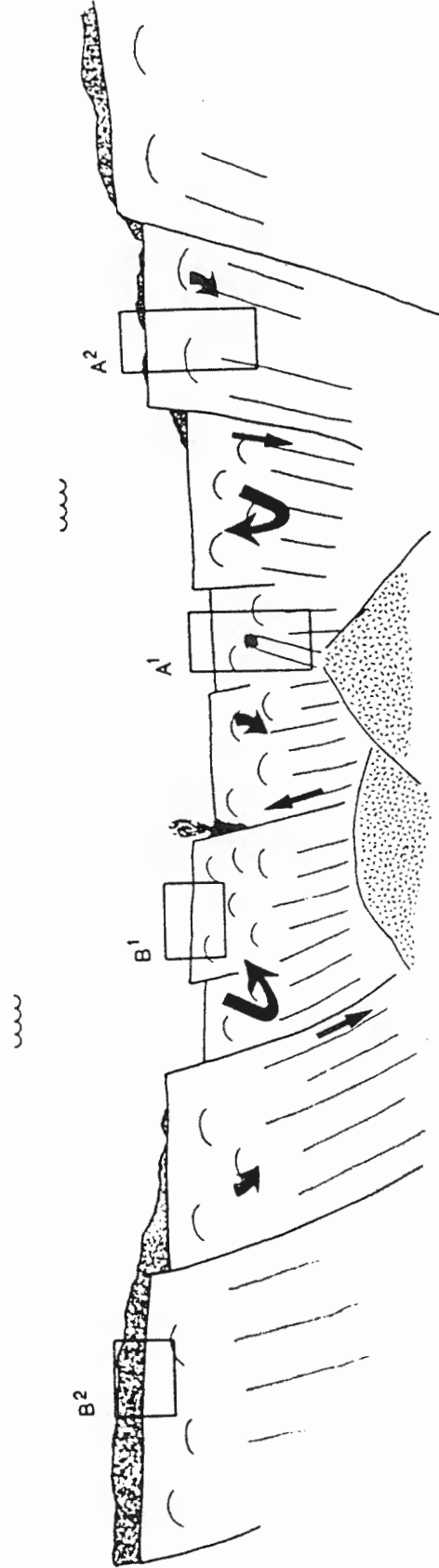
single ridge axis because there is no obvious younging direction for the position of the deposits in the extrusive sequence. Episodic intrusion (Spooner 1976) and the location of large faults (Point 3) could control the spatial distribution of these convection cells.

The boundary between the "permeable" and "less permeable" layers lies approximately at the lava/dyke transition. Below this transition zone, the movement of seawater to deeper levels became more restricted, resulting in a sharp rise in the thermal gradient and alteration under rock-dominated conditions. It is not known if the volume of seawater which could flow from the "permeable" to "less permeable" layer would be adequate to produce a deposit the size of those in Cyprus.

It has been suggested that structural features, such as faults, act as conduits which localize the upward movement of "evolved" seawater (Schiffman et al. 1985). It is reasonable to assume that such structural features not associated with mineralization could also effectively allow transfer of seawater to deeper crustal levels at much faster rates than could be achieved by migration through the lava pile. Water/rock ratios in structural conduits would probably be high and seawater-dominated conditions might prevail. To produce the rock-dominated conditions necessary to form the metal-enriched fluids, the permeability of these structural features and the flow-rate would have to decrease with depth. Evidence in the field for these "conduits", however, is minimal. Resistant vertical zones, composed of reddish-grey basalt fragments in a sparry calcite matrix, are present throughout the extrusive sequence. These zones are 1 - 2 m wide and commonly have an oxidation halo which extends several metres into the surrounding rock. Oxygen and carbon isotopic data for the carbonates

from these zones (Table VI-5) indicate that they precipitated from normal seawater at temperatures between 20 and 40°C. These structural features may have acted as recharge conduits which brought large volumes of seawater to the base of the extrusive sequence. Other than the large-scale fault boundaries described by Schiffman et al. (1985), however, there is little evidence that faults or fractures acted as conduits for seawater flow within the sheeted dyke complex (Baragar, pers. comm., 1986). It is obvious that further investigation is necessary to resolve how seawater is transported to depths below the extrusive sequence.

Smaller convection cells also probably existed during crustal construction. Sub-surface mixing of descending seawater with ascending "evolved" seawater resulted in localized distribution of small sulfide showings and metal-enriched rocks throughout the lavas and dykes, such as in the lower 350 m of CY-1a or small deposits such as Agrokipia "B" (CY-2a) (ICRDG 1984) (Figure VIII-2). Metal enrichment in the rocks from both CY-1a and the Agrokipia "B" deposit is restricted to the lowermost flows and dykes (Figure VI-1) (ICRDG 1984) (Points 9 & 10). The solubility of metals would be reduced in this zone of mixing, causing the precipitation of sulfides and metal enrichment where permeability change. The injection of high-level dyke swarms could localize convective flow. This convection would be short-lived, however, because the dykes would cool faster than a magma chamber (Mottl 1983) and would be less likely to produce a large deposit.

Above the metal-enriched zones of both CY-1a and CY-2a, there is no evidence that the evolved seawater passed upward into the "permeable" layer. Dilution by mixing with unmodified seawater already within this

Figure VIII-2. Schematic diagram showing the flow of unmodified and "evolved" seawater in the vicinity of a high-level dyke swarm, within the ridge axis (A^1). A^2 represents the same section, at same time later, away from the ridge axis.

KEY:
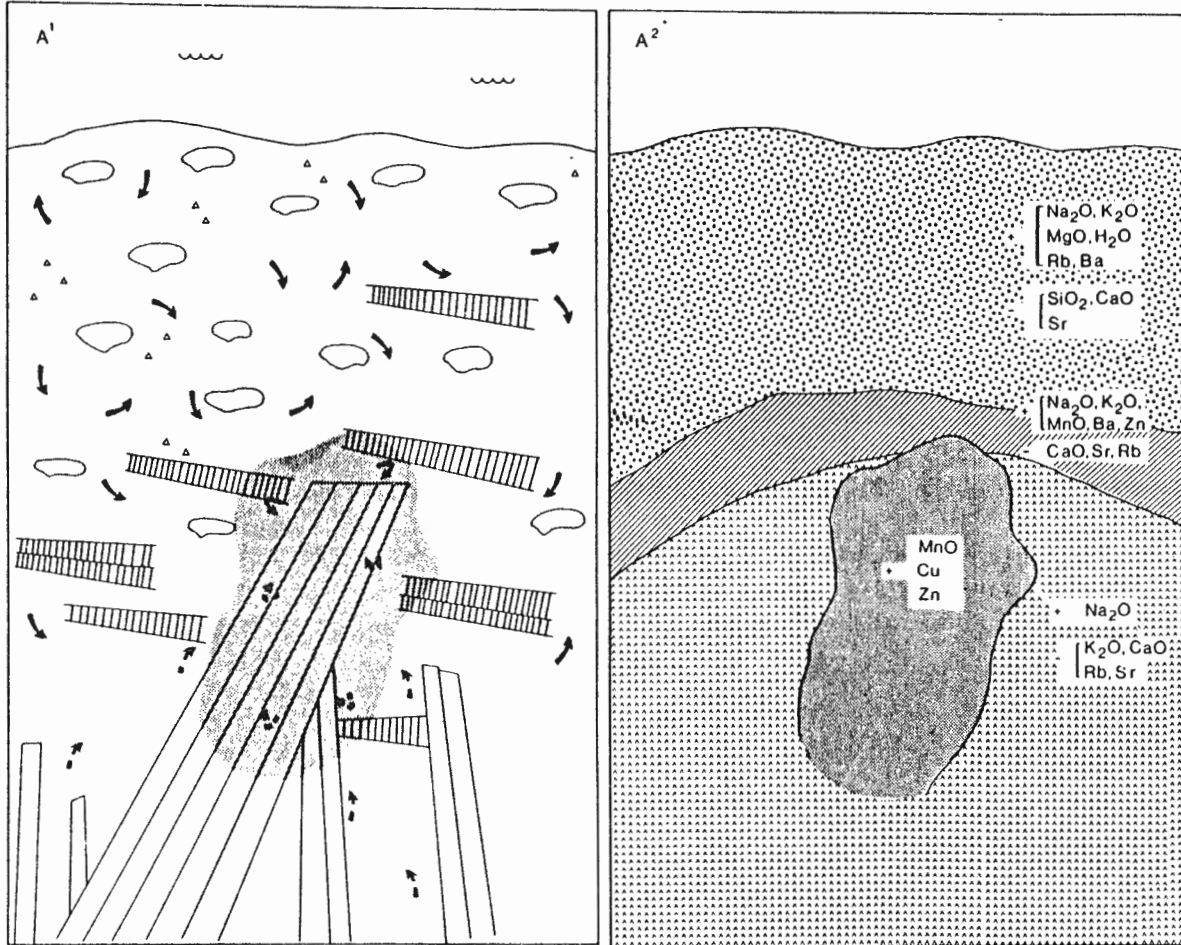
→ flow of unmodifed seawater

⇢ flow of evolved seawater

⫿ massive flows

◯ pillows

ⲛ dykes

▨ zone of mixing

KEY:

☐ Sedimentary Rocks

⬚ Sm-Ce-Ze Zone

▨ La-Sm/Ch-Qz Zone

⬛ Ep-Ch-Qz Zone

■ Zone of mixing

layer most likely dispersed its chemical signature. It is unlikely that this "evolved" seawater was trapped within the "less permeable" layer.

The volume of seawater within the "permeable" layer would be much greater than the volume which could pass downward into the "less permeable" layer. To compensate for this reduction in volume, secondary convection cells within the "permeable" layer would probably develop independently from the deep-rooted, heat-driven convection cells.

8.5.2 Crustal Aging

Crustal aging began as soon as the lavas were extruded onto the seafloor and continued until the rocks were effectively sealed from seawater by the deposition of an impermeable layer of sediment and/or by the clogging of fractures due to the deposition of secondary minerals. In the uppermost 100 - 200 m of the extrusive sequence, where permeability was greatest, the influx of cold seawater at higher water/rock ratios than in the underlying rocks led to pervasive oxidation, intense alteration, and enrichment in alkalis. The intensity of alteration in the rocks below this zone, but still within the "permeable" layer, was not uniform and the rocks were only locally oxidized and enriched in alkalis. Zones of high permeability, such as the margins of flows and intrusions, were most intensely altered, whereas zones of lower permeability were variably altered.

As alteration proceeded, the initial permeability of the crust was progressively reduced by the precipitation of secondary minerals in fractures and voids. The greatest change in permeability occurred where initial permeabilities were high because alteration at higher water/rock ratios promoted the deposition of secondary minerals. These zones of

high permeability also generally contain abundant glass which, upon hydration alters to smectite and zeolites, swells and effectively lowers permeability (Honnorez 1981). Elsewhere in the permeable zone, the initial permeability was reduced but to a lesser degree. Therefore, permeability within the "permeable" layer remained heterogeneous although the average difference between this zone and the lower, "less permeable" zone was reduced.

The movement of seawater into the "less permeable" layer probably became restricted by the clogging of the "permeable" layer. In addition, cooling of the heat source at depth reduced the driving mechanism for deep seawater penetration. Below the lithologic transition zone, there is no evidence for continued reaction, after the initial hydrothermal stage, between circulating seawater and the host rock, suggesting that the "less permeable" layer became relatively impermeable.

Later, perhaps "off-axis", circulation led to the deposition throughout the extrusive sequence of carbonate derived from seawater depleted in MgO. The source of this fluid is not known but it may have originated at deeper crustal levels. This would mean that the entire extrusive sequence passed through a zone of discharge at some time during its evolution.

Syn-volcanic umbers in topographic lows restricted the penetration of seawater into the underlying pillows (Figure VIII-3). It is difficult to estimate if, and when, the lavas in the intervening areas became sealed from seawater penetration because the sedimentary cover was discontinuous at least until the Eocene. The minimum duration of secondary mineral deposition associated with "in situ" alteration in

Figure VIII-3. Schematic diagram showing the flow of unmodified
seawater through the upper few hundred metres of the oceanic
basement, near the ridge axis (B^1). B^2 represents the same
section, at some time later, away from the ridge axis where the
rocks are overlain by sedimentary rocks. I is analogous to the
alteration in the Pediaeos River area; II is analogous to the Akaki
River area.

KEY:
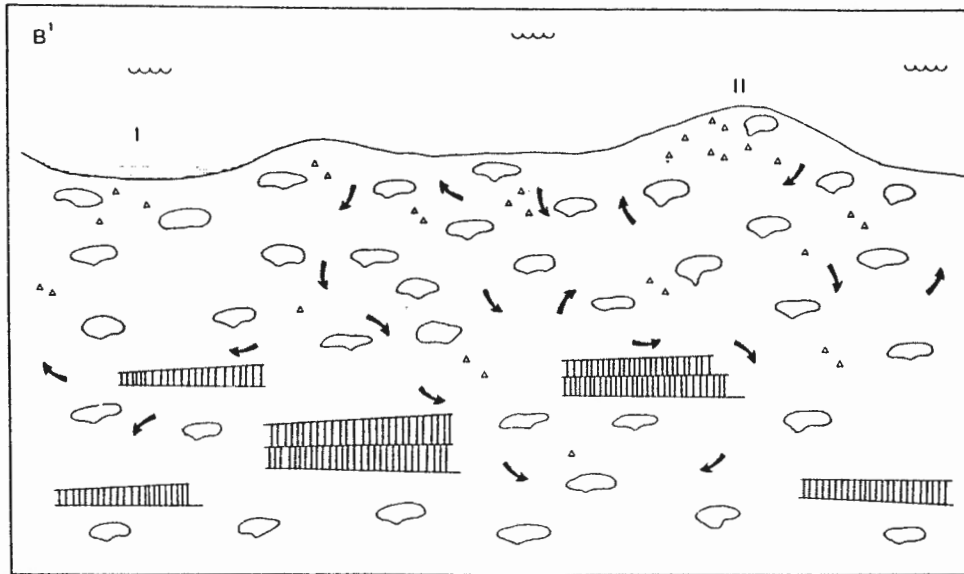
→ flow of unmodifed seawater

▥ massive flows

⬭ pillows

△△ breccias

▤ umbers
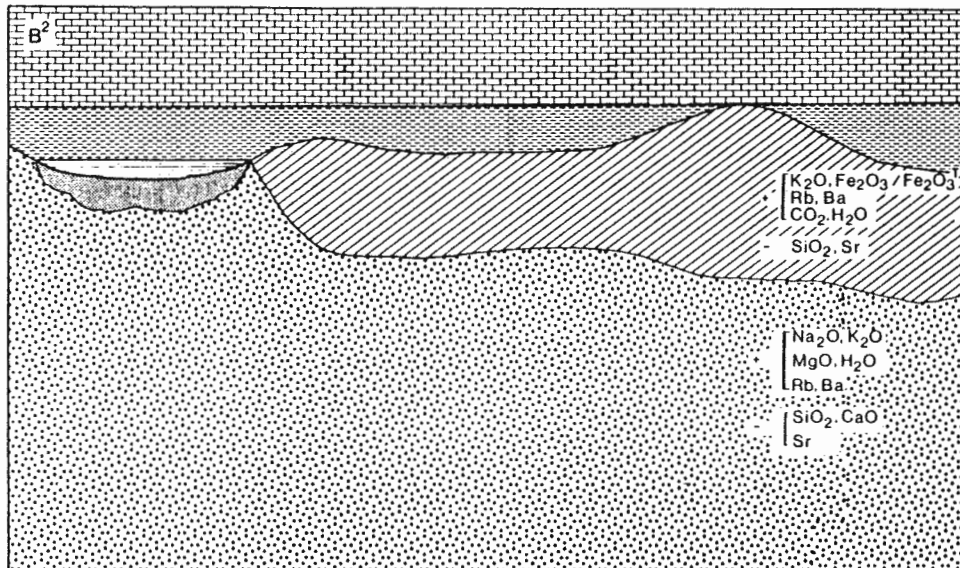
KEY:

▤ Upper Lefkara Chalks

▦ Middle Lefkara Marls & Chalks

▨ Perapedhi Umbers

▧ Sm-Pa-Ca Zone

▨ Sm Zone

⬚ Sm-Ce-Ze Zone

$K_2O, Fe_2O_3/Fe_2O_3$
Rb, Ba
CO_2, H_2O

SiO_2, Sr

Na_2O, K_2O
MgO, H_2O
Rb, Ba

SiO_2, CaO
Sr

the upper 500 m of the Troodos ophiolite was 17 Ma indicating that seawater circulation continued at least until the Maastrichtian (Point 14).

Pervasive palygorskite, gypsum, and calcite veining, which overprints the upper few hundred metres of the ophiolite, has been associated with a period of seawater circulation during the Miocene or later. It is unrelated to "in situ" oceanic alteration but may be related to the emplacement of the Kyrenia Range.

It may be concluded that aging of the oceanic crust results in a reduction of bulk permeability and modification of its bulk composition. The rate of change of permeability appears to be variable, particularly in the "less permeable" layer. The uppermost permeable zone is pervasively oxidized and enriched in alkalis and CO_2 and depleted in SiO_2. Below this zone, but still within the "permeable" layer, rocks are variably enriched in alkalis and MgO and slightly depleted in CaO, SiO_2, and Sr. In contrast, the rocks in the "less permeable" layer are enriched in Na_2O, and locally in metals, and depleted in CaO, K_2O, Rb, and Sr. MgO shows no consistent trend and therefore these rocks cannot be considered a source or sink for MgO.

8.6 COMPARISON WITH MODELS FOR AGING OF "IN SITU" OCEANIC CRUST

Only the products of crustal aging may be directly compared to establish how "representative" the alteration of ophiolites is of "in situ" oceanic crust. Two locations drilled by DSDP proved to be analogous to the alteration pattern observed in the Troodos ophiolite: Sites 417 and 418, drilled in Cretaceous crust south of the Bermuda Rise and Site 504, drilled in 5.9 Ma crust 200 km south of the Costa Rica

Rift. The secondary mineralogy and the alteration geochemistry of these cores were described and compared to the alteration zones defined for the Troodos ophiolite in Sections 3.4 and 5.7 respectively.

In the following discussion, the physical parameters believed to control the distribution and style of alteration in both "in situ" crust and the Troodos ophiolite are outlined and compared. To minimize confusion, the alteration zones described for the DSDP sites have been given the same nomenclature used in this study (Figures VIII-4 & VIII-5).

Alteration of the rocks in the Sm-Pa-Ca Zone of the Troodos ophiolite is most similar to Hole 417A as both were initially zones of high permeability, open to seawater circulation for a prolonged period of time. The lateral variation in thickness of the Sm-Pa-Ca Zone documented in the field exposures (Figure III-12) is also evident in "in situ" crust (Figure VIII-4). It has been documented that Hole 417A is a topographic high relative to Holes 417D and 418A and that the rocks at Hole 417A remained open to seawater circulation for 10-20 Ma longer than the surrounding areas (Shipboard Scientific Crew, Legs 51, 52, & 53, 1979 a&b). This suggests that the original seafloor morphology influenced the rate of sediment accumulation and, therefore, the duration of open circulation. A similar situation is evident in the Troodos ophiolite. The extrusive sequence exposed along the Akaki River section is thicker than in other areas along the northern flank of the ophiolite and is overlain by the Upper Lefkara Formation. In the surrounding areas, the older Perapedhi and Middle Lefkara Formations overlie the lavas. This suggests that the Akaki River area may have been a topographic high, left exposed to open circulation for 10 -

Figure VIII-4. Alteration zones for DSDP Holes 417A, 417D, and 418A

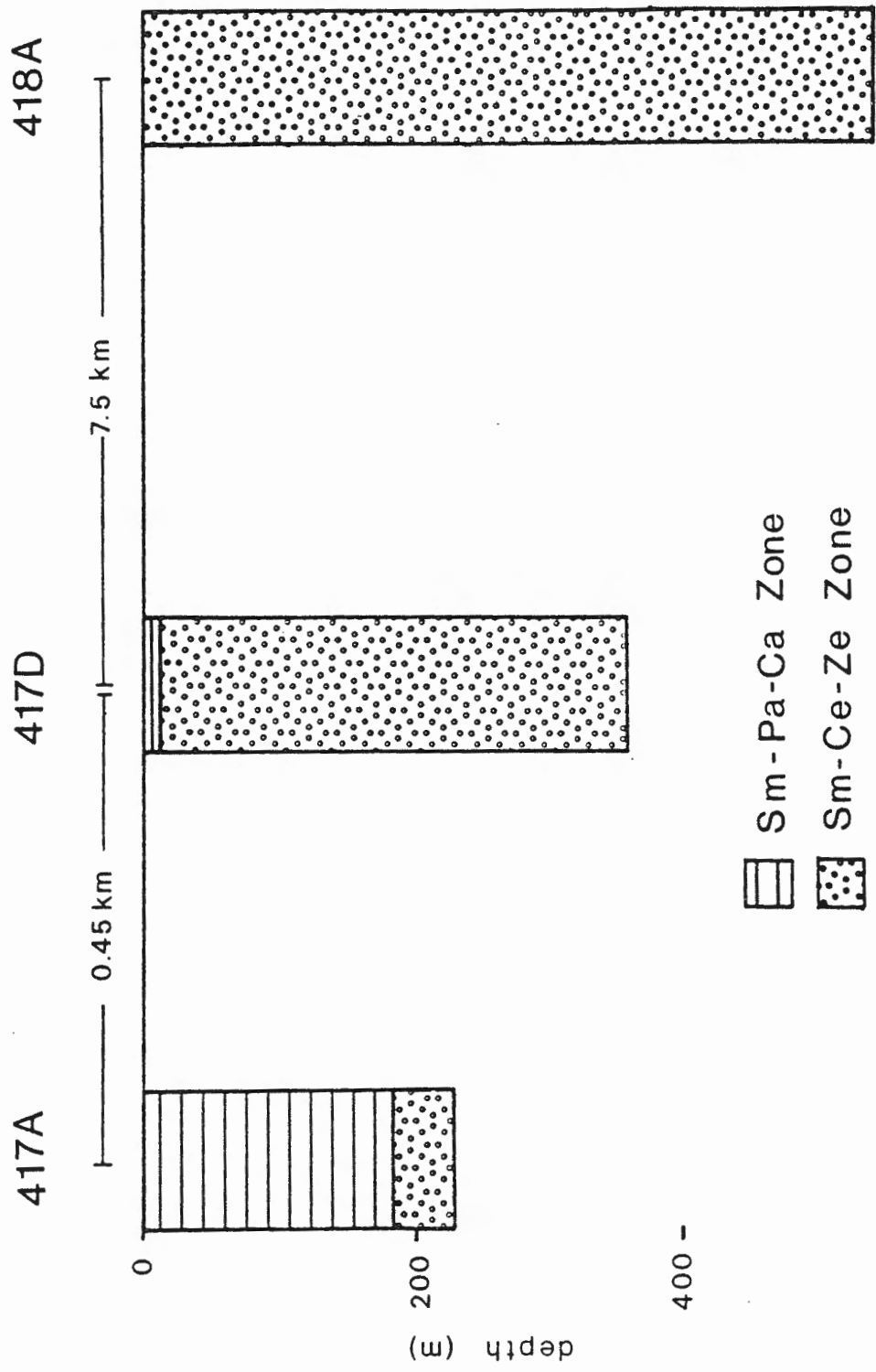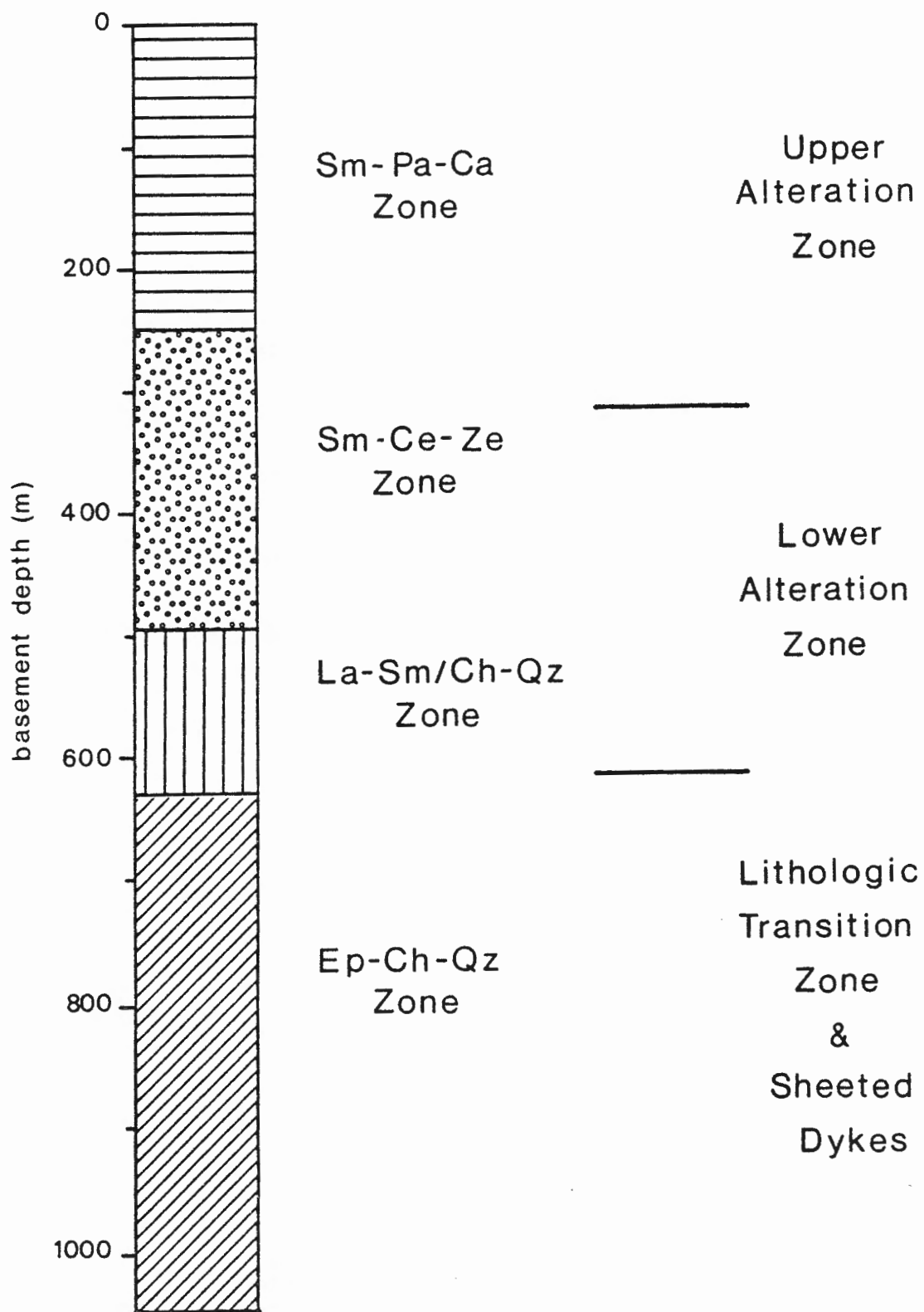(modified after Shipboard Scientific Crew, Legs 51, 52, & 53, 1979

a&b).

Figure VIII-5.   Alteration zones for DSDP Hole 504B (modified after Alt
et al. 1985; Honnorez et al. 1983).

Hole 504B

Sm-Pa-Ca Zone
Sm-Ce-Ze Zone
La-Sm/Ch-Qz Zone
Ep-Ch-Qz Zone

Upper Alteration Zone
Lower Alteration Zone
Lithologic Transition Zone & Sheeted Dykes

30 Ma. Because the Sm-Pa-Ca Zones in the Akaki River area and at Hole 417A are thicker than in their surrounding areas, it may be concluded that prolonged exposure to open circulation resulted in more pervasive alteration. The areal distribution of the Sm-Pa-Ca Zone, therefore, is dependent upon permeability, the rate of sedimentation, and seafloor morphology. It is believed that alteration equivalent to the Sm-Pa-Ca Zone is common in the oceanic crust, particularly in regions like the Atlantic where sedimentation rates are slow. In areas where sedimentation is fast, such as Site 504, this zone is not as well developed and the alteration associated with open circulation is overprinted by subsequent "less oxidizing" alteration.

In the underlying Sm-Ce-Ze Zone, both seawater- and rock-dominated conditions locally prevailed during the early stages of alteration. In the Sm-Ce-Ze Zone of the Troodos ophiolite, intense alteration was generally restricted to zones of high permeability, such as flow margins. Seawater-dominated conditions prevailed in these zones and produced secondary mineral assemblages different from those which formed in zones of lower permeability where rock-dominated conditions prevailed. The absence of such zones of intense alteration in the Sm-Ce-Ze Zones of the DSDP drillcores suggests the high water/rock ratios necessary to form these assemblages were not widespread or, alternatively, that the low recovery rates precluded their sampling.

The lower boundary of the Sm-Ce-Ze Zone was not sampled at Holes 417A, 417D, and 418A. At Hole 504B, a lithologic change (Figure VI-2) marks a transition from permeable approximately isothermal conditions to less permeable conditions with a steep thermal gradient (Alt et al. 1986). This lithologic change corresponds to the La-Sm/Ch-Qz Zone

whereas the underlying rocks correspond to the Ep-Ch-Qz Zone (Figure VIII-4). The sharp increase in temperature across this transition zone indicates that the thermal gradient was stepped. This has also been inferred for the Troodos ophiolite.

During axial hydrothermal convection, it is believed that ascending "evolved" seawater and descending seawater mixed within this transition zone. Recovery of the products of such zones of mixing in the only deep basement hole and in the CY-la drillcore combined with the common small sulfide showings in the sheeted dyke complex, suggests that sub-surface mixing is a common phenomenon in the oceanic crust. The coincidence of these zones with a lithologic, and thus permeability, change indicates that the upward flow of hot, metal-enriched solutions are cooled where they reach the upper "permeable" layer and that upwelling, ore-forming solutions must be focussed, for example along a fault, to reach the seafloor. The driving mechanism for the small deposits may be the intrusion of dyke swarms which act as a localized heat source for a short time period. However, the influence of a deeper-seated magma chamber cannot be ruled out.

Systematic high and low heat flow measurements away from the Galapagos Spreading Centre have been associated with deep, off-axis convection of seawater (e.g. Green et al. 1981; Williams et al. 1974). It is believed that the location of convection cells within the ridge axis is fixed. As rocks move away from the ridge axis, they pass through one stationary convection cell before becoming fixed either in a zone of recharge or discharge within the moving plate (Fehn et al. 1983). The alteration stages recognised at Hole 504B indicate that the rocks passed through zones of discharge and recharge near the ridge axis

before becoming fixed within a zone of discharge as the rocks moved away
from the ridge (Alt et al. 1986). It is difficult to recognise the
effects of off-axis circulation in the Troodos ophiolite because the
geometry of the spreading centre and the rate of spreading are not
known. The precipitation of carbonates from MgO-depleted seawater at
low temperatures during a later stage of alteration may indicate that
the rocks moved into a zone of discharge after they passed through axial
hydrothermal cells. The widespread distribution of laumontite and
calcite throughout the sheeted dyke complex and the plutonic suite would
also be consistent with a model for deep, off-axis circulation. Stable
isotopic studies of these minerals, however, suggest they were
precipitated from a fluid which evolved as a result of the
serpentinization and fracturing of the underlying peridotites (Kerrich &
Vibetti 1985; Vibetti et al. 1985) and, therefore, are not necessarily
related to off-axis circulation.

The permeability of young oceanic crust is stratified, with an
upper "permeable" layer ($\geq 10^{-13} - 10^{-15}$ m^2) and a lower "less
permeable" layer ($\leq 10^{-17}$ m^2) (Anderson et al. 1985; Becker 1985;
Hickman et al. 1984). Within the upper tens of metres of the
"permeable" layer, permeability is consistently high whereas, below this
zone, the distribution of permeability is not uniform. This
stratification of permeability correlates with the seismic velocity
layers defined for the upper oceanic crust (Ewing & Houtz 1979).
Seismic layer 2A is equivalent to the uppermost highly "permeable" zone,
layer 2B to the variably "permeable" layer below this zone of highest
permeability, and layer 2C to the "less permeable" layer. Seismic
studies have shown that layer 2A disappears as the crust ages. It is

believed that a reduction in permeability by the filling of cracks and fractures and/or compaction would make layers 2A and 2B indistinguishable (Ewing & Houtz 1979). In the Troodos ophiolite, the filling of voids suggests that permeability decreased throughout the extrusive sequence as alteration proceeded; however, the rate of change was probably greatest in the zones of highest permeability. Therefore, permeability of layer 2A after alteration may be similar to that in the underlying rocks (layer 2B) and thus correlate with the disappearance of layer 2A.

8.7 COMPARISON WITH OTHER OPHIOLITES

Of the ophiolites believed to preserve their original ocean floor alteration pattern (Troodos, Sarmiento, Semail, East Taiwan, Del Puerto), only the "permeable" layer of the Troodos ophiolite is analogous to alteration zones outlined for "in situ" oceanic crust. It has been suggested that the extrusive sequences of the Semail, East Taiwan, and Del Puerto ophiolites were altered at high temperatures due to conditions peculiar to their geologic setting. For example, Alabastar et al. (1985) suggested that a 10 - 20 m thick layer of sediments effectively sealed the lavas of the Semail ophiolite from cold seawater and thus, promoted repeated circulation of seawater at higher temperatures than would prevail in an open system. In their study of the Sarmiento ophiolite, Stern & Elthon (1979) proposed that steep thermal gradients, in the vicinity of a ridge system, would result in high temperature assemblages in the permeable zone which would be overprinted by low temperature, retrograde metamorphism as the rocks moved away from the ridge axis. It is difficult to envisage, however,

how high temperatures could be maintained in the "permeable" layer during the early hydrothermal stage. Below the lava-dyke transition, alteration in all the ophiolites is similar to the Troodos ophiolite and "in situ" crust.

The general model proposed for the evolution of the Sarmiento ophiolite (Stern et al. 1984; Stern & Elthon 1979; Stern et al. 1976) is similar to the model outlined for the Troodos ophiolite and "in situ" oceanic crust in many respects. An inverse relationship was recognised between temperature and water/rock ratio such that temperatures were greatest at deep crustal levels where water/rock ratios were lowest (Elthon et al. 1984). The degree or intensity of metamorphic effects (decreased whereas the grade of metamorphism increased with increasing depth. Retrograde effects throughout the igneous succession suggested that deep, hydrothermal convection and high grade metamorphism were restricted to the ridge axis whereas outside this zone, circulation was shallower and lower temperatures promoted a retrograde overprint. Although this model is generally in agreement with models proposed for the Troodos ophiolite and "in situ" oceanic crust (e.g. Alt et al. 1986), there are several differences. First, Stern & Elthon suggest that steep, but continuous, thermal gradients prevailed during crustal construction whereas a stepped thermal gradient seems more appropriate for "in situ" crust and the Troodos ophiolite. Second, the regional metamorphic zones proposed for Sarmiento are not prevalent in "in situ" oceanic crust or Troodos. It is evident that variation in the thickness of the "permeable" layer and the localization of discharge zones preclude the usefulness of such regional metamorphic zones, which imply lateral continuity. Third, bulk compositional trends in the extrusive

sequence are similar to those documented for "in situ" crust and for Troodos; however, the high temperature assemblages documented in the pillow lavas have not been documented for "in situ" crust.

Prior to this thesis, models for Troodos (e.g. Spooner 1976; Gass & Smewing 1973) were similar to those proposed for Sarmiento (e.g. Stern & Elthon 1979; Stern et al. 1976). It is possible that a re-investigation of Sarmiento with a "DSDP" approach would clarify the discrepancies.

8.8 SUMMARY

It is apparent from this study of the extrusive sequence of the Troodos ophiolite and from studies of "in situ" oceanic crust that the movement of solutions through the extrusive sequence and the sheeted dyke complex depends upon several variables: permeability, cooling rate of the heat source, temperature, reaction rate, and sedimentation rate. The relationship among these variables is illustrated in Figure VIII-6. It is evident that the sedimentation rate is the only independent variable.

The cooling rate of the heat source is partly a function of permeability because the deep circulation of seawater is the most effective heat transport mechanism (Lister 1974). Temperature also depends upon permeability because the influx of seawater depresses the thermal gradient imposed from the heat source. The rate of reaction depends upon temperature because higher temperatures promote reactions that produce secondary minerals which, in turn, clog voids and thus reduce permeability.

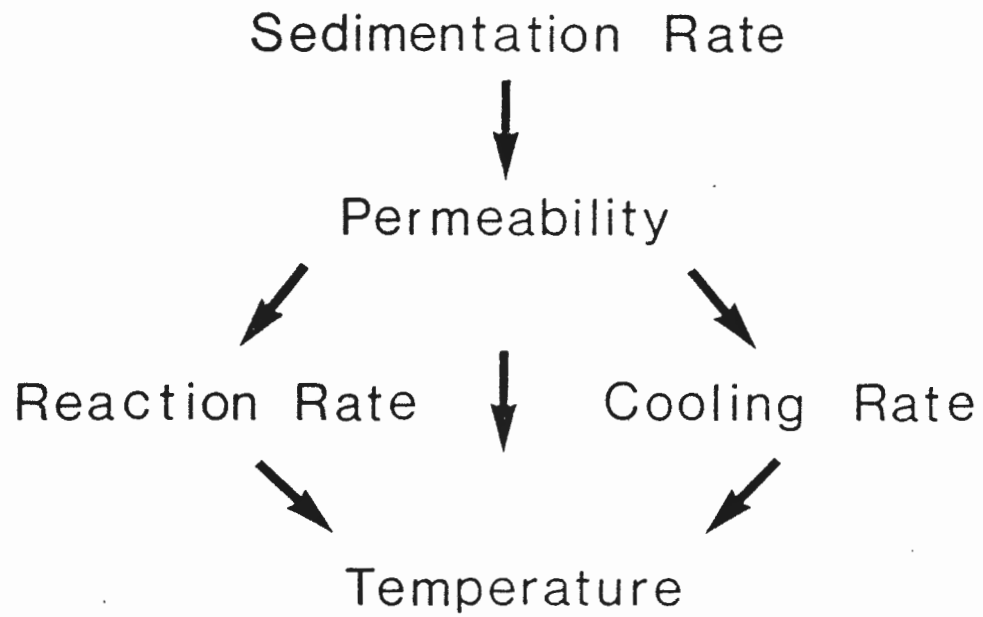It is apparent that the flow of seawater and the extent to which

Figure VIII–6.   Interrelationship of variables which influence the movement of seawater in the oceanic crust.

it reacts with the rocks through which it passes are dependent upon several interrelated variables. To improve our understanding of hydrothermal alteration and crustal aging it is necessary to increase our knowledge of these variables and the rate at which they change. Obviously, these are only the most important of many variables which influence the composition and structure of the oceanic crust.

The most important conclusions from this study, combined with comparable studies of "in situ" oceanic crust, are summarized in the following list.

1. Rocks from the "permeable" layer are highly oxidized and enriched in alkalis and $CaCO_3$; the greatest enrichment is in the zones of highest permeability. Rocks in the "less permeable" layer are depleted in alkalis and CaO and enriched in Na_2O. MgO has no consistent trend and therefore the rocks are neither a sink nor a source for MgO. Compositions of the rocks in the transition zone between these layers have the compositional characteristics of both.

2. The downhole variation in lithology reflects the measured permeability stratification at Sites 504B (Anderson et al. 1985; Becker 1985) and 395A (Hickman et al. 1985). Similar lithologic trends with increasing depth are evident in the Troodos extrusive sequence; however, there is significant lateral variation in the thickness of this "permeable" layer in the Troodos ophiolite, from <150 m to >1400 m. In addition, it is evident from field exposures that the permeability within the "permeable" layer is also heterogeneous.

3. The thickness and distribution of the Sm-Pa-Ca Zone is dependent upon permeability, the sedimentation rate, and the original seafloor morphology.

4. The thermal gradient in the extrusive sequence is stepped. A sharp increase in temperature across the lithologic transition zone from pillows to dykes corresponds to a decrease in permeability. It is evident from the lateral variation in the thickness of the "permeable" zone that the temperature gradient within the upper crust is not uniform.

5. Sub-surface mixing of ascending, metal-enriched solutions with descending seawater may be a common phenomenon in the oceanic crust.

CHAPTER IX

SUMMARY OF CONCLUSIONS

9.1 SUMMARY OF CONCLUSIONS

1. Six alteration zones for the extrusive sequence were defined on the basis of field appearance and consistent secondary mineral assemblages. Each zone, listed below, was named for its typical mineral assemblage.

   1. Smectite-Palygorskite-Calcite Zone (Sm-Pa-Ca Zone)

   2. Smectite Zone (Sm Zone)

   3. Smectite-Celadonite-Zeolite Zone (Sm-Ce-Ze Zone)

   4. Lamontite-Smectite/Chlorite-Quartz Zone (La-Sm/Ch-Qz Zone)

   5. Epidote-Chlorite-Quartz Zone (Ep-Ch-Qz Zone)

   6. Sulfide-Chlorite-Quartz Zone (Su-Ch-Qz Zone)

Because these minerals were deposited sequentially, they do not represent equilibrium assemblages.

2. The lateral and vertical extent of these zones varies significantly. For example, the Sm-Ce-Ze Zone along the Akaki River section is >1200 m thick whereas in the Agrokipia area, only 4 km to the west, it is 150 m thick.

3. There is no systematic increase in the pervasiveness of alteration with depth as has been previously proposed (Smewing 1975; Gass & Smewing 1973). Outside of the Su-Ch-Qz Zone, alteration is most pervasive in the Sm-Pa-Ca, Sm, and Ep-Ch-Qz Zones whereas the Sm-Ce-Ze and La-Sm/Ch-Qz Zones are characterized by significant variation in the intensity of alteration.

4. Qualitative and semi-quantitative estimates of element mobility for rocks from the CY-1 and CY-1a drillcores shows that each alteration zone

310

has a distinctive signature. The Sm-Pa-Ca Zone is oxidized, enriched in K_2O, H_2O+, Rb, Ba, and CO_2, and depleted in SiO_2 and Sr. The Sm-Ce-Ze Zone is locally oxidized and enriched in K_2O, Na_2O, MgO, H_2O, Rb, and Ba, and depleted in SiO_2, CaO, and Sr. The La-Sm/Ch-Qz Zone is enriched in Na_2O, MnO, Zn, and Ba and depleted in CaO, Sr, and Rb. The Ep-Ch-Qz Zone is enriched in Na_2, depleted in K_2O, CaO, Rb, and Sr and locally enriched in Zn, Cu, and MnO.

5. Bulk rock compositions of pillows are modified to a greater degree than massive flows; the outer margins of pillows are modified more than their cores.

6. Permeability in the extrusive sequence is stratified, with an upper "permeable" layer and a lower "less permeable" layer. Their boundary correlates with a lithologic change from pillows, breccias, and flows to flows and dykes. Permeability within the "permeable" layer is also stratified, with an upper 50 - 250-m-thick permeable zone, comprised of pillows and breccias. Below this zone, but still in the "permeable" layer, permeability is laterally heterogeneous. Initial permeability in both layers was reduced by the progressive deposition of secondary minerals in voids.

7. Four stages of alteration, which record progressive changes in the physical and chemical conditions, have been recognised. Stages 1 through 3 are continuous and are associated with hydrothermal and crustal aging prior to obduction. Stage 4 palygorskite, gypsum, and calcite veining, which overprints the upper few hundred metres of the ophiolite, is associated with a period of seawater circulation during the Miocene or later and may record the emplacement of the Kyrenia mountain range.

8. During Stages 1 and 2, the thermal gradient was stepped. Nearly isothermal conditions prevailed in the "permeable" layer, temperatures increasead sharply across the transition from the "permeable" to "less permeable" layer, and below this zone, a steep gradient prevailed. During Stage 3 the thermal gradient was more gradual and temperatures were lower.

9. Seawater-dominated conditions prevailed in the zones with the highest permeability; elsewhere rock-dominated conditions prevailed.

10. Sub-surface mixing of descending seawater with ascending "evolved" seawater at the boundary between the "permeable" and "less permeable" layers resulted in the deposition of sulfides. These replacement deposits are much smaller than the exhalative deposits.

11. The thickness and distribution of the Sm-Pa-Ca Zone is dependent upon permeability, the sedimentation rate, and the original seafloor morphology.

12. Alteration of the extrusive sequence of the Troodos ophiolite is analogous to "in situ" oceanic crust whereas alteration of other ophiolites, whose original alteration pattern has not been overprinted by a later alteration event, is generally higher grade. Alteration of the upper part of the Troodos sheeted dyke complex is similar to both "in situ" oceanic crust and other ophiolites.

9.2 RECOMMENDATIONS FOR FUTURE WORK

The list that follows contains suggestions to both fine-tune and extend the work presented in this thesis.

1. Further ^{87}Rb - ^{87}Sr studies of secondary minerals to better establish their age relationships. Minerals of particular importance

are: palygorskite, gypsum, and the clay minerals.

2. Stable isotope and fluid inclusion studies of secondary minerals to further characterize the composition and temperature of their depositing fluids.

3. Correlation of the ore deposits with the igneous stratigraphy and the axial grabens outlined by Moores & Varga (1984) to establish if there is a consistent younging direction and thus locate the position of the spreading centre(s).

4. Correlation of the location of the ore deposits with the plutonic suite to determine if the deposits are related to episodic intrusion. Such a study would provide boundary conditions for modelling the rate of cooling of the plutons and thus the duration and style of hydrothermal activity.

5. Further field mapping along the extrusive sequence - sheeted dyke complex boundary, particularily in areas included in this study (i.e., the area between the Pediaeos and Akaki Rivers). The purpose of this mapping is to test the models for localized zones of mixing associated with dyke swarms, lithologic control of permeability and stepped thermal gradient during the early stages of alteration.

6. Detailed mapping between ore deposits to further investigate the recharge zones of hydrothermal systems to determine boundary conditions for modelling. The area between the Kokkinopesula and Agrokipia deposits would be an excellent location for such a study because the ore deposits and intervening volcanic rocks have been extensively studied.

7. A structural study of the extrusive sequence and sheeted dyke complex to establish the scale of fracturing and the paths of fluid flow prevalent during hydrothermal circulation.

APPENDIX I   ANALYTICAL METHODS

1.   Whole Rock Analyses (Cooling-Unit Suite)

i) Sample preparation:

Samples were put into a heavy plastic bag and broken with a
hammer into fragments < 1 cm in size. Approximately 50 g of each sample
was crushed in a tungsten carbide ring mill. All rock powders were then
sieved through a -80 mesh teflon sieve.

ii) Major, minor, and trace element analyses

Samples were analysed for 10 major and minor element oxides and
14 trace elements on a Philips PW1400 sequential x-ray fluorescence
spectrometer using a Rh-anode tube. Major oxide analyses were carried
out on fused glass discs whereas trace elements were done on pressed
powder pellets. International standards with recommended values from
Abbey (1983) as well as inhouse standards were used for calibration
(Cameron, pers. comm., 1985). Analytical precision, as determined on
replicate analyses, is generally better than 5% for major oxides and
between 5-10% for trace elements. Loss on ignition (LOI) was determined
by heating the sample for 1.5 hours at 1050°C in an electric furnace.
Analyses were performed at St. Mary's University.

iv) Ferrous Iron

The ferrous iron content of each sample was determined using the
Wilson method of visual titration at Dalhousie University (Johnson &
Maxwell 1981). For more detailed description of the method see
Blanchard (1982).

314

v) Sulfur

Total sulfur was determined turbometrically as barium sulfate for 21 samples at Dalhousie University (Shapiro 1973).

vi) H_2O+, H_2O-, and CO_2

H_2O+ was evolved by a Leco induction furnace and measured using a Karl Fisher Aquameter (Troll & Farzaneh 1978). H_2O- was determined by heating the samples in an oven overnight at $110^{\circ}C$ (Parikh, pers. comm., 1986). CO_2 was measured in an automatic Leco titrator following an acid evolution method (Bouvier et al. 1972).

2. Whole rock analyses for ICRDG samples

i) CY-1

Major elements were measured at the Geological Survey of Canada (XRF), Memorial University of Newfoundland (AA), and the Open University (XRF). Interlab variability is generally <3 % for elements >10 wt%, <6 % for elements between 10 and 2 wt%, 25-70% for elements <2 wt% except TiO_2 and P_2O_3 which is < 7%. CO_2, H_2O+, and H_2O- were measured at the Geological Survey of Canada by wet chemical techniques and trace elements were measured at Memorial University of Newfoundland by XRF.

ii) CY-1a

Major and trace elements were measured at Memorial Univeristy of Newfoundland by AA and XRF, respectively.

3. Oxygen and Carbon Analyses of Carbonates

i) Sample preparation

Carbonate samples from vesicles, vugs, and veins were separated, gently crushed and sieved to 300-1000 m. Clear to milky white monomineralic samples were hand picked using a binocular microscope, washed in ethyl alcohol in an ultrasonic bath, and crushed with an agate mortar and pestal. Two grains were choosen from each sample for microprobe analysis.

ii) Analytical method

d^{18} O and d ^{13} C contents were determined by the CO_2 gas – phosphoric method (McCrea 1950) using a VG Micromass 602D "online" mass spectrometer at Dalhousie University. The results are reported as per mil $^o/oo$ and were corrected according to Craig 1957. Cavarra Marble was used as an internal lab standard. Its ^{18} O and ^{13} C content with respect to PBB is -1.19 and +2.79 $^o/oo$ repectively (N. J. Shackleton 1981 pers. comm.).

4. $^{87}Sr/^{86}Sr$ analyses

i) Sample preparation

Zeolite, clay mineral, and carbonate samples were separated from vesicles, vugs, and veins, gently crushed, and sieved to 200 - 1000 m. Zeolite and carbonate separates consisted of clear or consistently colored monomineralic grains. Several homogeneous, different colored fractions of celadonite (HSRT8 and HSTR9) were separated whilst smectite separates consisted of grains with minor variation in color and texture. All hand-picked mineral separates were pure, based on macroscopic appearance under the binocular microscope and XRD patterns. Microscopic inclusions of calcite were identified by microprobe in the palygorskite sample (CY-1:155.55 m) and trace amounts of analcime were identified in

the x-ray diffractogram of smectite (CY-1:243.3 m). Samples were washed
in ethyl alcohol in an ultrasonic bath and hand-crushed in an agate
mortar and pestal.

ii) Analytical method

K, Rb, Sr, and $^{87}Sr/^{86}Sr$ analyses were performed at
Lamont-Doherty Geological Observatory using the cation exchange and
solid source mass-spectrometry techniques outlined in Zindler et al.
(1984). $^{87}Sr/^{86}Sr$ ratios are relative to 0.70800 for the Eimer and
Amend $SrCO_3$ and $^{86}Sr/^{88}Sr$ is normalized to 0.1194.

The samples weighed between 10 - 50 mg with a weighing error of $\pm$
0.01 mg. All samples were spiked with a mixed spike and errors in
concentration ratios are: $Rb/Sr \pm 1\%$.

5. Mineral analyses

Mineral analyses were obtained using a fully automated JEOL
JXA-50A wavelength dispersive microprobe at Memorial University of
Newfoundland, a JEOL 733 microprobe at Dalhousie University, and a MARKV
Cambridge EDS microprobe at Dalhousie Univerity. The operating
conditions were: 1) JEOL JXA-50A: 22 na, 20 kV accelerating voltage, 10
sec counting time, 2) JEOL 733: 15 kv, 5 na, 10 sec counting time, 3)
Cambridge: 15 kv, 5 na, 100 sec counting time.

Natural standards were routinely run during operation of the
microprobes to monitor data quality. Precision was generally $\pm 1\%$ for
elements > 8 wt% and $\pm 2\%$ for the remaining elements. Iron, measured
as total iron, is expressed as FeO. To minimize the loss due to
volatilization in the hydrous phases, Na, Ca, and K were analysed first

and counted for 10 seconds on the WDSs. Counts for up to 5 minutes for volcanic glasses (wt% volatiles), however, showed no significant change in these elements (Rautenschlein, pers. comm., 1985; H. Longrich, pers. comm., 1984).

Due to the high volatile content of the majority of secondary minerals and the heterogeneity of most clay minerals, the quality of the data was difficult to access. Structural formulas were calculated for all analyses; if these were stoichiometric the analyses were deemed "good".

Structural formulas for saponite, celadonite, and smectite-chlorite were calculated assuming 22 (O,OH) following the method of Ross & Hendricks (1945). Si and the necessary Al were assigned to the tetrahedral site to total 8.00. The excess Al, Mg, Fe, and Ti were assigned to the octaheral site. Ca, Na and K were assigned to the interlayer position. All Fe was considered FeO. Published analyses of Fe^{3+}/Fe^T in saponites range from 0.1 to 0.9 (Alt 1984). A value of 0.3 was reported for a saponite from the pillow section at Site 504B (Andrews et al. 1983) but this value increased to 0.5 after one year. Increasing oxidation, for Fe^3/Fe^T ratios from 0 to 0.3, resulted in a more negative tetrahedral layer charge, a more positive octahedral layer charge, a lower interlayer charge, and lower Al, Si, and Mg (Alt 1984). Structural formulas for chlorite were similarily calculated assuming 28 (O,OH).

METHOD

Over 700 samples containing either single phases or assemblages of phases were scanned using a Phillips x-ray diffractometer with Cu kα radiation. Clay minerals were gently crushed in water in an agate mortar, pipetted onto a frosted glass slide, and air dried. These oriented smear mounts were scanned from 3° to 30° 2Q at a scanning speed of 1^O 2Q per minute, treated with ethylene glycol at 60° C for 36 to 48 hours, and rescanned under the same conditions from 3° to 15° 2Q. Selected samples were heated at 500° C for two hours, slowly cooled, and rescanned. Smear mounts of the remaining secondary minerals were scanned from 3° to 45°. Identification of secondary feldspars was facilitated by scanning between 20° and 28° 2Q at a scanning speed of $1/4^O$ 2Q per minute.
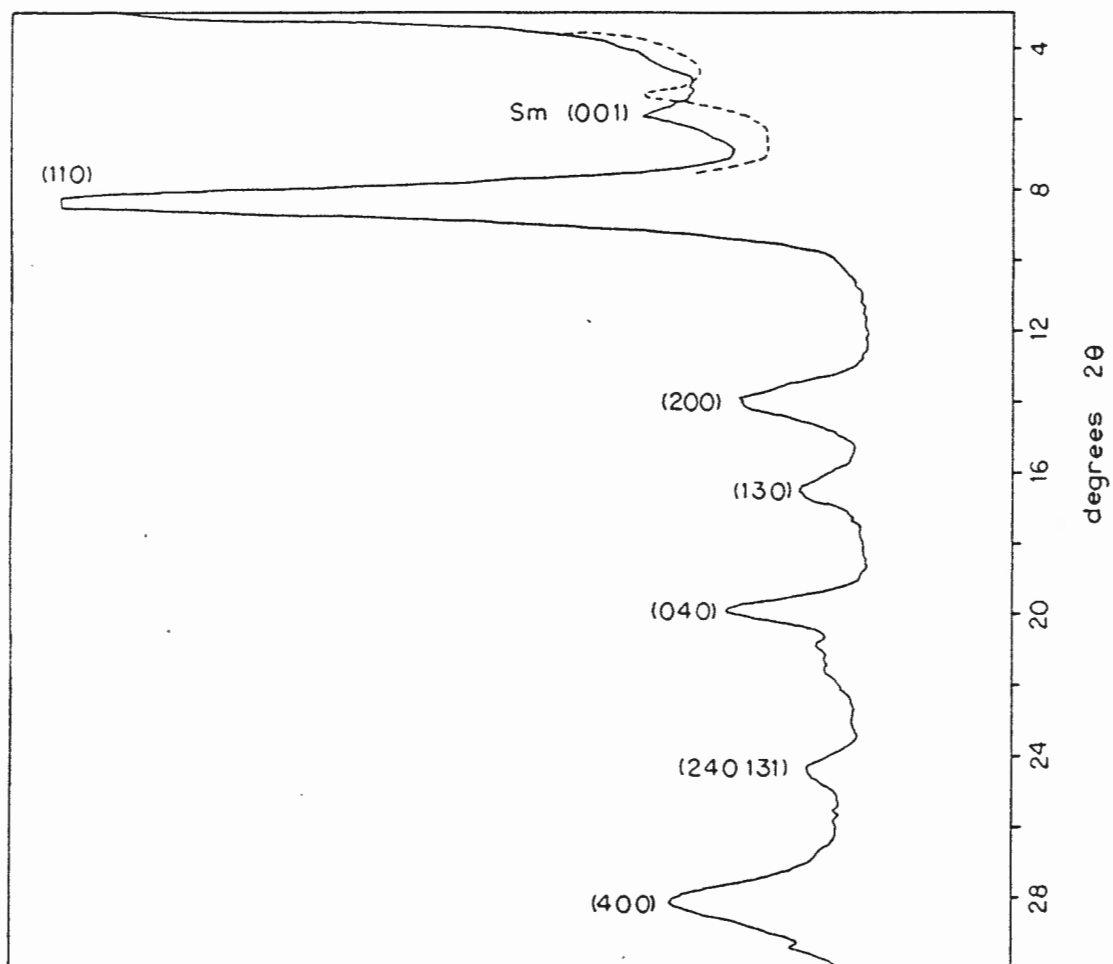
Quartz was periodically added to some samples for internal calibration with satisfactory results.
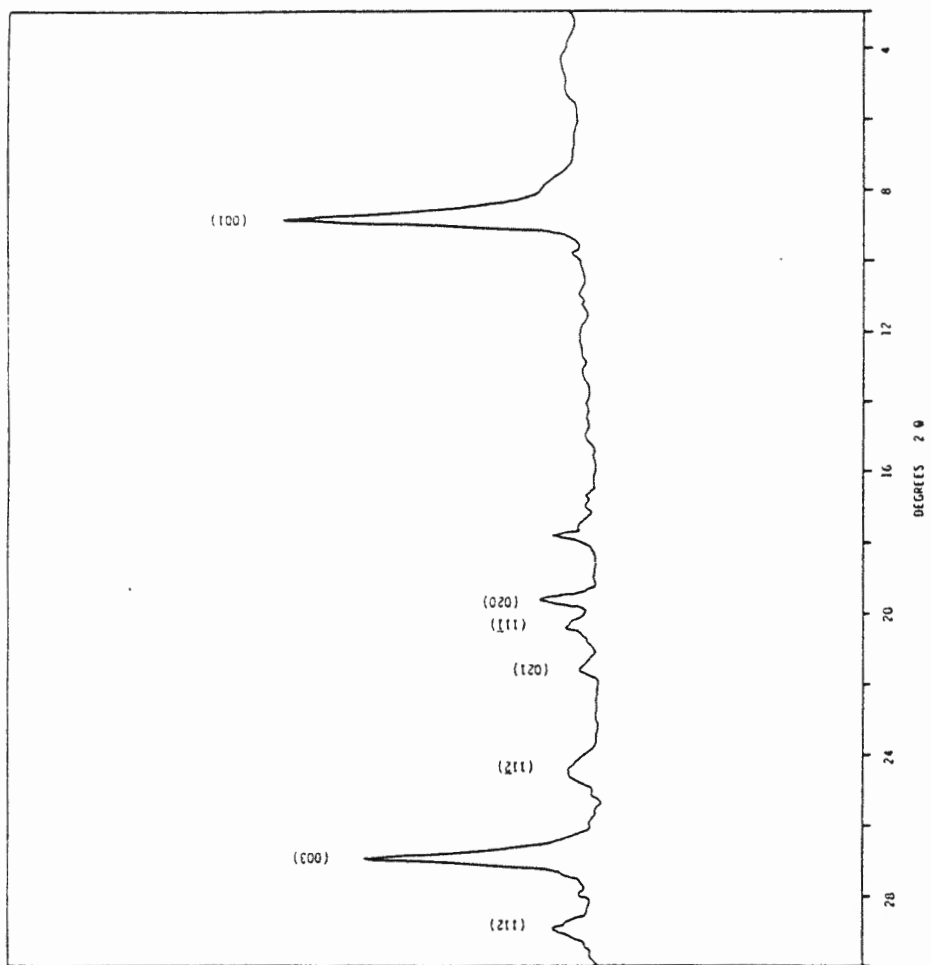
Appendix II-1. X-ray pattern of œladonite (KG:83:086).

Appendix II-2. X-ray pattern of palygorskite (P) and smectite (Sm) (KG:83:003). Untreated: solid line; treated with ethylene glycol: dashed line.
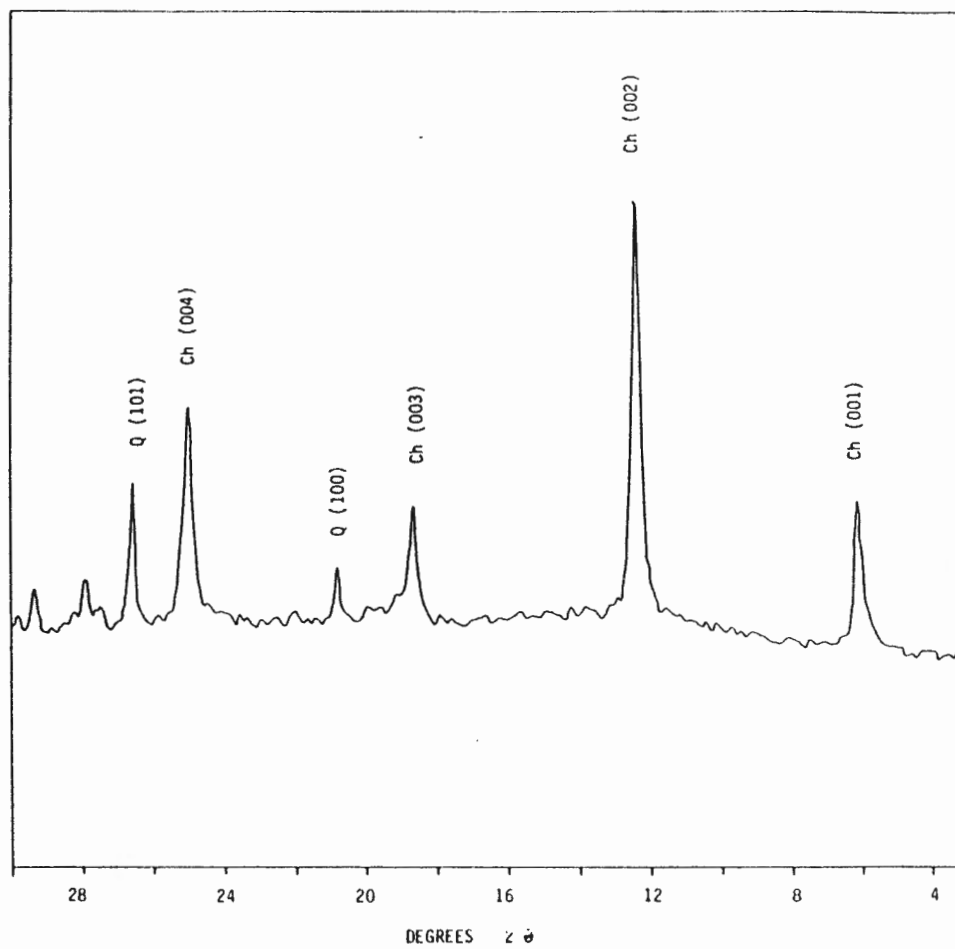
Appendix II-3. X-ray pattern of chlorite (Ch) and quartz (Q) (CY-1a:303.25).

Appendix II-4. Partial x-ray patterns for:

    A. Smectite (CY-la:83.3 m).

    B. Physical mixture of celadonite and smectite (KG:82:171).

    C. Physical mixture of sepiolite and smectite (CY-la:76.95 m).

    AD = air dried; EG = treated with ethylene glycol.

DEGREES 2 Θ
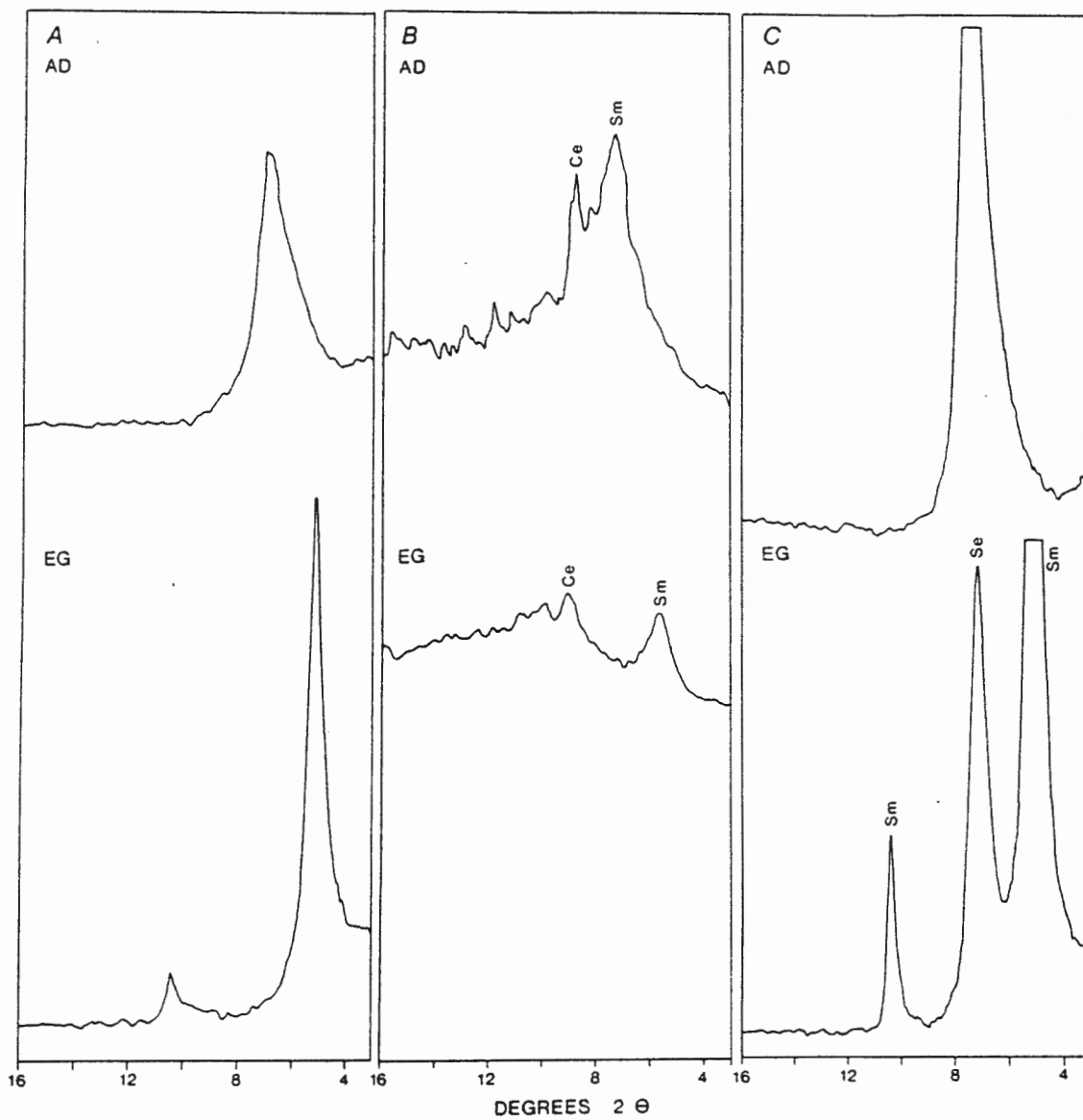
Appendix II-5. Partial x-ray patterns for smectite-chlorite mixtures.

A. Smectite >> chlorite

The intensity of the 001 peak is much greater than that of the 002 peak; both peaks shift toward larger d-spacings upon glycolation.

B. Smectite > chlorite

The intensity of the 001 peak is greater than that of the 002 peak; both peaks shift toward larger d-spacings upon glycolation and the 002 peak becomes asymmetric toward the 001 peak or splits into two peaks.

C. Chlorite and smectite = chlorite

The intensity of the 001 is greater than that of the 002 peak; the 002 peak of smectite=chhlorite is intermediate between smectite and chlorite. Upon glycolation, the 001 peak of smectite=chlorite and smectite shift toward larger d-spacings; the 001 and 002 peaks of chlorite are unaffected; the 002 peak of smectite=chlorite moves toward the chlorite peak.

D. Chlorite > smectite

The intensity of the 002 peak is greater than the 001 peak; the 001 reflection splits into two peaks and the 002 peak becomes asymmetric upon glycolation.

AD = air dried; EG = treated with ethylene glycol.

DEGREES 2 θ
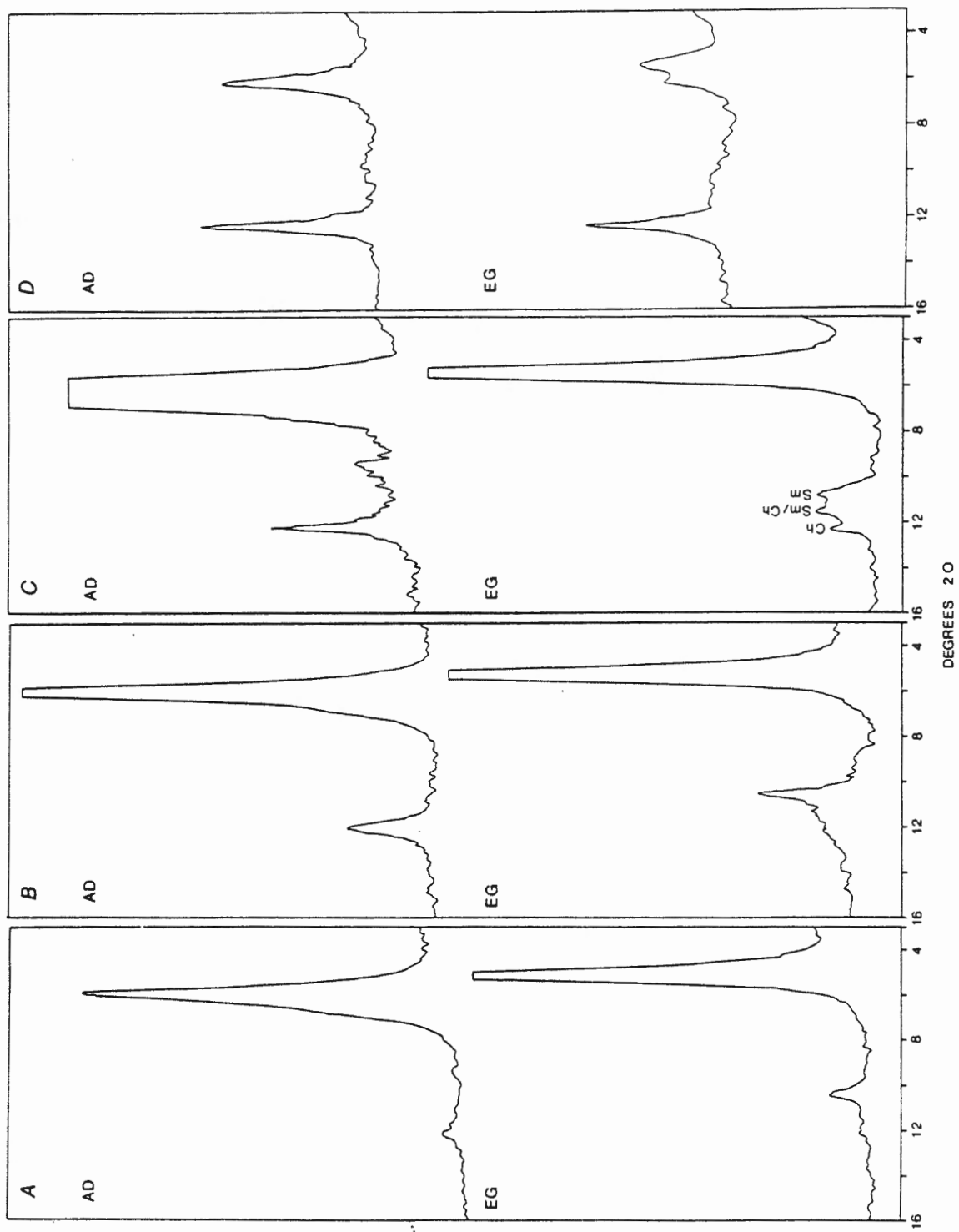
Appendix II-1Ø. X-ray pattern of mordenite (CY-1a:182.25 m).
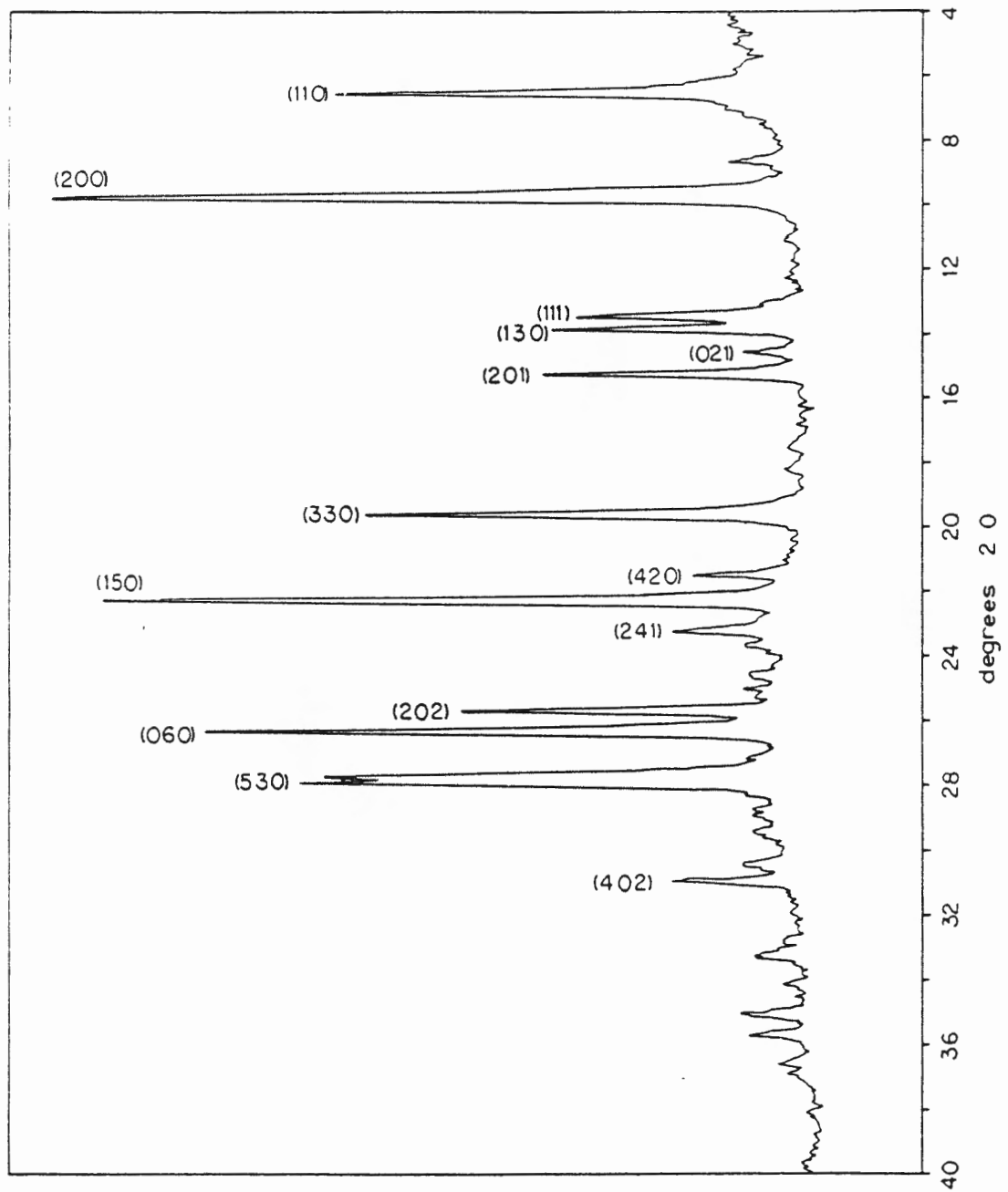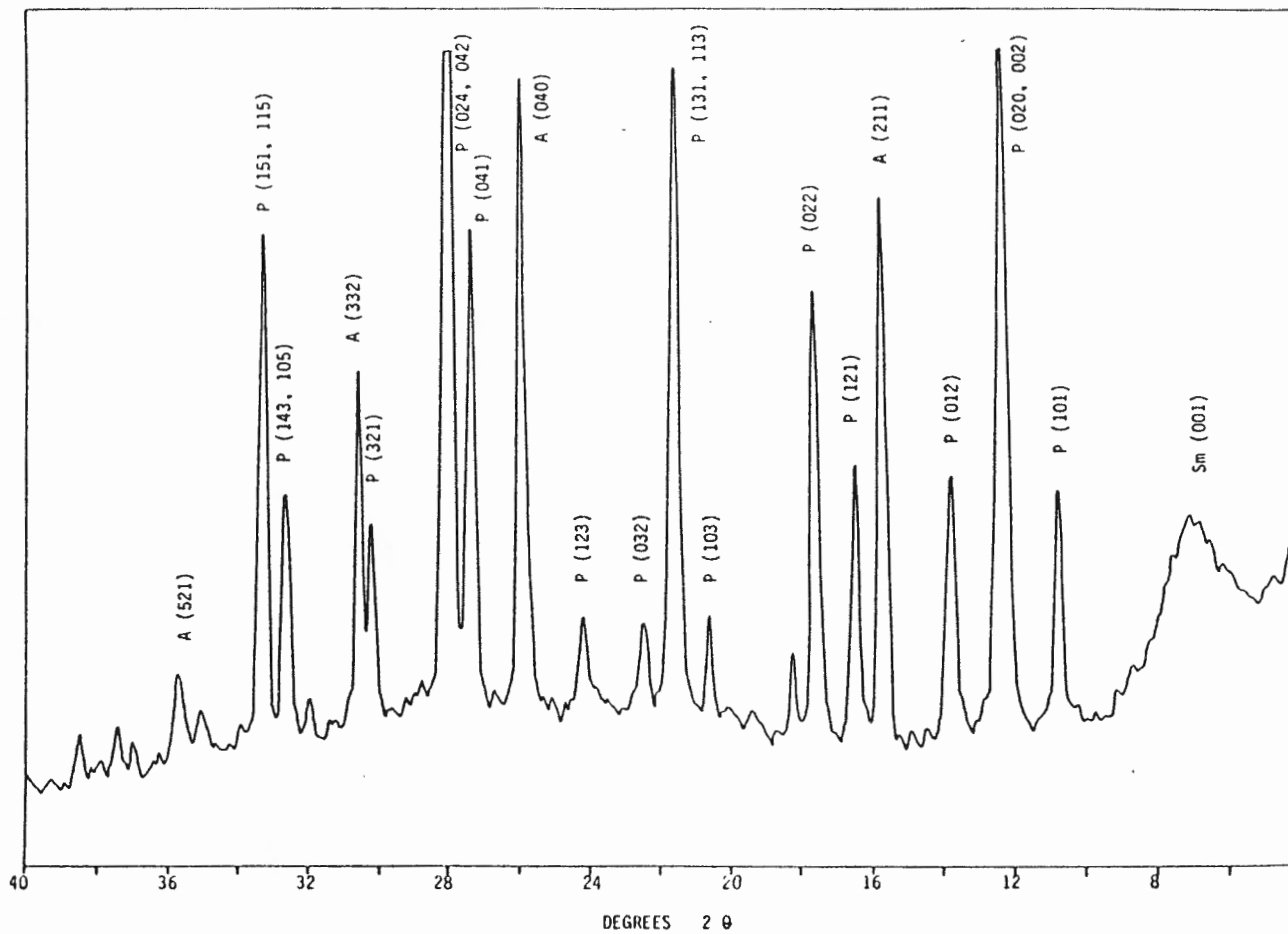
Appendix II-6. X-ray pattern of analcime (A), phillipsite (P), and smectite (Sm) (CY-la:5.0 m).
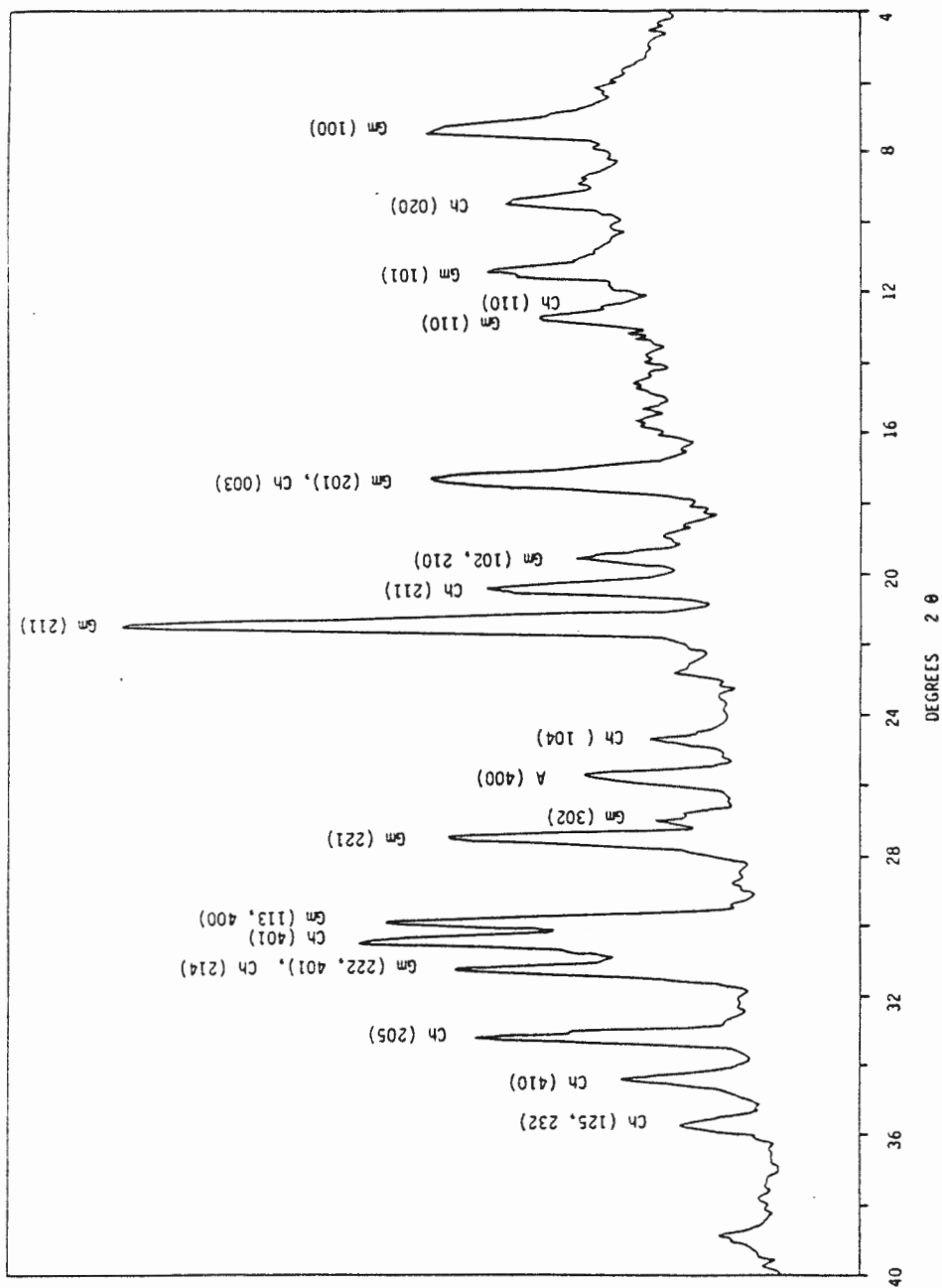
Appendix II-7. X-ray pattern of gmelinite (Gm), chabazite (Ch), and analcime (A) (KG:83:203).
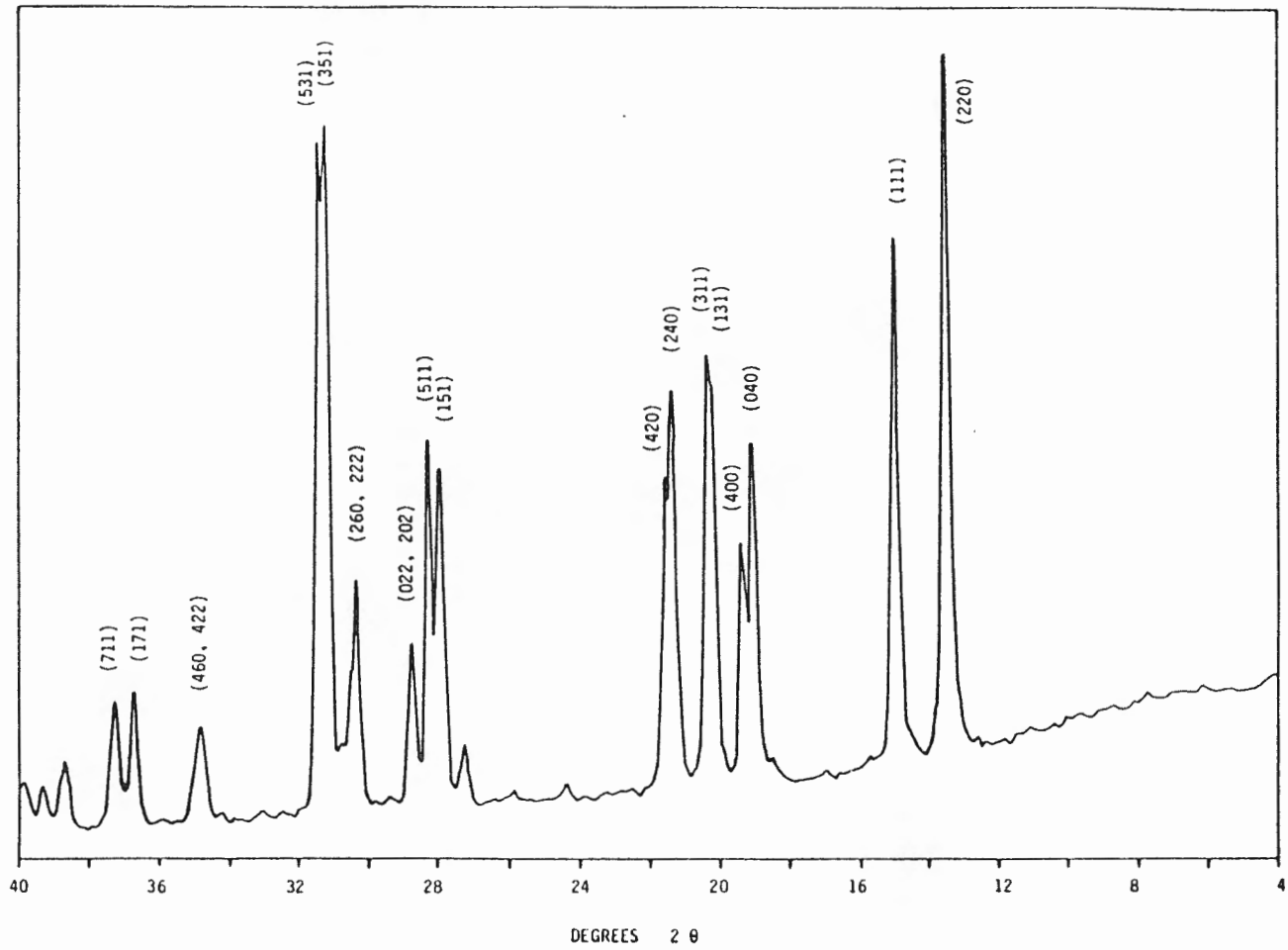
Appendix II-8.   X-ray pattern of natrolite (KG:83:292).
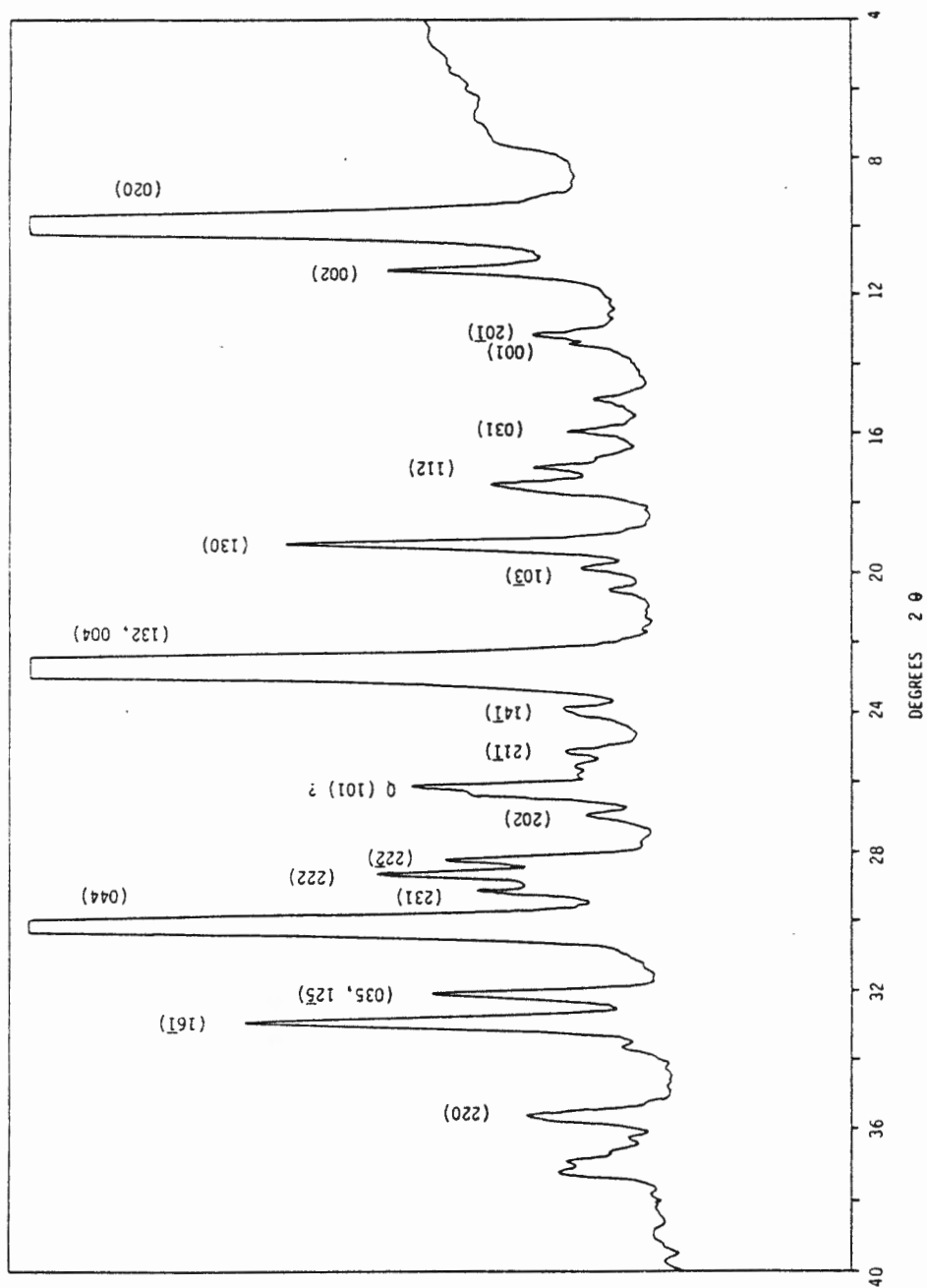
Appendix II-9. X-ray pattern of clinoptilolite (KG:83:167).
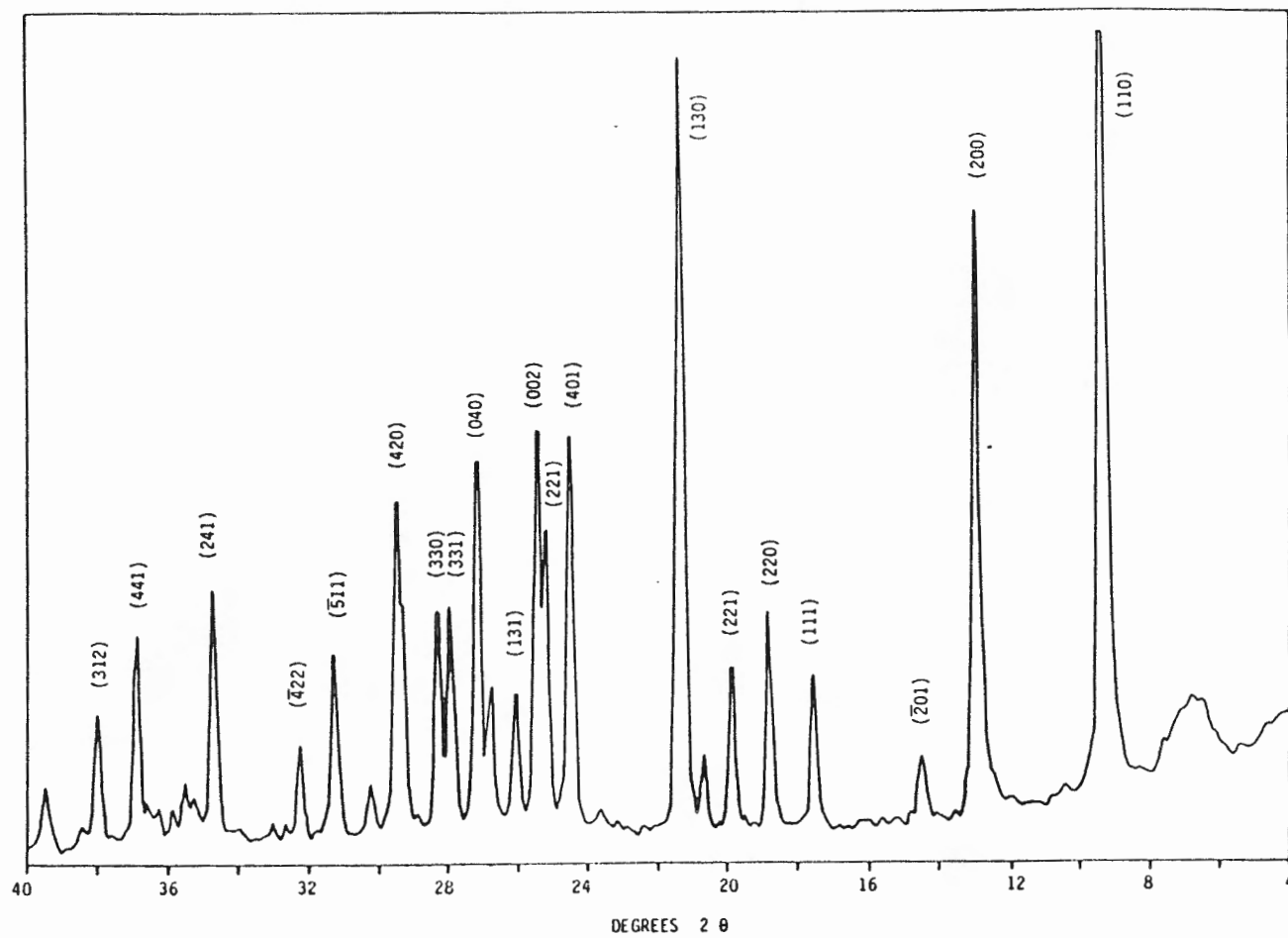
Appendix II-11. X-ray pattern of leonhardite (laumontite)
(CY-1a:196.5 m).
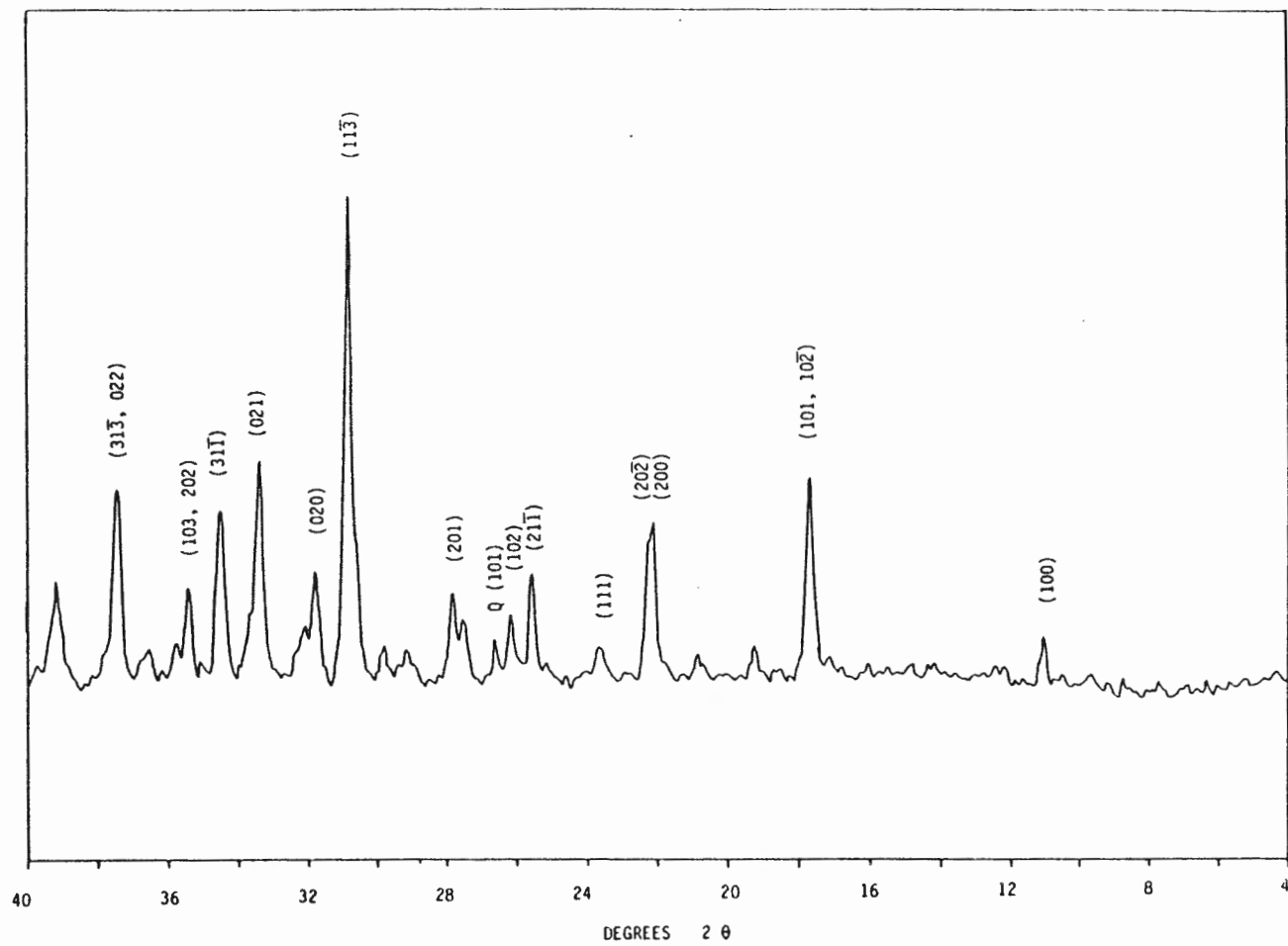
Appendix II-12. X-ray pattern of epidote and quartz (Q)

APPENDIX III   VARIATION IN BULK ROCK COMPOSITION WITH DEPTH

III-1   CY-1 Drillcore

III-2   CY-1a Drillcore

KEY:

1.   Major elements are expressed as weight percent (wt %).

2.   Trace elements are expressed as parts per million (ppm).

3.   Open circles are bulk rock samples.

4.   Closed circles are glass samples.

III-1b

III-1e

III-1g

III-1j

III · 2a

III-2b

III-2c

351

III · 2g

III·2h

III-2j
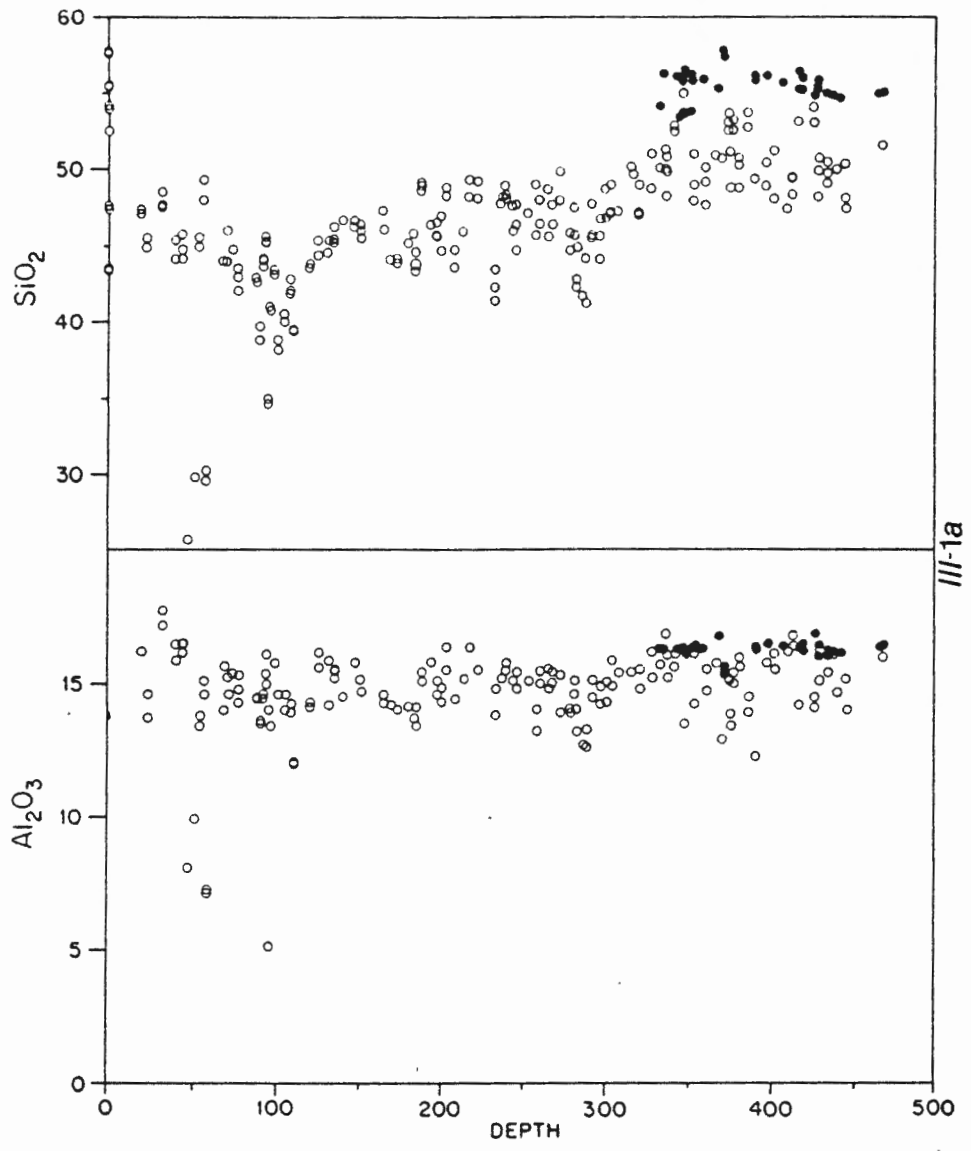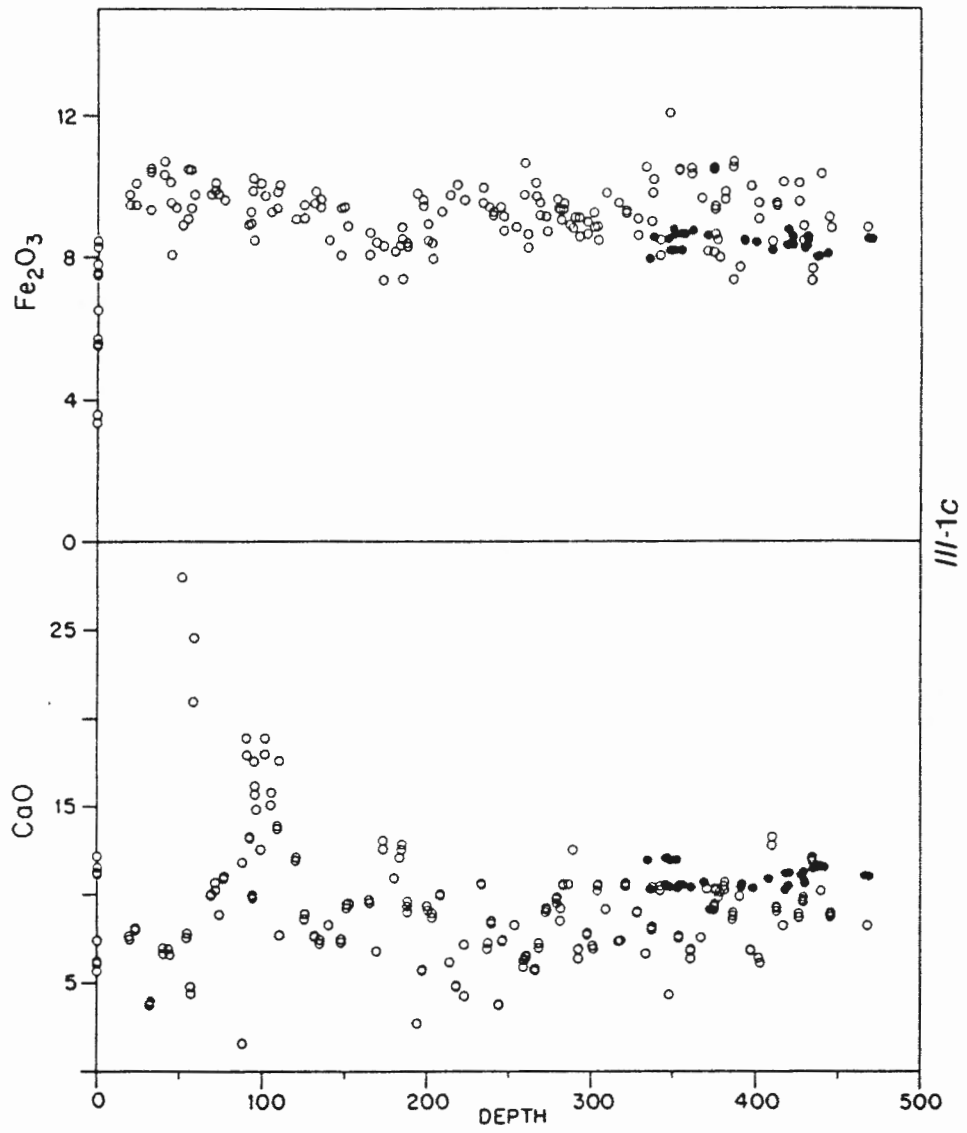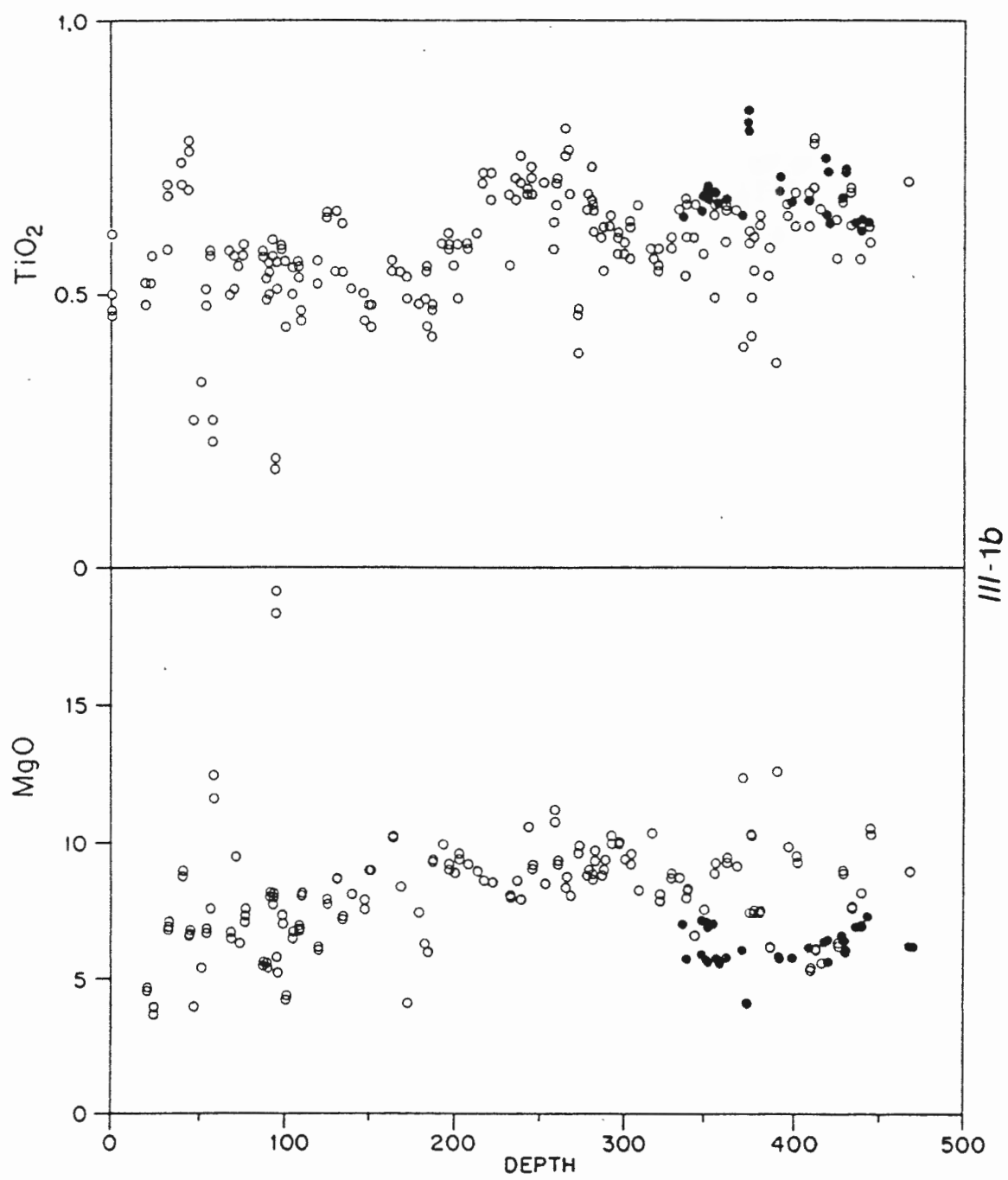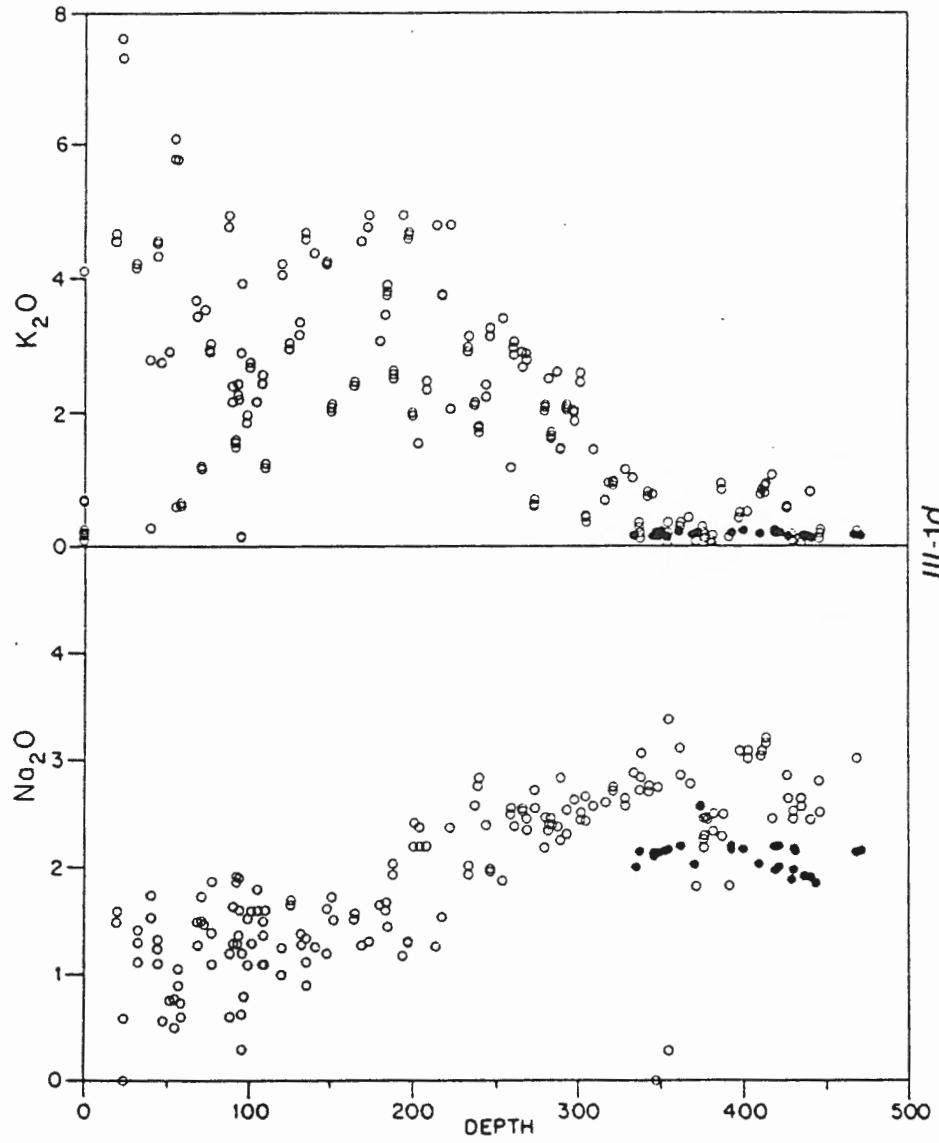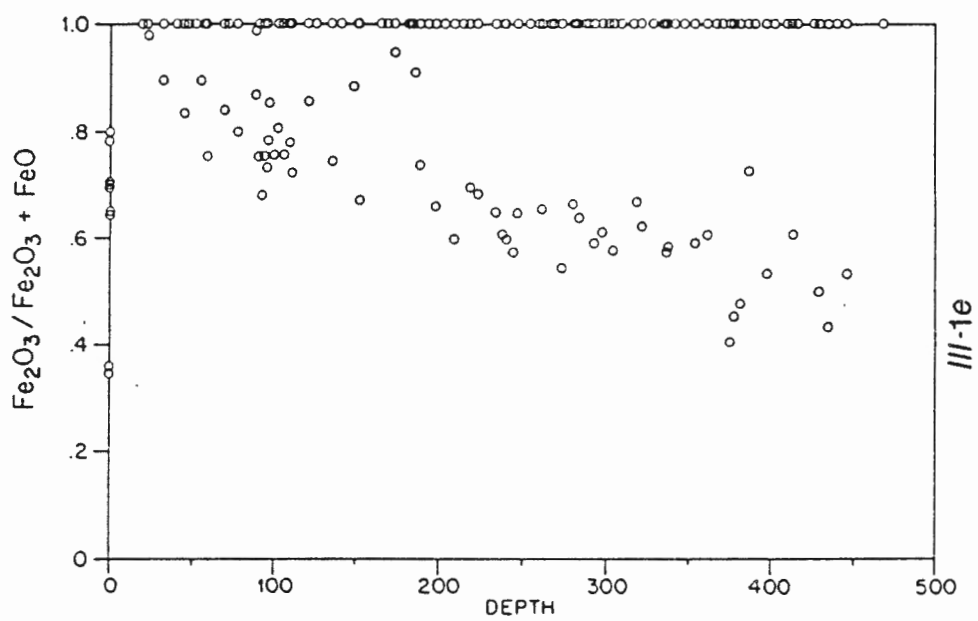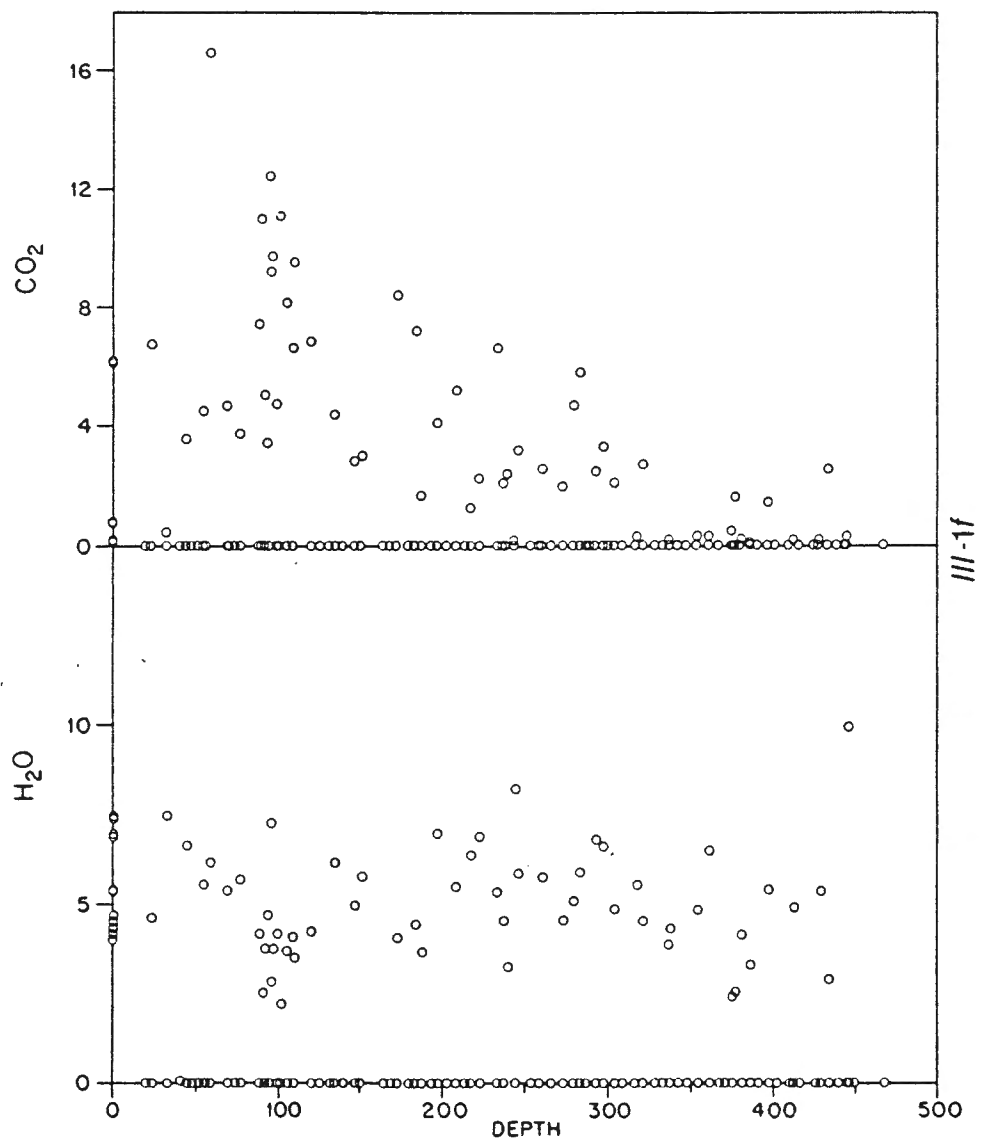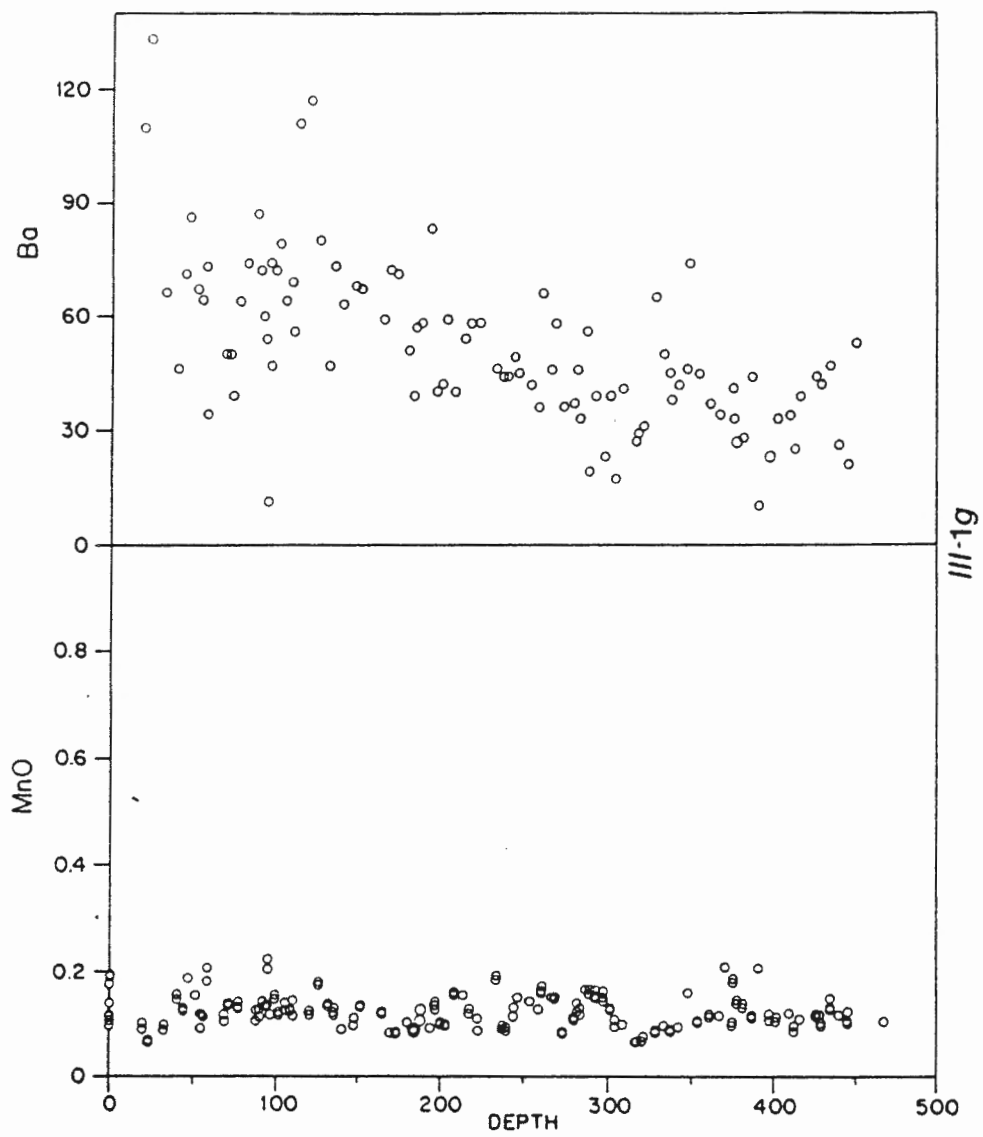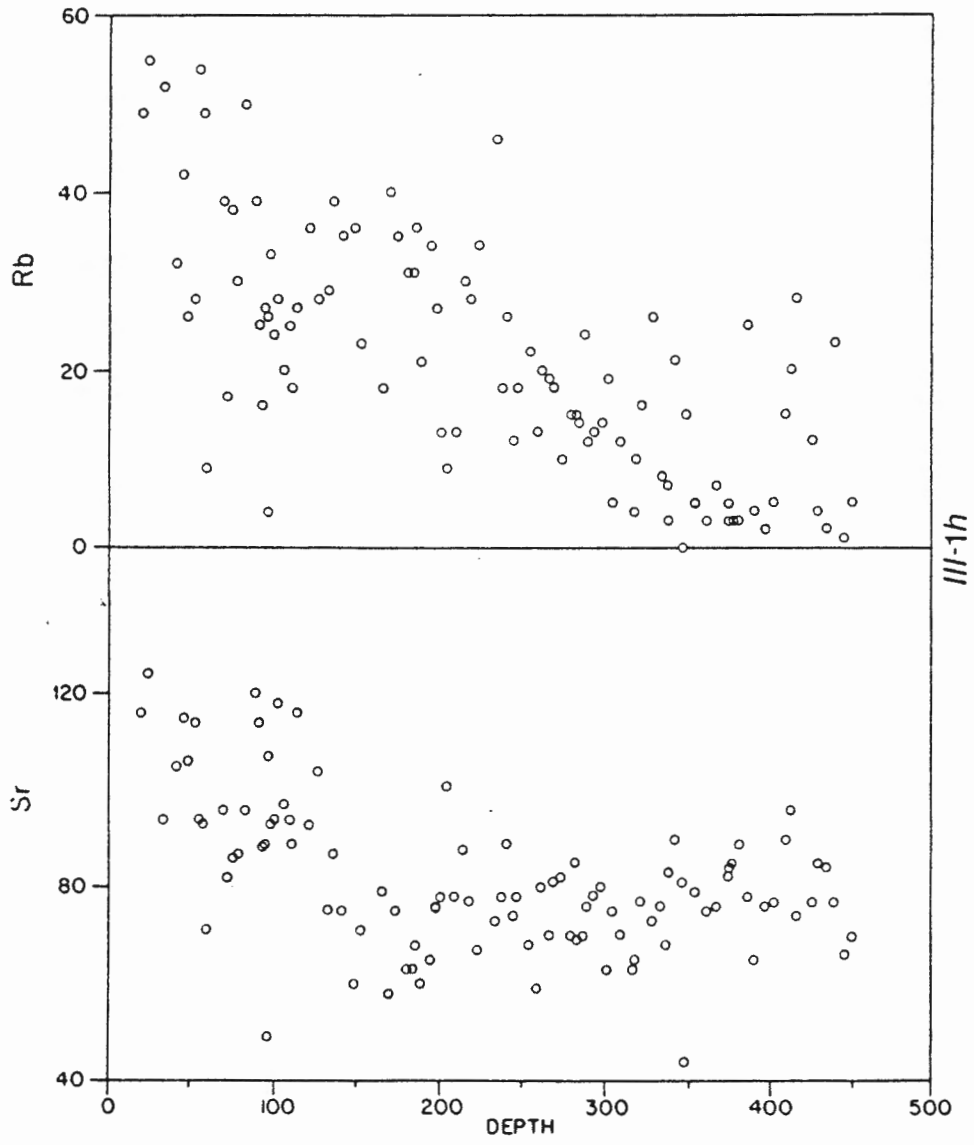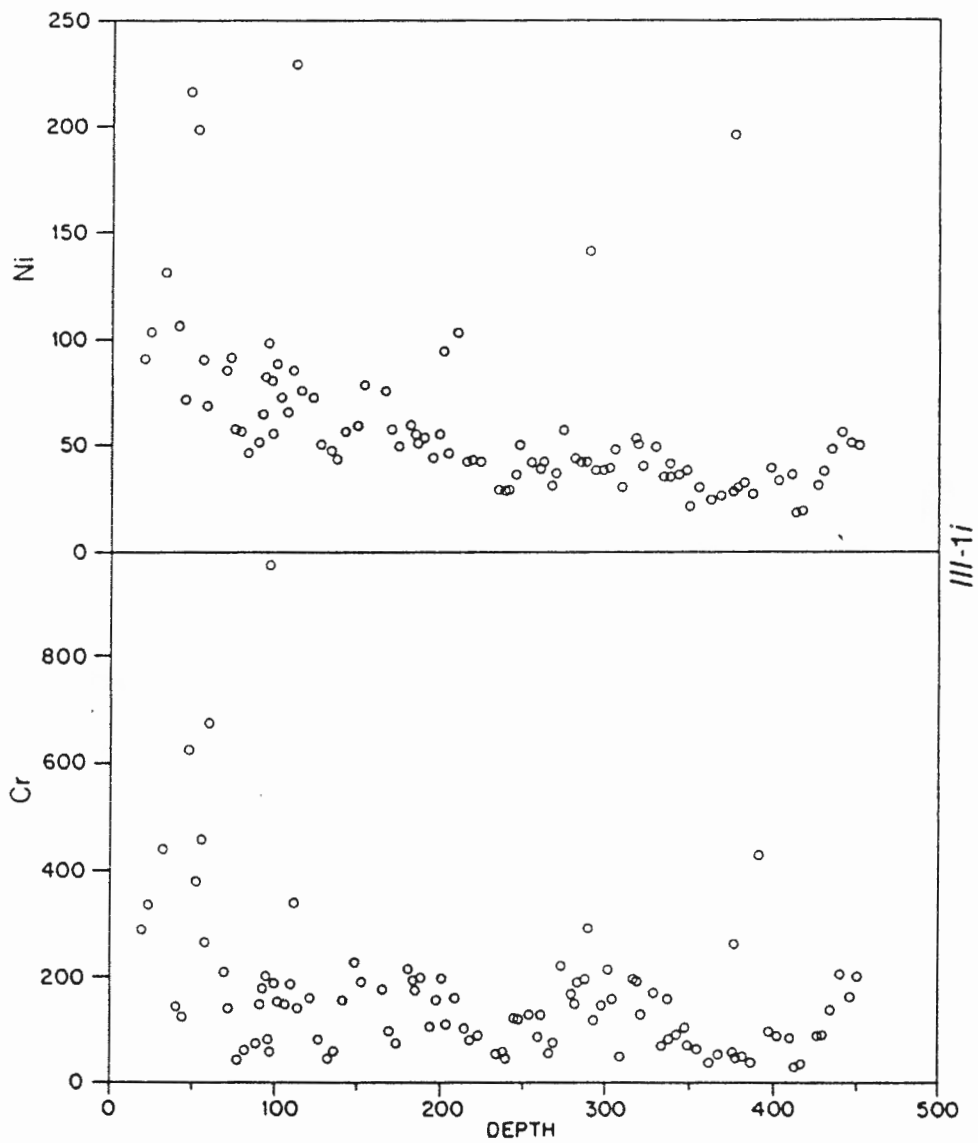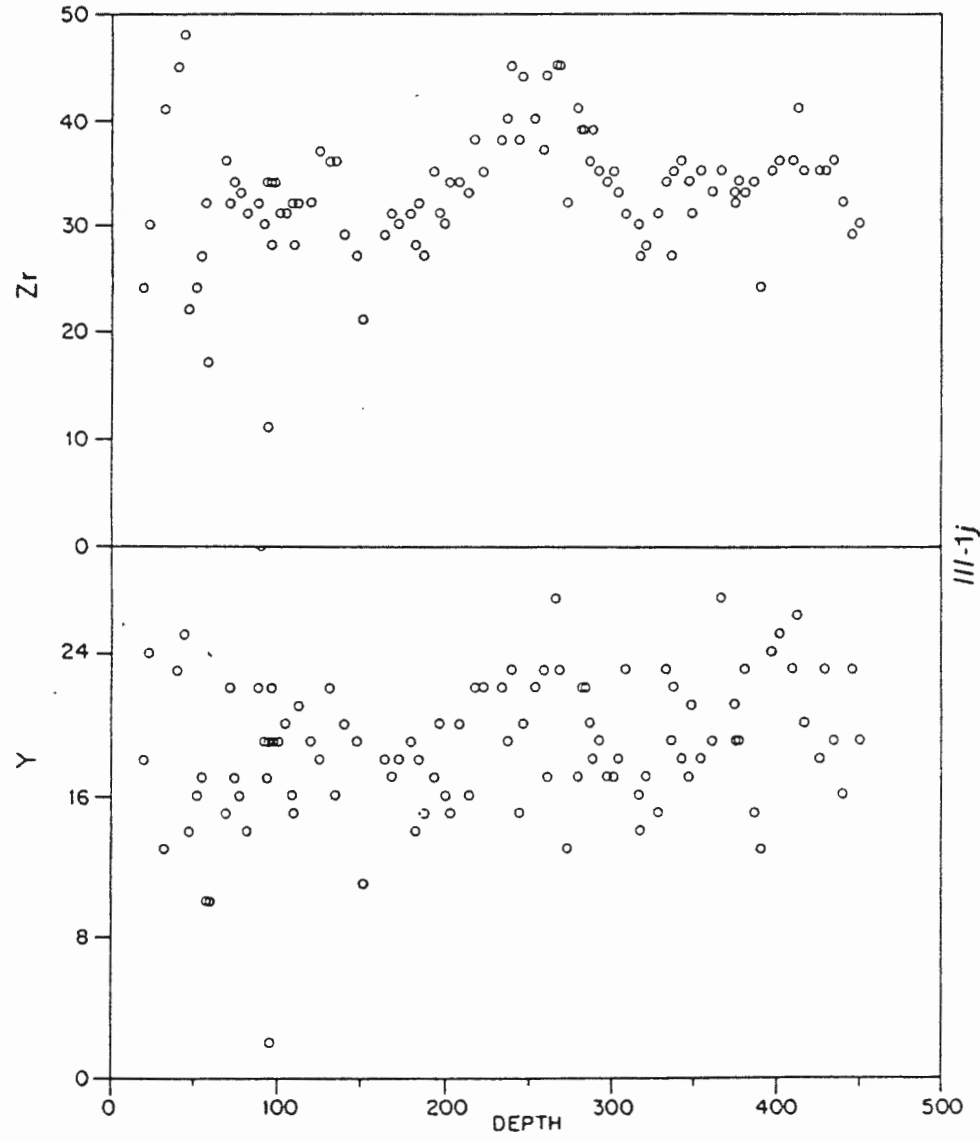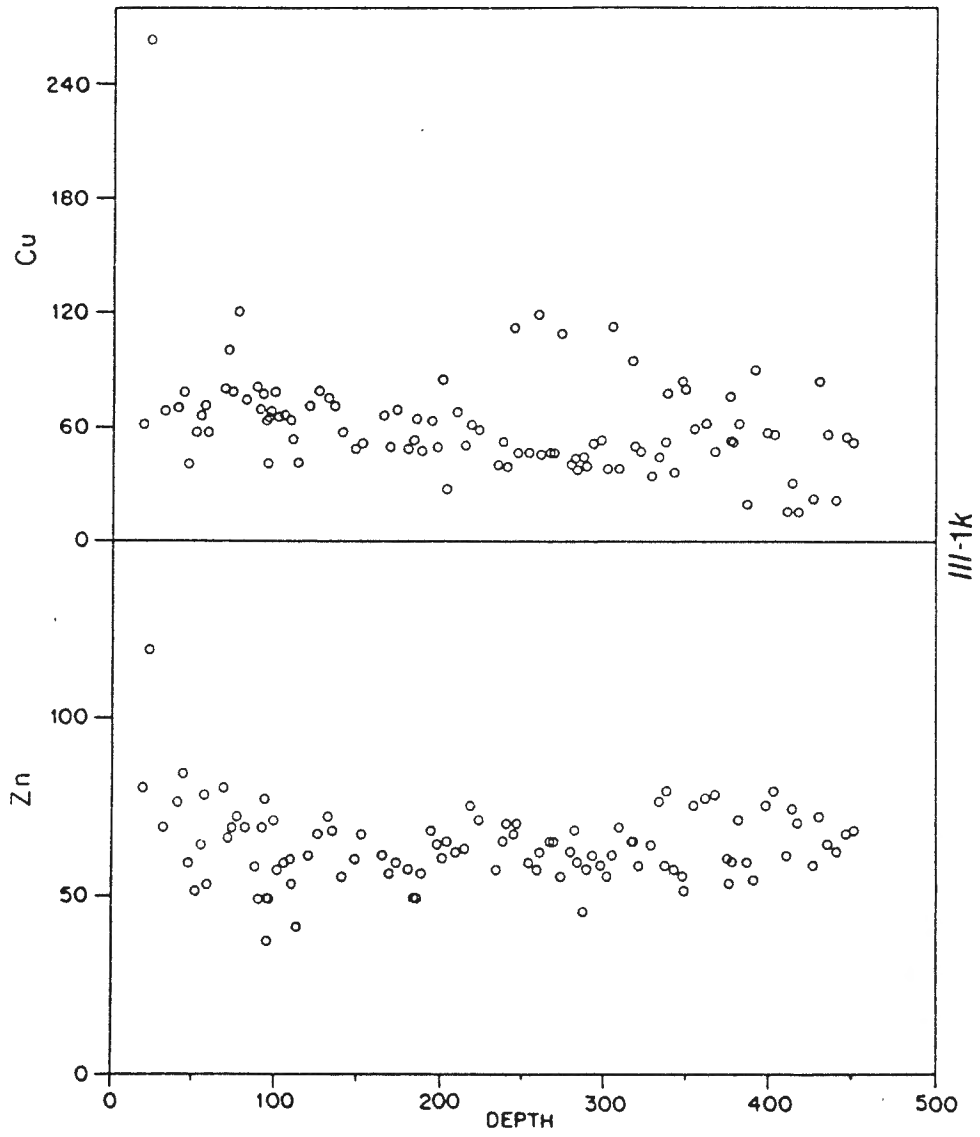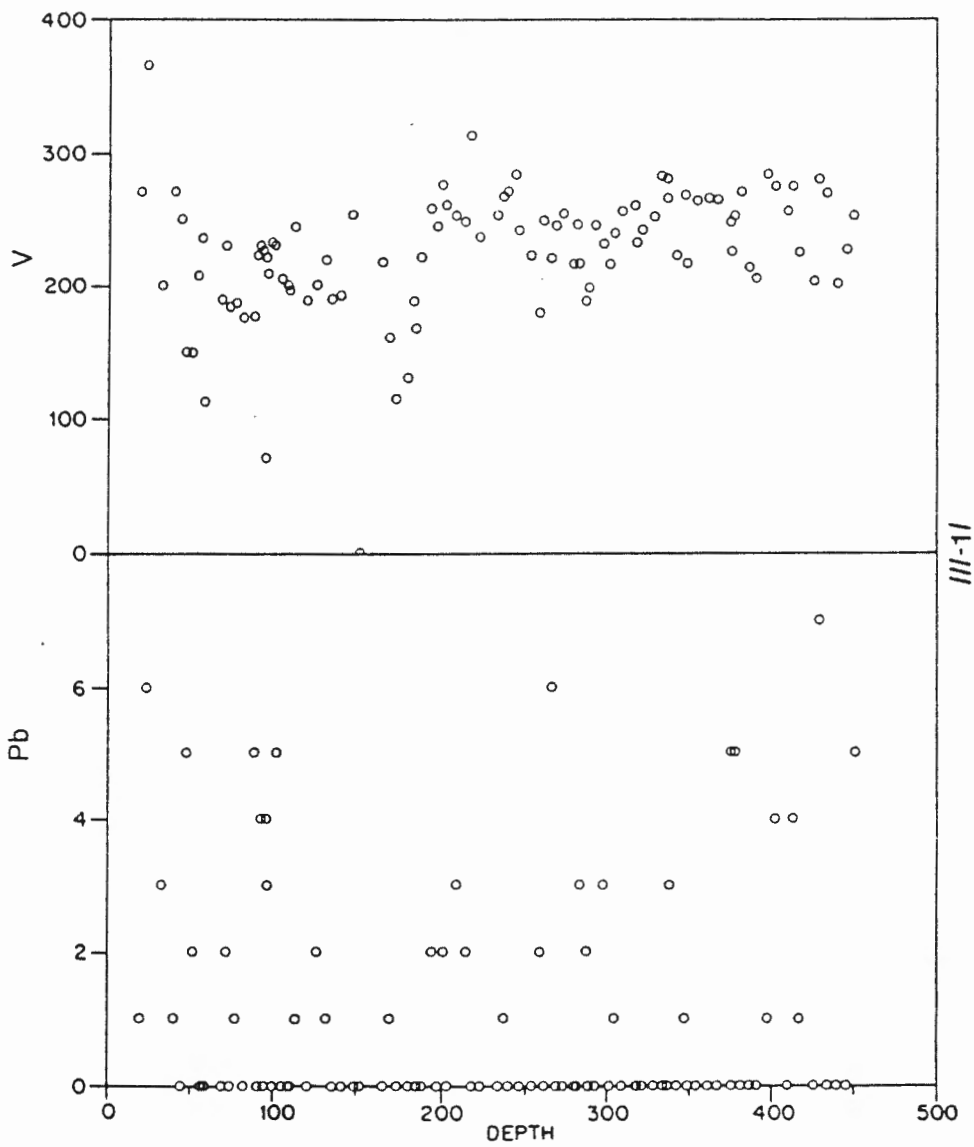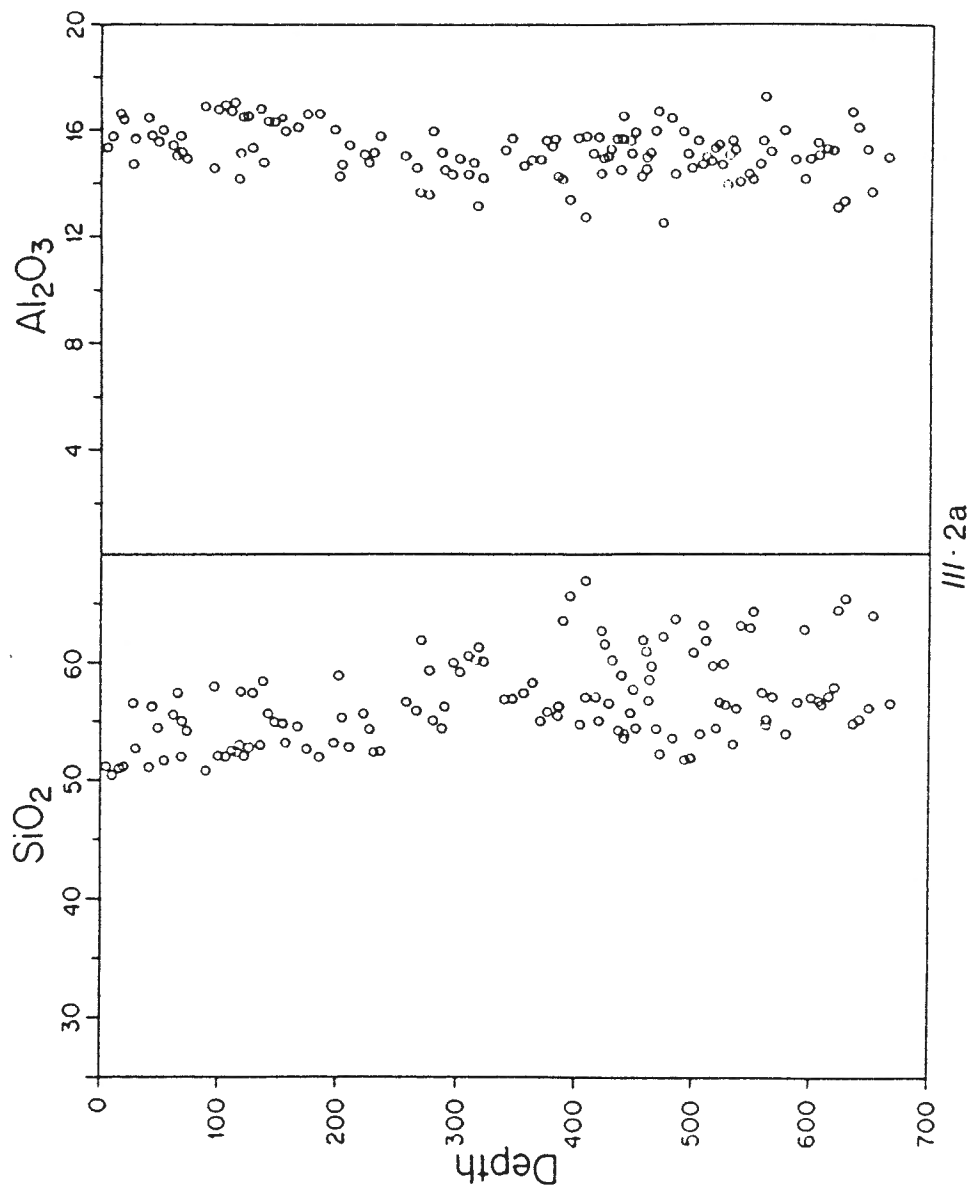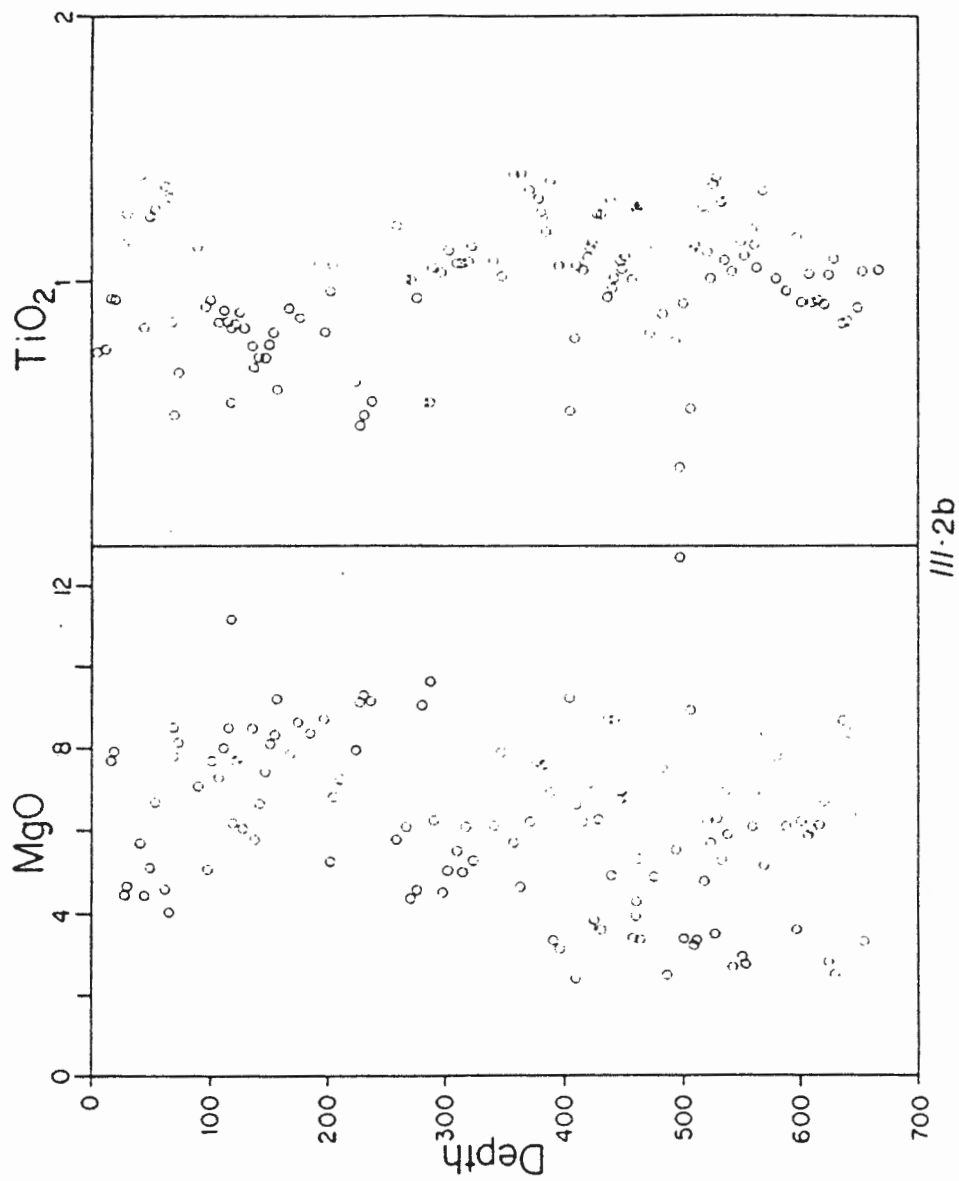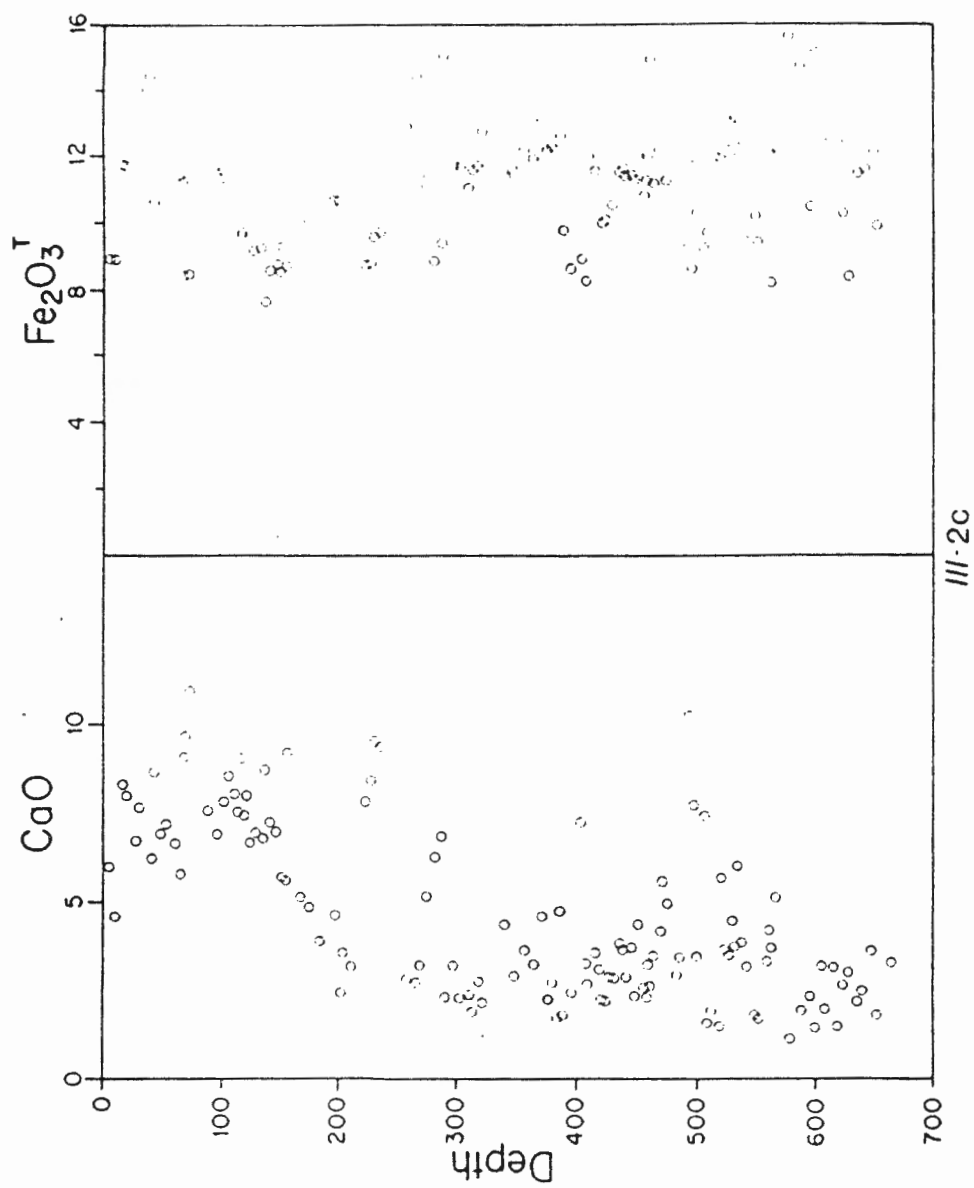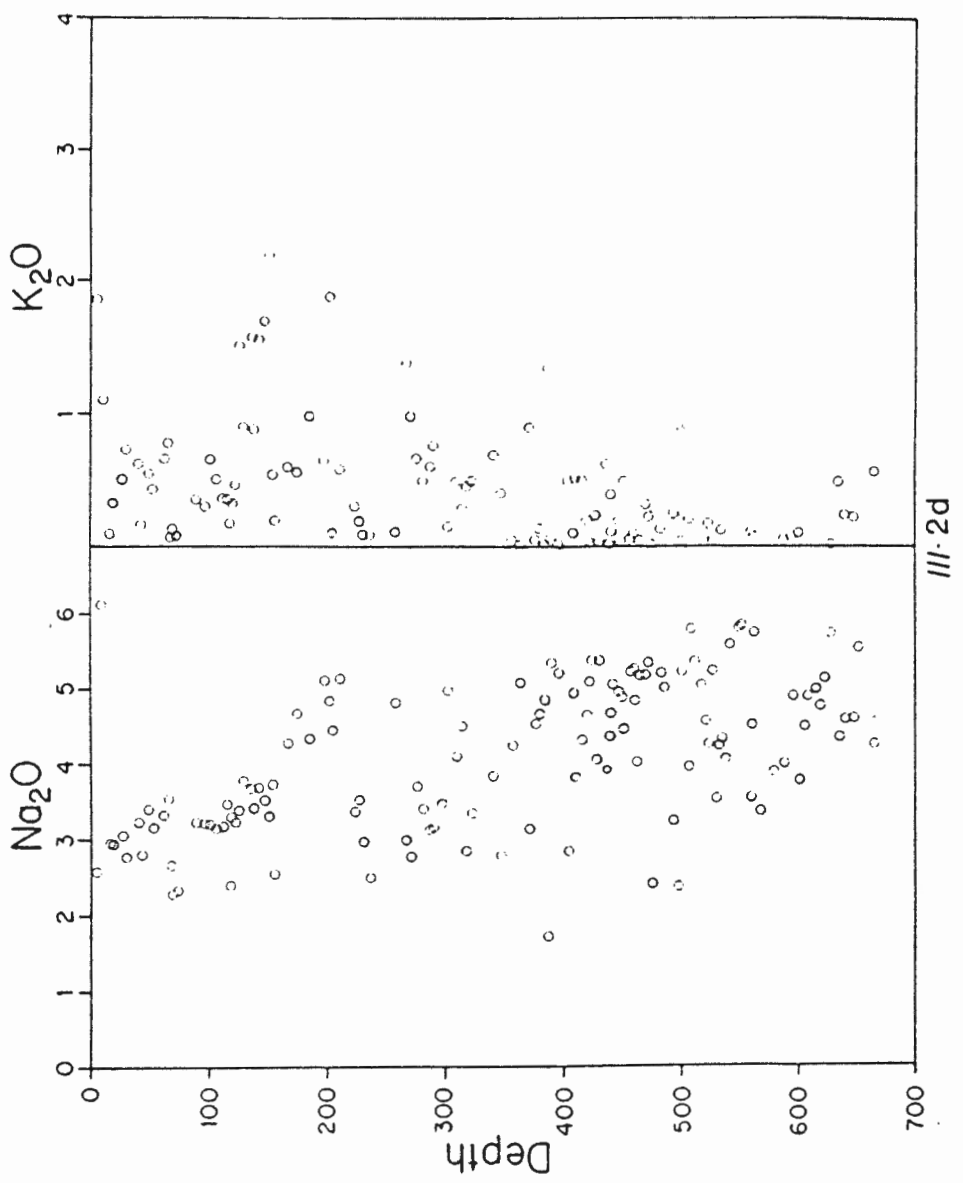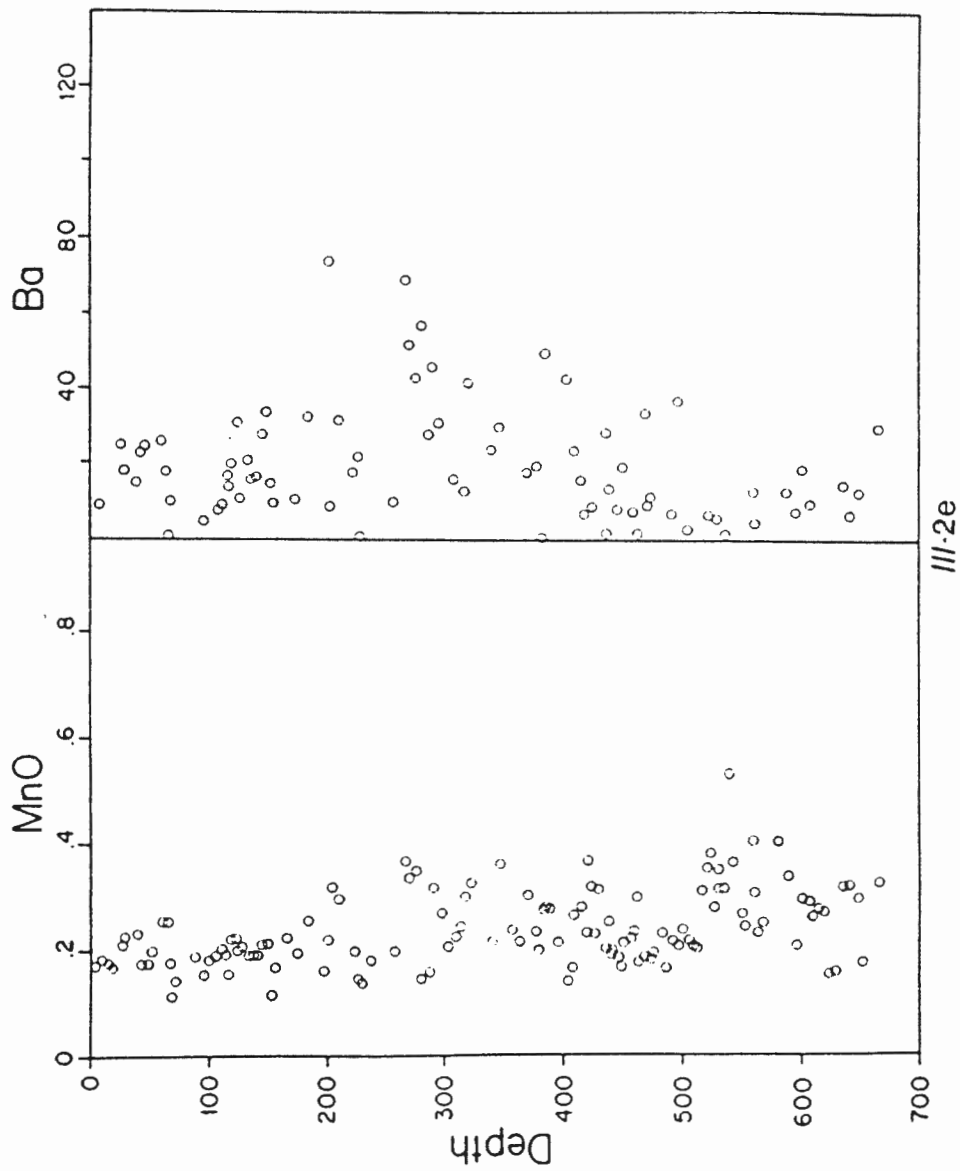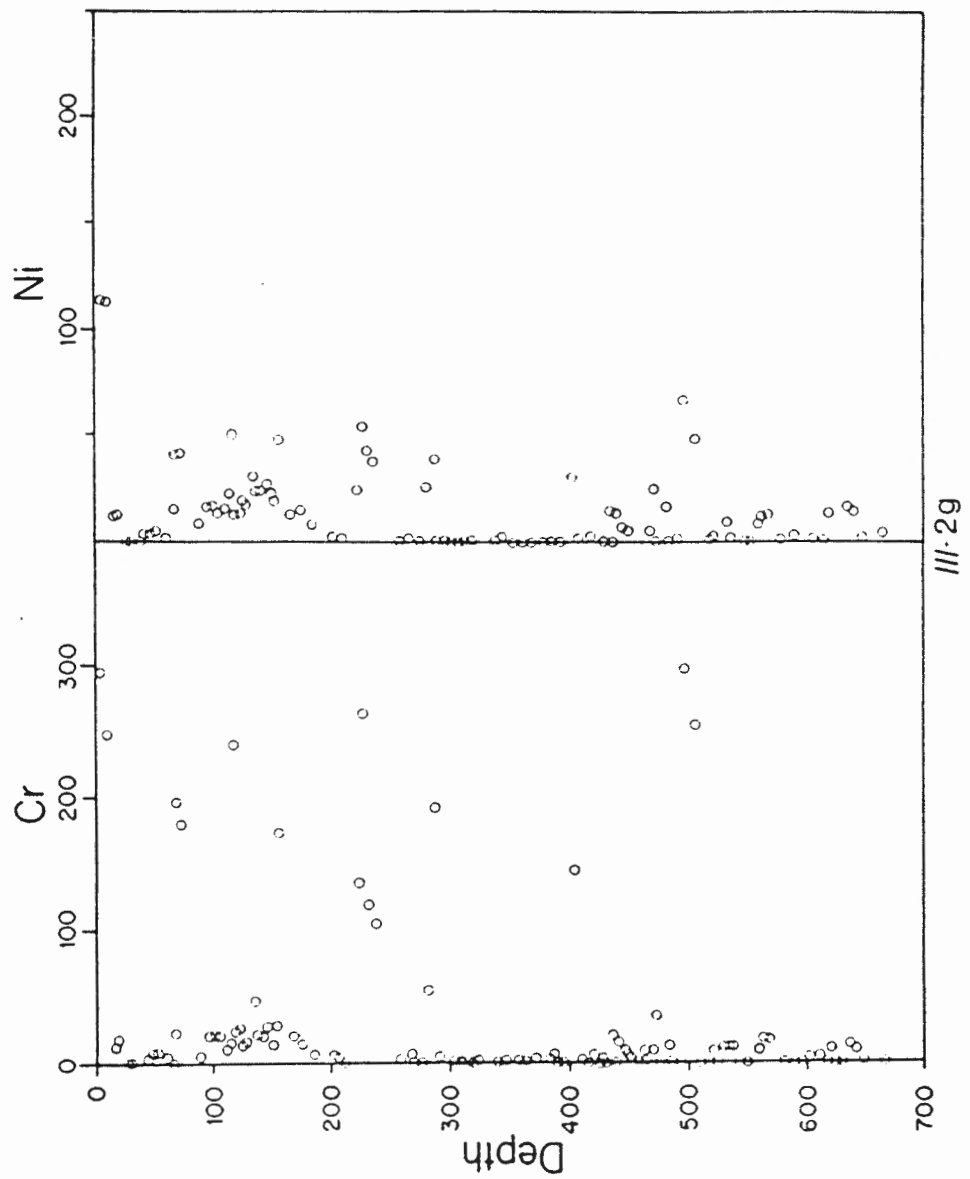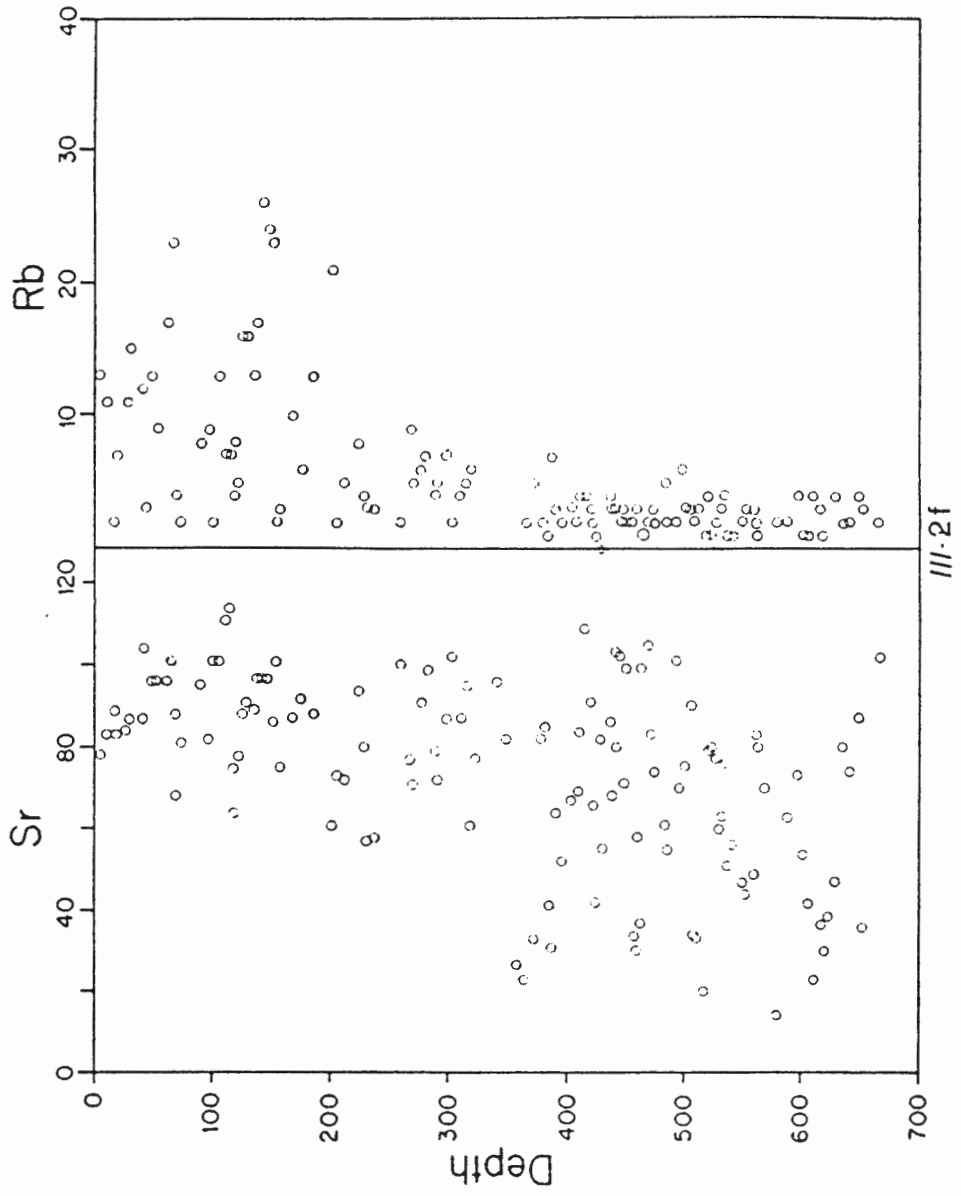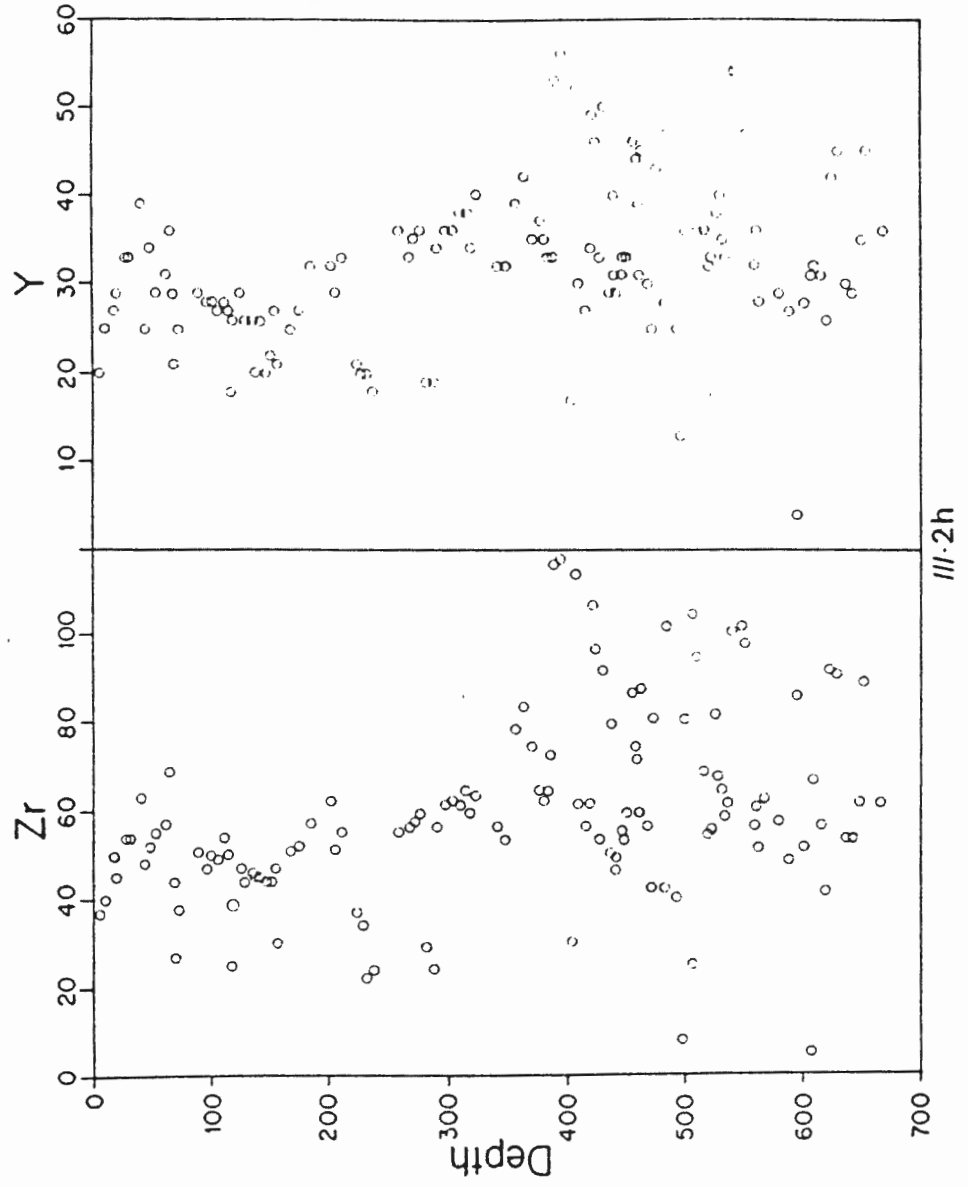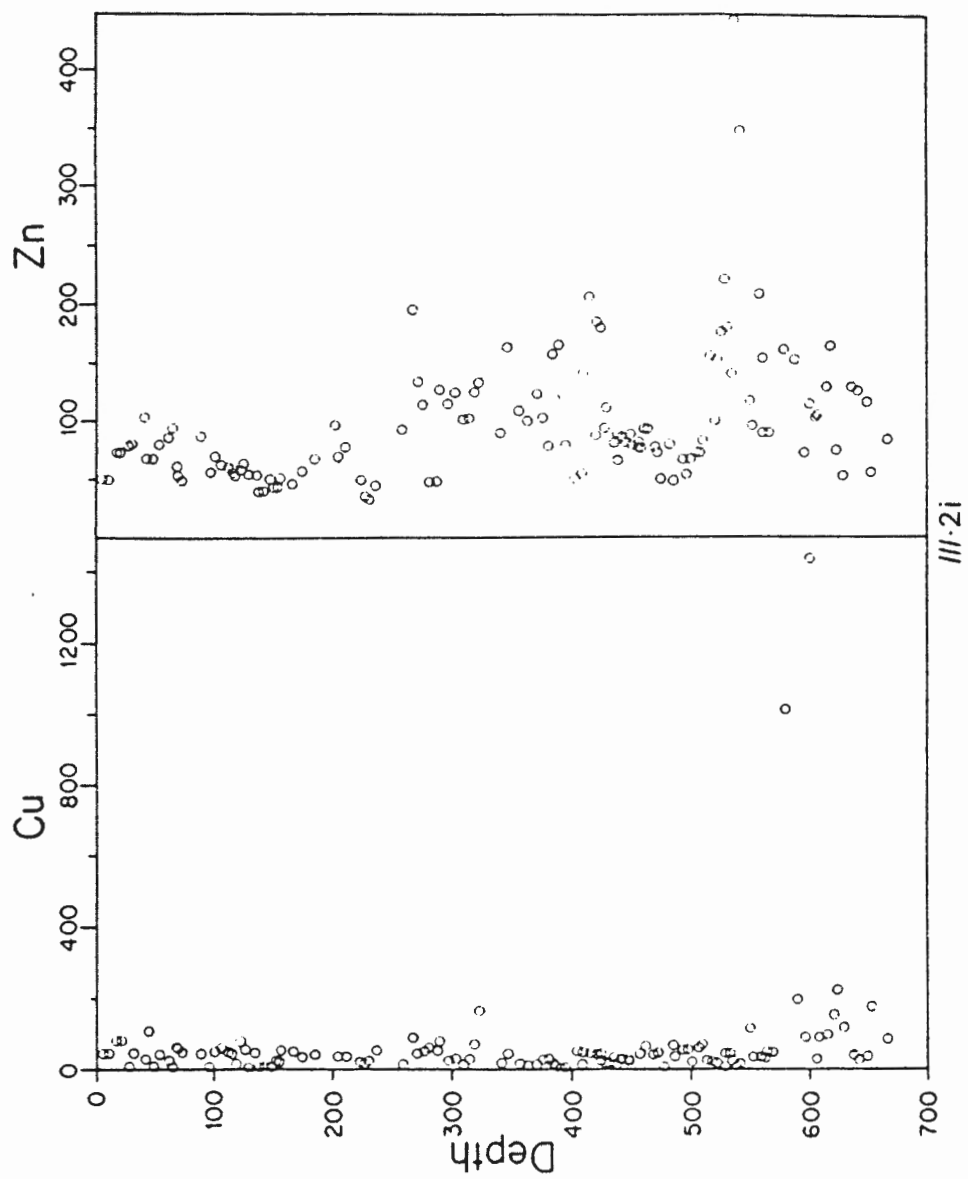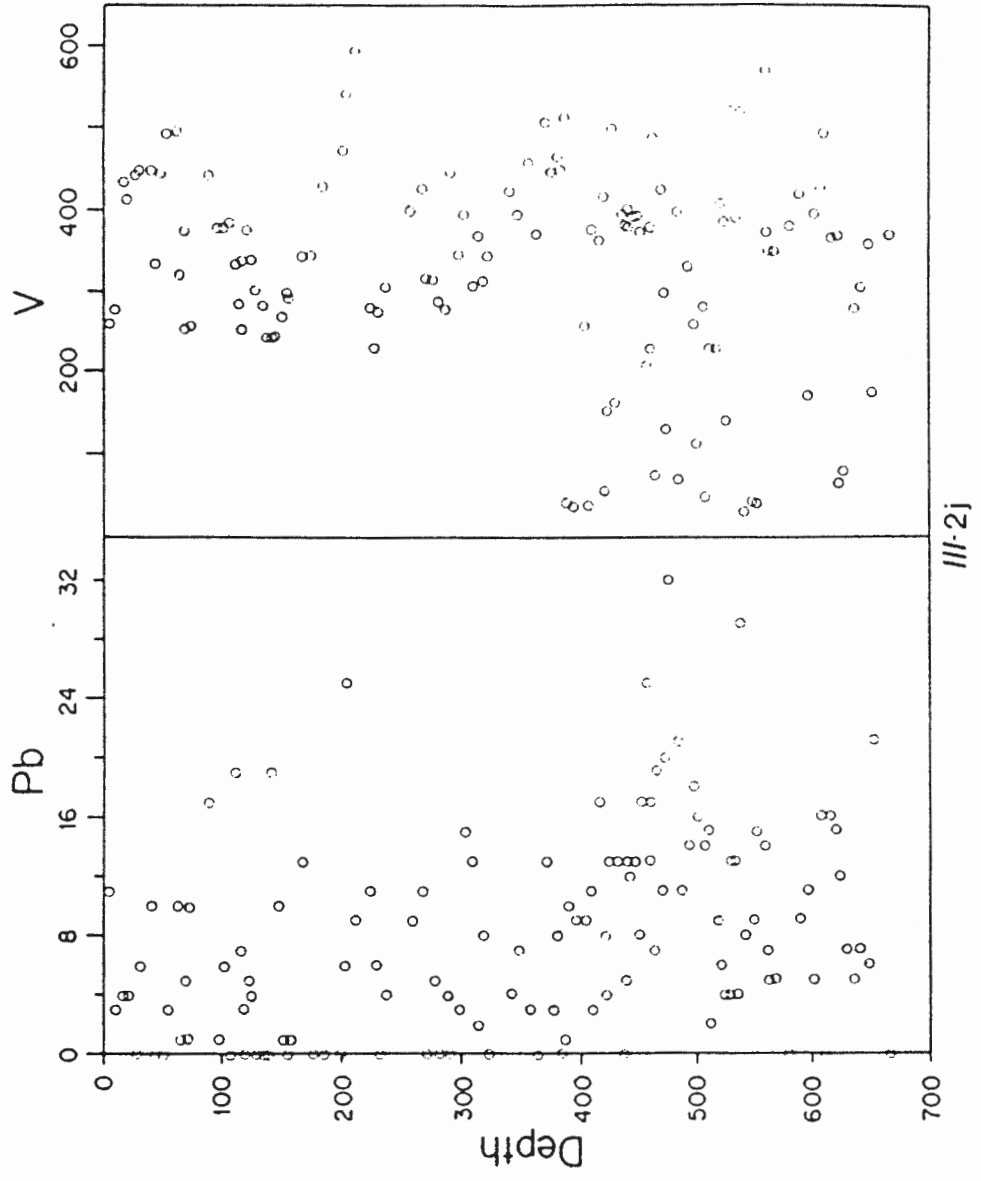
APPENDIX IV   Major and trace element analyses of the standards
              used for flux calculations

1. Samples with the prefix M are from Bailey (1984); the remaining
samples are from Mehegan, unpublished data, (1985).

2. n.a. = not analysed;   - = not detected.

4. N - number of samples

3. $FeO^* = Fe_2O_3 + FeO$

APPENDIX IV   STANDARDS FOR HIGH MgO - HIGH SiO_2 SUITE

STD	A	B	C	D	E	F
TiO_2 range	0.151–0.200	0.201–0.250	0.251–0.300	0.301–0.350	0.351–0.400	0.401–0.450

Majors (wt%)

SiO_2	45.86	45.74	48.60	58.10	50.13	54.70
TiO_2	0.19	0.23	0.33	0.37	0.42	0.50
Al_2O_3	4.89	5.04	7.40	12.53	15.32	14.98
FeO*	9.09	8.97	9.78	8.31	8.69	9.12
MnO	n.a.	n.a.	n.a.	0.16	0.15	?
MgO	35.45	35.15	28.36	9.15	7.74	7.87
CaO	4.04	4.45	5.14	7.84	15.76	11.08
Na_2O	0.43	0.27	0.29	3.49	1.39	1.45
K_2O	0.02	0.13	0.05	n.d.	0.24	0.32
P_2O_5	0.02	0.03	0.04	0.04	–	0?
Total	100.00	100.00	100.00	100.00	100.00	100.00

traces (ppm)

Rb	2	4	2	1	7	7
Sr	26	35	29	46	80	123
Y	6	6	9	12	15	13
Ba	–	1	–	2	2	–
Zr	12	8	11	14	24	29
V	76	88	108	263	238	226
Zn	54	54	60	57	62	64
Cu	26	30	32	67	16	62
Ni	1426	1402	899	108	76	61
Cr	2608	2430	1894	532	244	269
N	1	1	1	1	1	1

A – M53; B – M127; C – M75; D – DEL-1; E – YI-2; F – YI-2

STD TiO$_2$ range	G 0.501– 0.550	H 0.551– 0.600	I 0.601– 0.650	J 0.651– 0.700	K 0.701– 0.750	L 0.751– 0.800
			Majors (wt%)			
SiO$_2$	54.16	51.92	54.23	53.06	52.88	53.52
TiO$_2$	0.52	0.59	0.62	0.69	0.72	0.78
Al$_2$O$_3$	13.52	15.47	15.73	15.97	15.40	15.31
FeO	8.79	7.52	9.28	8.91	8.79	12.26
MnO	n.a.	0.14	0.16	0.12	n.a.	0.22
MgO	10.96	8.84	7.07	8.08	8.92	5.80
CaO	10.40	13.70	10.90	11.27	11.84	9.10
Na$_2$O	1.23	1.41	1.55	1.52	1.12	1.69
K$_2$O	0.36	0.31	0.45	0.38	0.27	0.63
P$_2$O$_5$	0.05	0.14	0.06	0.03	0.06	0.07
Total	100.00	100.00	100.00	100.00	100.00	100.00
			traces (ppm)			
Rb	7	7	9	6	6	12
Sr	98	96	118	107	98	102
Y	14	18	19	16	19	25
Ba	–	12	8	2	13	–
Zr	32	33	32	36	43	38
V	214	262	235	295	258	329
Zn	63	66	64	70	70	92
Cu	64	19	51	66	66	281
Ni	136	78	52	248	146	19
Cr	648	224	170	196	669	44
N	3	2	6	2	1	1

G – M10, M97, M28; H – PED-9, YI-3; I – XER-2b, YI-54, YI-32b, YI-41, M86, M181; J – PED-1, YI-40; K – M102; L – TR10; M – YI13

APPENDIX V-1   DESCRIPTION OF COOLING UNIT SAMPLES

Cooling Unit #	Unit Type	Sample #s	Locality	Lava Suite	Alteration Zone	Description
1	F	KG:84:140– KG:84:146	Akaki	B	Sm–Ce–Ze	
2	P	KG:84:162a– KG:84:162b	Akaki	B	Sm–Ce–Ze	
3	P	KG:84:163– KG:84–169	Akaki	B	Sm–Ce–Ze	
4	F	KG:84:147a– KG:84:147b	Akaki	B	Sm–Ce–Ze	aphyric
5[*]	P	CY1:136.10– CY1:139.75	CY-1	B	Sm–Pa–Ca	cpx–oliv phyric
6[*]	P	CY1:151.46– CY1:153.05	CY-1	B	Sm–Pa–Ca	sp. cpx phyric
7[*]	P	CY1:167.45– CY1:168.38	CY-1	B	Sm–Pa–Ca	aphyric
8[*]	P	CY1:291.95– CY1:293.22	CY-1	B	Sm–Ce–Ze	aphyric
9[*]	P	CY1:345.90– CY1:346.85	CY-1	B	Sm–Ce–Ze	aphyric

[*] from Aucoin et al. 1986.

APPENDIX V-2 MAJOR AND TRACE ANALYSES OF COOLING UNITS

SAMPLE #	KG84[1] 140	KG84[1] 142	KG84[1] 145	KG84[1] 146	CY-1a[2] 162a
Majors (wt%)					
SiO_2	52.25	51.23	52.15	52.07	47.30
TiO_2	0.72	0.75	0.76	0.76	0.78
Al_2O_3	16.11	17.42	17.00	17.16	15.69
FeO	2.46	2.34	2.18	2.18	2.52
Fe_2O_3	5.42	5.24	5.13	4.60	4.60
MnO	0.12	0.14	0.14	0.10	0.11
MgO	6.21	6.38	5.16	5.19	9.12
CaO	8.90	8.20	8.22	8.45	8.15
Na_2O	2.64	2.36	2.35	2.47	2.16
K_2O	0.78	0.57	0.93	0.94	1.90
P_2O_5	0.06	0.11	0.11	0.11	0.11
Total	95.23	94.74	94.13	94.03	92.44
H_2O+	1.60	2.28		1.68	3.04
H_2O-	2.27	2.68		2.45	2.98
CO_2	0.21	0.15		0.70	1.07
L.O.I.	4.50	4.15	5.31	4.62	7.15
$\dfrac{Fe_2O_3}{FeO+Fe_2O_3}$	0.69	0.69	0.70	0.68	0.64
traces (ppm)					
Rb	15	10	18	19	16
Sr	111	112	110	111	165
Y	16	18	17	19	18
Ba	16	–	13	17	12
Zr	46	47	48	46	43
V	232	236	234	236	237
Nb	4	4	4	4	5
Zn	56	53	59	46	62
Cu	12	22	15	10	53
Ni	32	33	27	35	98
Cr	40	40	33	40	323
Th	1	0	1	–	–
Ga	16	15	15	16	13
S	–	n.a.	n.a.	n.a.	15

[1] massive flow; Sequence II; Sm-Ce-Ze Zone; Akaki River section
[1] f.g. pillow; Sequence II; Sm-Ce-Ze Zone; Akaki River section

APPENDIX V-2 (continued)

SAMPLE #	KG84[2] 162b	KG84[3] 163	KG84[3] 165	KG84[3] 169

Majors (wt%)				
SiO_2	45.32	46.81	46.36	47.04
TiO_2	0.85	0.71	0.65	0.70
Al_2O_3	16.35	14.87	15.87	15.99
FeO	2.03	2.31	3.10	2.93
Fe_2O_3	4.94	4.96	4.04	4.47
MnO	0.12	0.13	0.15	0.14
MgO	9.69	9.86	10.52	9.38
CaO	6.94	6.10	6.35	4.77
Na_2O	2.59	3.85	3.50	4.48
K_2O	0.98	1.27	1.14	1.31
P_2O_5	0.10	0.09	0.10	0.10
Total	89.91	90.96	91.78	91.31
H_2O+	3.72	5.72	6.76	6.53
H_2O-	4.36	3.34	3.05	3.23
CO_2	1.28	0.67	0.37	0.16
L.O.I.	10.00	8.92	9.08	9.46
$\dfrac{Fe_2O_3}{FeO+Fe_2O_3}$	0.71	0.82	0.57	0.60

traces (ppm)				
Rb	8	17	9	13
Sr	98	35	188	111
Y	17	16	18	18
Ba	2	4	-	-
Zr	44	36	33	34
V	263	242	232	244
Nb	3	4	3	2
Zn	62	60	60	60
Cu	61	55	49	49
Ni	113	97	92	71
Cr	428	408	332	244
Th	5	2	0	2
Ga	15	8	14	14
S	5	n.a.	20	2

[2] f.g. pillow; Sequence II; Sm-Ce-Ze Zone; Akaki River section
[3] f.g.pillow; Sequence II; Sm-Ce-Ze Zone; Akaki River section

APPENDIX V-2 (continued)

SAMPLE #	KG84[4] 147a	KG84[4] 147b
Majors (wt%)		
SiO_2	52.37	50.63
TiO_2	0.79	0.75
Al_2O_3	16.44	17.64
FeO	2.34	2.61
Fe_2O_3	5.50	3.40
MnO	0.14	0.16
MgO	5.34	6.20
CaO	7.91	9.31
Na_2O	2.53	2.39
K_2O	1.26	0.17
P_2O_5	0.11	0.11
Total	94.73	93.37
H_2O+	1.43	2.08
H_2O-	2.11	2.17
CO_2	0.54	1.42
L.O.I.	4.08	5.54
$\dfrac{Fe_2O_3}{FeO+Fe_2O_3}$	0.70	0.57
traces (ppm)		
Rb	27	3
Sr	108	115
Y	18	19
Ba	13	10
Zr	50	47
V	247	244
Nb	4	4
Zn	58	66
Cu	62	66
Ni	23	35
Cr	34	41
Th	-	1
Ga	17	15
S	6	2

[8] f.-m.g. aphyric massive flow;
Sequence II; Sm-Ce-Ze Zone;

APPENDIX VI-1   DESCRIPTION OF CALCITE SAMPLES ANALYSED
                FOR OXYGEN AND CARBON ISOTOPES

CY-1 DRILLCORE

DEPTH (m)	OCCURRENCE
58.30	7 mm thick vein rimmed by smectite cutting grey green olivine phyric pillow
86.30	3 mm thick light green smectite & calcite vein cutting aphyric pillow parallel to margin
123.65	sparry calcite vug filling in olivine phyric pillow
291.85	calcite matrix in greyish-green breccia
299.05	smectite & calcite stringer within margin of dark grey pillow
410.43	calcite vesicle fill in aphyric greyish-green pillow

CY-1a DRILLCORE

DEPTH(M)	OCCURRENCE
36.35	sparry calcite associated with clinoptilolite in vug within massive flow
138.75	calcite associated with celadonite and gmelinite in vesicle within massive flow
242.09	calcite associated with zeolite?
314.05	calcite associated with pyrite in vuggy zone of a massive flow
406.45	calcite vein in brecciated zone within massive flow
434.50	calcite associated with pyrite and epidote in vein cross-cutting massive flow
518.08	coarse-grained calcite in epidosite, associated with hematite
617.20	sparry calcite associated with hematite on fracture surface within epidotized zone of massive flow
390.00	calcite associated with prismatic epidote in vug within a dyke

APPENDIX VI-1 (continued)

PEDIAEOS AND AKAKI RIVER SECTIONS

SAMPLE #	LOCATION	SEQUENCE #	OCCURRENCE
KG83017	Pediaeos	III	calcite filled fracture in oliv phyric pillow
KG83012	Pediaeos	III	vesicle fill, rim of aphyric pillow
KG83032	Pediaeos	III	vesicle fill, slightly olivine phyric pillow
KG83063	Pediaeos	I	vug filling within massive flow
KG83093	Pediaeos	I	vesicle fill, bottom of greyish-green flow
KG83089	Pediaeos	I	sparry calcite vug filling, Fe-stained within massive flow
KG83147	Pediaeos	I	vug filling within pliiow, associated with heulandite
KG83154	Pediaeos	I	vesicle fill, within brown massive flow
KG82255	Akaki	II	calcite vein within brecciated unit
KG82383A	Akaki	II	sparry calcite in brecciated zone
KG82360	Akaki	II	vein within brecciated zone

APPENDIX VI-2   DESCRIPTION OF SAMPLES ANALYSED FOR $^{87}Sr/^{86}Sr$

CY-1 DRILLCORE

DEPTH (m)	MINERAL	OCCURRENCE
58.30	calcite	7 mm thick vein rimmed by smectite cutting grey green olivine phyric pillow
86.30	calcite, smectite	3 mm thick light green smectite & calcite vein cutting aphyric pillow parallel to margin
123.65	calcite	sparry calcite vug filling in olivine phyric pillow
155.55	palygorskite	palygorskite & calcite vein cutting sparsely olivine phyric pillow
243.30	smectite	12 mm thick smectite & calcite vein cutting greyish-green massive flow
291.85	calcite	calcite matrix in greyish-green breccia
293.35	analcime	analcime associated with phillipsite & smectite within margin greyish-green aphyric pillow
299.05	calcite	smectite & calcite stringer within margin of dark grey pillow
327.90	gypsum	4 mm thick gypsum vein cutting greyish green massive flow
410.43	calcite	calcite vesicle fill in aphyric greyish green pillow

AKAKI RIVER SECTION AND THE MARGI AREA

SAMPLE #	LOCATION	SEQ #	MINERAL	OCCURRENCE
HSTR 8	Akaki R	II	celadonite	massive celadonite zone within near vertical fissure in flow
HSTR 9	Akaki R.	II	celadonite	massive celadonite zone with chalcedony core within near vertical fissure within flow
HSTR10	Akaki R.	II	mordenite	zeolite rich celadonite zone along cooling joint in flow
KG82107	Akaki R.	II	analcime	fracture filling within pillow associated with calcite
KG82135	Akaki R.	II	heulandite	fracture filling within pillow
KG83203	Margi	III	gmelinite	fracture filling within pillow, orange, rosettes are associated with smectite

Abbey, S. (1983). Studies in "standard samples" of silicate rocks and
    minerals 1969 - 1982. Geol. Surv. Can. Pap. 83-15, 114 pp.

Adamides, N.G. (1984). Cyprus volcanogenic sulphide deposits in
    relation to their environment of formation. Unpublished Ph.D.
    thesis, University of Leicester, 383 pp.

Adamides, N.G. (1975). Geological history of the Limni concession,
    Cyprus, in light of the plate tectonics hypothesis. Trans. Inst.
    Min. Metal. Sec. B 84, B17-B23.

Adamson, A. (1985). Basement lithostratigraphy, Deep Sea Drilling
    Project Hole 504B. In: Anderson, R.N., Honnorez, J., Becker, K.,
    et. al., Initial Reports DSDP, 83: Washington (U.S. Govt. Printing
    Office), 121-128.

Alabaster, T. and Pearce, J.A. (1985). The interrelationship between
    magmatic and ore-forming hydrothermal processes in the Oman
    ophiolite. Econ. Geol. 80, 1-16.

Alabaster, T., Pearce, J.A., Mallick, D.I.J. and Elboushi, I.M. (1980).
    The volcanic stratigraphy and location of massive sulphide deposits
    in the Oman ophiolite. In: Panayiotou, A.,(ed.), Ophiolites,
    Proceedings, International Ophiolite Symposium, Cyprus 1979.
    Ministry of Agriculture and Natural Resources, Geol. Surv. Dept.,
    751-757.

Alt, J.C. (1984). The structure, chemistry, and evolution of a
    submarine hydrothermal system, DSDP Site 504. Unpublished Ph.D.
    dissertation, University of Miami, Miami, Florida, 286 pp.

Alt, J.C., Honnorez, J., Laverne, C. and Emmerman, R. (1986).
    Hydrothermal alteration of a 1 km section through the upper oceanic
    crust, Deep Sea Drilling Project Hole 504B: Mineralogy, chemistry,
    and evolution of seawater-basalt interactions. J. Geophys. Res.
    91, 10,309-10,335.

Alt, J.C., Laverne, C. and Muehlenbachs, K. (1985). Alteration of the
    upper oceanic crust: Mineralogy and processes in Deep Sea Drilling
    Project Hole 504B, Leg 83. In: Anderson, R.N., Honnorez, J.,
    Becker, K., et. al., Initial Reports DSDP, 83: Washington (U.S.
    Govt. Printing Office), 217-247.

Alt, J.C. and Emmermann, R. (1985). Geochemistry of hydrothermally
    altered basalts: Deep Sea Drilling Project Hole 504B, Leg 83. In:
    Anderson, R.N., Honnorez, J., Becker, K., et. al., Initial Reports
    DSDP, 83: Washington (U.S. Govt. Printing Office), 249-262.

Alt, J. C. and Honnorez, J. (1984). Alteration of the upper oceanic crust, DSDP Site 417: Mineralogy and chemistry. Contrib. Mineral. Petrol. 87, 149-169.

Andrews, A.J. (1980). Saponite and celadonite in layer 2 basalts DSDP Leg 37. Contrib. Mineral. Petrol. 73, 323-340.

Andrews, A.J., Dollase, W.A. and Fleet, M.E. (1983). A Mossbauer study of saponite in layer 2 basalt, Deep Sea Drilling Project Leg 69. In: Cann, J.R., Langseth, M.G., Honnorez, J., Von Herzen, R.P., White, S.M., et al., Initial Reports DSDP, 69: Washington (U.S. Govt. Printing Office), 585-588.

Anderson, R.N. and Skilbeck, J.N. (1981). Oceanic heatflow. In: Emiliani, C. (ed.), The Oceanic Lithosphere, The Sea 7. John Wiley & Sons, New York, 489-524.

Anderson, R.N., Langseth, M.G., Sclater, J.G. (1977). The mechanisms of heat transfer through the floor of the Indian Ocean. J. Geophys. Res. 82, 3391-3409.

Anderson, R.N. and Hobart, M.A. (1976). The relation between heat flow, sediment thickness, and age in the eastern Pacific. J. Geophys. Res. 81, 2968-2989.

Anderson, R.N., Zoback, M.D., Hickman, S.H. and Newmark, R.L. (1985). Permeability versus depth in the upper oceanic crust: In situ measurements in Deep Sea Drilling Project Hole 504B, eastern equatorial Pacific. In: Anderson, R.N., Honnorez, J., Becker, K., et al., Initial Reports DSDP, 83: Washington (U.S. Govt. Printing Office), 429-442.

Aubert, M. and Baroz, F. (1974). Structure profonde de la chaine Zu Pentadaktylos et de la Misasoria (Chypre). Rev. Inst. Fr. Pet. Paris 29, 361-373.

Auclair, F., Baragar, W. and Ludden, J. Alteration of the upper pillow lavas of the Troodos ophiolite: Evidence from the CY-1 drillcore of the ICRDG. Initial Reports ICRDG, CY-1, in press.

Bailey, D.G. (1984). Stratigraphy and geochemistry of the Troodos ophiolite extrusive sequence in the Margi area, Cyprus. Unpublished M.Sc. thesis, Dalhousie University, Halifax, N.S., 215 pp.

Baker, P.A., Gieskes, J.M. and Elderfield, H. (1982). Diagenesis of carbonates in deep-sea sediments - evidence from Sr/Ca ratios and interstitial dissolved Sr^{2+} data. J. Sed. Petrol. 52, 71-82.

Baragar, W.P.A., Lambert, M., Baglow, N. and Gibson, I. Sheeted dykes of the Troodos ophiolite, Cyprus. Initial Reports ICRDG, CY-4, in press.

Baragar, W.P.A., Lambert, M., Baglow, N. and Gibson, I. (1984). Sheeted dyke complex, Troodos Ophiolite. Geol. Assoc. Can. - Mineral. Assoc. Can. Joint Annual Meeting Program with Abstracts 9, 44.

Baroz, F. (1980). Volcanism and continent-island arc collision in the Pentadaktylos Range, Cyprus. In: Panayiotou, A., (ed.), Ophiolites, Proceedings, International Ophiolite Symposium, Cyprus 1979. Ministry of Agriculture and Natural Resources, Geol. Surv. Dept., 73-85.

Baroz, F. (1977). Observation nouvelles sur l'Eocene de la Chaine de Kyrenia (Chypre). Bull. Soc. geol. Fr. 18, 429-437.

Baroz, F., Desmet, A. and Lapierre, H. (1976). Les traits dominants de la geologie de Chypre. Bull. Soc. geol. Fr. 18, 429-437.

Baroz, F., Desmet, A. and Lapierre, H. (1975). Trois familles volcaniques pre-orogeniques a Chypre: Comparison et discussion geotectonique. 3e. Reun. ann. Sci. Terre Monpellier, 126 pp.

Barrows, K.J. (1980). Zeolitization of Miocene volcaniclastic rocks, southern Desatoya Mountains, Nevada. Geol. Soc. Am. Bull. 91, 199-210.

Barth, T.F.W. (1948). Oxygen in rocks: A basis for petrographic calculations. J. Geol. 56, 50-60.

Bass, M.N. (1976). Secondary minerals in oceanic basalt, with special reference to Leg 34, Deep Sea Drilling Project. In: Yeats, R. S., Hart, S. R., et al., Initial Reports DSDP, 34: Washington (U.S. Govt. Printing Office), 393-432.

Bayliss, P. (1975). Nomenclature of the trioctahedral chlorites. Can. Mineral. 13, 178-180.

Bear, L.M. (1960). The geology and mineral resources of the Akaki-Lythrodonda area. Cyprus Geol. Surv. Dept. Memoir 3, 122 pp.

Becker, K. (1985). Large-scale electrical resistivity and bulk porosity of the oceanic crust, Hole 504B, Costa Rica Rift. In: Anderson, R.N., Honnorez, J., Becker, K., et al., Initial Reports DSDP, 83: Washington (U.S. Govt. Printing Office), 419-428.

Biju-Duval, B., Lapierre, H. and Letouzey, J. (1976). Is the Troodos Massif (Cyprus) allochthonous? Bull. Soc. geol. Fr. 18, 1347-1356.

Bischoff, J.L. (1980). Geothermal system at $21^{\circ}N$, East Pacific Rise: Physical limits on geothermal fluid and role of adiabatic expansion. Science, 207, 1465-1469.

Bischoff, J.L. and Dickson, F.W. (1975). Seawater-basalt interaction at 200°C and 500 bars: Implication for the origin of sea-floor heavy metal deposits and regulation of seawater chemistry. Earth Planet. Sci. Lett. 25, 385-397.

Bischoff, J.L. and Seyfried Jr., W.E. (1978). Hydrothermal chemistry of seawater from 25° to 350°C. Amer. J. Sci. 278, 838-860.

Blanchard, M.-C. (1982). Geochemistry and petrogenesis of the Fisset Brook Formation, Western Cape Breton Island, Nova Scotia. Unpublished M.Sc. thesis, Dalhousie University, Halifax, Nova Scotia.

Bleil, U., Donnelly, T., Francheteau, J. and Leg 51 Scientific Party (1977). Paleomagnetic and structural evidence for a tectonic event in the Leg 51 basement. EOS 58, 1174.

Blome, C.D. and Irwin, W.P. (1985). Equivalent radiolarian ages from ophiolite terranes of Cyprus and Oman. Geology 13, 401-404.

Bohlke, J.K., Alt, J.C. and Muehlenbachs, K. (1984). Oxygen isotope-water relations in altered deep-sea basalts: Low-temperature mineralogical controls. Can. J. Earth Sci. 21, 67-77.

Bohlke, J.K, Honnorez, J., Honnorez-Guerstein, B.M., Muehlenbachs, K. and Petersen, N. (1981). Heterogeneous alteration of the upper oceanic crust: Correlation of rock chemistry, magnetic properties, and O isotope ratios with alteration patterns in basalts from Site 396B, DSDP. J. Geophys. Res. 86, 7935-7950.

Bohlke, J.K, Honnorez, J. and Honnorez-Guerstein, B.M. (1980). Alteration of basalts from Site 396B DSDP: Petrographic and Mineralogic Studies. Contrib. Mineral. Petrol. 73, 341-369.

Boles, J.R. (1972). Composition, optical properties, cell dimensions and the thermal stability of some heulandite group zeolites. Amer. Mineral. 57, 1463-1493.

Boles, J.R. and Coombs, D.S. (1977). Zeolite facies alteration of sandstones in the Southland syncline, New Zealand. Amer. J. Sci. 277, 982-1012.

Bouvier, J.G., Gupta, S. and Abbey, S. (1972). Use of an "automatic sulfur titrator" in rock and mineral analyses: Determination of sulfur, total carbon, carbonate and ferrous iron. Geol. Surv. Can. Pap. 72-31, 21 pp.

Boyle, J.F. and Robertson, H.F. (1984). Evolving metallogenesis at the Troodos spreading axis. In: Gass, I.G., Lippard, S.J. and Shelton, A.W., (eds.), Ophiolites and Oceanic Lithosphere. Blackwell Scientific Publications, Oxford, 169-181.

Brass, G.W., Southam, J.R. and Peterson, W.H. (1982). Warm saline bottom water in the ancient ocean. Nature 296, 620-623. 373

Brindley, G.W. and Brown, G. (1980). Crystal Structures of Clay Minerals and their XRD identification. Mineralogical Society of London, 495 pp.

Buckley, H.A., Bevan, J.C., Brown, K.M. and Johnson, L.R. (1978). Glauconite and celadonite: Two separate mineral species. Mineral. Mag. 42, 373-382.

Cann, J.P. (1979). Metamorphism in the ocean crust. In: Talwani, M., Harrison, C.G., and Hayes, D.E. (eds.), Deep Drilling Results in the Atlantic Ocean: Ocean Crust, Maurice Ewing Series 2. Am. Geophys. Union, Washington, 230-238.

Cann, J.R. (1970). Rb, Sr, Y, Zr and Nb in some ocean floor basaltic rocks. Earth Planet. Sci. Lett. 10, 7-11.

Cann, J., Oakley, P., Richards, H. and Richardson, C. Geochemistry of hydrothermally altered rocks from Cyprus drill holes CY-2 and CY-2a compared with other Cyprus stockworks. Initial Reports ICRDG, CY-2 & CY-2a, in press.

Carr, J.M. and Bear, L.M. (1960). The geology and mineral resources of the Peristerona-Lagoudhera area. Cyprus Geol. Surv. Memoir 2, 79 pp.

Chapman, H.J. and Spooner, E.T.C. (1977). ^{87}Sr enrichment of ophiolitic sulfide deposits in Cyprus confirms ore formation by circulating seawater. Earth Planet. Sci. Lett. 35, 71-78.

Chudayev, O.V., Kurnosov, V.B., Petrachenko, E.D. and Kholodkevich, I.V. Secondary Minerals from the extrusive section, ophiolites of Troodos, Cyprus, CY-1 and CY-1a holes, Initial Reports ICRDG, CY-1 and CY-1a, in press.

Coish, R.A. (1977). Ocean floor metamorphism in the Betts Cove ophiolite, Newfoundland. Contrib. Mineral. Petrol. 60, 255-270.

Coleman, R.G. (1977). Ophiolites: Ancient oceanic lithosphere? Springer-Verlag, Berlin, 229 pp.

Colman, S.M. (1982). Chemical weathering of basalts and andesites: Evidence from weathering rinds. Geol. Survey Prof. Pap. 1246, U.S. Govt. Printing Office, 51 pp.

Constantinou, G. (1980). Metallogenesis associated with the Troodos ophiolite. In: Panayiotou, A. (ed.), Ophiolites, Proceedings, International Ophiolite Symposium, Cyprus 1979. Ministry of Agriculture and Natural Resources, Geol. Surv. Dept., 663-674.

Constantinou, G. (1976). Genesis of the conglomerate structure, porosity and collomorphic textures of the massive sulfide ores of Cyprus. In: Strong, D.J., (ed.), Metallogeny and Plate Tectonics, Geol. Assoc. Can. Spec. Pap. 14, 187-210.

Constantinou, G. and Govett, G.J.S. (1973). Geology, geochemistry and genesis of Cyprus sulfide deposits. Econ. Geol. 68, 843-858.

Constantinou, G. and Govett, G.J.S. (1972). Genesis of sulfide deposits, ochre, and umber of Cyprus. Trans. Inst. Min.Met., Sec. B, 81, B32-46.

Coombs, D.S. (1952). Cell size, optical properties and chemical composition of laumontite and leonhardite. Amer. Mineral. 37, 812-830.

Coombs, D.S., Ellis, A.J., Fyfe, W.S., and Taylor, A.M. (1959). The zeolite facies with comments on the interpretation of hydrothermal syntheses. Geochim. Cosmoschim. Acta 17, 53-107.

Couture, R.A. (1977). Composition and origin of palygorskite-rich and montmorillonite-rich zeolite-containing sediments from the Pacific Ocean. Chem. Geol. 19, 113-130.

Deer, W.A., Howie, R.A. and Zussman, J. (1962). Rock forming minerals, First edition, 1 - 5. Longmans Green, & Co. Ltd., London.

Delaloye, M., de Souza, H., Wagner, J.-J. and Hedley, I. (1980). Isotopic ages of ophiolites from the eastern Mediterranean. In: Panayiotou, A., (eds.), Ophiolites, Proceedings, International Ophiolite Symposium, Cyprus 1979. Ministry of Agriculture and Natural Resources, Geol. Surv. Dept., 292-295.

Delaney, J.R., Mogk, D.W. and Mottle, M.J. (1980). High-temperature, sulfide-bearing hydrothermal system on the Mid-Atlantic Ridge at 23.6° North. Geol. Soc. Amer. Programs with Abstracts 12, 411.

Donahoe, R.J. and Liou, J.G. (1985). An experimental study on the process of zeolite formation. Geochim. Cosmoschim. Acta 49, 2349-2360.

Donnelly, T.W., Pritchard, R.A., Emmermann, R. and Puchelt, H. (1979a). The aging of oceanic crust: Synthesis of the mineralogical and chemical results of DSDP, Legs 51 through 53. In: Donnelly, T.W., Francheteau, J., Bryan, W., Robinson, P., Flower, M., Salisbury, M., et al., Initial Reports DSDP, 51-53 Pt.2: Washington (U.S. Govt. Printing Office), 1563-1577.

Donnelly, T.W., Thompson, G. and Salisbury, M.H. (1979b). The chemistry of altered basalt at Site 417, Deep Sea Drilling Project Leg 51. In: Donnelly, T.W., Francheteau, J., Bryan, W., Robinson, P., Flower, M., Salisbury, M., et al., Initial Reports DSDP, 51-53 Pt.2: Washington (U.S. Govt. Printing Office), 1319-1330.

Douma, L. and Robinson, P. (1984). Cyprus Crustal Study Project, Hole CY-1. Edited core descriptions. Unpublished report, Dalhousie University, Halifax, 1000 pp.

Douma, L. and Robinson, P. (1984). Cyprus Crustal Study Project, Hole CY-2a. Edited core descriptions. Unpublished report, Dalhousie University, Halifax, 513 pp.

Drever, J.L. (1974). The magnesium problem. In: Goldberg, E.D., (ed.), Ideas and observations on progress in the study of the seas, The Sea 5, John Wiley & Sons, New York, 337-358.

Dunsworth, S. and Calon, J. (1984). Relationships between deformation and magmatism in the plutonic complex, Troodos Ophiolite, Cyprus. Geol. Assoc. Can. - Mineral. Assoc. Can. Joint Annual Meeting Program with Abstracts 9, 59.

Edmond, J.M., Measures, C., Mangum, B., Grant, B., Sclater, F.R., Collier, R., Hudson, A., Gordon, L.J. and Corliss, J.B. (1979). On the formation of metal-rich deposits at ridge crests. Earth Planet. Sci. Lett. 46, 19-30.

Elsbree, H.C. (1985). Clay alteration in three ore deposits and associated volcanics of the Troodos Ophiolite, Cyprus. Unpublished M.Sc. thesis, University of Illinois at Urbana-Champaign, 132 pp.

Elthon, H.C., Lawrence, J.R., Hansen, R.E. and Stern, C. (1984). Modelling of oxygen-isotope data from the Sarmiento ophiolite complex, Chile. In: Gass, I.G., Lippard, A.W., & Shelton, A.W. (eds.), Ophiolites and Oceanic Lithosphere. Blackwell Scientific Publications, 185-197.

Elthon, D. and Stern, C. (1978). Metamorphic petrology of the Sarmiento Ophiolite Complex, Chile. Geology 6, 464-468.

Emmermann, R. (1985). Basement geochemistry, Hole 504B. In: Anderson, R.N., Honnorez, J., Becker, K., et al., Initial Reports DSDP, 83: Washington (U.S. Govt. Printing Office), 183-200.

Evarts, R.C. and Schiffman, P. (1983). Submarine hydrothermal metamorphism of the Del Puerto ophiolite, California. Am. J. Sci. 283, 289-340.

Ewing, J. and Houtz, R. (1979). Acoustic stratigraphy and structure of the oceanic crust. In: Talwani, M., Harrison, C.G., and Hayes, D. (eds.), Deep drilling results in the Atlantic ocean: Oceanic crust, Maurice Ewing Series 2. Am. Geophys. Un., Washington, 1-14.

Fehn, U., Green, K.E., Von Herzen R.P., and Cathles, L.M. (1983). Numerical models for the hydrothermal field at the Galapagos Spreading Centre. J. Geophys. Res. 88, 1033-1048.

Finlow-Bates, T. and Stumpft, E.F. (1981). The behavior of so-called immobile elements in hydrothermally altered rocks associated with volcanogenic submarine exhalative ore deposits. Mineral. Deposita. 16, 319-328.

Floyd, P.A. and Winchester, J.A. (1978). Identification and discrimination of altered and metamorphosed volcanic rocks using immobile elements. Chem. Geol. 21, 291-306.

Franklin, J.M., Sangster, D.M. and Lydon, J.W. (1981). Volcanic-associated massive sulphide deposits. In: Skinner, B.J., (ed.), Econ. Geol. 75th Anniv. vol., 485-627.

Friedrichsen, H. (1983). Strontium, oxygen, and hydrogen isotopic studies on primary and secondary minerals in basalts from the Costa Rica Rift, Deep Sea Drilling Project Hole 504B. In: Cann, J.R., Langseth, M.G., Honnorez, J., Von Herzen, R.P., White, S.M., et al., Initial Reports DSDP, 69: Washington (U.S. Govt. Printing Office), 289-296.

Fuchtbauer, H. and Hardie, L.A. (1976). Experimentally determined homogeneous distribution coefficients for precipitated magnesian calcites. Abs. Ann. Prog. Meet. Geol. Soc. Amer. 8, 877.

Gass, I.G. (1980). The Troodos Massif: Its role in the unravelling of the understanding of constructive plate margin processes. In: Panayiotou, A. (ed.), Ophiolites, Proceedings, International Ophiolite Symposium, Cyprus 1979. Ministry of Agriculture and Natural Resources, Geol. Surv. Dept., 23-35.

Gass, I.G. (1960). The geology and mineral resources of the Dhali area. Cyprus Geol. Surv. Dept. Memoir 4, 116 pp.

Gass, I. and Smewing, J.D. (1973). Intrusion, extrusion and metamorphism at constructive margins: Evidence from the Troodos Massif, Cyprus. Nature 242, 26-29.

Green, K.E., Von Herzen, R., P., and Williams, D.L. (1981). The Galapagos Spreading Center at 86° W: A detailed geothermal field study. J. Geophys. Res. 86, 979-986.

Gresens, R.L. (1967). Composition-volume relationships of metasomatism. Chem. Geol. 2, 47-65.

Hajash, A. (1975). Hydrothermal processes along mid-ocean ridges: An experimental investigation. Contrib. Mineral. Petrol. 53, 205-226.

Hall, J.M., Walls, C., Williamson, M., and Wang, B.-X. Depth trends in magnetic properties in an area of prolonged cold sea water drawdown in uppermost Troodos type ooceanic crust, Can. J. Earth Sci., in press.

Hartland, W.B., Cox, A.V., Llewellyn, P.G., Pickton, C.A.G., Smith, A.G., and Walters, R. (1982). A geologic timescale. Cambridge University Press, Cambridge, England, 131 pp.

Hay, R.L. (1966). Zeolites and zeolitic reactions in sedimentary rocks. Geol. Soc. Amer. Spec. Pap. 85, 130 pp.

Hawkins, D.B., Sheppard, R.A. and Gude, A.J. (1978). Hydrothermal synthesis of clinoptilolite and comments on the assemblage phillipsite-clinoptilolite-mordenite. In: Sand, L.B. and Mumpton, F.A., (eds.), Natural Zeolites: Occurrence, Properties, Use. Permagon Press, New York, 337-344.

Heaton, T.H.E. and Sheppard, S.M.F. (1977). Hydrogen and oxygen isotope evidence for seawater - hydrothermal alteration and ore deposition, Troodos ophiolite, Cyprus. In: Volcanic processes in ore genesis, Special Publication 7 of the Geological Society of London, 42-57.

Hendricks, D.M. and Whittig, L.P. (1968). Andesite weathering, Part II, Geochemical changes from andesite to saprolite. J. Soil Sci. 19, 147-153.

Herzig, P.M. & Friedrich, G.H. Sulphide mineralization, hydrothermal alteration and chemistry in the drill hole CY-2a, Agrokipia, Cyprus. Initial Reports, ICRDG, CY-2 and CY-2a, in press.

Hess, J., Bender, M. and Schilling, J.G. (1986). Seawater $^{87}Sr/^{86}Sr$ evolution from Cretaceous to present, applications to paleoceanography. Science 231, 979-984.

Hickman, S.H., Svitek, J.F. and Langseth, M.G. (1984). In situ permeability and pore pressure measurements near the mid-Atlantic ridge, Deep Sea Drilling Project Hole 395A. In: Hyndman, R.D., Salisbury, M.H., et al., Initial Reports DSDP, 78B: Washington (U.S. Govt. Printing Office), 699-709.

Hoffman, J. and Hower, J. (1979). Clay mineral assemblages as low grade metamorphic geothermometers: Application to the thrust faulted disturbed belt of Montana, U.S.A. In: Scholle, P.A., and Schluger, P.R., (eds.), Aspects of Diagenesis, Soc. of Econ. Paleontologists and Mineralogists, Spec. Publ. 26, 55-79.

Honnorez, J. (1981). The aging of the oceanic crust at low temperature. In: Emiliani, C., (ed.), The Oceanic Lithosphere, The Sea, 7. John Wiley & Sons, New York, 525-588.

Honnorez, J. (1978). Generation of phillipsites by palagonitization of basaltic glass in seawater and the origin of K-rich deep-sea sediments. In: Sand, L.B. and Mumpton, F.A., (eds.), Natural Zeolites: Occurrence, Properties, Use. Permagon Press, New York, 245-258.

Honnorez, J., Alt, J., Honnorez-Guerstein, B.-M., Laverne, C., Muehlenbachs, K., Ruiz, J. and Saltzman, E. (1985). Stockwork-like sulphide mineralization in young oceanic crust: Deep Sea Drilling Project Hole 504B. In: Anderson, R.N., Honnorez, J., Becker, K., et al., Initial Reports DSDP, 83: Washington (U.S. Govt. Printing Office), 263-282.

Honnorez, J., Laverne, C., Hubberten, H.-W., Emmermann, R. and Muehlenbachs, K. (1983). Alteration processes in layer 2 basalts from Deep Sea Drilling Project Hole 504B Costa Rica Rift. In: Cann, J.R., Langseth, M.G., Honnorez, J., Von Herzen, R.P., White, S.M., et al., Initial Reports DSDP, 69: Washington (U.S. Govt. Printing Office), 509-542.

Holler, H. and Wirsching, U. (1978). Experiments on the formation of zeolites by hydrothermal alteration of volcanic glasses. In: Sand, L.B. and Mumpton, F.A., (eds.), Natural Zeolites: Occurrence, Properties, Use. Permagon Press, New York, 329-336.

Horne, L. and Robinson, P. (1986). Cyprus Crustal Study Project, Hole CY-1A. Edited core descriptions. Unpublished report, Dalhousie University, Halifax, Nova Scotia, 700 p.

Humphris, S. and Thompson, G. (1978). Hydrothermal alteration of oceanic basalts by seawater. Geochim. Cosmoschim. Acta 42, 107-125.

Humphris, S.E. and Thompson, G. and Marriner, G.F. (1979). The mineralogy and geochemistry of basalt weathering, Holes 417A and 418A. In: Donnelly, T., Francheteau, J., Bryan, W., Robinson, P., Flower, M., Salisbury, M., et al., Initial Reports DSDP, 51-53 Pt. 2: Washington (U.S. Govt. Printing Office), 1201-1217.

Iijima, A. (1974). Clay and zeolitic alteration zones surrounding Kuroko deposits in the Hokuroku District, Norther Akita, as submarine hydrothermal-diagenetic alteration products. In: Ishihara, S., Kanehira, K., Sasaki, A., Sako, T., and Shimazaki, Y., (eds.), Geology of Kuroko Deposits, Mining Geology Special Issue 6: 267-289.

Iijima, A. and Utada, M. (1971). Present-day zeolitic diagenesis of the Neogene geosynclinal deposits in the Niigata oil field, Japan. Molecular Sieve Zeolites - I Advances in Chem. Ser. 101, 342-349.

ICRDG (1984). Are Troodos deposits an East Pacific analog? Geotimes 29, 12-14.

Johnson, W.M. and Maxwell, J.A. (1981). Rock and mineral analysis (Second Edition). John Wiley and Sons, New York.

Jones, J.B. and Segnit, E.R. (1971). The Nature of opal: I Nomenclature and constituent phases. J. geol. Soc. Aust. 18, 57-68.

Kastner, M. and Gieskes, J.M. (1976). Interstitial water profiles and sites of diagenetic reactions. Leg 35, DSDP, Bellingshausen abyssal plain. Earth Planet. Sci. Lett. 33, 11-20.

Katz, A., Sass, E. and Stavinsky, A. (1972). Strontium behavior in the aragonite-calcite transformation: An experimental study at 40-98°C. Geochim. Cosmoschim. Acta 36, 481-496.

Kay, R.W. and Senechal, R.G. (1976). The rare earth geochemistry of the Troodos ophiolite complex. J. Geophys. Res. 81, 964-970.

Kempton, P.D., Autio, L.K., Rhodes, J.M., Holdaway, M.J., Dungan, M.A. and Johnson, P. (1985). Petrology of basalts from Hole 504B, Deep Sea Drilling Project, Leg 83. In: Anderson, R.N., Honnorez, J., Becker, K., et al., Initial Reports DSDP, 83: Washington (U.S. Govt. Printing Office), 129-164.

Kerrich, R. and Vibetti, N.J. (1985). Evolution of Ca-chloride brine in Cyprus ophiolite: Evidence from C and O isotopes. EOS 66, 1128.

Kristmannsdottir, H. (1975). Hydrothermal alteration of basaltic rocks in Icelandic geothermal areas. Proceedings, 2nd U.N. Symposium on the development and use of geothermal resources, 20-29 May 1975, San Francisco, California, U.S.A., 441-445.

Kristmannsdottir, H. and Tomasson, J. (1978). Zeolite zones in geothermal areas in Iceland. In: Sand, L.B. and Mumpton, F.A., (eds.), Zeolites: Occurrence, properties, use. Permagon Press, Oxford, 277-284.

Lapierre, H. (1975). Les formations sedimentaire et eruptives des nappes de Mamonia et leurs relations avec le Massif de Troodos (Chypre occidentale). Mem. Soc. geol. Fr. 123, 132 pp.

Leg 106 Scientific Party (Detrick, R., Honnorez, J., Adamson, A., Brass, G., Gillis, K., Humphris, S., Mevel, C., Meyer, P., Petersen, N., Rautenschlein, M., Shibata, T., Staudigel, H., Yamamoto, K., and Woolridge, A.). Drilling the Snake Pit hydrothermal sulfide deposit on the mid-Atlantic ridge. Geology, in press.

Liou, J.G. (1979). Zeolite facies metamorphism of basaltic rocks from the East Taiwan Ophiolite. Amer. Mineral. 64, 1-14.

Liou, J.G. (1971a). Stilbite-laumontite equilibrium. Contrib. Mineral. Petrol. 31, 171-177.

Liou, J.G. (1971b). Analcime equilibrium. Lithos 4, 389-402.

Liou, J.G. and Ernst, W.G. (1979). Oceanic ridge metamorphism of the East Taiwan Ophiolite. Contrib. Mineral. Petrol. 68, 335-348.

Liou, J.G., Maruyama, S. and Cho, M. (1985). Phase equilibria and mineral parageneses of metabasalts in low-grade metamorphism. Mineral. Mag. 49, 321-333.

Lister, C.R.B. (1983). On the intermittency and crystallization mechanisms of sub-spreading magma chambers. Geophys. J. Roy. astr. Soc. 73, 351-366.

Lister, C.R.B. (1982). "Active" and "passive" hydrothermal systems in the oceanic crust: Predicted physical conditions. In: Fanning, K.A. and Manheim, F.T. (eds.), The dynamic environment of the ocean floor. Lexington Books, Massachusetts, 441-459.

Lister, C.R.B. (1977). Qualitative models of spreading-center processes, including hydrothermal penetration. Tectonophysics 37, 203-218.

Lister, C.R.B. (1974). On the penetration of water into hot rock. Geophys. J. Roy. astr. Soc. 39, 465-509.

Lydon, J.W. (1984). Some observations on the mineralogical and chemical zonation patterns of volcanogenic sulfide deposits of Cyprus. Current Research, Part A, Geol. Sur. Can. Pap. 84-1A, 611-616.

Malpas, J. and Langdon, G. (1984). Petrology of the upper pillow lava suite, Troodos ophiolite, Cyprus. In: Gass, I.G., Lippard, S.J., and Shelton, A.W., (eds.), Ophiolites and oceanic lithosphere. Blackwell Scientific Publications, Oxford, 155-167.

Mariner, R.H. and Surdam, R.C. (1970). Alkalinity and formation of zeolites in saline lakes. Science 170, 977-980.

McCrea, J.M. (1950). The isotope chemistry of carbonates and a paleo-temperature scale. J. Chem. Phys. 18, 849-857.

McCulloch, M.T. and Cameron, W.E. (1983). Nd-Sr isotopic study of primitive lavas from the Troodos ophiolite, Cyprus: Evidence for subduction - related setting. Geology 11, 727-731.

McCulloch, M.T., Gregory, R.T., Wasserburg, G.J. and Taylor, H.P. (1980). Sm-Nd, Rb-Sr, and $^{18}O/^{16}O$ isotopoic systematics in an ocean crustal section: Evidence from the Semail ophiolite. J. Geophys. Res. 86, 2721-2735.

Mehegan, J. and Robinson, P. (1985). Lava compositions of the Troodos ophiolite, Cyprus. EOS 66, 1123.

Mehegan, J., Robinson, P. and Delaney, J. (1982). Secondary mineralization and hydrothermal alteration in the Reydarfjordur drillcore, eastern Iceland. J. Geophys. Res. 87, 6511-6524.

Miyashiro, A. (1973). The Troodos Ophiolite Complex was probably formed in an island arc. Earth Planet. Sci. Lett. 19, 218-224.

Moore, T.A. (1960). The geology and mineral resources of the Astromeritis–Kormakiti area. Cyprus Geol. Surv. Dept. Memoir 6, 96 pp.

Moores, E.M., Robinson, P.T., Malpas, J. and Xenophontos, C. (1984). A model for the origin of the Troodos Massif, Cyprus and other mideast ophiolites. Geology 12, 500–503.

Moores, E.M. and Varga, R.J. (1984). Extensional tectonics and possible abandoned axial valley, Troodos ophiolite, Cyprus. EOS 65, 1115.

Moores, E.M. and Vine, F.J. (1971). The Troodos Massif, Cyprus and other ophiolites as oceanic crust: Evaluation and implications. Phil. Trans. Roy. Soc. London A 268, 443–466.

Mottl, M.J. (1983). Metabasalts, axial hot springs and the structure of hydrothermal systems at mid–ocean ridges. Geol. Soc. Am. Bull. 94, 161–180.

Mottl, M.J. and Holland, H.D. (1978). Chemical exchange during hydrothermal alteration of basalt by seawater – 1. Experimental results for major and minor components of seawater. Geochem. Cosmoschim. Acta 42, 1103–1115.

Mottl, M.J. and Seyfried Jr., W.E. (1980). Sub–seafloor hydrothermal systems rock– versus seawater–dominated. In: Rona, P.A. and Lowell, R.P, (eds), Seafloor spreading centers: Hydrothermal systems. Dowden, Hutchinson and Ross, Inc., Stroudsburg, PA, 66–82.

Mucci, A. and Morse, J.W. (1983). The incorporation of Mg^{2+} and Sr^{2+} into calcite overgrowths: Influence of growth rate and solution composition. Geochim. Cosmoschim. Acta 83, 217–233.

Muehlenbachs, K. (1979). The alteration and aging of the basaltic layer of the seafloor: Oxygen isotope evidence from DSDP/IPOD Legs 51, 52 and 53. In: Donnelly, T., Francheteau, J., Bryan, W., Robinson, P., Flower, M., Salisbury, M., et al., Initial Reports DSDP, 51–53 Pt. 2: Washington (U.S. Govt. Printing Office), 1159–1167.

Mukasa, S. and Ludden, J. (1986). A Cenomanian–Turonian U–Pb zircon age for plagiogranites from the Troodos ophiolite. EOS 67, 400.

Mumpton, F.A. (1960). Clinoptilolite redefined. Amer. Mineral. 45, 351–369.

Munha, J., Fyfe, W.S. and Kerrich, R. (1980). Adularia, the characteristic mineral of felsic spillites. Contrib. Mineral. Petrol. 75, 15–19.

O'Neil, J.R., Clayton, R.N. and Mayeda, J.K. (1969). Oxygen isotope fractionation in divalent metal carbonates. J. Chem. Phys. 51, 5547–5558.

382

Oudin, E. and Constantinou, G. (1984). Black smoker chimney fragments in Cyprus sulfide deposits. Nature 308, 349-353.

Palmason, G., Arnorsson, S., Fridleifsson, I.B., Kristmannsdottir, H., Saemundsson, K., Stefansson, V., Steingrimsson, B., Tomasson, J. and Kristjansson, O. (1979). The Iceland crust: Evidence from drillhole data on structure and processes. In: Talwani, M., Harrison, C.G., and Hayes, D.E., (eds.), Deep Drilling Results in the Atlantic Ocean: Ocean crust, Maurice Ewing Series 2. Am. Geophys. Un., Washington, 43-65.

Pantazis, T. M. (1967). The geology and mineral resources of the Pharmakas-Kalavasos area. Cyprus Geol. Surv. Dept. Memoir 8, 190 pp.

Parmentier, E.M., and Spooner, E.T.C. (1978). A theoretical study of hydrothermal convection and the origin of the ophiolitic sulfide deposits of Cyprus. Earth Planet. Sci. Lett. 40, 33-44.

Pearce, J.A. (1975). Basalt geochemistry used to investigate past tectonic environments on Cyprus. Tectonophysics 25, 41-67.

Pearce, J.A. and Cann, J.R. (1973). Tectonic setting of basic volcanic rocks determined using trace element analyses. Earth Planet. Sci. Lett. 19, 290-300.

Pearce, J.A. and Norry, M.J. (1979). Petrogenetic implications of Ti, Zr, Y, and Nb variations in volcanic rocks. Contrib. Mineral. Petrol. 69, 33-47.

Pechersky, D.M., Tikhonov, L.V. and Pertsev, N.N. (1983). Magnetic properties of basalts, Deep Sea Drilling Project Leg 69 and 70. In: Cann, J.R., Langeth, M.G., Honnorez, J., Von Herzen, R.P., White, S.M., et al., Initial Reports DSDP, 69: Washington, (U.S. Govt. Printing Office), 705-710.

Ramshen, T.W. & Moores, E.M. (1985). Development and structural relations of domains in the sheeted dike complex, Troodos ophiolite, Cyprus. EOS 66, 1124.

Rautenschlein, M., Jenner, G., Hertozen, J., Hofmann, A.W., Kerrich, R., Schmincke, H.-U. and White, W.M. (1985). Isotopic and trace element composition of volcanic glass from the Akaki Canyon, Cyprus: Implications for the origin of the Troodos ophiolite. Earth Planet. Sci. Lett. 75, 369-383.

Richardson, S.H., Hart, S.R. and Staudigel, H. (1980). Vein mineral ages of old oceanic crust. J. Geophys. Res. 85, 7195-7200.

Robertson, A.H.F. (1977). Tertiary uplift history of the Troodos massif, Cyprus. Geol. Soc. Am. Bull. 88, 1763-1772.

Robertson, A.H.F. and Boyle, J.F. (1983). Tectonic setting and origin of metalliferous sediments in the Mesozoic Tethys ocean. In: Rona, P.A., Bostrom, K., Laubier, L. and Smith, K.L., (eds.), Hydrothermal processes at seafloor spreading centers. Plenum Press, New York, 595-663.

Robertson, A.H.F. and Hudson, J.D. (1974). Pelagic sediments in the Cretaceous and Tertiary history of the Troodos Massif, Cyprus. In: Hsu, K.J. and Jenkyns, H.C. (eds.), Spec. Publ. Int. Assoc. Sediment. 1, 403-434.

Robertson, A.H. and Woodcock, N. (1980). Tectonic setting of the Troodos massif in the east Mediterranean. In: Panayiotou, A., (ed.), Ophiolites, Proceedings, International Ophiolite Symposium, Cyprus 1979. Ministry of Agriculture and Natural Resources, Geol. Surv. Dept., 36-49.

Robinson, P.T. (1977). Alteration of Cretaceous basalts, DSDP Sites 417 and 418. EOS 58, 1174.

Robinson, P.T. and Gibson, I.L. (1984). Cyprus Crustal Study Project, Hole CY-1. Lithologic unit summaries. Unpublished report, University of Waterloo, Waterloo, Ontario, 18 pp.

Robinson, P.T., Melson, W. and Schmincke, H.-U. (1983). Volcanic glass compositions of the Troodos Ophiolite, Cyprus. Geology 11, 400-404.

Rosenbauer, R.J. and Bischoff, J.L. (1983). Uptake and transport of heavy metals by heated seawater: A summary of the experimental results. In: Rona, P.A., Bostrom, K., Laubier, L. and Smith Jr, K.L., (eds.), Hydrothermal processes at seafloor spreading centers. Plenum Press, New York, 177-197.

Ross, C.S. and Hendricks, S.B. (1945). Minerals of the montmorillonite group. Their origin in relation to soils and clays. Geol. Surv. Prof. Pap. 205-B, 23-79.

Savin, S.M. (1977). The history of the earth's surface temperature during the past 100 million years. Ann. Rev. Earth Planet. Sci. 5, 319-355.

Salisbury, M. and Christensen, N. (1978). The seismic velocity structure of a traverse through the Bay of Islands ophiolite complex, Newfoundland: An exposure of oceanic crust and upper mantle. J. Geophys. Res. 83, 805-817.

Schiffman, P., Smith, B., Varga, R., Eddy, C. and Moores, E. (1985). Low ^{18}O epidosites along fossil hydrothermal feeders for massive sulfide deposits, Solea Graben, northern Troodos ophiolite, Cyprus. EOS 66, 1128.

Schmincke, H.-U., Rautenschlein, M., Robinson, P.T. and Mehegan, J.M. (1983). Troodos extrusive series of Cyprus: A comparison with oceanic crust. Geology 11, 405-409.

Seyfried Jr., W.E. and Bischoff, J.L. (1981). Experimental seawater-basalt interaction at 300°C, 500 bars, chemical exchange, secondary mineral formation and implications for the transport of heavy metals. Geochim. Cosmoschim. Acta 46, 135-147.

Seyfried Jr., W.E. and Bischoff, J.L. (1979). Low temperature basalt alteration by seawater: an experimental study at 70°C and 150°C. Geochim. Cosmoschim. Acta 43, 1937-1947.

Seyfried Jr., W.E. and Mottl, M.J. (1982). Hydrothermal alteration of basalt by seawater under seawater-dominated conditions. Geochim. Cosmoschim. Acta 46, 985-1002.

Seyfried Jr., W.E., Shanks III, W.C. and Dibble Jr., W.E. (1978). Clay mineral formation in DSDP Leg 34 basalt. Earth Planet. Sci. Lett. 41, 265-276.

Shapiro, L. (1973). Rapid determination of sulfur in rocks. J. Res. U.S. Geol. Survey 1, 81-84.

Shipboard Scientific Crew (1985). Hole 540B, Leg 83. In: Anderson, R.N., Honnorez, J., Becker, K., et al., Initial Reports DSDP, 83: Washington (U.S. Govt. Printing Office), 13-120.

Shipboard Scientific Crew (1983). Sites 501 and 504: Sediments and ocean crust in an area of high heat flow on the southern flank of the Costa Rica Rift. In: Cann, J.R., Langseth, M.G., Honnorez, J., Von Herzen, R.P., White, S.M., et al., Initil Reports DSDP, 69: Washington (U.S. Govt. Printing Office), 31-176.

Shipboard Scientific Crew (1979a). Site 417. In: Donnelly, T., Francheteau, J., Bryan, W., Robinson, P., Flower, M., Salisbury, M., et al., Initial Reports DSDP, 51-53 Pt.2: Washington (U.S. Govt. Printing Office), 23-350.

Shipboard Scientific Crew (1979b). Site 418. In: Donnelly, T., Francheteau, J., Bryan, W., Robinson, P., Flower, M., Salisbury, M., et al., Initial Reports DSDP, 51-53 Pt.2: Washington (U.S. Govt. Printing Office), 351-626.

Smewing, J. (1975). Metamorphism of the Troodos Massif, Cyprus. Unpublished Ph.D. thesis, Open University, U.K., 132 pp.

Smewing, J.D., Simonian, K.O. and Gass, I. (1975). Metabasalts from the Troodos Massif, Cyprus: Genetic implication deduced from petrography and trace element geochemistry. Contrib. Mineral. Petrol. 51, 49-54.

Smith, R.E. and Smith, S.E. (1976). Comments on the use of Ti, Zr, Y, Sr, K, P and Nb in classification of basaltic magmas. Earth Planet. Sci. Lett. 32, 114-120.

Spooner, E.T.C. (1980). Cu-pyrite mineralization and seawater convection in oceanic crust: The ophiolitic ore deposits of Cyprus. In: Strangway, D.W., (ed.), The continental crust and its mineral deposits, Geol. Assoc. Can. Spec. Pap. 20, 685-704.

Spooner, E.T.C. (1977). Hydrodynamic model for the origin of the ophiolitic cupriferous pyrite ore deposits of Cyprus. In: Volcanic processes in ore genesis. The Institute of Mining and Metallurgy Spec. Publ. 7, Geol. Soc. London, 58-71.

Spooner, E.T.C. and Bray, C.J. (1977). Hydrothermal fluids of sea water salinity in ophiolitic sulphide ore deposits in Cyprus. Nature 266, 808-812.

Spooner, E.T.C., Beckinsale, R.D., England, P.C. and Senoir, A. (1977a). Hydration, ^{18}O enrichment, and oxidation during ocean floor hydrothermal metamorphism of ophiolitic metabasic rocks from E. Liguria, Italy. Geochim. Cosmoschim. Acta 41, 857-871.

Spooner, E.T.C., Chapman, H.J. and Smewing, J.D. (1977b). Strontium isotopic contamination and oxidation during ocean floor hydrothermal metamorphism of the ophiolitic rocks of the Troodos Massif, Cyprus. Geochim. Cosmoschim. Acta 41, 873-890.

Spooner, E.T.C., Beckinsale, R.D., Fyfe, W.S. and Smewing, J.D. (1974). ^{18}O enriched ophiolitic metabasic rocks from E. Liguria (Italy), Pindos (Greece) and Troodos (Cyprus). Contrib. Mineral. Petrol. 47, 41-62.

Spooner, E.T.C. and Fyfe, W.S. (1973). Sub-sea-floor metamorphism, heat and mass transfer. Contrib. Mineral. Petrol. 42, 287-304.

Stakes, D.S. and O'Neil, J.R. (1982). Mineralogy and stable isotope geochemistry of hydrothermally altered oceanic rocks. Earth Planet. Sci. Lett. 57, 285-304.

Staudigel, H., Kastner, M. and Sturz, A. ^{18}O and $^{87}Sr/^{86}Sr$ of calcites from the basaltic basement of DSDP Site 597: Timing, and temperatures of alteration. In: Initial Reports DSDP, 92: Washington (U.S. Govt. Printing Office), in press.

Staudigel, H., Gillis, K. and Duncan, R. (1986). K/Ar and Rb/Sr ages of celadonites from the Troodos ophiolite, Cyprus. Geology 14, 72-75.

Staudigel, H. and Hart, S.R. (1985). Dating of ocean crust alteration: Strontium isotopic ratios from 504B carbonates and a re-interpretation of Sr isotope data from DSDP Sites 105, 332, 417 and 418. In: Anderson. R., Honnorez, J., Becker, K., et al., Initial Reports DSDP, 83: Washington (U.S. Govt. Printing Office), 297-303.

Staudigel, H., Bryan, W.B. and Thompson, G. (1979). Chemical variation in glass - whole and rock pairs from individual cooling units in Holes 417D and 418A. In: Donnelly, T., Francheteau, J., Bryan, W., Robinson, P., Flower, M., Salisbury, M., et al., Initial Reports DSDP, 51-53 Pt.2: Washington (U.S. Govt. Printing Office), 977-986.

Staudigel, H., Hart, S.R. and Richardson, S.H. (1981). Alteration of the oceanic crust: Processes and timing. Earth Planet. Sci. Lett. 52, 311-327.

Staudigel, H. and Hart, S.R. (1979). Ocean crust-seawater interactions Sites 417 and 418. In: Donnelly, T., Francheteau, J., Bryan, W., Robinson, P., Flower, M., Salisbury, M., et al., Initial Reports DSDP, 51-53 Pt.2: Washington (U.S. Govt. Printing Office), 1169-1176.

Stern, C., DeWit, M.J. and Lawrence, J. (1976). Igneous and metamorphic processes associated with the formation of Chilean ophiolites and their implications for ocean floor metamorphism, seismic layering and magnetism. J. Geophys. Res. 81, 4370-4380.

Stern, C. and Elthon, D. (1979). Vertical variations in the effects of hydrothermal metamorphism in Chilean ophiolites: Their implications for ocean floor metamorphism. Tectonophysics 55, 179-213.

Strens, M.R. and Cann, J.R. (1982). A model of hydrothermal circulation in fault zones at mid-ocean ridge crests. Geophys. J. Roy. astr. Soc. 71, 225-240.

Sunkel, G., Bednarz, U. and Schmincke, H.-U. The basaltic andesite - andesite and the andesite - dacite series from the ICRDG drill-holes CY-2 and CY-2a: II. Alteration. Initial Reports ICRDG, CY-2 and CY-2a, in press.

Surdam, R.C. and Shepperd, R.A. (1978). Zeolites in saline, alkaline-lake deposits. In: Sand, L.B. and Mumpton, F.A. (eds.), Natural Zeolites: Occurrence, Properties, Use. Pergamon Press, Oxford, 145-174.

Swarbrick, R.E. (1980). The Mamonia Complex of southwest Cyprus: A Mesozoic continental margin and its relationship to the Troodos complex. In: Panayiotou, A., (ed.), Ophiolites, Proceedings, International Ophiolite Symposium, Cyprus 1979. Ministry of Agriculture and Natural Resources, Geol. Surv. Dept., 86-92.

Thompson, G. (1983). Basalt-seawater interaction. In: Rona, P.A.,

Bostrom, K., Laubier, L. and Smith, K.L., (eds.), Hydrothermal processes at seafloor spreading centers. Plenum Press, New York, 225-278.

Thy, P., Brooks, C.K. and Walsh, J.N. (1985). Tectonic and petrogenetic implications of major and rare earth element chemistry of Troodos glasses, Cyprus. Lithos 18, 165-178.

Turner, W.M. (1973). The Cyprian gravity nappe and the autochthonous basement of Cyprus. In: De Jong, K.A. and Scholten, R., (eds.), Gravity and Tectonics. Wiley, New York, 287-307.

Troll, G. and Farzaneh, A. (1978). Determination of fluorine and total water in thirty-three international geochemical reference samples. Geostandard Newsletter 2, 43-47.

Vibetti, N.J., Kerrich, R. and Fyfe, W. (1985). Presence of Ca-Na dominated hypersaline brines in quartz - calc silicate veins of Troodos ophiolite (Cyprus). EOS 66, 1129.

Von Damm, K.L., Edmund, J.M., Grant, B., Measures, C.I., Walden, B. and Weiss, R.F. (1985). Chemistry of submarine hydrothermal solutions at 21° N, East Pacific Rise. Geochim. Cosmoschim. Acta 49, 2197-2220.

Williams, D.L., Von Herzen, R.P., Sclater, J.G. and Anderson, R.N. (1974). The Galapagos spreading center: Lithospheric cooling and hydrothermal circulation. Geophys. J. Roy. astr. Soc. 38, 587-608.

Wilson, R.A.M. (1959). The geology and mineral resources of the Xeros-Troodos area. Cyprus Geol. Surv. Dept. Memoir 1, 135 pp.

Wise, W.S. and Eugster, H.P. (1964). Celadonite: Synthesis, thermal stability and occurrence. Amer. Mineral. 49, 1031-1083.

Wood, D.A., Joron, J.L. and Treuil, M. (1979). A re-appraisal of the use of trace elements to classify and discriminate between magma series erupted in different tectonic settings. Earth Planet. Sci. Lett. 45, 326-336.

Wolery, T.J. and Sleep, N.H. (1976). Hydrothermal circulation and geochemical flux at mid-ocean ridges. J. Geol. 84, 249-275.

Zindler, A., Staudigel, H. and Batiza, R. (1984). Isotopic and trace element geochemistry of young Pacific seamounts: Implications for the scale of upper mantle heterogeneity. Earth Planet. Sci. Lett. 70, 175-195.